Natural modulators of amyloid formation in Alzheimer's disease

Sirwan M. Amin Al-Jaf

A Thesis Submitted for the degree of Doctors of Philosophy

July 2016

University of Sheffield

Department of Molecular Biology and Technology

For Sirwan’s Family;

Mother, father, wife, children, brothers and sisters.

Abstract

Alzheimer's disease (AD) is the most common cause of dementia, and the deposition of amyloid β (Aβ) peptide in the AD brains is a hallmark of the disease. Other amyloidogenic proteins like Transthyretin (TTR) and human Cystatin C (hCC) can modulate the aggregation of Aβ. These two proteins are proposed to play a role in the pathophysiology of AD as they are found co-deposited in amyloid deposits in the brains of AD patients, most notably at the cell surface. Animal models and cell line assays showed protective roles for TTR and hCC against Aβ-induced toxicity, and Aβ fibril formation is inhibited through interaction with TTR and hCC.

This study investigated the mechanism of *in vitro* interaction of TTR with Aβ. The ability of WT TTR to inhibit Aβ fibrillisation in the presence of Aβ binding surfaces was higher than in the presence of non-binding surfaces. Then, the interaction between different TTR mutants with different multimeric stabilities and different alloforms of Aβ showed that TTRs with less stable tetramers and unfolded monomers are the best inhibitors of Aβ fibrillisation. Analysing the thioflavin T curves of Aβ aggregation in the presence of TTRs and the interaction of TTRs with different forms of Aβ showed that the interaction between the two proteins occurs mainly through binding to early nucleating species of Aβ rather than to the monomer.

The dose-dependent inhibition of Aβ fibrillisation and the promotion of amorphous aggregates by hCC were validated. However, the previous suggestion of simple monomer to monomer interaction between Aβ and hCC was not confirmed. Instead, a proposed hCC binding to oligomeric species of Aβ was supported by the observed hCC interaction with different aggregated species of Aβ. The dimeric form of hCC was found to be a less effective inhibitor compared to WT monomer, indicating that the active site could be the hydrophobic loops involved in dimerisation and protease inhibition. This interpretation was supported, as mutation of hydrophobic residues in the active site significantly reduced the intensity of hCC to inhibit Aβ fibrillisation.

We showed that these two proteins are mainly inhibit Aβ fibrillisation through interaction with the early aggregated structures of Aβ (some form of oligomers). As it is known that oligomers are responsible for Aβ toxicity *in vivo*, the potential of these two proteins to be used as natural modulators is supported by this study.

Acknowledgements

First and foremost I must thank my supervisor Rosie Staniforth who has been wonderful, both for supervising my PhD in the first place and for all her guidance, support and encouragement throughout the last four years, especially during the painful writing up process. I would also like to thank my advisors Jon Waltho, John Rafferty and Mike Williamson for all their help and guidance. Andrea Hounslow has been amazing, assisting me with the NMR experiments and analysis. Thank you also to Svet Tzokov for all of his help with EM.

Thank you also to amyloid group, particularly Abi, Pete, Amy, Liam and Alex. Abi has been simply a great colleauge, she was always around for a help and a part of my research has been based on her work, for which I am very grateful. The NMR group have been great; it would be impossible to name everybody (and I would undoubtedly forget someone), but thank you all so much for the help and advice. Thank you also to the NMR group Nicky, Claire, Luke and Angus. Thanks for all the excellent cakes, I have enjoyed Friday cakes a lot.

Outside the lab, I have met many wonderful people since moving to Sheffield, but special thanks must go to Taib, Isam, Salar, and Omed. I'm so glad I met you all, and I definitely wouldn't have made it through without you all.

Outside the university, I would like to thank Sarwat, Sartip and Barzan, especially Sarwat for his help at the early days on arriving to UK and been a great friend all the time.

Thank you to my wonderful family, to Mum, Dad and the whole family (brothers and sisters) for all their love and support, it means so much to me and I am truly grateful.

Thanks to The Higher Committee for Education Development in Iraq, for sponsoring my PhD. Thanks to my friends and university colleagues back home, they were always happy to help for anything I needed there.

Last but not least, thank you to my wonderful wife, Srwa, for companionship, as I made her to live away of her family and friends for 4 years, putting up with me and for always believing in me. I couldn't have done it without you.

Table of contents

List of Figures

List of Tables

List of Abbreviations

Aβ	Amyloid β
AD	Alzheimer's disease
ALS	Amyloid Lateral Sclerosis
AFM	Atomic Force Microscopy
β2m	β2-Microglobulin
DMSO	Dimethyl sulfoxide
EM	Electron Microscopy
FAC	Familial Amyloidotic Cardiomyopathy
FAP	Familial Amyloidotic Polyneuropathy
GLTI	Glutamate/ Aspartate transport protein
hCC	Human Cystatin C
H/D	Exchange Hydrogen/Deuterium Exchange of protein backbone amides
HSQC	Hetero-Nuclear Single Quantum Coherence NMR Spectroscopy
LTP	Long term potentiation
MS	Mass Spectroscopy
N-terminal	Amide End Protein Region
NMR	Nuclear Magnetic Resonance Spectroscopy
OD	Optical Density
PEG	Polyethylne glycol
PMSF	Phenylmethanesulfonyl Fluoride
PrP^C	Prion Protein (Cellular)
PS	Polystyrene
SDM	Site-Directed Mutagenesis
SDS-PAGE	Sodium Dodecyl Sulphate Polyacrylamide Gel Electrophoresis
SEC HPLC	Size Exclusion Chromatography High-Pressure-Liquid-Chromatography
ssNMR	Solid State Nuclear Magnetic Resonance Spectroscopy
TEM	Transmission Electron Microscopy
ThT	Thioflavin-T
TTR	Transthyretin
UV	Ultra-Violet

Chapter 1: Introduction

Background

There are a growing number of human diseases, known as amyloid diseases, which are identified by the deposition of protein aggregates in the body (Westermark *et al.*, 1990, Dobson, 2002, Horwich, 2002, Westermark *et al.*, 2002). Alzheimer's disease (AD) (Selkoe and Schenk, 2003a), Parkinson's disease (Lang and Lozano, 1998), prion diseases (Prusiner, 1998, Collinge, 2001) and Huntington's disease (Perutz, 1999) are among these diseases. Most of these diseases are late-onset diseases and as the world's population gets older these diseases are becoming more prevalent. Alzheimer's is the most common cause of dementia, an estimated 46.8 million people worldwide were living with dementia in 2015, with 9.9 million new cases per year (Alzheimers.co.uk). For that reason, understanding the cause and developing new drugs for amyloid diseases is important.

Amyloid diseases are identified by the deposition of amyloid fibril in affected tissues. Amyloid fibrils are formed through conformational change and aggregation of normally soluble proteins to insoluble, highly ordered and typically highly stable protein deposits (Fandrich, 2012a).Whereas in the past, each disease was usually associated with one amyloid-forming protein, current data suggest the involvement of multiple amyloid-forming proteins in the pathophysiology of the amyloid disease. *In vitro*, the aggregation behaviour of different proteins has been characterised extensively but the effect of individual proteins on each other's aggregation is not well known. In order to develop novel ways for targeting amyloid formation for therapeutic purposes, we need a better understanding of natural protection mechanisms occurring in the body. An increasing number of studies suggest amyloid aggregation is perturbed by other amyloid proteins under physiological conditions (Li and Buxbaum, 2011). As we search for a cure, the

purpose of this project is to study the natural regulation of amyloid β aggregation by two other amyloidogenic proteins, transthyretin and cystatin C.

1. 1. Classification of Amyloid

An increasing number of proteins have been found to form amyloid deposits in the human body. At least 31 proteins have been recognized to form extracellular amyloid plaques, and some others are found to form intracellular amyloids where they form fibril-like intracellular deposits (Table 1.1) (Sipe *et al.*, 2014). The majority of deposited amyloids are extracellular and may be found in an organ or throughout all the body (Sipe and Cohen, 2000, Dobson, 2004). The amount of deposited amyloid is hugely variable from nearly undetectable to kilograms found in the case of systemic amyloidosis (Dobson, 2004). Most amyloid protein mutants are associated with induced fibril formation because of native state destabilisation, therefore increasing the steady state concentration of the partially unfolded species. Amyloidogenic diseases can be categorized into different groups according to deposition site and affected organs. Three main groups of amyloidogenic diseases can be classified: non-neurodegenerative systemic amyloidosis where amyloid deposition occurs in multiple organs, non-neurodegenerative localised amyloidosis where the amyloid deposition is localised in only one organ, and neurodegenerative amyloidogenic diseases where the deposition is confined only to the brain (Chiti and Dobson, 2006a).

Amyloidogenic protein	**Precursor protein**	**Disease**	**Systemic or localized**	**Target organs**
AL	Immunoglobulin light chain	Systemic amyloid light chain amyloidosis Nodular amyloidosis	S, L	All organs except CNS
AH	Immunoglobulin heavy chain	Immunoglobulin heavy chain associated amyloidosis (Eulitz *et al.*, 1990)	S, L	All organs except CNS

AA	(Apo) Serum amyloid A	AA amyloidosis	S	All organs except CNS
ATTR	Transthyretin, wild type	Senile systemic amyloidosis	S	Heart mainly in male, Ligaments, Tenosynovium
	Transthyretin, variants	Familial amyloid polyneuropathy, Familial amyloid cardiomyopathy	S	PNS, ANS, heart, eye, leptomen
Aβ2M	β_2-Microglobulin, wild type	Haemodialysis-related amyloidosis	L	Musclo-skeletal system
	β_2-Microglobulin, variant	Familial systemic amyloidosis (Stoppini and Bellotti, 2015)	S	ANS
AApoAI	Apolipoprotein A I, variants	Hereditary systemic amyloidosis	S	Heart, liver, kidney, PNS, testis, larynx (C-terminal variants), skin (C-terminal variants)
AApoAII	Apolipoprotein A II, variants		S	Kidney
AApoAIV	Apolipoprotein A IV, wild type		S	Kidney medulla and systemic
AGel	Gelsolin, variants	Hereditary systemic amyloidosis	S	PNA, cornea
ALys	Lysozyme, variants	Hereditary systemic amyloidosis	S	Kidney
ALECT2	Leukocyte chemotactic factor-2	Leukocyte chemotactic factor amyloidosis (Benson *et al.*, 2008)	S	Kidney, primarily
AFib	Fibrinogen α, variants	Hereditary renal amyloidosis	S	Kidney, primarily
ACys	Cystatin C, variants	Hereditary cystatin c amyloid angiopathy	S	PNA, skin
ABri	ABriPP, variants	Familial British/Dutch amyloidosis	S	CNS
Adan	ADanPP, variants	Familial Danish dementia (Holton *et al.*, 2002)	L	CNS
Aβ	Aβ protein precursor, wild type Aβ protein precursor, variant	Alzheimer's Disease	L	CNS
APrP	Prion protein, wild-type Prion protein variants	Creutzfeldt-Jakob disease Gerstmann-Strassler-Schneiker syndrome Fatal familial insomnia Bovine spongiform encephalopathy	L	CJD, fatal insomnia
ACal	(Pro)calcitonin	Medullary carcinoma of the thyroid	L	C-cell thyroid tumors
AIAPP	Islet Amyloid Polypeptide	Type 2 Diabetes	L	Islet of Langerhans, Insulinomas

AANF	Atrial Natruritic factor	Atrial amyloid	L	Cardiac atria
APro	Aprolactin	Ageing pituitary gland amyloidosis	L	Pituitary polycarcinomas, aging pituitary
AIns	Insulin	Injection-localized amyloidosis	L	Iatrogenic, local injection
ASPC	Lung Surfactant Protein	Pulmonary alveolar proteinosis (Gustafsson *et al.*, 1999)	L	Lung
AGal7	Galectin 7	Skin amyloidosis	L	Skin
ACor	Corneodensomin	Cornified epithelia, hair follicles amyloidosis	L	Cornified epithelia, Hair follicles
AMed	Lactadherin	Aortic medial amyloid	L	Senile aortic, Media
AKer	Kerato-epithelin	Lattice corneal dystrophy	L	Cornea, hereditary
ALac	Lactoferrin	Corneal amyloidosis	L	Cornea
AOAAP	Odontogenic Ameloblast-Associated Protein		L	Odontogenic tumors
ASem1	Semenogelin 1		L	Vesicula seminalis
Enf	Enfurvitide		L	Iatrogenic

Table 1.1. The amyloidogenic proteins and amyloid-related diseases, mainly adapted from (Sanders *et al.*, 2009, Sipe *et al.*, 2014).

1. 2. Alzheimer's disease

Alzheimer's disease (AD) is the most common cause of dementia (Prince *et al.*, 2015). The probability of being diagnosed with AD over the age of 65 is 6% (Burns and Iliffe, 2009), and this figure increases to 50% over the age of 85 (Irvine *et al.*, 2008). Although AD diagnosis is based on specific criteria, currently the only accurate technique of diagnosis is post-mortem autopsy. Advancements in the magnetic resonance imaging (MRI) and/or single photon emission computed tomography (SPECT) imaging techniques will improve diagnosis and allow pre-symptomatic identification of AD (Coimbra *et al.*, 2006).

The presence of extracellular amyloid plaques and intracellular neurofibrillary tangles (NFT) in the brain is one of the characteristic features of AD (Annaert and De Strooper,

2002). Amyloid plaques contain fibrils mostly formed from the Aβ peptide, while the neurofibrillary tangles are formed from hyper-phosphorylated tau protein. Besides the deposition of plaques and tangles, there is a gradual decline in cognitive ability (Caughey and Lansbury, 2003). The pyramidal neurons of the third and fourth layers of the cerebral cortex are most susceptible to loss in AD, and enlarging of the ventricles, widening of the sulci and thinning of the cortical gyri results in a complete loss of grey matter (Deng *et al.*, 2001). The molecular basis for the connection between Aβ peptide levels and neurotoxicity is not well understood (Annaert and De Strooper, 2002). It is believed that Aβ is involved in various toxic activities such as apoptosis, generation of radicals, complement activation, calcium homeostasis disruption and the pore formation in the cell membrane (Small *et al.*, 2001, Benilova *et al.*, 2012). The prominent hypothesis is that the oligomeric forms of Aβ are the toxic species responsible for degeneration.

There are two types of AD: late-onset (sporadic), which accounts for the majority (90%) of the cases, and early-onset (familial), which is usually caused by a mutation that either causes overproduction of $A\beta_{1-42}$ or increases its tendency to form fibrils (Caughey and Lansbury, 2003). The presenilin-1 gene encodes for one of the enzymes responsible for the Aβ peptide cleavage from its precursor, mutations in this gene leads to an increase in both brain and extracellular concentrations of Aβ (Scheuner *et al.*, 1996). Polymorphisms are also noticed in the presenilin-2 (PS2) gene encoding an enzyme which is responsible for the further downstream processing of Aβ. Mutations in the gene for the amyloid precursor protein (APP) itself lead to overproduction of both $A\beta_{1-40}$ and $A\beta_{1-42}$ or changes in the Aβ peptides production spectrum (Ancolio *et al.*, 1999, Kumar-Singh *et al.*, 2000). These polymorphisms can also be linked to cerebral amyloid angiopathy (CAA) and late-onset AD (Yamada *et al.*, 1997, Yamada, 2000). Down's syndrome patients above the

fourth decade normally develop AD; this is most possibly because of the chromosome 21 trisomy which houses the APP gene (Caughey and Lansbury, 2003).

Amyloid-β (Aβ) is a short peptide generated from the amyloid precursor protein (APP) cleavage. The Aβ fragments are different in length, ranging from 38 to 43 amino acids (Benilova *et al.*, 2012), however, $A\beta_{1-40}$ and $A\beta_{1-42}$ are the most common fragments (Jarrett *et al.*, 1993). $A\beta_{1-40}$ is present at higher levels compared to $A\beta_{1-42}$ (ratio 10:1) (Kuperstein *et al.*, 2010), where the latter is the most toxic form of the peptide (Storey and Cappai, 1999). Although studies show that oligomerisation of these different Aβ alloforms occurs by different assembly pathways, there is enough evidence to prove formation of similar intermediates by both peptides, although at different concentrations of the peptide (Bitan *et al.*, 2003). The peptides are very hydrophobic, particularly the C-terminal and central cluster (residues 17-21) (Serpell, 2000).

The amyloid cascade hypothesis (Hardy, 1997, 1999, Sisodia *et al.*, 2001, Annaert and De Strooper, 2002) proposes that the amyloid β peptide, and in particular its aggregates are the cause of all of the Alzheimer's disease pathophysiology, including the characteristic hyperphosphorylation of tau proteins and the consequent formation of intracellular tangles.

1. 3. The structure of amyloid

Despite the differences in the amino acid sequence of the native forms of amyloid precursor proteins, the deposited amyloid fibrils exhibit similar basic structural features (Serpell *et al.*, 1995, Sunde *et al.*, 1997, Serpell *et al.*, 2000), and similar toxicity mechanisms (Makin and Serpell, 2005). For example, amyloid beta peptide (40-42 residues) which is the Alzheimer's disease (AD) amyloid (Selkoe and Schenk, 2003b), and a >3000 residue huntingtin which is the Huntington's disease amyloid, form similar

fibrils. Furthermore, structurally different proteins varying from the all-β tetrameric transthyretin in senile systemic amyloidosis to small α-helical prion protein in Creuzfeld-Jacob disease (Zahn *et al.*, 2000), also form similar fibrils.

Actually, it appears that nearly all proteins can assemble to amyloid fibrils *in vitro*, suggesting that amyloid is a model structure that proteins will adopt when subjected to certain conditions (Guijarro *et al.*, 1998, Chiti *et al.*, 1999, Dobson, 1999, Fandrich *et al.*, 2001). However, even in the absence of accessory components, protein self-assembly into amyloid can still occur *in vitro* (Dobson, 2004), implying a more subtle role, probably analogous to molecular chaperones in the folding of the protein (Thomas *et al.*, 1995, Revesz *et al.*, 2003).

Early electron microscopic investigations showed that amyloid fibrils are unbranching and straight, with a diameter of 70-120 Å (Shirahama and Cohen, 1967), and formed from several protofibrils arranged in parallel. Amyloid fibrils have a specific cross-β structure formed by an organised core of β-strands that run perpendicular to the fibril axis. It is believed that the fibril is stabilised via hydrogen bonding from main chain interactions (Makin *et al.*, 2005), explaining not only the amyloid fibrils' common structure but also the process by which any protein can make fibrils when it is exposed to the correct conditions (Fandrich *et al.*, 2001).

Because amyloid fibrils are heterogeneous, large and insoluble, it is difficult to gather structural information applying conventional techniques like X-ray crystallography and NMR (Serpell, 2000). However, biophysical techniques such as X-ray diffraction and solid-state NMR (ssNMR) can be adopted to great effect, in combination with other techniques like electron microscopy, limited proteolysis and hydrogen-deuterium (H/D) exchange to evolve structural information leading to improvements in structural models.

1. 4. Atomic-level structural determination

1. 4. 1. X-Ray Fibre Diffraction

X-ray fibre diffraction provided the key structural details on the amyloid fibrils (Blake and Serpell, 1996). Fibre diffraction creates diagnostic reflections in two positions: strong meridional reflections of 4.7Å correspond to repeated inter-strand hydrogen bond spacing between the β-sheets along the fibril axis whilst weaker equatorial reflections 10 Å created from electron density due to intersheet interactions vertical to the fibril axis, which is characteristic of a cross-β structure (Figure 1.1) (Geddes *et al.*, 1968, Blake and Serpell, 1996). Further structural information can be obtained through using well-aligned fibril preparations, information like helical pitch/helical repeating unit, precise overall appearances, dimensions and even the existence of a hydrated fibril core (Blake and Serpell, 1996, McDonald *et al.*, 2012). However, fibril diffraction can only disclose these molecular features in exceptionally appropriate situations (Stubbs, 1999, Chandrasekaran and Stubbs, 2006).

Based on the fact that all amyloid fibrils demonstrate the same diffraction pattern, the "cross-β structure" model was proposed (Figure 1.2). According to this model, the β-sheets run parallel to the fibril axis and their component β-strands are perpendicular to the axis of the fibril (Blake and Serpell, 1996, Sunde *et al.*, 1997, Makin and Serpell, 2005). The cross β structure was originally noticed in silk fibrils (Geddes *et al.*, 1968).

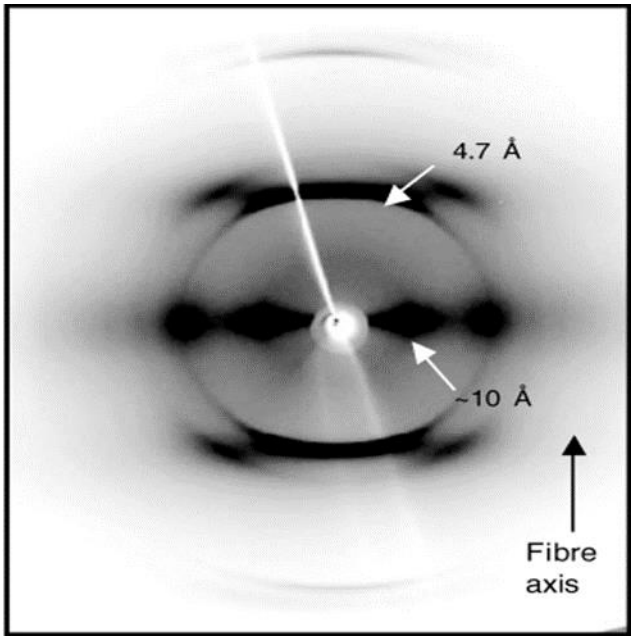

Figure 1.1. X-ray fibril diffraction from aligned islet amyloid polypeptide (IAPP) fibrils, showing the positions of the 4.7 Å meridional and approximately 10 Å equatorial reflections in a cross-β pattern. Taken from (Makin and Serpell, 2005).

1.4.2. Microscopy Techniques

Transmission electron microscopy (TEM) and atomic force microscopy (AFM) are useful techniques not only for identification of amyloid fibrils, but are also used to explore oligomer formation and fibrillisation by discontinuous and continuous methods (Figure 1.2 A) (Goldsbury *et al.*, 1999). Improvements in real-time AFM techniques could provide some exciting insights into the fibrillisation mechanism. Mass per unit length (MPL) measurements can be performed applying specific scanning transmission electron microscopy (STEM) which is employed to calculate the spaces between repeating units in amyloid fibril (Wall *et al.*, 2008). Thus, these calculations have been conducted on a number of amyloid fibril-forming proteins and play a major part in the structural modelling of amyloid fibrils (Petkova *et al.*, 2002a).

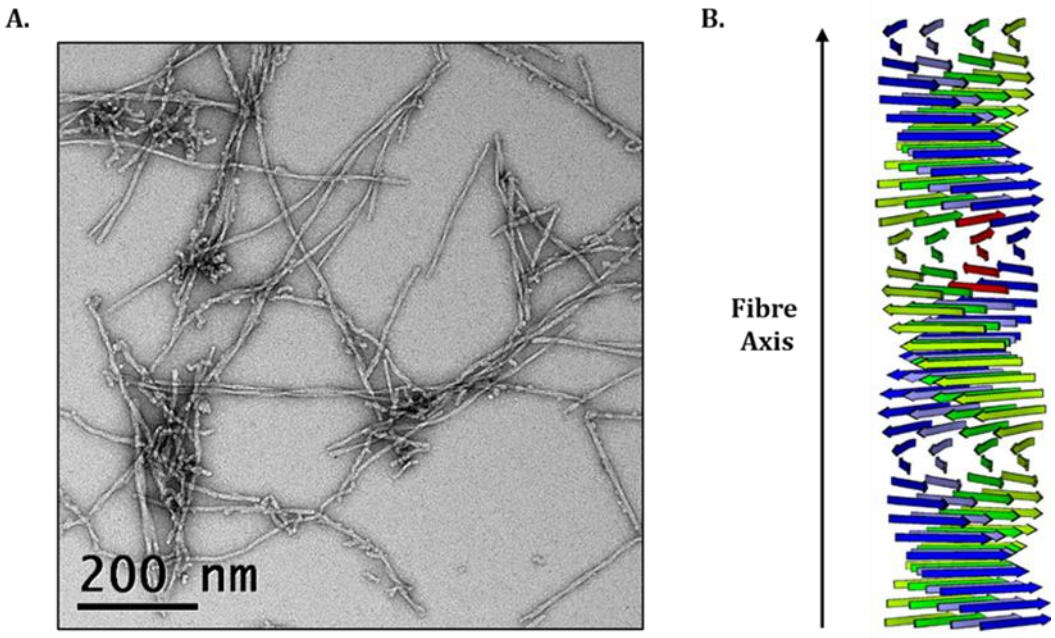

Figure 1.2. Amyloid Fibril Structure. (A) Electron micrograph of negatively stained $A\beta_{1-42}$ amyloid fibrils. (B) Model of the cross-β fibril structure consisting of β-strands running perpendicular to the fibril axis, with inter-strand hydrogen bonds in the direction of the fibril axis. Adapted by Prof. Peter Artymiuk from (Sunde *et al.*, 1997).

1.4.3. Cryo-electron microscopy

The three-dimensional structure of amyloid fibrils can be revealed by cryo-electron microscopy, by averaging several sections of EM images of amyloid fibril. Cryo-EM investigations have shown that fibrils are made of filamentous subunit structures named protofilaments. Twisting of protofilaments around one another along the axis of the fibril gives a helical appearance (Goldsbury *et al.*, 2000, Serpell, 2000, Jimenez *et al.*, 2002). Cryo-EM examinations verified the cross-β model, as striations can be observed running across the fibril with a 4.7 Å repeat in fibrils produced from Aβ ($A\beta_{11-25}$) (Serpell and Smith, 2000a). This observation also confirms that the β-strands are in direct register and run perpendicular to the fibril axis. Microscopy is particularly beneficial for characterizing common species within a mixture as the different structural families can

be investigated individually. This technique has been used to study fibrils formed by the SH3 domain of phosphatidylinositol-39-kinase (Jimenez *et al.*, 1999), $A\beta_{1-40}$ (Serpell and Smith, 2000b), insulin (Figure 1.3 A) (Jimenez *et al.*, 2002), and β_2 microglobulin (White *et al.*, 2009). More recently, a high resolution structure has been proposed for $A\beta_{1-42}$ fibrils (Figure 1.3 B).

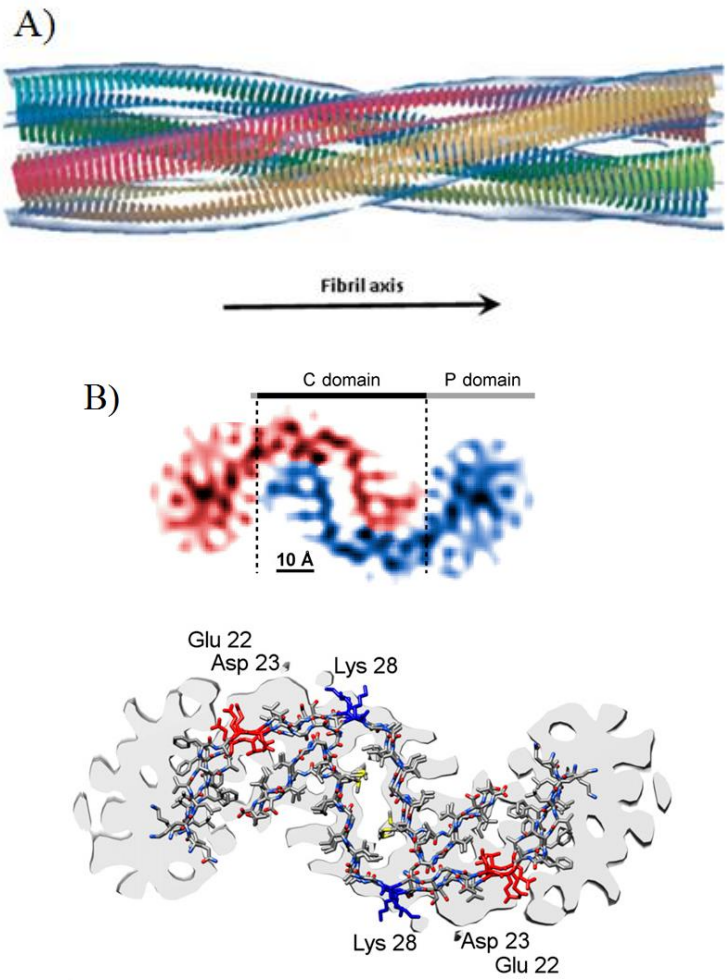

Figure 1.3. Cryo-EM reconstructions of amyloid fibrils. (A) Insulin protofilaments within a mature amyloid fibril, where the four protofilaments are coloured separately, Taken from (Jimenez *et al.*, 2002). B) Top; cross-sectional view of the Cro-EM reconstruction (rendered at 5A°. down; best fits for the sequence of $A\beta_{1-42}$ superimposed on electron density, taken from (Schmidt *et al.*, 2015).

1.4.4. Hydrogen-deuterium exchange (HX)

HX is an effective technique that can be used to resolve the secondary structure and solvent accessibility of single protein chains within the fibrils. The proton exchange rate between the amide and the solvent deuterated water can be measured by this technique. Faster rates of proton exchange happen between the exterior amide protons and solvent deuterons compared to amides involved in hydrogen bonds or that are hidden within the protein structure. The latter amides are thus "protected" from exchange (Bai *et al.*, 1993, Scholtz and Robertson, 1995, Englander *et al.*, 1996, Raschke and Marqusee, 1998). The magnitude of amide proton resistance to exchange can be evaluated and indicated as a protection factor which correlates with the regions protected by the structure of the fibril. This can be considerably helpful in identifying which residues are involved in the formation of the hydrogen bond; i.e. secondary structure.

Successful conjugation of HX with NMR spectroscopy has been performed. As deuterons are invisible to 1H NMR (i.e. proton NMR) experiment, the decrease in the intensity of amide proton peaks can be detected. Quantitative estimation of the exchange rate can be achieved by monitoring weakened resonances. Labelling of protein with ^{15}N can provide residue-specific information from an assigned 2D transverse relaxation optimised spectroscopy - heteronuclear single quantum coherence - NMR (TROSY HSQC) spectrum (Pervushin *et al.*, 1997), which displays a single peak for each amide proton in the protein.

Basically, HX is accomplished on the intact fibril, then the fibril is dissociated and unfolded to monomers by adding dimethyl sulfoxide (DMSO) to trap the hydrogen exchange state of the amides. This approach formed the basis of investigating amyloid fibrils from the HET-s prion protein (Ritter *et al.*, 2005), β2-microglobulin (Hoshino *et*

al., 2002, Yamaguchi *et al.*, 2004), a 10 residue fragment of Aβ (Ippel *et al.*, 2002), an SH3 domain (Carulla *et al.*, 2005) and cystatin B (Morgan *et al.*, 2008). HX has also been applied to study the dynamic nature of the amyloid fibril, as dissociation and re-association rates of the molecules with the fibril are detected (Carulla *et al.*, 2005, Sanchez *et al.*, 2011).

HX can also be combined with mass spectrometry (MS). Changes in the mass of protein can be detected as deuteration occurs. HX-MS has been employed on Aβ peptide to identify the protected regions within both the precursor states and the amyloid core (Kheterpal *et al.*, 2000, Nettleton *et al.*, 2000, Kheterpal *et al.*, 2003).

1. 4. 5. Limited proteolysis

Similar to HX, limited proteolysis can be used to identify the accessible regions of the amyloid fibril (Hubbard, 1998). The amyloid fibrils are subjected to proteolytic enzymes; then proteolytic products are investigated with MS to find the regions which are protected and therefore construct a model of the fibril structure. Regions that are exposed on the outside of the amyloid fibril are in contact with proteases and accordingly can be quickly hydrolysed, however, regions within the fibril's secondary structure are not accessible to proteolysis and allow the protected fibril core to be determined.

Limited proteolysis has been employed to analyse the structural features of the $A\beta_{1-40}$ fibril. The data collected indicate that the first ten residues from the N-terminal region are not involved in the amyloid fibril core (Kheterpal *et al.*, 2001). SH3 domain analysis showed that intermediates in the fibrillisation pathway are less folded than the native form of the protein (Polverino de Laureto *et al.*, 2003a).

Limited proteolysis has been used to obtain structural information for fibrils in several systems including $A\beta_{1-40}$ peptide (Kheterpal *et al.*, 2001), α-synuclein (Miake *et al.*, 2002), HET-s (Balguerie *et al.*, 2003, de Laureto *et al.*, 2003), Ure2p (Baxa *et al.*, 2003), PI3-SH3 (Polverino de Laureto *et al.*, 2003b) bovine α-lactalbumin (de Laureto *et al.*, 2005), β2-microglobulin (Myers *et al.*, 2006), lysozyme (Frare *et al.*, 2006) and cystatin B (Davis *et al.*, 2015).

1. 4. 6. Solid-state nuclear magnetic resonance spectroscopy

Solid-state NMR (ssNMR) spectroscopy is now accepted as a powerful technique to provide insight into the atomic level of amyloid fibril structure. The insolubility of amyloid fibrils makes it difficult to reveal its structure by solution state NMR (Naito and Kawamura, 2007).

Solid-state NMR (ssNMR) provides high-resolution information which is not obtainable applying other techniques. A range of different ssNMR techniques has been utilised which are basically very similar to those used in the solution. Labelling strategies have been developed to label residues selectively with ^{15}N and ^{13}C and minimize the number of peaks obtained in each spectrum. This labelling allows measurements of distance constraints between specific residues, which provide details on secondary, tertiary and quaternary structures as well as dynamic data. From these measurements, a structural model can be developed.

ssNMR has been used to resolve the structure of the prion-forming domain of the HET-s protein describing a left-handed β-solenoid model, which was the first theorized model of what is thought to be an infectious fibrillar state (Wasmer *et al.*, 2008). Other structures of fibrils include transthyretin (Correia *et al.*, 2006) and β2-microglobulin (Iwata *et al.*,

2006) and of course the different structures proposed for $A\beta_{1-40}$ (Figure 1.4) (Petkova *et al.*, 2002b).

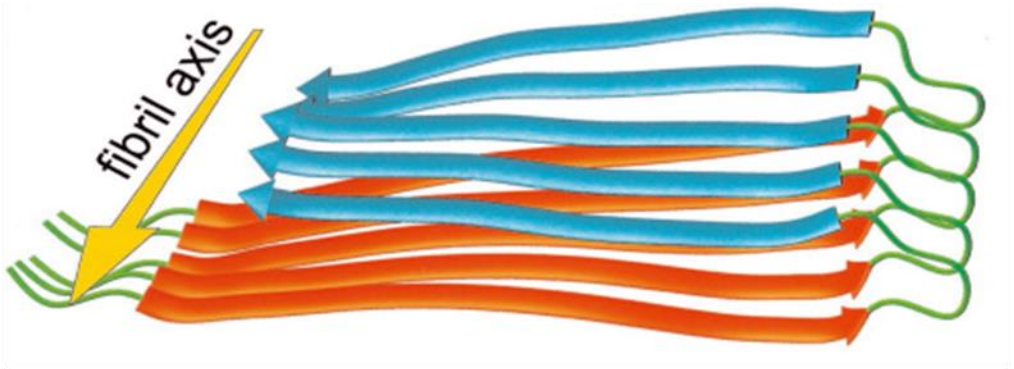

Figure 1.4. Structural model of the $A\beta_{1-40}$ fibril as resolved by SSNMR. Residues 1 – 8 are thought to be fully disordered and are omitted. Adapted from (Petkova *et al.*, 2002b).

1. 5. Amyloid probing

Amyloid identification is performed through displaying characteristic properties at the time of binding to some specific dyes, most notably Congo red and thioflavin T (ThT).

1. 5. 1. Congo red

Congo red staining is one of the most valuable diagnostic methods in clinical practice for the detection and screening of amyloid. Upon staining with Congo red, fibrils display the characteristic pink-orange colour by light microscopy and exhibit a characteristic green birefringence when observed under a cross-polarized light microscope (Elghetany *et al.*, 1989, Sipe and Cohen, 2000, Makin and Serpell, 2005). Depending on its polarization, the light splits into two rays when it passes through a specific type of material. This is birefringence, which will only happen when the structure is anisotropic. When the

amyloid fibril is bound to Congo red, the observed birefringence is evidence of the presence of a sub-microscopic ordered structure (Glenner *et al.*, 1972). It is proposed that these changes originate from the molecular alignment of the dye upon binding to the exposed specific epitope on the fibril. It is believed that binding is specific and associative, either via the extended β-sheet or intercalation (Wolfe *et al.*, 2010).

1. 5. 2. Thioflavin T (ThT)

Specific binding between the benzothiazole dye ThT and amyloid fibrils leads to a dramatic increase in fluorescence intensity of ThT spectra. The ThT excitation maximum is 385 nm and emission is 445nm, when it is unbound. Upon interaction with amyloid fibrils, it exhibits a different excitation maximum of 450 nm and enhanced emission of 482 nm. The resulting shift from ThT binding to amyloid fibrils can be measured over time to monitor amyloid fibrillisation in solution (LeVine, 1993, Sipe and Cohen, 2000, Khurana *et al.*, 2005, Makin and Serpell, 2005).

1. 6. Definitions of amyloid structures

1. 6. 1. Amyloid fibril

Amyloid fibrils are unbranched, long protein fibrils with diameters of 2-20 nm and a length of several micrometres (Kodali and Wetzel, 2007, Fandrich, 2012a). Amyloid fibrils are usually formed of 2-6 protofilaments and can be flat or twisted around each other to form obvious fibril constrictions at fixed intervals, called crossovers. The helicity of fibrils is often left-handed, with few exceptions (Fandrich, 2012b). Despite the fact that amyloid fibril toxicity is not yet confirmed, however, they should be investigated because they are tough with extensive hydrogen bonding, therefore may deposit and remain inside the cells for a prolonged period of time and are suggested to act as toxic oligomer and protofibril reservoirs (Harper *et al.*, 1997, Walsh *et al.*, 1997, Benilova *et al.*, 2012). The amyloid fibril ability to act as a reservoir species is recommended because

of its dynamic nature which exhibits extensive, but slow molecular recycling by which the protein constituents of a fibril dissociate and re-associate over (Carulla *et al.*, 2005, Sanchez *et al.*, 2011). Therefore, studying amyloid fibril structure as one of the therapeutic targets is important by which stabilisation or ablation of fibrils can reduce harmful levels of toxic species.

1. 6. 2. Protofilament

Protofilaments are single strands which together form mature amyloid fibrils.

1. 6. 3. Amyloid intermediates

Amyloid intermediates can be categorized into different groups including protofibrils, annular aggregates, oligomers (Fandrich, 2012a), and Aβ-derived diffusible ligands (ADDLs) (Figure 1.5). It is thought that a large number of different species and subspecies are present which makes classification of diverse intermediates complicated. The study of these intermediates is very difficult because of their transient heterogeneous nature. The investigation of soluble oligomeric species is highly important as they are proposed to be the toxic species (Lansbury, 1999).

1. 6. 3. 1. Protofibrils

Protofibrils can be differentiated from oligomers by their elongated, filamentous structures. They are believed to represent late-stage intermediate species in the formation of amyloid fibrils. They are characteristically thinner (< 10 nm), shorter (< 400 nm in length) and more curved compared to mature fibrils. Protofibrils are not highly ordered and do not exhibit amyloid fibrils periodic symmetry. They usually have a lower affinity for ThT and CR dyes compared to mature fibrils but still encompass high levels of β-sheet structure as shown by CD, FTIR, and x-ray fibre diffraction (Fandrich, 2012a). Stabilisation of Aβ by applying a specific protofibril antibody (B10AP) allowed the

observation of high levels of typical β-sheet structure, which were shown by ssNMR to surround two β-strands expanding from residues 16-22 and 30-36 (Scheidt *et al.*, 2011), this is a smaller number of residues than in mature fibrils but is consistent with the idea of protofibrils representing a precursor to the fibrils.

1. 6. 3. 2. Annular aggregates

Annular aggregates maintain a donut-like appearance confining a central channel, which is assumed to be filled with water (Lashuel *et al.*, 2002). Some amyloidogenic proteins, like Aβ and α-synuclein variants, have been shown to make ring-like aggregates (Lashuel *et al.*, 2002, Caughey and Lansbury, 2003). Exploring the detailed molecular structures of these samples is difficult because of the high levels of heterogeneity, yet because of their similarity to pore forming toxins it has been suggested that these species are able to penetrate the cell membrane and disrupt its integrity and consequently lead to cell death (Caughey and Lansbury, 2003, Butterfield and Lashuel, 2010, Fandrich, 2012a).

1. 6. 3. 3. Oligomers

The term 'oligomer' is derived from the Greek oligos meaning 'a few', thus it is suggested that this terminology is preferable for the description of small assemblies with few units, like dimer and trimers, and employing the term 'non-fibrillar aggregates' (Morgado and Fandrich, 2011) for bigger multimeric species. However, in the amyloid field, oligomer is an umbrella term used to describe any structure larger than monomer which has a non-fibrillar morphology. Low and high molecular weight oligomers are also used in the literature to describe non-fibrillar structures. Soluble oligomeric intermediates form both on and off-pathway to amyloid fibril formation. For example, from the Aβ peptide, these can include dimers, small multimers (3-10mers) all the way up to several mega-Dalton large macromolecular structures (Haass and Selkoe, 2007).

It is accepted that amyloid fibrils possess a characteristic cross-β structure; however a similar common structural conformation has not yet been found for oligomers (Fandrich, 2012a). While different oligomeric species share both β-sheet and random coil conformations, characteristic secondary structures can be remarkably different (Habicht *et al.*, 2007, Campioni *et al.*, 2010, Sandberg *et al.*, 2010). Nonetheless oligomer preparations from different polypeptides found to be recognized by the same oligomer-specific antibodies such as A11 (Kayed *et al.*, 2003) and these oligomers exhibit similar effects in the metabolic assays of cells (Bucciantini *et al.*, 2002), indicating the presence of common structural properties. Oligomers are highly heterogonous, with variability in size and structure happening within the same sample, or from different preparations (Glabe, 2008). Because of their transient, dynamic properties, oligomeric species usually aggregate further and grow to more mature forms (Fandrich, 2012a).

1. 6. 3. 4. Aβ-derived diffusible ligands (ADDLs).

ADDLs are highly ordered soluble oligomers of $A\beta_{1-42}$ peptide. They are formed from multiple units of trimers, tetramers, or 12mers. ADDLs are highly neurotoxic (Lambert *et al.*, 1998).

1. 6. 4. Amorphous aggregate

Accumulation of protein molecules without a defined structural characteristics detectable by electron microscopy, while it is possible that structure could exist at the molecular level.

1. 6. 5. Amyloid fibril seed

Seeds are small amyloid fibril fragments usually developed through sonication of mature fibrils. Kinetically stable protein molecules might be induced to aggregate upon addition of seeds, the aggregation usually occur through growth of the seed itself (Kodali and Wetzel, 2007).

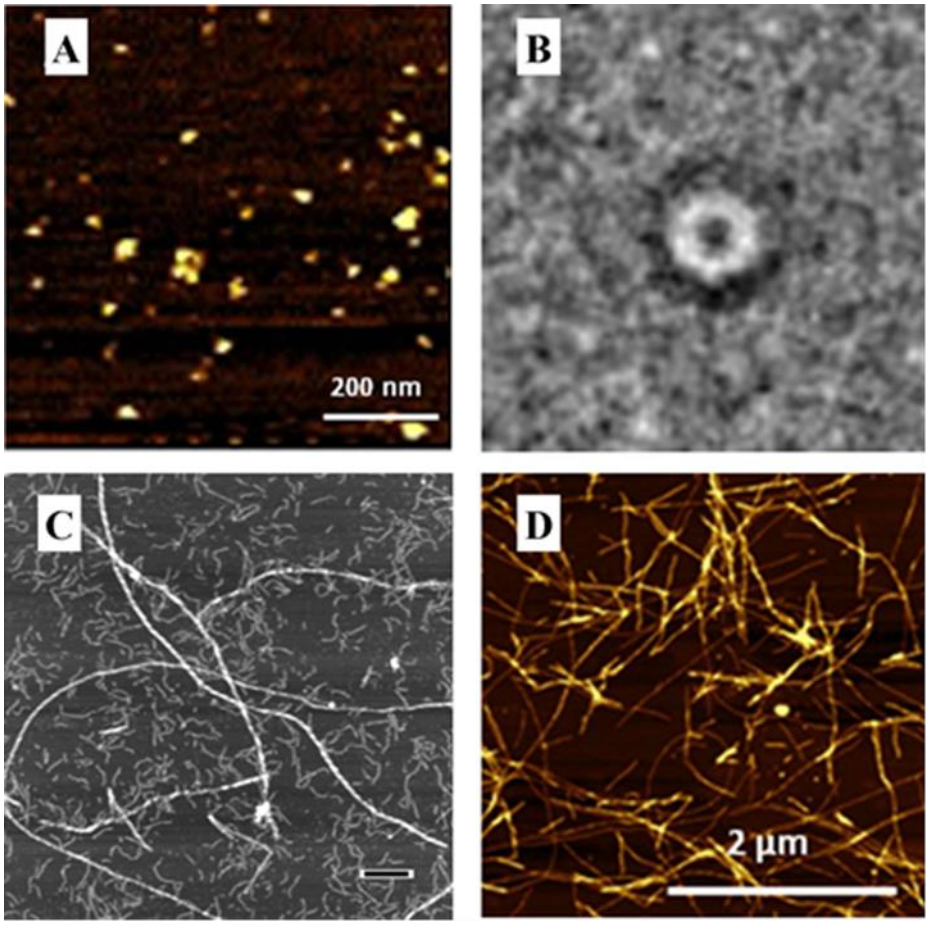

Figure 1. 5. Amyloid Fibrils, Protofibrils and Oligomeric Structures

EM and AFM images of structures formed by amyloid-forming proteins. (A) Globular Aβ oligomers (B) Annular Aβ oligomer (C) Small curly α-synuclein protofibrils and thicker mature fibrils (D) Mature Aβ amyloid fibril. Figure adapted from (Bartolini *et al.*, 2011) (A, D), (Lashuel *et al.*, 2002) (B) and (Koo *et al.*, 1999) (C).

1. 7. Transformation to the amyloid-forming competent state

It has been shown that even non-amyloidogenic proteins can form fibrils under destabilising conditions (Fandrich *et al.*, 2001), this has given rise to the hypothesis that amyloid fibril formation is a potential shared by all proteins and that this is not only restricted to disease-associated amyloid proteins (Guijarro *et al.*, 1998). However,

amyloid peptides and proteins which aggregate promptly, primarily acquire unstructured conformations in their normal biological state (Chiti *et al.*, 2003), and consequently become more liable to form partially unfolded intermediates which is a key triggering event in amyloidogenesis (Kelly, 1998, Calamai *et al.*, 2005, Chiti and Dobson, 2006a). Amyloid protein, if not natively unstructured, becomes partially unfolded before amyloid formation. Similar to fibril formation, partial unfolding is also found in amorphous aggregation. It is believed that amorphous aggregation is driven by interactions between exposed hydrophobic interiors of the protein (Ohnishi and Takano, 2004) but in amyloids, further stabilization happens as a result of more specific interactions between complementary sections of the polypeptide chains. The protein in the fully folded state is therefore not directly transformed into an amyloid fibril. The lack of interactions between side chains or its destabilization, for instance because of changes in the conditions or mutations can cause a rise in unfolded or partially folded protein, and accordingly increases subjection of hydrophobic amino acids and the normally hidden main chain to the solvent (Dobson, 2003). The crucial driving force for the formation of amyloid is the need of partially unfolded protein to bury the exposed hydrophobic residues and find an alternative energetically favourable conformation that is kinetically accessible in specific conditions (Chiti and Dobson, 2006b). The idea of partially unfolded conformations having a major effect in amyloidogenesis comes from the fact that less stable mutant versions of amyloidogenic proteins are more aggregation prone compared with their wild-type counterparts (Hurle *et al.*, 1994, Abrahamson, 1996, Booth *et al.*, 1997, Wei *et al.*, 1998, Kad *et al.*, 2001). Furthermore, native state stabilization by ligand binding decreases fibril formation (Peterson *et al.*, 1998, Chiti *et al.*, 2001, Hammarstrom *et al.*, 2003).

1. 8. Mechanism of fibril formation

Amyloidogenic proteins are different in terms of both amino acid sequence and conformation. However, they all form similar amyloid structures through similar mechanisms (Glabe, 2006). Amyloidogenesis followed by thioflavin T assays and other kinetic methods exhibit three major steps with typical sigmoidal kinetics. The first step is the lag phase, where little fibril is produced, followed by an exponential growth phase, and finally ends up with an equilibrium plateau phase. The protein species populated in the lag phase are not well characterized. The existence of a lag phase on its own indicates the multistep nature of the process. However, when combined with the observation that the lag phase can significantly reduce or be completely removed by the addition of 'seeds', a nucleated growth mechanism can be suggested, where the rate limiting step relies on the presence of a rare possibly stochastically created nucleus (Figure 1.6) (Hortschansky *et al.,* 2005). The infrequency of the nucleus can be explained by its production not being thermodynamically favourable where the resultant intermolecular interactions cannot exceed the association entropy. The simplest description of the exponential phase is that monomer addition is becoming more favourable thermodynamically by intensifying intermolecular interactions and outweighing the entropic barrier (Jarrett and Lansbury Jr., 1993). Other researchers correlated the exponential phase with fibril fragmentation and introduction of new growing fibril ends (Kodali and Wetzel, 2007). Others still suggest adhering of the oligomers to form protofibrils, which are short beaded fibrils, followed by mature fibrils forming either by a conformational change or protofibril association.

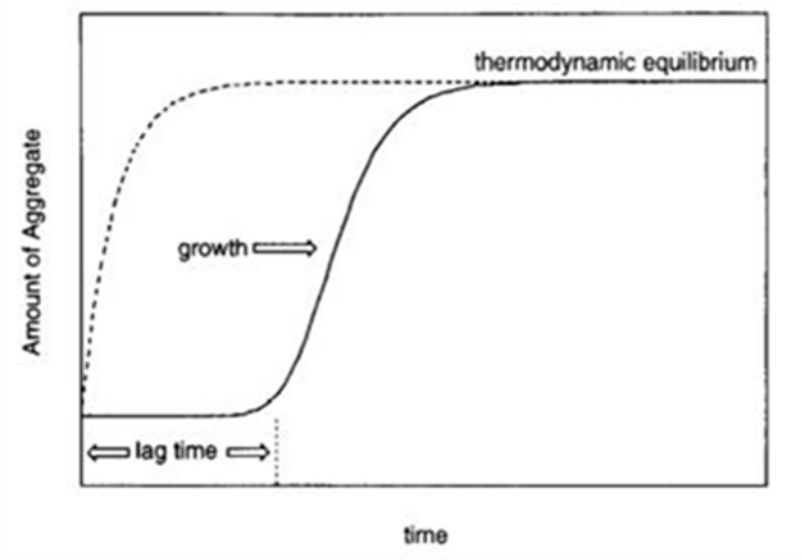

Figure 1.6. Typical Fibrilisation Kinetics. Amyloid fibril (aggregate) formation typically follows a kinetic profile of a nucleation-dependent process which exhibits a lag phase followed by an exponential growth period and subsequent thermodynamic equilibrium (solid line). At a high concentration or very favourable environmental conditions, nucleation is so rapid no lag phase is observed (dashed line). The addition of a nucleus or seed eliminates the nucleation step and therefore also ablates the lag phase. Diagram from (Jarrett and Lansbury Jr., 1993).

1. 9. Kinetic models

There are four conspicuous models of amyloid formation (Figure 1.7), the latest one, nucleated conformational conversion, integrate the elements of the other three (Kelly, 2000, Serio *et al.*, 2000).

The first model is known as **templated assembly,** in which an amyloidogenic (A-state) pre-assemble to form a nucleus, then bind to a soluble non-amyloidogenic (S-state) peptide, causing a rate-limiting structural conversion in the latter followed by peptide addition to the end of growing amyloid fibril (Griffith, 1967). This model implies a direct change in the lag phase with a change in soluble protein concentration, but the fibril elongation rate will stay unaltered. The addition of seed should reduce the lag time.

The second model is **monomer-directed conversion** and predicts that a monomeric peptide will adopt an amyloid-competent conformation (A-state). This species will induce transformation of further monomeric peptides which initiates aggregation and fibrilisation. This model suggests that the addition of seed will not alter the fibrillisation rate or shorten the lag time, as the rate-limiting step occurs with the transformation of the soluble protein (Prusiner, 1982).

The third model is **nucleated polymerisation**. This paradigm assumes that nucleus formation happens through association of soluble amyloid-competent species, then addition of the assembly-competent monomers to the nucleus leads to fibril formation. An equilibrium between both amyloid-competent and amyloid-incompetent protein species occur, with the equilibrium greatly favouring the incompetent species. Thus, the process is rate-limited by the amount of amyloid-competent species associated to create a nucleus. In this model, high levels of soluble protein will increase the rate of fibril assembly and shorten the lag time (Jarrett and Lansbury, 1993). *In vitro* assembly of amyloid fibrils usually have a lag phase before a rapid growth phase. In many circumstances preformed aggregate addition reduces the lag phase which is known as 'seeding' (Dobson, 2003). In addition to amyloid fibril formation, the nucleation model is also common among a number of well-defined processes, such as protein crystallisation, actin polymerisation and microtubule association (Jarrett and Lansbury, 1993).

The fourth model is **nucleated conformational conversion** which suggests that formation of nuclei is enhanced by conformational rearrangements of structurally dynamic oligomers. These oligomers have not a defined quaternary structure, but it is thought that they might have a micelle-like structure. The formed nuclei interact with

other structurally flexible oligomers, then generate a group of subunits which can either add onto the end of the fibril or associate with similar structures. This model explains the often observed low level concentration dependence and suggests that higher molecular weight complexes formed by oligomers at higher protein concentrations are assembly-incompetent. This model can also explain why higher concentrations of seed produce sometimes minimal rate enhancements, because the oligomer concentration is limiting, not fibril ends (Serio *et al.*, 2000).

The discovery of secondary processes which involve the generation of new nuclei suggests that the nucleation process is greatly determined by the aggregates produced during the assembly reaction (Buell *et al.*, 2014). These secondary processes involves fragmentation and secondary nucleation. When a critical concentration is achieved, the fibrillar structures act as a catalytic surface for the formation of new nuclei, and causes a rapid generation of toxic oligomeric species and amyloid fibrils in a secondary nucleation event (Cohen *et al.*, 2013). Amyloid fibril fragmentation increases the number of available elongation sites for soluble protein attachment, bring on further production of fibrils (Xue *et al.*, 2009). Fibril fragmentation can cause a negative concentration dependence, as fragmentation is enhanced by a low concentration, therefore the seed concentration increases (Bernacki and Murphy, 2009, Xue *et al.*, 2009). As the amyloid assembly mechanism is intrinsically complex and heterogeneous, it is hard to find a concrete or general model to describe aggregation. Most models rely on nucleation, and seeding is a characteristic feature of most amyloids. However, as argued by (Bernacki and Murphy, 2009), these models can only clearly be differentiated with a complete set of data, not only on the disappearance of monomer, but also on quantity and size distribution of intermediate aggregates and the amount of fibrillar structure.

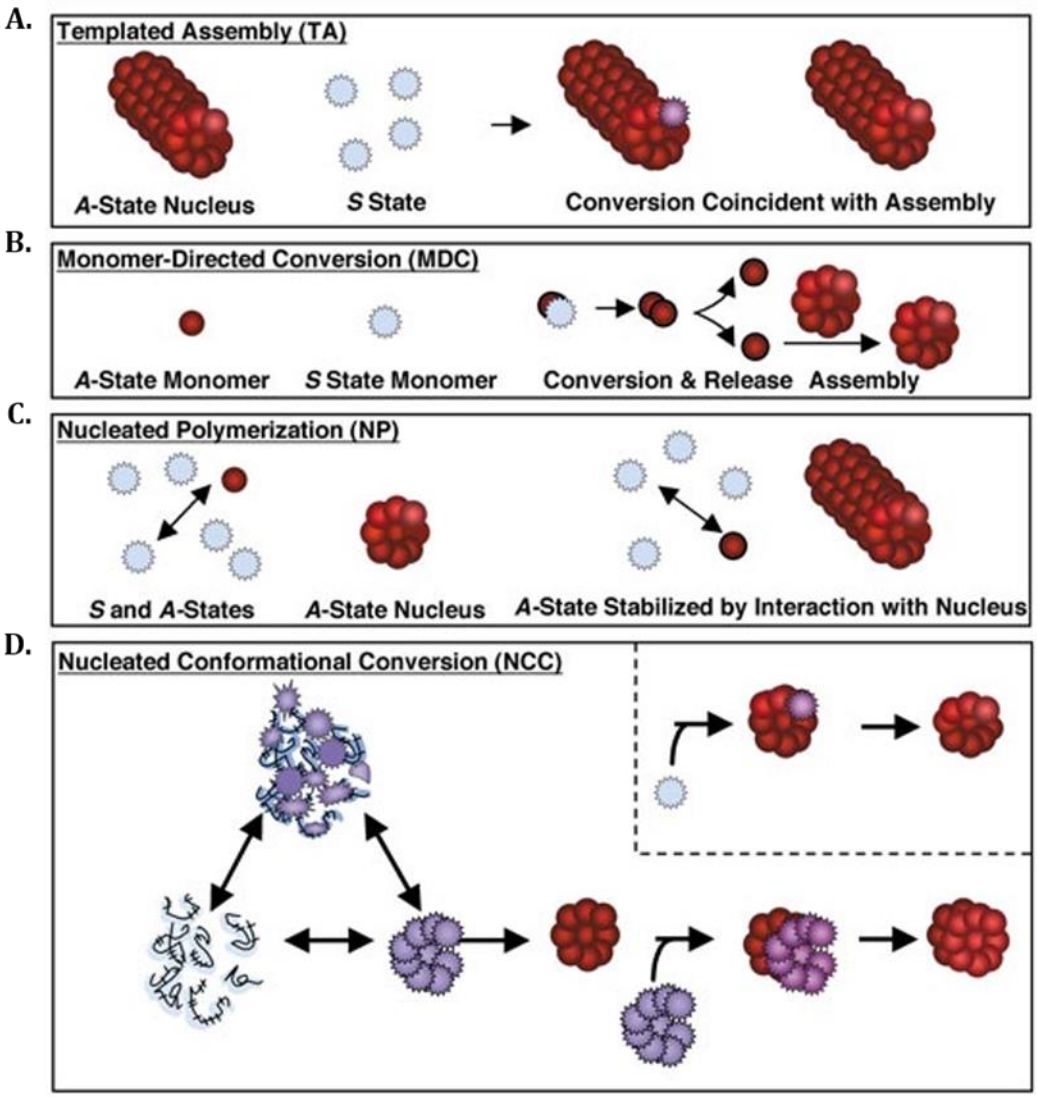

Figure 1.7. Models of Fibril Formation. Proposed models for amyloidogenic peptide conversion into amyloid fibrils. Jagged circles represent soluble (S-state) protein, smooth circles represent amyloid-competent (A-state) protein which takes a similar structure to that adopted in amyloid fibrils and open circles represent potential conformational heterogeneity in A) templated assembly, B) monomer-directed conversion, C) nucleated polymerisation and D) nucleated conformational conversion. Figure taken from (Kelly, 2000).

1.10. Alzheimer's disease and related proteins

1. 10. 1. Transthyretin (TTR)

Transthyretin (formerly known as pre-albumin) is a homotetrameric protein made up of 127 amino acid subunits. The TTR structure is mainly β-sheet, most of the residues except ten N-terminal and five C-terminal residues are involved in the β-strands, with a small helix and small loops connecting them (Figure 1.8A) (Blake *et al.,* 1971). The monomer is composed of two four-stranded β-sheets, an outer sheet and an inner sheet. While the dimer forms by extensive hydrogen bonding between two monomers, the tetramer assembles largely through hydrophobic interactions (Hamilton and Benson, 2001).

TTR is produced in the liver and choroid plexus and its function is to transport thyroid hormone and retinol via the retinol binding protein (RBP) (Hamilton and Benson, 2001). Thyroxin and RBP bind the TTR tetramer non-competitively (Raghu and Sivakumar, 2004): thyroxin binds the tetramer pocket (Richardson, 2007b) while RBP binds residues in the loop between the strands E and F (Monaco, 2000) (Figure 1.8B). The concentration of TTR in plasma is around 3.16 μM with a range of 3-6 μM, however, although it constitutes 25% of cerebrospinal fluid (CSF) total proteins, the TTR concentration is 18 times less in the CSF 0.26 μM with a range of 0.1-0.4 μM (Weisner and Roethig, 1983, Herbert *et al.,* 1986). TTR plays an important role in the body: in serum, TTR normally binds and transports 30% of RBP and 15-20% of thyroxin (Richardson, 2007a), but it transports 80% of thyroxin in the central nervous system (Hamilton and Benson, 2001), and thus serves as a major thyroxin transporter there. Thyroxin is important for the development of the nervous system, and influences mood and cognition (Bauer *et al.*, 2008). TTR gene silencing in mice leads to a behavioural deficit and neuropathological changes in the brain (Buxbaum and Reixach, 2009). Silencing of the RBP gene in mice

leads to cortical and hippocampal neuronal loss, some degree of gliosis and a major reduction in neuroblast proliferation (Buxbaum *et al.*, 2014).

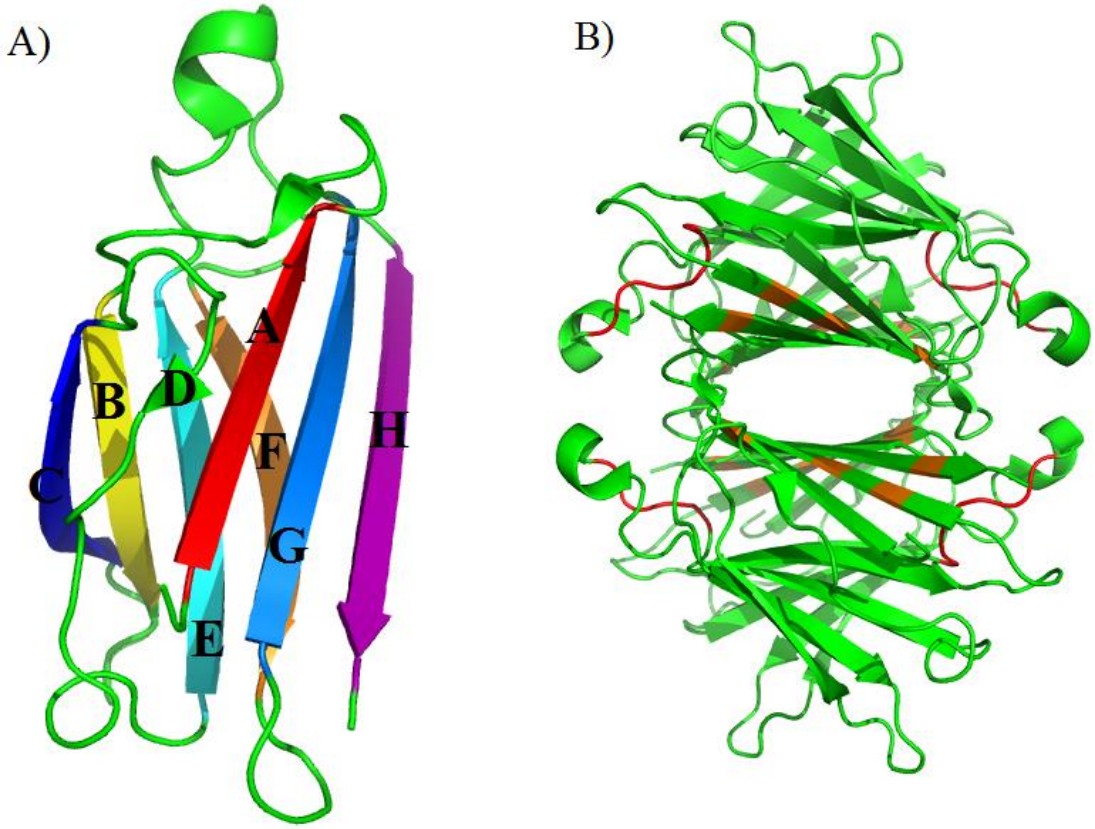

Figure 1.8. X-ray structure of Transthyretin. TTR is a homotetrameric protein. The contacts between the dimers form two hydrophobic pockets where thyroxin binds. A) The monomer structure of TTR with the sheets colour coded and labled, the monomer is composed of two four stranded β-sheets (DAGH and CBEF). B) The residues involved in thyroxin binding are coloured in orange and residues involved in retinol binding protein coloured in red. The structures made using Pymol (DeLano, UK).

1. 10. 1. 1. TTR amyloidosis

TTR is one of the approximately 30 known amyloidogenic proteins. Wild-type TTR is normally stable at neutral pH, but acidic conditions facilitate tetramer dissociation to monomer and consequent formation of fibrils. Several mutants that form fibrils at physiological pH have also been discovered (Lashuel *et al.*, 1998). There are currently 124 TTR naturally occurring mutants listed in the amyloid protein mutations database

(http://www.amyloidosismutations.com/mut-attr.php, last accessed on March 26, 2016). Crystallographic data shows that most of the amyloidogenic TTR variants retain their normal tetrameric structures (Hornberg *et al.*, 2000); and function. Thus, it is the increased tendency of the mutant to dissociate and misfold, not their incapacity to fold and function; that results in disease through a gain-of-toxic function mechanism (Hammarstrom *et al.*, 2001, Sousa *et al.*, 2001, Reixach *et al.*, 2004). Wild-type TTR is the precursor of Senile Systemic Amyloidosis (SSA) (Westermark *et al.*, 1990) whereas mutants are responsible for Familial Amyloid Polyneuropathy (FAP), (Saraiva *et al.*, 1984) and Familial Amyloidotic Cardiomyopathy (FAC) (Jiang *et al.*, 2001). These diseases are characterized by the deposition of aggregated WT TTR or variants in extracellular tissues. The deposition occurs throughout the body (SSA) or in specific organs, like peripheral nervous system (FAP) or heart (FAC). SSA affects, 25% of the population above 80 years of age and this involves amyloid deposition in the heart causing congestive heart failure. With FAC, cardiac involvement is noticeable, whereas in FAP deposition of amyloid in the peripheral nervous system is more prominent (Miller *et al.*, 2004).

1. 10. 1. 2. TTR and Aβ

The first suggestion of a relevant relationship between TTR and Aβ was revealed by (Schwarzman *et al.*, 1994), who showed that TTR, as a major constituent of the CSF, can sequester Aβ. This finding was followed by several animal model studies further supporting this interaction. Co-expression of TTR and Aβ lowered the number of Aβ deposits in muscle and controlled abnormal motility in *Caenorbiditis elegans* (Link, 1995). It has also been shown that levels of TTR expression increased 8 fold in Tg2576 transgenic mice over-expressing the Swedish mutation of APP (APPsw) (Stein and Johnson, 2002), and unilateral anti-TTR antibody infusion in the brains of Tg2576

transgenic mice triggered Aβ related pathology compared to the non-injected hemisphere (Stein *et al.*, 2004). A later study showed that a hemizygous deletion of the TTR gene in *ceAPPswe/PS1_E9* transgenic mice led to the elevation of soluble Aβ levels and acceleration of its deposition in the brain (Choi *et al.*, 2007). Buxbaum *et al.* (2008) observed cognitive and behavioural improvement in progeny from human TTR expressing mice crossed with APPsw mice. Collectively these findings mark TTR's ability to sequester Aβ and protect cells from Aβ's cytotoxic effects.

Cell line experiments also show TTR's protective ability against Aβ cytotoxicity. Physiological levels of TTR protected neuroblastoma cells form Aβ induced apoptotic changes (Giunta *et al.*, 2005). It has been shown that TTR abolishes apoptosis and cell death caused by Aβ toxicity in human neuroblastoma cells (Costa *et al.*, 2008) and murine cortical neuronal cultures (Yang *et al.*, 2013b). Substoichiometric concentrations of TTR significantly restored cell viability and prevented Aβ's apoptotic effects in murine cortical neurons (Liu *et al.*, 2009) and human SH-SY5Y neuroblastoma cells, probably by reducing Aβ's tendency to acquire cytotoxic properties (Li *et al.*, 2011).

Although there is evidence for a direct interaction between WT-TTR and Aβ, contradictory results were achieved regarding which species of TTR and Aβ were interacting when different methodologies were used. In general, methodologies depending on immobilizing one of the proteins like surface plasmon resonance (SPR) and ELISA show that TTR tetramers bind all forms of Aβ (Costa *et al.*, 2008) with preferential binding of TTR tetramers to Aβ aggregates than to Aβ monomers (Du and Murphy, 2010) and fibrils (Yang *et al.*, 2013a). Using the same methodology, Murphy and colleagues showed that TTR monomers bind more strongly to Aβ monomers than TTR tetramers (Du and Murphy, 2010). In contrast, and more accurately, liquid phase NMR experiments

showed that only TTR tetramers bind to Aβ monomers despite the greater inhibitory effect of TTR monomers on Aβ fibrillisation. This suggests that TTR monomers play a different role by binding to a larger Aβ species and preventing its further aggregation (Li *et al.*, 2013a).

It has been suggested that the co-incubation of wild type and variant TTRs with Aβ lead to a triggering of tetramer dissociation which exposes the hydrophobic inner sheet of the TTR monomer and consequently inhibits Aβ aggregation (Yang *et al.*, 2013a). In support of this, it was found that kinetically unstable tetramers are better inhibitors of Aβ aggregation than highly kinetically stable tetramers (Li *et al.*, 2013a). Solution NMR assays suggest that the TTR tetramer pocket which is also the thyroxin binding site is involved in Aβ binding. Indeed, Aβ binding is less effective when this site is occupied by small molecules (Li *et al.*, 2013a). This result is consistent with the binding site identified through peptide array and site-directed mutagenesis assays (Du *et al.*, 2012, Cho *et al.*, 2014) (Figure 1.9). Thioflavin T assays have shown that the TTR monomer is a greater inhibitor of Aβ fibrillogenesis *in vitro*. However, HSQC NMR assays failed to show TTR monomer binding to Aβ monomers. It can be concluded that TTR monomers prevent Aβ aggregation through binding to larger oligomers and suppress any further aggregation of Aβ to make fibrils (Li *et al.*, 2013a).

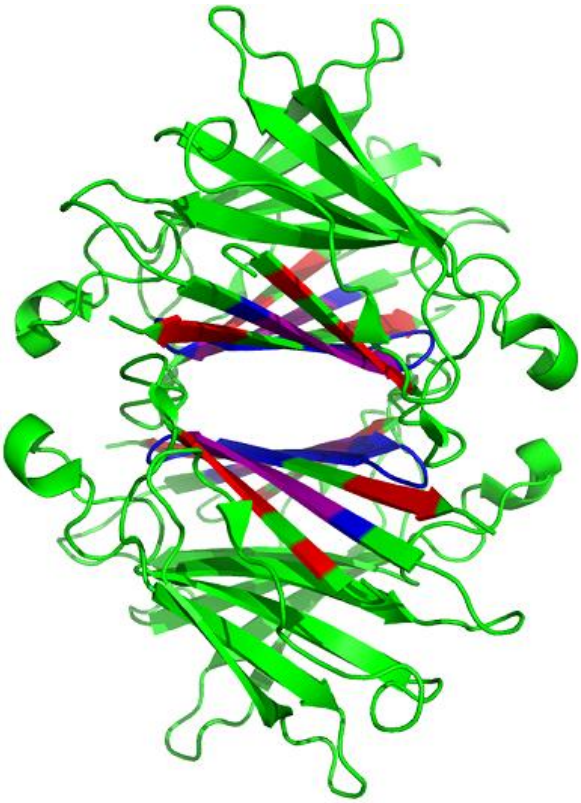

Figure 1.9. The crystal structure of tetrameric TTR with the Aβ binding sites. The residues coloured in red are showed chemical shifts upon $A\beta_{1\text{-}40}$ binding investigated by NMR (Li *et al.*, 2013a), the residues found to bind to Aβ detected by peptide array are coloured in blue (Du *et al.*, 2012), and the residues showed binding in both studies are coloured in purple. The crystal structure by (Klabunde *et al.*, 2000). The structure made by using Pymol (DeLano, UK).

The TTR equilibrium greatly favours tetramer *in vivo* and TTR tetramer is in equilibrium with only a small population of monomer in the body (Buxbaum *et al.*, 2012). The concentration of TTR tetramer is 0.25-0.5μM in human CSF and 3-5μM in human serum, much higher than the monomer. Based on a WT TTR $K_{association}$ of 1.1X $10^{24}M^{-3}$, the TTR monomer concentration (Hurshman Babbes *et al.*, 2008), is predicted to be ~25 nM in CSF and ~46nM in serum, consistent with the detected TTR monomer concentration in human serum (5-10nM) (Sekijima *et al.*, 2001). The Aβ monomer concentration in the human brain is in the high picomolar to low nanomolar range (Cirrito *et al.*, 2003,

Buxbaum *et al.*, 2008, Moore *et al.*, 2012). Thus, the *in vivo* concentration of TTR monomer may be present in excess compared to Aβ, however, the absolute concentration of TTR tetramer is much higher. Based on the above facts, it seems that binding of tetrameric TTR to Aβ monomers and possibly Aβ oligomers is the main mechanism of inhibition of Aβ fibrillogenesis *in vivo*.

1. 10. 2. Human Cystatin C

Cystatin C is also known as γ-trace (Hochwald *et al.*, 1967) and was initially identified in the CSF before being observed in all body fluids and tissues (Bobek and Levine, 1992, Turk *et al.*, 2008). Cystatin C is an inhibitor of papain-like cysteine protease inhibitors which include some of the cathepsins (cathepsin B and D) in humans, which are required for protein degradation during protein turnover (Turk *et al.*, 2000). Different neurological diseases which have been related to uncontrolled proteolysis happen when the balance between active proteases and their inhibitors is disturbed (Nakamura *et al.*, 1991). As well as its main protease inhibition activity, cystatin C has a diverse range of biological functions, including, regulation of the inflammatory response (Warfel *et al.*, 1987, Bobek and Levine, 1992), cell growth and proliferation (Sun, 1989, Tavera *et al.*, 1992), and astrocytic differentiation during mouse brain development (Kumada *et al.*, 2004). Cystatin C expression is also enhanced in patients with epilepsy (Tizon *et al.*, 2010c). Cystatin C is a brain-specific protein as the bulk of cystatin present in CSF is produced by the choroid plexus (Tu *et al.*, 1992) and, unlike other protein constituents, its normal CSF concentration is five times higher than in serum, indicating a possible important role in the brain (Grubb, 1992).

1. 10. 2. 1. Cystatin C amyloidosis

Cystatin C was recognised as an amyloidogenic protein causing a dominantly inherited disorder known as hereditary cystatin C amyloid angiopathy (HCCAA) (Cohen *et al.*,

1983). This disease is systemic since immuno-histochemical assays have detected amyloid deposits of cystatin C in diverse tissues including the brain, spleen, salivary glands, and the skin (Abrahamson and Grubb, 1994). As cystatin C is found in all body fluids, so its systemic deposition is expected. However, the highest plaque burden is found in brain arteries and arterioles, causing vessel wall thickening and causing brain haemorrhage (Palsdottir *et al.*, 2006). This disease is normally found in 20 to 40 year old Icelandic individuals.

The cystatin C variant (L68Q) causes the hereditary cystatin C amyloid angiopathy (HCCAA) disease (Ghiso *et al.*, 1986a). Although the mutation does not directly participate in amyloid-formation interactions, it destabilises the monomer and makes it more susceptible to dimerisation. L68Q hCC is similarly effective in inhibiting cathepsin B with similar equilibrium constants for dissociation (Kd) as WT hCC, suggesting that the mutant is able to fold into the right conformation; the dissimilarities are in their propensity to dimerise and form aggregates (Abrahamson and Grubb, 1994). Both hCC dimers and monomers are found in the blood plasma of patients with the disease when only monomeric species are detected in healthy individuals (Palsdottir *et al.*, 2006). The existence of inactive dimers in CSF caused a decrease in the total cysteine protease inhibition capacity, this could cause cerebral haemorrhages in HCCAA (Olafsson *et al.*, 1990). Despite the L68Q mutation, the variant detected in HCCAA amyloid deposits also has an N-terminal truncation of 10 amino acids when compared to normal hCC (Grubb and Lofberg, 1985, Ghiso *et al.*, 1986b). It is suggested that leucocyte elastase is responsible for this truncation (Abrahamson *et al.*, 1991).

1. 10. 2. 2. Cystatin C and Aβ

The link between hCC and AD was initially proposed because of their co-localisation in amyloid plaques. Human immunohistochemical investigations demonstrated that hCC is mainly detected in amyloid deposits encircling blood vessels and less frequently in parenchymal deposits (Deng *et al.*, 2001, Sastre *et al.*, 2004b). Co-localisation of hCC and β-APP have been detected inside both mouse neuroblastoma N2a cells and human embryonic kidney HEK293 cells. Cell culture assays show intracellular localisation of hCC and β-APP in both mouse neuroblastoma N2a cells and human embryonic kidney HEK293 cells. Co-localisation of hCC with Aβ has also been detected in the brains of transgenic mice over-expressing human APP (Tizon *et al.*, 2010a). Cystatin C co-localization with Aβ is not only limited to AD, it is found in the core of amyloid senile plaques in brains of patients with Down's syndrome, HCHWA-D (hereditary cerebral haemorrhage with amyloidosis – Dutch type), intracranial haemorrhage, cerebral infarction, and of elderly individuals without any neurological disorder (Maruyama *et al.*, 1990, Vinters *et al.*, 1990b, Itoh *et al.*, 1993, Haan *et al.*, 1994, Levy *et al.*, 2001). Studies were performed to reveal whether hCC co-exists with Aβ as amyloid fibrils or soluble hCC trapped or adsorbed in Aβ fibril bundles. An ELISA based study found hCC included in crude Aβ fibrils in a ratio of 1:100 in amyloid plaques isolated from cerebral blood vessels (Nagai *et al.*, 1998). Cystatin C was found to be soluble in fibrillar Aβ samples isolated in leptomeningeal vessels in another case of sporadic CAA (cerebral amyloid angiopathy) (Maruyama *et al.*, 1992). One interpretation is that hCC deposition is driven by Aβ deposition (Itoh *et al.*, 1993), and leads to an increased local concentration of hCC and this leads to cerebral haemorrhage (Kaur and Levy, 2012). Despite that, the main deposited amyloidogenic protein in HCCAA is hCC. However, Aβ co-deposition has not

been confirmed using different anti-Aβ antibodies (Vinters *et al.*, 1990a, Haan and Roos, 1992).

hCC levels are found to be increased in susceptible parts of the human brain (Deng *et al.*, 2001) and in animal models, indicating a physiological response to the disease pathology, by which hCC expression is increased (Steinhoff *et al.*, 2001). Transgenic mice studies demonstrated that overexpressing hCC to twice the normal levels inhibits Aβ deposition in transgenic mice expressing the Swedish mutant APP (Kaeser *et al.*, 2007b, Mi *et al.*, 2007a).

1. 10. 2. 3. Genetic studies

Genetic studies reveal an association between AD and hCC at the genetic level. The Cystatin C gene, CST3, is located on chromosome 20 (Abrahamson *et al.*, 1989, Saitoh *et al.*, 1989), studies show a link between CST3 polymorphism and an increased risk of AD (Crawford *et al.*, 2000, Bertram *et al.*, 2007). A reduction in hCC levels has been observed as a result of a mutation in which threonine substitutes for alanine at position -2. This leads to a reduced signal peptide cleavage and impaired secretion (Tizon *et al.*, 2010a) such polymorphism increases the risk of AD for homozygous individuals (Selenica *et al.*, 2007a). Late onset AD is also related to other polymorphisms including the CST3 +73 G/A mutation (Crawford *et al.*, 2000) or the CST3 –157 G/C polymorphism (Finckh *et al.*, 2000). However, some studies have failed to prove the link between CST3 polymorphism and AD in a German cohort (Dodel *et al.*, 2002), a Dutch sample with early onset AD (Roks *et al.*, 2001), Japanese AD patients (Maruyama *et al.*, 2001), a Finnish population (Helisalmi *et al.*, 2009) and in early onset AD families (Parfitt *et al.*, 1993). Other researchers have found a connection between AD and the *CST3* polymorphism AD in Caucasian populations, but not in Asian populations (Hua *et al.*,

2012), including Chinese (Wang *et al.*, 2008). Many of these findings are difficult to reproduce, probably due to the diversity of different risk factors associated with AD which lead to considerable difficulties in selecting controls (Bertram and Tanzi, 2008). However, these genetic studies with accumulated evidences on physiological roles of hCC in animal and cell line models of AD and evidences on biochemical interactions of hCC with Aβ in test tube models strengthen the suggested protective role for hCC in AD.

1. 10. 2. 4. Mechanisms of neuroprotection

Cystatin C can protect neuronal cells through different mechanisms meaning there could be direct and indirect roles of hCC in Alzheimer's disease. The indirect mechanisms include cysteine protease inhibition, inducing autophagy and enhancing neurogenesis, while a direct mechanism exists through interaction with Aβ and inhibition of its aggregation.

1. Inhibition of cysteine proteases: The balance between cathepsins and hCC as an inhibitor is important for neuronal health. The inhibitory effect of cystatin C against cathepsin B was investigated by knocking out the cystatin C gene in mice. This resulted in an increased cathepsin B activity (Sun *et al.*, 2008). In a separate study, it was shown that cathepsin B and D activity decreased, and neuropathological symptoms were rescued by over-expressing cystatin C in cystatin B knocked out mice (Kaur *et al.*, 2010).

2. Induction of autophagy: Using different methodologies, it was revealed that hCC enhances autophagy in cells under basal conditions, and induces autophagic activation in cells subjected to oxidative stress and nutritional deprivation (Tizon *et al.*, 2010c). Autophagy is lysosomal degradation of cytoplasmic components. It is essential for normal cell growth and survival. It is important for destruction and removal of undesirable

contents such as misfolded protein, aberrant protein aggregates, dysfunctional organelles and invading pathogens (Lamark and Johansen, 2012).

3. Protection by neurogenesis: Cystatin C can also adjust proliferation of cells (Sun, 1989, Tavera *et al.*, 1992). Levels of both cystatin C mRNA and protein are elevated in the dentate gyrus and hippocampus in rats experiencing status epilepticus-induced epileptogenesis and acute hippocampal injury (Aronica *et al.*, 2001, Lukasiuk *et al.*, 2002). The increase in hCC expression and prominent neurogenesis was observed to occur at the same time (Parent *et al.*, 1997, Nairismagi *et al.*, 2004). Additionally, in hCC knockout mice, the basal level of neurogenesis in the dentate gyrus was reduced and newborn granule cell proliferation and migration in the dentate gyrus were impaired (Pirttila and Pitkanen, 2006), supporting an hCC role in neurogenesis. Thus, induction of neurogenesis might be another mechanism of neuroprotection enhanced by hCC.

4. Protection by inhibition of Aβ oligomerization and amyloid fibril formation: -

ELISA was used as one of the first techniques to investigate the hCC interaction with Aβ (Sastre *et al.*, 2004a). This revealed high-affinity binding between two proteins at physiological pH and temperature, with a dissociation constant (K_d) in the nanomolar range. Only 5nM of a monoclonal antibody 6E10 was needed to block hCC binding to Aβ. This antibody specifically binds to residues 1-17 (the N-terminal region of the peptide), proposing that hCC also bind in this region. A concentration dependence of the binding of hCC to Aβ was first investigated by this study.

Further investigation by Sastre *et al.* (2004a) using electron microscopy showed inhibition of Aβ fibril formation by hCC *in vivo* in a concentration-dependent manner. Direct and sub-stoichiometric binding between hCC and Aβ was suggested which led to reduced Aβ fibril formation. Selenica *et al.* (2007b) suggest that the *in vitro* formation of

protofibrils and oligomers of Aβ, including toxic ADDLs can be prevented by hCC. This finding could have important implications because Aβ oligomers are potentially causative in AD. The hCC binding to Aβ was detected using size-exclusion chromatography (SEC) and immunoprecipitation, with a one to one equimolar complex observed by the authors. The concerned species was not resolved by the chromatography used which makes the results somewhat ambiguous. Despite this, the authors suggested that hCC and Aβ react rapidly to form high-affinity one to one molar complexes, involving the N-terminal region of Aβ in the binding (Selenica *et al.*, 2007a). When the mixture was incubated for longer, the initial complexes had less tendency than the monomeric Aβ to produce higher species such as ADDLs, protofibrils or even fibrils. Rather larger, amorphous aggregates are assembled without the structural characteristics of the preceding species and precipitate from solution.

1. 10. 3. Neuroserpin

Neuroserpin is a member of the serine protease inhibitor (serpin) superfamily (Osterwalder *et al.*, 1996) and its main function is the inhibition of tissue plasminogen activator (tPA) (Miranda and Lomas, 2006). Low levels of tPA are produced within the CNS and are believed to contribute to the development of synaptic plasticity and learning and memory (Yepes and Lawrence, 2004). Neuroserpin was initially found in neurons of the central and peripheral nervous system, and then in other organs like kidney, testis, pancreas and heart (Hastings *et al.*, 1997).

1. 10. 3. 1. Neuroserpin amyloidosis

Four different neuroserpin variants (Ser49Pro, Ser52Arg, His338Arg and Gly392Glu) have been found in humans (Davis *et al.*, 1999, Davis *et al.*, 2002). Neuroserpin mutants polymerise spontaneously and form inclusion bodies in neurons causing an inclusion

body dementia which is called “familial encephalopathy with neuroserpin inclusion bodies” (FENIB).

1. 10. 3. 2. Neuroserpin and Aβ

Recently, neuroserpin has been reported as another protein associated with extracellular Aβ plaques in the brains of AD patients. Neuroserpin has been found at the periphery and within the Aβ plaques (Kinghorn *et al.*, 2006a). Neuroserpin specifically interacts with Aβ to form a 1:1 binary complex, in which Aβ fills the β-Sheet A of neuroserpin. The dissociation constant for the neuroserpin- Aβ complex is 10± 5nM (Chiou *et al.*, 2009). Pre-incubation of neuroserpin with Aβ irreversibly inactivated its inhibitory action against serine protease (tPA). Formation of homopolymers at elevated temperatures through loop sheet polymerisation is a distinctive character of the serine superfamily (Figure 1.10). The N-terminal and middle part fragments but not the C-terminal of Aβ also inhibit neuroserpin loop sheet polymerisation, suggesting that the N-terminal and middle parts of Aβ are involved in the interaction. Neuroserpin reduces Aβ cytotoxicity in both cell culture and in an *in vivo* drosophila model, supporting a neuroprotective role for neuroserpin in AD. A fibrillisation assay where fibril formation is detected using Thioflavin T fluorescence showed an apparent acceleration of Aβ aggregation by neuroserpin, however electron microscopic inspection showed that different species of aggregate were formed (short amorphous aggregates) and so it is suggested these are off-pathway non-toxic aggregates (Figure 1.11) (Kinghorn *et al.*, 2006b).

Other studies have found an indirect role for neuroserpin regarding the accumulation of Aβ in the brain. It has been found that its substrate tPA plays a role in Aβ clearance through activation of inactive plasminogen to plasmin which consequently degrades both Aβ monomers and fibrils (Selkoe, 2001, Melchor *et al.*, 2003, Medina *et al.*, 2005). The

activity of plasmin (Ledesma *et al.*, 2000) and tPA are both remarkably diminished, while neuroserpin levels significantly increased in the brain of AD compared to age-matched control brains (Fabbro and Seeds, 2009). High levels of neuroserpin can inhibit tPA activity through the tPA-neuroserpin complex formation in the AD brain tissue (Fabbro and Seeds, 2009), and consequently, inhibit Aβ clearance. Furthermore, AD mice model studies showed that knocking out the neuroserpin gene results in decreased levels of brain Aβ (Fabbro *et al.*, 2011) which also confirm a negative role of neuroserpin in Alzheimer's disease.

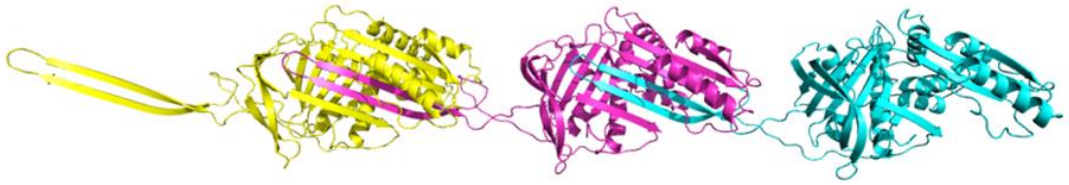

Figure 1.10. Model of a domain-swapped serpin polymer. Both sheet 5A and the reactive centre loop (RCL) insert into the A-sheet of another serpin monomer (Yamasaki *et al.*, 2008).

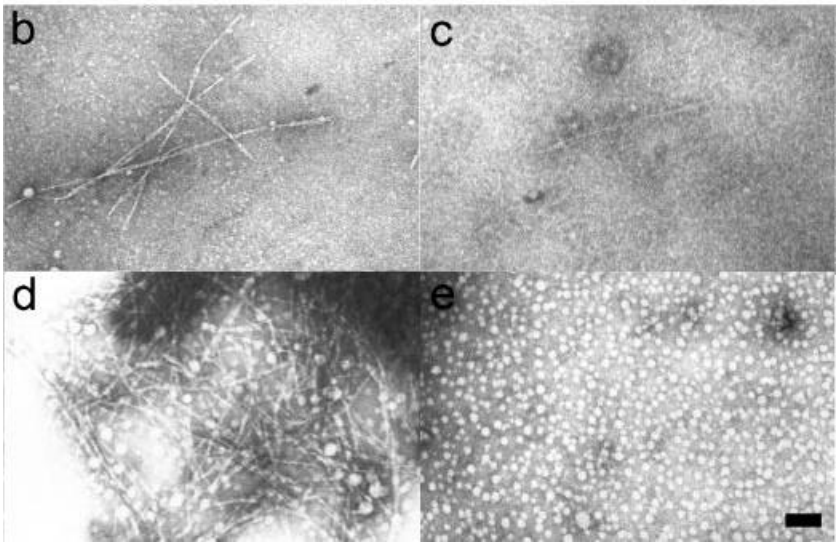

Figure 1. 11. TEM of neuroserpin / $A\beta_{1-42}$ mixtures. Monomeric $A\beta_{1–42}$ was incubated at 1 mg/ml for 1 h at pH 7.4 and 37 °C in the absence (*b* and *d*) or presence of 12 μM neuroserpin

(*c* and *e*). Samples were diluted 1:1 with buffer and placed directly onto the electron microscopy grid (*b* and *c*) or centrifuged at 10,000 x *g* for 10 min, and the pellet placed on the grid (*d* and *e*). The morphology of the resulting protein species was examined by transmission electron microscopy. $A\beta_{1–42}$ incubated in the absence of neuroserpin formed amyloid fibrils (*b* and *d*), whereas co-incubation $A\beta_{1–42}$ and neuroserpin abolished fibril formation and promoted the formation of smaller species (*c* and *e*). *Scale bar*, 100 nm (Kinghorn *et al.*, 2006b).

1. 10. 4. Albumin

Serum albumin reduction with age is one of the known AD risk factors. Human serum albumin (HSA) has been found bound to 89-95% of Aβ in blood plasma (Biere *et al.*, 1996, Kuo *et al.*, 2000b) with a Kd of 5-10 µM and with a 1:1 stoichiometry (Kuo *et al.*, 2000a). HSA concentration in blood serum is 640 µM (Carter and Ho, 1994) which is the highest among all serum proteins. However, its concentration is much lower in CSF at only 3 µM, which is comparable to levels of TTR and cystatin C (Stevens *et al.*, 1979). It is suggested that the decreased HSA level in the CSF results in a diminished availability for Aβ binding, and this could explain the presence of extracellular Aβ plaques only in the brain, instead of peripheral tissues (Stanyon and Viles, 2012a).

It is still a subject of controversy as to whether HSA binds Aβ monomer or oligomers. Some researchers have demonstrated that HSA binds monomers of Aβ (Kuo *et al.*, 2000a, Rozga *et al.*, 2007). Stanyon and Viles (2012a) suggested that HSA interacts with Aβ monomers and small oligomers of less than five monomers. Another study employing biotin labelling and immobilized Aβ polymers showed that HSA inhibits soluble Aβ monomer in addition to immobilized Aβ seeds, indicating inhibition of Aβ aggregation (Bohrmann *et al.*, 1999). However, results obtained through a series of STD NMR experiments on Aβ and HSA binding showed that HSA binds to Aβ oligomers but not monomers and fibrils (Milojevic *et al.*, 2007, Milojevic *et al.*, 2009, Milojevic *et al.*,

2014). It is well known that HSA binds to many hydrophobic molecules, especially pharmaceuticals and endogenous fatty acids (Carter and Ho, 1994). The hydrophobic pockets of HSA have been described through the investigation of the crystal structure of HSA bound to fatty acids (Curry *et al.*, 1998), hemin (Zunszain *et al.*, 2003) and bilirubin (Vander Jagt and Garcia, 1987), which might be the pocket where the hydrophobic C-terminal part of Aβ binds. It has also been proposed that hydrophobic molecules such as cholesterol (Peng *et al.*, 2008) and pharmaceuticals compete with Aβ to bind to HSA (Bohrmann *et al.*, 1999). Recent studies have found that HSA binds to Aβ oligomers through multiple binding sites, distributed evenly across the three albumin domains (Milojevic and Melacini, 2011).

Since HSA is not observed within amyloid plaques in brains of AD patients, it is believed that it does not interact or become incorporated into the plaques. However, Thioflavin T experiments showed that a micromolar human CSF concentration of HSA significantly elongates the lag phase and the bulk of produced fibril by both $A\beta_{1-40}$ and $A\beta_{1-42}$ variants *in vitro* (Stanyon and Viles, 2012b). Given the fact that a large proportion of serum Aβ is bound to HSA, it is hypothesized that the replacement of plasma albumin could lower Aβ levels in the CSF and brain because Aβ peptides are able to cross the blood brain barrier (Mackic *et al.*, 1998). Promising results have been obtained in phase II (Boada *et al.*, 2009) and phase III clinical trials through plasma albumin exchange schedule (http://grifols.com/en/web/uk/view-news/-/new/grifols-achieves-ten-years-of-research-into-alzheimers, last accessed on 17/February /16).

1. 10. 5. Prion (PrPC)

Prion is a ubiquitously expressed cell surface glycoprotein with its highest concentration in the brain. The cellular prion protein has recently been recognized as a cell surface receptor for Aβ oligomers (Zhou and Liu, 2013). Lauren *et al.* (2009) found that prion is able to intervene in Aβ oligomer toxicity. They showed that Aβ oligomers bound to prion with high affinity and specificity. They also found that nanomolar concentrations of Aβ oligomers are capable of halting LTP in cultured hippocampal slices, however, this affect is not observed in slices without PrPC receptors or when receptors are occupied with an antibody. This suggests that LTP is specifically suppressed by Aβ oligomers binding to PrPC. Lauren *et al.* (2009), then attempted to test whether, *in vivo*, PrPC is crucial to the ability of Aβ to arrest cognitive function. They crossed transgenic mice encoding β-APP gene with mice encoding the PrPC gene or not. They, found that mice containing Aβ plaques but lacking PrPC demonstrated no detectable impairment of spatial learning and memory, while the AD transgene mice with PrPC developed considerable deficits in spatial learning and memory, suggesting that PrPC is specifically needed for the toxicity of naturally occurring Aβ in the brain. Deletion analysis, antibody binding (Lauren *et al.*, 2009) and surface plasmon resonance (Chen *et al.*, 2010) experiments identified two specific binding sites of Aβ oligomers on PrPC. One is at the N-terminal and the other is close to middle part of the protein and both are rich in positively charged basic residues. Deletion of either part significantly reduced the binding affinity for Aβ oligomers, suggesting that both parts act together to render high-affinity binding to oligomers (Chen *et al.*, 2010, Biasini *et al.*, 2012).

The PrPC role in mediating Aβ oligomer toxicity was questioned by other researchers' findings. Roberto Malinos' group demonstrated that PrPC is not needed for Aβ-induced synaptic toxicity. The Aβ mediated synaptic plasticity was noticed in both wild-type and

prnp-1- mouse slices (Kessels *et al.*, 2010). Forloni and his team found that PrP expressing and PrPC knock-out mice were equally susceptible to cognitive impairment when they injected with Aβ oligomers into the lateral ventricle, proposing that PrPC is not necessary for Aβ oligomer-mediated cognitive impairment (Balducci *et al.*, 2010), yet they have verified nanomolar affinity binding between Aβ oligomers with PrPC. Other researchers found conflicting results on the role of PrPC in Aβ mediated toxicity. Overexpression or ablation of *PRNP* in AD model transgenic mice was shown not to prevent impairment of synaptic plasticity of neurones in the hippocampus (Calella *et al.*, 2010), nor improve abnormal neurone activity or improve cognitive dysfunction (Cisse *et al.*, 2011). These results indicate that Aβ toxicity is not dependent on PrPC. The wide variation in results may be due to the use of different preparations and concentrations of Aβ, and the use of different mouse models and cell lines (Freir *et al.*, 2011). Perhaps the Aβ oligomers used are capable of causing PrPC -independent damage but are not found *in vivo,* and hence were not isolated in the AD brain extracts used by (Freir *et al.*, 2011). Alternatively, perhaps Aβ requires PrPC for only some of the pathological effects observed in AD patients, for example, prevention of LTP.

Despite the controversial results found by different researchers on the role of PrPC as a mediator of Aβ oligomer toxicity, there are no conflicts on two end points: high-affinity binding between PrPC and Aβ oligomers and Aβ oligomer-mediated synaptic toxicity. The challenge remaining to researchers is to make the two ends meet.

1. 11. Sugars and Polysaccharides

1. 11. 1. Simple sugars

Sugar molecules interact with peptides and proteins using their hydrophobic surface to form contacts with hydrophobic pockets of proteins, as well as hydrogen-bonds. It has

been proposed that this characteristic is crucial to binding amyloidogenic proteins (Fung *et al.*, 2005). Less mobile sugar molecules are likely to form more stable and stronger H-bonds with amyloid proteins and consequently stabilise the soluble forms of protein and prevent fibrillogenesis.

In contrast, some carbohydrates enhance fibrillogenesis by induction of nucleation (Kim *et al.*, 2001) or mature fibril formation (Yang *et al.*, 1999). Indeed, it has been shown that glucose enhances nucleation and seeding of the amyloid Aβ peptide fibrillogenesis, while galactose and maltose enhance amyloid fibril formation (Fung *et al.*, 2005). In contrast, other disaccharides have been shown to prevent protein unfolding and inhibit amyloid fibril formation. These disaccharides include sucrose, maltitol, turanose, cellobiose and trehalose (Tanaka *et al.*, 2005). The most effective of these disaccharides is trehalose, it is a simple disaccharide composed of two glucose molecules binding together through α,α-1,1 linkage (Liu *et al.*, 2005). It has been shown that trehalose is effective against protein denaturation by heat shock and might be able to prevent denatured protein from aggregation (Singer and Lindquist, 1998). Insulin aggregation can be delayed or inhibited by Trehalose (Arora *et al.*, 2004). Oral administration of trehalose reduced brain atrophy by decreasing polyglutamine aggregates and increasing the lifespan of a transgenic mouse model of Huntington's disease (Tanaka *et al.*, 2004). Trehalose efficiently reduced Aβ aggregation and toxicity in human neuroblastoma cell lines (Liu *et al.*, 2005).

Other simple saccharides such as sucrose increase Aβ protein stability and consequently its fibrillogenesis (Fung *et al.*, 2005). This shows that carbohydrates with similar molecular weights have different effects on amyloid fibril formation according to their pattern of potential H-bonding.

1. 11. 2. Glucose metabolism

The most energy-demanding organ in the body is the brain and glucose is the main energy source used by the brain to generate the ATP it requires to function (Hoyer, 1998). Anumber of *in vivo* studies have therefore focused on the relationship between glucose metabolism and AD. The endothelial cells lining cerebral blood vessels are responsible for transporting glucose across the blood-brain barrier (BBB), yet constitutes less than 1% of brain cells. They are high in GLUT1, a specific protein transporter that aids glucose to pass the BBB and enters the brain (Harik *et al.*, 1990).

A substantial decrease of glucose metabolism in affected areas of the brain is one of the evident features of Alzheimer's disease. Applying positron emission tomography (PET) with 2-[F-18]-fluoro-2-deoxy-D-glucose as a label shows a gradual decrease in brain glucose metabolism and flow in association with the dementia severity. Interestingly, regional brain glucose hypometabolism was shown not only in patients but also in younger family members with familial AD in a preclinical phase before the onset of disease (Perani, 1999), indicating a causal involvement in the disease process. Subsequently, the depletions in the endothelial GLUT1 transporter were shown in the brains of AD patients, suggesting that reduced utilization of glucose was a result of the deficiency in glucose transport across the BBB (Harik *et al.*, 1990, Mooradian *et al.*, 1997). However, the effect of the endothelial GLUT1 transporter reductions on brain performance and disease progress remained unresolved for over twenty years. Winkler *et al* (2015) started to answer this question employing GLUT1 gene deficit mice (*Slc2a1*+/– mice). They showed that *Slc2a1* haploinsufficiency in the brain gives rise to a decline in vascular length, blood flow and glucose uptake with age, and to an increase in BBB permeability. With ageing, *Slc2a1*-deficent mice also display evidence of cortex and hippocampus neurodegeneration. These findings revealed an unpredicted impact of

deficiency in endothelial GLUT1 on the brain and its vessels that leads to brain dysfunction and neurodegeneration.

Therefore (Winkler *et al.*, 2015), investigated the effect of the brain GLUT1 deficiency on AD pathology by crossing *Slc2a1*-haploinsufficient mice with mice overexpressing the amyloid precursor protein containing the Swedish mutation (*APPSw* mice). They found that the endothelial GLUT1 reduction noticed in AD could potentially work synergistically with AD pathology to intensify its detrimental effects on the brain and stimulate the development of dementia.

One explanation of the reduced brain glucose metabolism is that the hypometabolism is the outcome of diminished neuronal activity and accordingly, a depletion in energy expenditure. However, an alternative explanation would be that the reduction in GLUT1 could decrease glucose uptake and restrain the brain's energy supply, which, could impair neuronal activity and, eventually, bring on neurodegeneration (de la Monte and Tong, 2014).

GLUT1 has been investigated as a potential target for the development of new therapeutic interventions aimed at restoring GLUT1 levels for the relief of brain dysfunction and damage in AD. To begin to address this possibility, Winkler *et al.* (2015) conducted adenoviral gene transfer in *APPSw* mice deficient in *Slc2a1*. They discovered that GLUT1 restoration in the hippocampus notably decreased local Aβ levels. This may open new therapeutic approaches for this devastating neurodegenerative disease.

1. 11. 3. Polysaccharides

Extensive investigation into amyloid diseased tissues has confirmed the presence of a large amount of polysaccharide along with amyloid proteins in the deposits. The

deposited polysaccharides are mainly glycosaminoglycans (GAGs). Heparan sulphate (HS) is among the most commonly deposited GAGs, being observed in a number of amyloid diseases including Alzheimer's disease, type II diabetes, light chain amyloidosis, and prion-related diseases (Snow *et al.*, 1990, Young *et al.*, 1992).

Recent studies propose that GAGs can enhance misfolding through favouring the formation of β-sheet rich intermediates by polypeptides, and accordingly increases the number of nucleation seeds. Furthermore, GAGs can act as a template for amyloid assembly. GAGs can also interfere with amyloid formation in its late stages by promoting lateral association of small fibrils affording insolubility and avoiding proteolysis (McLaurin *et al.*, 1999, Ancsin, 2003).

In vitro studies further disclosed the link between GAGs and amyloid formation. Heparan sulphate has been shown to trigger fibril formation by the Aβ peptide *in vitro* (Castillo *et al.*, 1997, Castillo *et al.*, 1999, McLaurin *et al.*, 1999). The interaction of GAGs with both Aβ peptides ($A\beta_{1-40}$ and $A\beta_{1-42}$) were investigated to reveal their effect on peptide conformation and fibril formation. In the presence of heparin, the transition of the Aβ peptide from random-coil to amyloidogenic β-sheet is accelerated, with $A\beta_{1-42}$ quickly adopting a β-sheet conformation. This stimulation is followed by amyloid fibril formation, indicating that $A\beta_{1-42}$ nucleation is enhanced. These results obviously suggest that GAGs affect amyloid fibril formation at the very early stages. The crucial part of GAGs, which enhance Aβ fibril formation is the sulphates, its complete removal causing a full disappearance of the enhancing effect (Castillo *et al.*, 1999, Valle-Delgado *et al.*, 2010).

It has been suggested that surface HS mediates the internalization and toxicity effects of Aβ (Sandwall *et al.*, 2010). These authors showed that HS-deficient cells were unable to

internalise Aβ and were substantially resistant to Aβ toxicity. Over-expression of heparanase in cells also debilitated $A\beta_{1-40}$ toxicity. Furthermore, heparin addition to cells blocked $A\beta_{1-40}$ internalisation and inhibited Aβ toxicity.

Low-molecular-weight heparins (LMWHs) can prevent the formation of β-plated structure and inhibit fibril formation (Bergamaschini *et al.*, 2009, Ariga *et al.*, 2010). Scholefield *et al.* (2003) showed that heparin can also inhibit the activity of β-secretase activity in neurons, *i.e.*, the β-site APP-cleaving enzyme 1 (BACE-1), whose activity is essential for the production of the amyloidogenic Aβ peptide (Walsh *et al.*, 1997). The ability of heparin to interfere with both Aβ production and fibril formation, suggesting a possible role of heparin in a therapeutic approach (Bergamaschini *et al.*, 2009, Ariga *et al.*, 2010).

1. 12. Lipids

Post-mortem brain tissue investigations showed biochemical alterations of lipid composition as a first clue to a link between Alzheimer's and lipid metabolism. Subsequently, a closer link was built when the e4 allele of the Apo lipoprotein E (APOE) gene was confirmed as a genetic risk factor for AD (Corder *et al.*, 1993, Bertram and Tanzi, 2008). APOE encodes a ~34-kDa protein that acts as an important cholesterol metabolism regulator in the brain. It mediates the lipoprotein particle uptake in the brain through the very low-density family lipoprotein receptor and low-density lipoprotein (LDL) receptor-related protein (LRP) (Bu, 2009, Kim *et al.*, 2009). Data on the binding, clearance and modulation of Aβ aggregation by the e4 allele of APOE, support its role in the pathology of Alzheimer's disease. Moreover, the role of cholesterol in the pathophysiology of Alzheimer's is also supported by several epidemiological studies (Bu, 2009, Kim *et al.*, 2009).

Its now well-known that most of the lipids that modulate Alzheimer's pathology do so through different mechanisms which can be summarized as follows: firstly, they control the movement and activity of membrane-bound enzymes like APP, BACE1 and the presenilins. Secondly, Aβ exerts its effect on cell membranes by direct and indirect mechanisms which is responsible for the manifestation of Alzheimer's pathology. Thirdly, lipids can affect Aβ's propensity to aggregate and modulate its pathogenic potential.

1. 12. 1. Role of cholesterol metabolism and transport in amyloidogenesis.

The most cholesterol-containing organ in the body is the brain, which contains as much as 25% of the whole cholesterol present in the body. Cholesterol is a fundamental factor of cell membranes and plays a critical role in neuronal function and plasticity (Pfrieger, 2003). Nearly all of the brain cholesterol is acquired from *de novo* biosynthesis, rather than plasma, since the blood–brain barrier blocks any significant traffic between brain and plasma lipoproteins (Dietschy and Turley, 2001, Vance *et al.*, 2005). Exceptions include the cholesterol oxidisation products, 27-hydroxycholesterol and 24 Shydroxycholesterol (Papassotiropoulos *et al.*, 2000) which can cross the blood–brain barrier. The daily exchange rate of cholesterol between the brain and periphery is less than 1%. Accordingly, it has to be supposed that the brain cholesterol homeostasis is mainly, but not entirely independent of the cholesterol level in the blood (Dietschy and Turley, 2001).

Longitudinal, population-based studies reveal that cholesterol levels correlate with developing AD in later lifetime and hypercholesterolemia is an early risk factor for the development of amyloid pathology (Kivipelto *et al.*, 2001). Animal model studies using rabbits fed a cholesterol-enriched diet exhibited a progressively mild-to-moderate-to-

severe intracellular accumulation of immunolabeled Aβ (Sparks *et al.*, 2005). Furthermore, cerebral amyloid concentrations become elevated in APP transgenic mice fed on a cholesterol-enriched diet (Refolo *et al.*, 2001, Shie *et al.*, 2002).

Studies in which *de novo* synthesis of cholesterol is repressed by pharmacological drugs further justifies the vital role of cholesterol in APP processing. Cholesterol synthesis inhibitors were capable of diminishing extracellular and intracellular concentrations of $A\beta_{1-42}$ and $A\beta_{1-40}$ peptides in mixed cortical neurons and primary cultures of hippocampal neurons. *In vivo*, cerebrospinal and brain homogenate levels of $A\beta_{1-42}$ and $A\beta_{1-40}$ peptides were reduced in guinea pigs treated with high doses of simvastatin, an inhibitor of *de novo* cholesterol synthesis (Fassbender *et al.*, 2001). Similar results were obtained when cholesterol was depleted from the membrane by physical extraction with cyclodextrin (Fassbender *et al.*, 2001).

Cells convert excess free cholesterol to cholesteryl esters using the enzyme acyl CoA: cholesterol acyltransferase 1 (ACAT1) (Chang *et al.*, 2010). Aβ release in cultured cells is enhanced by increasing levels of cholesteryl esters, while inhibition of ACAT1 by drugs caused a reduction in both cholesteryl ester and Aβ levels (Puglielli and Kovacs, 2001, Hutter-Paier *et al.*, 2004). In a mouse model of AD, both Aβ pathology and cognitive impairment were reduced by genetic ablation of ACAT1 (Bryleva *et al.*, 2010). However, ablation of ACAT also raises the concentration of oxysterol, 24(S)-hydroxycholesterol which complicates interpretation and proposes a possible role of this cholesterol metabolite in decreasing amyloidogenesis (Bhattacharyya and Kovacs, 2010, Bryleva *et al.*, 2010). One presumed mechanism compatible with these results is that the excessive free brain cholesterol evolving from ACAT1 ablation can be changed to 24(S)-hydroxycholesterol and then travel across the blood–brain barrier to reach the periphery,

thus causing lowered brain cholesterol levels. Conclusively, these findings suggest that the equilibrium between free cholesterol and cholesterol esters is an essential parameter controlling amyloidogenesis. However, the molecular mechanism underlying this relationship is unclear (Bhattacharyya and Kovacs, 2010).

1. 12. 2. Role of sphingolipids in Aβ production.

Besides cholesterol, sphingolipids including ceramide, sphingomyelin and glycosphingolipids (GSLs) play some critical roles in cell function associated with normal as well as diseased states (Hannun and Obeid, 2008, Posse de Chaves and Sipione, 2010). Ceramide is a major component in sphingolipid metabolism and it is used as a backbone for developing GSLs and sphingomyelin via the addition of sugars or phosphocholine at the hydroxyl group, respectively. GSLs and Sphingomyelin are plentiful in the brain, and gangliosides, which are GSLs containing sialic acids, are the main constituents of neuronal membranes.

Initial reports reveal that ceramide concentrations are increased at the earliest clinically recognizable stage of AD, conceivably mediating neuronal death by oxidative stress induction. However, independently of its contribution in oxidative cell death (He *et al.*, 2010), ceramide also modulates BACE1-mediated processing of APP. The mechanism appears to be associated with the enhancement of BACE1 stability in cells, probably by the generation of ceramide-enriched platforms (Puglielli *et al.*, 2003)

Sphingolipids also directly participate in the metabolism of APP. Inhibition of the enzyme (sphingomyelinase) that favours the sphingomyelin conversion to ceramide, and the resulting sphingomyelin accumulation, decreases Aβ secretion which leads to γ-secretase inhibition. Sphingomyelinase activity enhancement is also observed in cells harbouring FAD mutations in PS1, further suggesting an important role for sphingolipids in AD

(Grimm *et al.*, 2005). However, complete suppression of sphingolipid biosynthesis causes an increase in $A\beta_{1-42}$ production, while the level of $A\beta_{1-42}$ remains unaffected. Consequent sphingosine addition restores the normal ratio of $A\beta_{1-40}$ to $A\beta_{1-42}$, suggesting that sphingolipids can act as a modulator of γ-secretase (Sawamura *et al.*, 2004).

Finally, the Aβ V3 loop domain has been identified as a sphingolipid-binding sequence (Fantini *et al.*, 2002), and suggests an Aβ affinity to raft-like sphingolipid and cholesterol-rich regions of cellular membranes, with important implications for Aβ aggregation, internalization and intracellular sorting, all of which can affect its pathogenic capability (Zhang *et al.*, 2009).

Altogether, these studies demonstrate that sphingolipids modulate γ-secretase and BACE1 activities as well as Aβ microdomain localization, even though additional research is required to decide the mechanistic details and to verify these lipid-dependent models *in vivo* (Di Paolo and Kim, 2011).

1. 12. 3. Other lipid changes in AD brains

During AD pathogenesis, along with the mentioned modifications, some other lipid changes occur. Brain autopsy samples from AD patients showed a selective and significant reduction in ethanolamine plasmalogens (PLs) concentrations relative to phosphatidyl ethanolamine. These changes happen neither in Parkinson's nor in Huntington's disease (Ginsberg *et al.*, 1995, Wells *et al.*, 1995, Guan *et al.*, 1999).

At a very early stage in AD, a substantial decrease up to 40 mol% in PL content in white matter and 10 mol% in grey matter was observed already. Once dementia is at a severe stage, up to 30 mol% in grey matter was also noted. However, the importance of PL reduction in AD is not well understood. It can be associated with synapse loss and

neurodegeneration since the decrease in PL might cause instability of the membrane (Ginsberg *et al.*, 1998). This reduction might be explained by the elevated oxidative damage in the AD brain caused by Aβ accumulation (Albers and Beal, 2000, Bassett and Montine, 2003), where Aβ itself has been identified as an oxidant species (Davis, 1996, Markesbery and Carney, 1999). Indeed, a significant decrease has been noticed in ethanolamine PL content of cultured embryonic rat brain oligodendrocytes treated with Aβ (Cheng *et al.*, 2003). In addition, reactive oxygen species (ROS) can affect PLs through their vinyl-ether bond that makes them susceptible to oxidation. Oxidative stress in AD creates ROS and accordingly ROS-mediated degradation may deplete PL (Han, 2005).

1. 13. Membrane surfaces

Investigations into membrane-stimulated fibrillogenesis have been motivated by various important medical and physiological questions, such as the cytotoxic effect of amyloid aggregates exerted at the cell membranes rather than in the bulk (Williams *et al.*, 2011). Recent findings have revealed the role of surfaces in favouring or disfavouringdisfavoring the aggregation process and in increasing the rate of formation of nuclei (Sani *et al.*, 2011, Burke *et al.*, 2013). The conformational state of the protein and its aggregates may be determined by different physicochemical properties of surfaces (Rocha *et al.*, 2012).

Fresh Aβ interactions with lipid vesicles of different compositions have revealed that the membrane hydrophobicity and surface charge can modulate Aβ binding to the surface of the membranes. Various studies have shown that anionic phospholipids which form most of the membrane constituent are responsible for the enhancement of fibril formation. It was noted that $A\beta_{1\text{-}40}$ is preferably bound to negatively-charged lipids of complex membranes and negatively-charged phosphatidylglycerol membranes compared to

neutrally charged membranes (Williams and Serpell, 2011). The degree of $A\beta_{1-40}$ fibrillisation increases upon association with anionic lipids (PA, PS, PI, PIP, PIP2, and CL), in contrast with to the neutral (cholesterol, cerebrosides, and diacylglycerol) and zwitterionic lipids (PC, PE, and SM), and phosphate group lacking anionic lipids (Knight and Miranker, 2004).

The phospholipids head-group charges have been proposed to contribute to the Aβ association to the membrane through electrostatic interactions. The affinity of $A\beta_{1-40}$ to 1-palmitoyl- 2-oleoyl-sn-glycero-3-phospho-rac-(1-glycerol) (POPG) is stronger than for 1-palmitoyl-2-oleoyl-sn-glycero-3-phosphocholine (POPC) (Kremer and Murphy, 2003), confirming the idea that the head-groups moderate binding. Furthermore, a 50–100% greater mass adsorption was detected between $A\beta_{1-40}$ and POPG compared with $A\beta_{1-40}$ mass adsorption to POPC membranes. It seems that, whilst POPC binding does not lead to aggregation of the Aβ peptide, POPG liposomes considerably boost aggregation (Williams and Serpell, 2011).

Several studies support that *in vitro* formation of amyloid fibrils is not only induced by anionic phospholipid containing membranes, but is also enhanced by bilayers composed of phospholipid (PC and PE) mixed with cholesterol or gangliosides, and the commonly named ‘raft’ containing cholesterol and sphingomyelin. Therefore, it does not appear possible to accredit the ability to enhance protein fibrillisation to specific lipid classes. Yet, it is believed that the chemical properties of the bilayer constituents have a capacity to determine the extent and mode of these proteins binding to the membranes, in favouring the aggregation-prone conformation of the protein. However, the molecular details of interactions between protein and lipids which lead to the transformation of protein into

aggregated structures may differ remarkably, according to the structural characteristics of the investigated peptides or proteins.

It was shown that adsorption of $A\beta_{1-42}$ oligomers to hydrophilic surfaces was not followed by further aggregation, while adsorption on hydrophobic surfaces was enhanced conformational changes and aggregation (Saraiva *et al.*, 2010). AFM imaging and single molecule fluorescence tracking were also applied to investigate the mechanism of $A\beta_{1-42}$ fibril formation following oligomer formation and adsorption on substrates covered with polymers of different hydrophobicity. Results confirmed that only weakly adsorbed peptides with enough mobility enhance peptides to interact and start fibrillisation at several orders of magnitude lower concentration of Aβ peptide than in bulk (Shen *et al.*, 2012). In summary, consistent with other works on lipid membranes, it was demonstrated that surface favoured fibrillisation, was crucially dependent on the physical properties of the polymer covered surfaces.

One day fibrillised $A\beta_{1-40}$ adsorption displayed small variations in the kinetics of membrane binding compared to fresh Aβ. The fibrillar Aβ affinity to neutrally charged membranes is higher than its affinity for negatively-charged membranes. Hydrophobic forces were argued to be more influential regarding fibrillar Aβ adsorption on membranes, although the electrostatic forces were noticed to be more important regarding fresh Aβ binding to membranes (Lin *et al.*, 2007). Generally, protein recruitment can be favored via interaction of surface charges with the amino acid residues of opposite charge, accordingly increasing protein concentration at the interface (Giacomelli and Norde, 2005).

Amyloid fibril formation is a multistep process which can be modulated by a number of different factors, specifically by lipid-protein interactions. Fibril formation in a membrane

environment can be enhanced through some principal factors including first: enhancing structural transformation in proteins to form partially folded conformation. Second: local concentration of protein increases up on binding to the membranes. Third: orientation of the bound protein into aggregation favouring direction. Fourth: influencing the membrane bound protein nucleation propensity.

Aβ-membrane interactions and permeation

The amyloid oligomers amphipathic nature has been proposed to contribute to the membranes insertion and penetration capacity, adsorbing to the membrane surfaces, or possibly act as cell-penetrating peptides (Lansbury and Lashuel, 2006). Three different models have been suggested for Aβ membrane induced toxicity. The first model is carpeting of the peptide on one side of the membrane surface, which cause small molecules to leakage through creating an asymmetric pressure between the two sides (Hebda and Miranker, 2009). The carpet model was suggested to explain the inexistence of the lag phase and exponential rather than sigmoidal leakage kinetics in hIAPP and mouse IAPP-induced LUV permeation (Engel *et al.*, 2008).

The second proposed model for amyloid-mediated toxicity is stable pores and ion channels formation. Ca2+ channels formation in lipid bilayers was suggested in AD cytotoxicity as the $A\beta_{1\text{-}40}$ adsorption into planar phosphatidylserine bilayers created channels that produced linear current–voltage relationships in symmetrical solutions (Arispe *et al.*, 1993). Direct observation of channels by AFM showed an 8–12 nm doughnut-shaped structure with a 1–2 nm internal pore diameter that extends 1 nm above the surface of the bilayer (Lin *et al.*, 2001).

The third model suggested is based on the detergent-like effect of amyloidogenic peptides on lipid membranes. The peptide electrostatically interacts with phospholipid head group

or membrane surface receptors, which accompanied by peptide alignment to the hydrophilic surface of the phospholipid head groups. The hydrophobic residues of the peptide orients towards the hydrophobic core of the membrane, and consequently the membrane disintegrate by bilayer curvature disruption (Shai, 1999). The detergent effect arises from the surfactant- like properties of the amphiphilic peptide, which causes a decrease in membrane surface tension. This reduction led to the removal of lipid and membrane thining when it happens on one side or formation of holes in the membrane bilayer when both sides are affected (Hebda and Miranker, 2009).

The amyloid forming peptides associated cytotoxicity might not entirely linked to only one mechanism but more possibly to a collection of mechanisms. Each mechanism may be involved at a specific stage amyloid formation. The carpeting and detergent models may only happen while the peptide is in its monomeric or small oligomeric phase and causes nonspecific membrane permeation; the formation of ion channels or amyloid-induced pores might happen through specific receptors of amyloid- induced permeation (Williams and Serpell, 2011).

1.14. Aims of this study

The initial aim of this study was to investigate the interactions between both Transthyretin (TTR) and human Cystatin C (hCC) with Aβ peptide. The studies on the interaction of TTR and Aβ showed contradictory results on the binding and inhibition intensity of TTR against Aβ using different methodologies. Studies in which one of the proteins immobilized showed strong binding of TTR to nearly all forms of Aβ, however the solution based studies showed a weak binding between the two proteins. In chapter 3, conditions were optimized for fibrillisation of Aβ in the presence of two different (binding and non-binding) surfaces. The intensity of WT TTR for inhibition of $A\beta_{1-42}$ fibrillisation

were investigated and compared in the presence of these two different surfaces. In chapter 4, in order to study the details of TTR interaction with Aβ, four different TTR mutants with different stabilities of their tetramers and monomers were developed and their inhibitory effect compared to WT TTR. The interaction of WT and mutant TTRs with different structures of Aβ were also investigated. $A\beta_{1-40}$ is less aggregation prone, however, it is more abundant *in vivo*. The ability of WT TTR and some mutants to inhibit $A\beta_{1-40}$ fibrillisation is also considered.

Previous study found monomer to monomer interaction between hCC and Aβ, however previous works in our group showed that this is not the case. Instead they suggested that hCC binds to oligomeric Aβ and inhibition of fibrillisation occurs as binding disfavours the fibrillisation pathway. In chapter 5, we confirm the dose dependence inhibition of Aβ fibrillisation by hCC and investigate the monomer-monomer interaction between the two proteins in different buffer conditions to the previous study. The hCC binding to aggregated Aβ structures were further supported by hCC binding to Aβ fibrils and monitoring the disappearance of both Aβ and hCC monomers in the mixture using 1D NMR experiments. In order to find the binding interface to Aβ on hCC some hydrophobic residues throughout the hCC structure were mutated to alanine and their inhibitory effect on Aβ compared to WT hCC. An *E. coli* contaminant protein was co-purified along with hCC purification and it was interfering with the hCCs inhibitory effect on Aβ fibrillisation. In chapter 6, the *E. coli* contaminant protein was sequenced by mass spectrometry and identified as glutamate/aspartate binding protein. Then, its inhibitory effect on Aβ aggregation were investigated using thioflavin T assays and electron microscopy.

Chapter two: Materials and Methods

This chapter covers the details of common experimental procedures used throughout the research work presented. Further details of materials and methods of specific experiments are found in relevant chapter.

2.1. Buffers and Reagents

All chemicals and reagents were purchased from, Sigma-Aldrich, Fisher Scientific or Melford, unless stated otherwise. Deionised water (18.2Ω) which was used throughout all experiments was from Elga Purelab 611 Classic UVF. Buffers were prepared according to the protocol described in (Sambrook *et al.*, 1989) and filtered through a 0.2 μm filter. Final concentration of 1 or 2 mM sodium azide (NaN_3) was added as standard to all buffers, except those used for bacterial growth and unless otherwise stated.

2.2. Growth Media and Solutions

2.2.1. Luria-Bertani Media

Taken from (Sambrook *et al.*, 1989). For each litre of deionised water, the following was added:

bacto-tryptone (Oxoid ltd, UK)	10 g
yeast extract (Oxoid)	5 g
NaCl (Melford)	10 g

The pH of media was adjusted to 7.0 and made up to 1L prior sterilisation by autoclaving, then antibiotics added after the media had cooled. If LB-agar was required, 28 g Nutrient agar (Oxoid Ltd, UK) was made up to 1L and autoclaved.

2.2.2. Minimal media

Per litre of deionized water:

Na_2HPO4	6 g
KH_2PO4	3 g
NaCl	0.5 g

The volume made up to 1L after adjusting pH to 7.4 and sterilized by autoclaving.

The following were added to the media directly before use (per litre):

trace elements	650 µl	(autoclaved)
glucose	3g	(filter sterilized)
10 mg/ml thiamine	0.1 ml	(filter sterilized)
0.5 mg/ml $(NH_4)_2SO_4$	2 ml	(filter sterilized)
1 M $MgSO_4$	1 ml	(autoclaved)
1 M $CaCl_2$	0.1 ml	(autoclaved and added last)

The flask was swirled immediately to disperse precipitate; if precipitate did not disperse then the preparation was discarded.

Trace elements

Per 100 ml deionised water:

$CaCl_2.2H_2O$	550 mg
$CuSO_4.5H_2O$	40 mg
$CoCl_2.6H_2O$	45 mg

H_3BO_4	40 mg
KI	26 mg
$MnSO_4.H_2O$	140 mg
$Na_2MoO_4.2H_2O$	26 mg
$ZnSO_4.H_2O$	220 mg

The above components were added to 70 ml of deionised water and the pH adjusted to 8.0 before adding:

EDTA	500 mg

The pH was again adjusted to 8.0 before adding:

$FeSO_4.7H_2O$	375 mg

The solution was made up to 100 ml with deionised water before autoclaving.

2.2.3. 2X TY media

Per litre of deionised water the following was added:

Bacto-tryptone (Oxoid ltd, UK)	16 g
Yeast extract (Oxoid, UK)	10 g
NaCl	5 g

The pH was adjusted to 7.2 and the volume made up to 1 litre. Media was transferred into conical flasks and sterilised by autoclaving. Antibiotics were added after the media had cooled.

2.2.4. Antibiotic Stock Solutions

Ampicillin (Melford, UK): stock solution (1000x) was produced by dissolving ampicillin sodium salt in water at a concentration of 100 mg/ml and then filter-sterilised with a 0.2 μm syringe filters. Aliquots were stored at -20°C until needed, when they were gently thawed and added to growth media to a final concentration of 100 μg /ml.

2.2.5. Isopropyl-β-D-galactosidase (IPTG)

IPTG (Melford): stock solution (1 M) was prepared by dissolving 120 mg/ml in water, and 0.2μm filter-sterilised. Fresh solution (or aliquots stored at -20°C and thawed on ice) was added to growth media to a final concentration of 1, 1.5 or 2 mM to induce protein overexpression.

2.3. DNA Manipulation

2.3.1. Bacterial strains and expression system

Transthyretin and variants; wild type TTR previously cloned into the pMMHa expression system, was provided by Gareth Morgan (Scripps Research Institute, California, USA). Expression was carried out in *Escherichia coli* BL21/DE3 strain. Site-directed mutagenesis was carried out on the wild type plasmid to produce the variants. Thre pMMHa plasmid contains ampicillin resistance (β-lactamase) gene.

Human cystatin c and variants; wild type hCC previously cloned into the pIN-III-ompA periplasmic expression system was provided by Dr. Adham Elshawaidhe. Expression was carried out in *E. coli* BL21/DE3 strain for which an efficient purification had been established (Elshawaihde, 2012). The rare codons found in genes for human proteins had been removed previously to allow expression in this strain. Site-directed mutagenesis was carried out on the wild type plasmid to produce the variants.

2.3.2. Competent cells

Escherichia coli cells of the XL10 blue (Novagen) strain were used for plasmid minipreps and BL21/DE3 strain were used for protein purifications. Competent cells were made using the following protocol.

The desired strain of *E. coli* cells from glycerol stock were plated onto LB agar and grown overnight at 37°C. Five ml of LB media inoculated by a single colony, which was grown overnight at 37°C, 200 rpm. 10 ml of LB was inoculated with 200 µl of starter culture, and grown at 37°C, 200 rpm until its OD600 reached 0.6. The cells were spun down by centrifugation, the supernatant was discarded, the cells resuspended in 3.3 ml RF1 buffer (30 mM KCH_3CO_2, 100 mM RbCl, 10 mM $CaCl_2$, 50 mM $MnCl_4$, 15% glycerol, pH 5.8) and incubated on ice for 30 minutes. The cells were pelleted again, the supernatant was discarded and the cells were resuspended in 1 ml RF2 buffer (10 mM MOPS, 10 mM RbCl, 75 mM $CaCl_2$, 15% glycerol, pH 6.5). After incubating on ice for a further 30 minutes, the cells were divided into 100 or 200 µl aliquots and either transformed immediately or stored at -80°C until needed.

2.3.3. Preparation of plasmid DNA

Plasmid DNA was extracted and purified from overnight grown cell cultures using QIAprep Spin Miniprep kits (Qiagen), according to the manufacturer's instructions. Plasmid was eluted with MilliQ water or Tris-Cl, pH 8.5 and stored at -20°C.

2.3.4. Transformation

200 µl competent cells thawed on ice and transferred to 15 ml falcon tube then 1.5 µl of plasmid DNA was added and incubated for 30 minutes on ice. Cells were heat-shocked for 90 s at 42°C in a water bath and incubated on ice for a further 2 minutes. 800 µl of LB

media was added and the cells were incubated at 37°C, 200 rpm for 90 minutes. 2, 20 and 200 µl of cells were plated onto selective LB agar (generally containing 100 µg/ml ampicillin) and grown overnight at 37°C.

2.3.5. Quantification of DNA Concentration

UV-Vis Spectrophotometer; The concentrations of plasmids and oligonucleotide primer solutions were estimated using the optical density at 260 nm, where an absorbance reading of 1 is equivalent to a nucleotide concentration of 33 µg/ml. Protein contamination of plasmid preparations were calculated using $A_{260\ nm}/A_{280\ nm}$ ratio. DNA samples considered free of contamination, if this value was greater than 2. Absorbance readings were taken with a Varian Cary 50-Bio UV-Vis spectrophotometer.

Nanodrop Spectrophotometer; the spectrophotometer cleaned, initialized and blanked by loading 1-2µl of deionized water. DNA concentration measured by loading 1µl of the sample on lower optic surface and lowering the lever arm to trap the sample between both optical surfaces and concentration measured as ng/µl. Absorbance readings were taken with a Thermo Nanodrop spectrophotometer.

2.3.6. Site- Directed Mutagenesis

Site-directed mutagenesis (SDM) for TTR and hCC genes were performed using QuikChange® II mutagenesis kit (Stratagene). The following protocol used for producing all the mutants and the manual can be referred to for more details.

PCR reaction mixture prepared as follow:

5 µl 10x reaction buffer (100 mM KCl, 100 mM $(NH_4)_2SO_4$, 200 mM Tris-HCl pH 8.8, 20 mM $MgSO_4$, 1 % Triton® X-100, 1 mg/ml nuclease-free BSA).

30 ng plasmid template.

1 µl dNTP mixture.

1µl Pfu Turbo DNA polymerase was added to the reaction.

125 ng of each forward and reverse primer containing the desired mutation

then final volume made up to a 50 µl with sterilised deionised water.

PCR was then performed in a Techne Progene thermocycler, using 18 cycles of:

30 seconds at 95°C (melting)

1 minute at 55°C (annealing)

9 minutes at 68°C (extension).

Reaction mixtures were subsequently digested with Dpn1 restriction endonuclease for 1 hour to selectively digest methylated template DNA. Plasmid DNA was transformed into competent XL1-Blue *E.coli* cells and plated onto selective LB-agar, containing the relevant antibiotic. Colonies which grew on the selective agar were grown overnight and the plasmid extracted as described previously. The primers were designed using the Stratagene QuikChange® Primer Design Program.

2.3.7. DNA Sequenceing

Wild type TTR Plasmid and its mutants produced by site-directed mutagenesis were sequenced to confirm the correct identity by the Core Genomic Facility, University of Sheffield. Wild type hCC Plasmid and its mutants produced by site-directed mutagenesis were sequenced to confirm the correct identity by GATC (Biotech, Germany). Sequences were aligned and analysed using Finch TV Version 1.4.0 (Geospiza, Inc) and the basic local alignment search tool (BLAST) available on the NCBI website (http://blast.ncbi.nlm.nih.gov/bl2.seq/wblast2.cgi).

2.4. Protein Expression and Purification

2.4.1. Expression and Purification of Transthyretin

2.4.1.1. Overexpression

Single colonies of freshly transformed *E. coli* BL21/DE3 were used to inoculate 50 ml starter culture of LB media, and incubated overnight at 37°C, 250 rpm. 6 ml of the starter culture was used to inoculate 0.6 litre of LB media containing 100 μg/ml ampicillin, and incubated at 37°C with 250 rpm shaking until OD_{600} reached 0.6. Cultures were then induced with IPTG to a final concentration of 2 mM and incubated for a further 19 hours.

2.4.2.2. Cell Harvesting

Harvesting of induced cells were performed by centrifugation at 10 000 rpm, 4°C for 10 minutes. The growth media was discarded, and the cell pellets resuspended in 25 mM Tris buffer, 2 mM EDTA, 0.1% (v/v) Triton X-100, pH 7.5. Cell resuspensions were directly frozen at -80C.

2.4.2.3. Cell Lysis

Cell resuspension were lysed by two cycles of freeze-thaw by freezing at -80°C and thawing at 60°C in a water bath, and then sonicated on ice for 4 x 30 seconds, operating at maximum intensity and allowing one minute rest between sonication cycles. The suspension was centrifuged at 15 000 rpm, 4°C for 15 minutes. The pellet was discarded and the supernatant used for purification.

2.4.2.4. Purification

The volume of supernatant was measured by a measuring cylinder and 50% of ammonium sulphate were added, then centrifuged at 18000 rpm for 20 minutes to precipitate contaminant proteins. The pellet discarded and TTR precipitated by addition of 90%

ammonium sulphate. The pellet resuspended in a minimal volume of 5 mM Tris buffer, pH 8.0, and desalted by overnight dialysis against 5L of 5 mM Tris buffer, pH 8.0 at 4°C. The desalted protein solution heated at 60°C for 30 min in order to precipitate out contaminating proteins.

The mixture centrifuged at 15000 rpm for 15 minutes and the supernatant was loaded onto a 100 ml Q-Sepharose (Pharmacia) ion-exchange column at 2 ml/min, equilibrated with 5 mM Tris buffer, pH 8.0. The column was washed with the same Tris buffer until the OD_{280} of the eluent stabilised. Bound protein was eluted with 400 ml total volume 0.20-0.35 M NaCl gradient employing 25mM Tris buffer, pH 8.0. Eluent was collected in 8 ml fractions and fractions containing TTR were pooled and Precipitated with ammonium sulfate (90%) and store as a pellet at 4°C.

2.4.2. Expression and Purification of Human Cystatin C

2.4.2.1. Over-expression

5 ml of LB broth inoculated with a single colony of *E. coli* BL21 (DE3). Culture was grown overnight at 37°C and used to inoculate 100 ml of LB broth for overnight at 37°C. 10 ml of starter culture was used to inoculate 600 ml of M9 minimal media. The total growth was 4.8 litres. Cultures were grown at 37°C with shaking at 220 r.p.m. Cell growth was followed by measuring the OD_{600}, and expression cultures were induced with IPTG to a final concentration of 0.75 mM when OD_{600} reached 0.4 – 0.6 and growth continued for 6 hours after induction.

2.4.2.2. Periplasmic Extraction

Induced cells were harvested by centrifugation at 10,000 rpm at 4°C for 10 minutes and the pellets re-suspended in 20% sucrose, 0.2 M Tris pH 8.0. The suspension was

centrifuged at 20,000 rpm at 20 °C for 15 minutes. Cold EDTA solution (2 mM), pH 8.0 was used to re-suspend pellets. Phenylmethylsulphonyl fluoride (PMSF) was added immediately to give a final concentration of 1 mM. The re-suspended sample was centrifuged at 20,000 at 4 °C for 15 minutes. The supernatant was recovered and protease inhibitors (EDTA-free, 1 tablet per 50ml), 0.1 mg/ml DNase and 20 mM $MgCl_2$ were added. The sample was dialysed into cold 10 mM sodium phosphate buffer pH 7.0 to remove small molecules.

2.4.2.3. Cation Exchange Chromatography

100 ml SP-Sepharose (Pharmacia) cation exchange column had been equilibrated with cold 10 mM sodium phosphate buffer pH 7.0, and cold periplasmic extract was loaded at a rate of 2 ml/min. The column was washed with 10 mM sodium phosphate pH 7.0 until A_{280} of the eluent stabilized. Elution of hCC has been performed using 10 mM sodium phosphate buffer pH 7.0, 0.2 M NaCl, and 5 ml fractions collected. Any remaining bound protein was eluted with sodium phosphate buffer pH 7.0, 1 M NaCl. Fractions were analysed by SDS-PAGE and those containing hCC were pooled and stored at -20°C.

2.4.2.4. Size-Exclusion Chromatography

The fractions containing hCC were pooled and concentrated to less than 10 ml using an Amicon ultra-filtration stirred-cell device in conjunction with a Millipore regenerated cellulose membrane with a molecular weight cut-off of 10,000 Da and filtered using a 0.2 μm filter. Superdex G75 (GE Healthcare, UK) gel filtration column (400 ml) equilibrated with 10 mM sodium phosphate buffer (pH 6.0) before loading of the sample. The column had been run at a rate of 3 ml/min and 6 ml fractions collected applying 0.1 M NaCl. Phosphate buffer pH 6. The fractions were analysed using SDS-PAGE and any containing hCC were pooled. The average yield of cystatin C was 1-2 mg per litre of cell growth.

2.5. Protein procedures

2.5.1. Electrophoresis

SDS-PAGE (polyacrylamide gel electrophoresis on proteins denatured using sodium dodecyl sulphate) was accomplished using a BioRad Mini Protean II apparatus, according to the method of Laemmli (1970), and described in Sambrook *et al*. (1989). A stacking gel (4% acrylamide, tris-HCl pH 6.8) was cast above a resolving gel (16% acrylamide, tris-HCl pH 8.8), with a ratio of acrylamide to bis-acrylamide of 37.5:1. The running buffer was tris-glycine pH 8.6. All buffers contained 0.1% SDS. The samples were loaded in 50 mM tris-HCl, pH 6.8, containing 20% glycerol, 0.2% bromophenol blue. Proteins were incubated at 90°C for 5 minutes to reduce any disulphide bonds.

A standard of low molecular weight proteins (Sigma) was run alongside the samples. Neuroserpin runs an apparent molecular weight of 46 kDa. The gels were run at a constant voltage of 180 V for around 55 minutes, until the loading dye approached the edge of the gel. After removing the gel from its glass plates, it was stained for 1-2 hours with Coomassie Blue (in 10% acetic acid, 45% water, 45% methanol), then destained with the same solvent until the bands were visible. The gels were scanned with an Epson Imagejet scanner.

2.5.2. SDS-PAGE buffers and markers

<u>SDS-PAGE buffers:</u>

4 x stacking gel buffer	0.5 M Tris/HCl, 0.4 % (w/v) SDS, pH 6.8
4 x resolving gel buffer	1.5 M Tris/HCl, 0.4 % (w/v) SDS, pH 6.8
Running buffer	25 mM Tris/HCl, 0.19 M glycine, 0.1 % (w/v) SDS, pH 8.3

Loading buffer	50 mM Tris/HCl, 100 mM DTT, 2 % (w/v) SDS, 0.1 % (w/v) Bromophenol blue, 10 % (v/v) glycerol	
Stain	0.4 % (w/v) Coomassie blue R, 8 % (v/v) acetic acid, 46 % (v/v) methanol	
Destain	10 % (v/v) acetic acid, 30 % (v/v) methanol	
16 % resolving gel	Lower buffer	2.5 mL
	40 % (w/v) acrylamide/Bis (29:1)	4 mL
	dH_20	3.5 mL
	10 % (w/v) APS	100 µL
	TEMED	10 µL
4 % stacking gel	Upper buffer	2.5 mL
	40 % (w/v) acrylamide/Bis (29:1)	1.125 mL
	dH_20	6.4 mL
	10 % (w/v) APS	110 µL
	TEMED	11 µL

TEMED and Acrylamide solutions were purchased from Bio-Rad.

Molecular Weight Marker

Bio-Rad pre-stained broad range molecular weight markers were used with the typical mass values stated below:

Myosin	200 000 Da
B-galactosidase	116 250 Da
Bovine serum albumin	86 000 Da

Ovalbumin	51 000 Da
Carbonic anhydrase	37 000 Da
Soybean trypsin inhibitor	29 000 Da
Lysozyme	19 700 Da
Aprotinin	7 000 Da

2.5.3. Protein concentration and buffer exchange

Large volumes of protein solutions were concentrated and using an Amicon ultrafiltration stirred cell conjugated with an appropriate Millipore 10kDa MWCO filter. Vivaspin centrifugal concentrators (Viva science) with 5-10kDa MWCO were used to concentrate smaller volumes (≥10 ml) of protein solutions. Buffer exchange was accomplished either using Vivaspin concentrators, or by dialysis against the desired buffer using Spectra/Por dialysis tubing or dialysis cassettes with a 10kDa MWCO (Spectrum labs, USA).

2.5.4. Determination of protein concentration

The protein concentrations were determined by measuring UV absorption spectra at 280 nm on a Cary spectrophotometer, and analysed using Cary Win-UV software. The concentrations were determined by using the Beer-Lambert Law:

$A = c \times l \times \varepsilon$

Absorbance = concentration x pathlength x molar extinction coefficient

The transthyretin tetramer has a molar extinction coefficient of 77600 $M^{-1}.cm^{-1}$, hCC has a molar extinction coefficient of 11050 $M^{-1}.cm^{-1}$, and W106A hCC variant has a molar extinction coefficient of 5550 $M^{-1}.cm^{-1}$. These values were calculated from the proteins'

sequences using the "ProtParam" tool at http://web.expasy.org/cgi-bin/protparam/protparam.

2.6. Analytical Size Exclusion Chromatography

The purity of the protein samples was analysed by size exclusion high-pressure liquid chromatography (SEC-HPLC). 20-180 µl samples were analysed using a Superdex 200 column (GE Healthcare, UK) with a Perkin Elmer Series 200 HPLC system equipped with a UV-visible absorbance detector (Perkin Elmer, UK). The OD of the eluent was monitored at OD_{280}. Specific HPLC experiments are discussed further in the appropriate chapters.

2.7. Spectroscopic Techniques

2.7.1. Fluorescence Spectroscopy

Thioflavin T fluorescence measurements were taken on a Fluostar Omega plate-reader (BMG Labtech, UK). The spectra were recorded at time-points with an excitation wavelength of 442 nm and an emission wavelength of 482 nm. Further details on specific fluorescence experiments are provided in the relevant chapters.

2.7.2. Nuclear Magnetic Resonance (NMR)

NMR spectra were recorded on Bruker DRX spectrometers operating at 500, 600 or 800 MHz controlled using XWinNMR (Bruker) and NMR data was processed using Felix (Accelrys). Experiments are discussed in further detail in the appropriate chapter.

2.7.3. Transmission Electron Microscopy (TEM)

Carbon-coated copper grids (Agar Scientific) were glow-discharged with 2x 20 second pulses using a Cressington 208 glow-discharge unit. Samples were adsorbed on a freshly glow-discharged grid for 1 minute and then blotted. Each grid was washed shortly in two

drops of water and two drops of 0.75% uranyl formate and blotted between each wash; the grid was held in the final drop of 0.75% uranyl formate for 30 seconds and dried with gentle vacuum suction after blotting. A Philips CM-100 electron microscope, operating at 100 kV and equipped with a 1024 x 1024 pixel Gatan CCD camera, was used to record micrographs.

2.8. Aβ peptide Manipulation

2.8.1. Preparation of Monomeric Aβ

1 mg aliquots of Hexafluoroisopropanol (HFIP) (HFIP- is a polar, volatile, organic solvent used to dissolve pre-aggregated peptides) -treated recombinant Aβ peptide were purchased from rPeptide (Georgia, USA) and stored at -20°C. To prevent condensation upon opening, each closed vial was allowed to equilibrate at room temperature for 10 minutes before dissolution. A 1 mg/ml solution was produced by adding 1 ml of cold HFIP to the lyophilised peptide and complete dissolution was ensured by sonication for 10 minutes in a DECON Ultrasonics sonicator bath (Sussex, UK). 0.1 mg aliquots were produced by transferring 0.1ml of the clear solution into sterile micro-centrifuge tubes. A nitrogen stream was used to remove excess HFIP and any remaining traces were then removed by lyophilisation. The lyophilised aliquots of peptide were stored as thin clear films at -20°C.

2.8.2. Aβ Fibril Formation

Each 0.1 mg aliquot of HFIP-treated Aβ was allowed to equilibrate to room temperature before the addition of 20 µl DMSO (peptide concentration 10 mM). The sample was then sonicated for 10 minutes before being further aliquoted depending on the number of experiments being performed. Phosphate buffered saline (PBS) (50 mM

Na_2HPO_4/NaH_2PO_4, 150mM NaCl, 2mM NaN_3, pH 7.4) containing 10μM thioflavin T was added to DMSO-dissolved Aβ aliquots, then 100 μl samples were added to 96 half-well plates (Corning) which were either polystyrene (3694) or PEG treated (non-binding-3686). These were incubated in a Biotech Omega fluorescence plate reader (BMG Labtech, UK) at 37°C with either double orbital shaking at 100 r.p.m for only 10 seconds before each reading (minimal shaking) or continuous double orbital shaking at 300 r.p.m. (continuous shaking) . Each condition was replicated 5 times and each experiment repeated at least 3 times. The mean of these replicates was plotted and standard errors of the mean were shown. The excitation wavelength was 440 nm and fluorescence emission was measured at 485 nm every 5 minutes.

Chapter Three: Transthyretin and Aβ interaction in the presence of different surfaces

3.1 Introduction

Accumulation of Aβ peptide aggregates into extracellular amyloid plaques in the brain is the hallmark of Alzheimer's disease. A number of other amyloidogenic proteins have been found co-deposited in these plaques. Recent findings suggest the involvement of these proteins in the plaques and in the pathophysiology of Alzheimer's disease. Transthyretin is one of the amyloidogenic proteins that have been found within amyloid plaques along with Aβ.

Transthyretin and Aβ

Transthyretin (TTR) is a homotetrameric protein of 127 amino acid subunits. In the serum, the 55KDa homotetramer is in equilibrium with a small proportion of monomer (Buxbaum *et al.*, 2012). Transthyretin is one of several proteins which have been found inside Alzheimer's plaques along with Aβ. It is a major constituent of the CSF and can sequester Aβ (Schwarzman *et al.*, 1994). This finding was followed by several studies using either animal models or cell culture assays which further supported this interaction and showed TTR's protective ability against Aβ cytotoxicity. *In vitro* studies then showed a direct inhibitory effect of wild-type and mutant TTRs on Aβ aggregation. Although there is clear evidence for the interaction between WT-TTR and Aβ, *in vitro* studies give contradictory results regarding the binding affinity between the two proteins. In general, methodologies depending on immobilising one of the proteins like surface plasmon resonance (SPR) and ELISA measured a K_D of 28nM (Costa *et al.*, 2008). However, liquid phase experiments (ITC) showed the K_D to be 24 μM in solution (Li *et al.*, 2013a), a difference of 3 orders of magnitude.

Binding of Aβ to surfaces has been suggested by a number of studies. The formation of sheet-like deposits of Aβ on graphite and micelle-like structures on mica have been observed by AFM (Kowalewski and Holtzman, 1999). Neutron reflectometry applied to show the formation of dense Aβ films on cationic or hydrophobic surfaces (Rocha *et al.*, 2005). Garai *et al.* (2008) and Morinaga *et al.* (2010) found that polypropylene was an effective catalyst for the aggregation of $A\beta_{1\text{-}40}$. Shen *et al.* (2012) found that $A\beta_{1\text{-}42}$ binds tightly on the polystyrene (PS) surface and loosely on the polyethylglycate (PEG) surface, however it fibrillises faster on the loosely bound surfaces better than tightly bound ones. The thickness of the film detected by Rocha was 2 nm which is nearly twice the hydrodynamic radius or gyration radius of Aβ monomer in solution (Massi *et al.*, 2001, Raffa and Rauk, 2007, Nag *et al.*, 2011). Thus, it is likely that these films might be Aβ monolayers. Given the fact that Aβ has a tendency to bind to different surfaces, even in solution phase experiments, Aβ will still interact with surfaces and the peptide's interactions with other proteins can therefore be affected. The observation of both the deposition of films of Aβ on hydrophobic surfaces as well as its nucleation in these films supports the idea that Aβ can tightly bind to polystyrene and nucleate in this environment. Work carried out by my colleague Alex Taylor during the writing of this thesis has suggested that the fibril yield reflects the available Aβ monomer concentration in solution (Taylor, MSc thesis, 2016 and manuscript in preparation). He observed the relationship between the initial Aβ monomer concentration and final fluorescence intensity for thioflavin T timecourse data at different $A\beta_{1\text{-}42}$ concentrations (Figure 3.1.). Each set of data was independently fitted to the equation:

$$Y \approx V\,([M]_0 - kg^-/\,kg^+) - \rho_{max}A,$$

where Y is the yield, V is the volume of reaction mixture, $[M]_0$ is monomer concentration, $kg+$ is the elongation rate constant, and $kg-$ is the disaggregation rate constant, ρ_{max} is the

maximum packing capacity and A is the surface area. Using the x-intercept of these graphs, a reaction volume of 100 µl, and the calculated surface area of the plates, the concentration of Aβ disappeared on surface binding and therefore the mean packing density were detected. The observed difference in the x-intercept between non-binding (treated with PEG) and untreated polystyrene (PS) plates was significant (compare Figures 3.1A and B), suggesting that tight binding was actually occurring on untreated (PS) plates. The likely packing densities and corresponding intermolecular spacings for idealised square-lattice monolayers of $A\beta_{1\text{-}42}$ were calculated. Given that the effective diameter of a random coil (RC) Aβ monomer in solution may be ~2 nm, these idealised spacings are consistent with the formation of tightly packed monolayers of structured or partially structured $A\beta_{1\text{-}42}$ on exposed polystyrene surfaces.

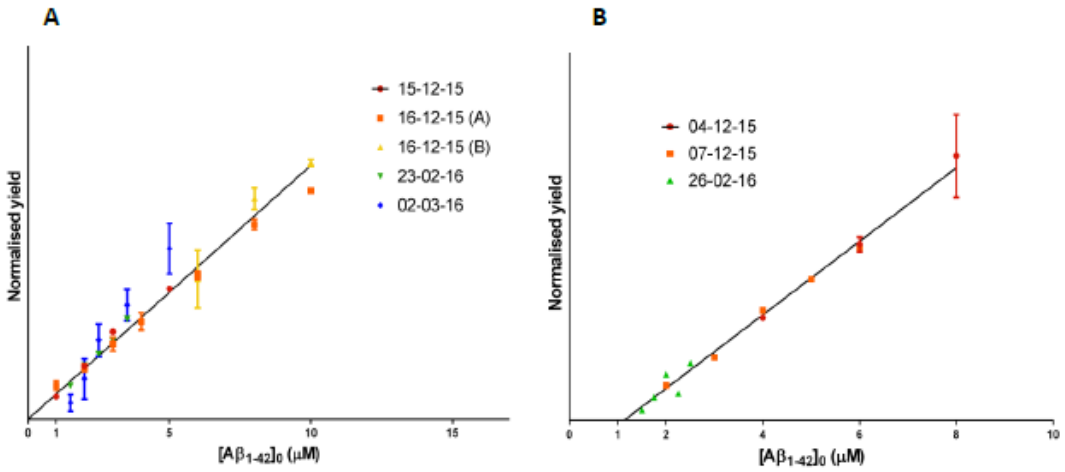

Figure 3.1.The effect of plate type on the fluorescence intensity change, measured in the early plateau phase. A) shows the relationship between initial $A\beta_{1\text{-}42}$ concentration and fluorescence intensity change ('yield') in nonbinding plates (PEG), while B) shows the equivalent experiments in untreated (PS) plates (Adapted from Taylor, 2016).

The efficiency of the TTR binding and inhibition of Aβ fibrillisation remains questionable in the absence of a detailed characterisation of the inhibition of fibril formation in the presence of different surfaces. This chapter is a study to further investigate binding affinity and inhibition of Aβ fibrillisation by TTR in the presence of two different

surfaces, widely used for the *in vitro* studies of $A\beta_{1-42}$ whether for biophysical analysis, cell assays or ELISA. Polystyrene (non-treated or binding) and polyethylglycate (PEG) treated (non-binding) microplates were used to show the influence of these two surfaces on TTR binding and Aβ fibrillisation inhibition intensity. The chemical structures of these molecules are shown in Figure 3.2.

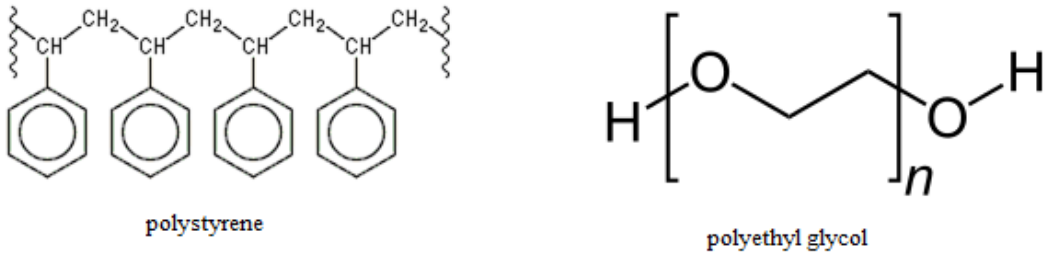

Figure 3.2. The structures of polystyrene (PS) and polyethyl glycol (PEG). The highly hydrophobic nature of PS and more hydrophilic nature of PEG.

3.2. Materials and Methods

Preparation of monomeric Aβ, fibrillisation and EM were performed as described in chapter 2.

3.2.1. Addition of TTRs to Aβ

TTR stocks were kept in PBS (50 mM Na_2HPO_4/NaH_2PO_4, 150mM NaCl, 2mM NaN_3, pH 7.4) at -20 °C. TTR stocks were thawed at room temperature, then filtered through 100KD filters to remove any aggregated structures. TTR solutions were then diluted by adding PBS to the correct final concentration then added directly to the lyophilised Aβ, to prevent the peptide from forming low molecular weight species before the addition of TTR. 100 µl of the mixture was then added to 96 half-well plates and incubated in minimal shaking conditions as previously mentioned in section 2.8.2.

3.3. Results

3.3.1. Aβ Fibrillisation

$A\beta_{1-42}$ fibril formation was monitored using thioflavin T fluorescence. Thioflavin T is an amyloid-specific dye that displays a characteristic shift of its emission spectrum as it binds to mature amyloid fibrils, and thus allows the time-dependent monitoring of fibrillisation. The dye binds only to mature fibrils, but not to monomers, oligomeric intermediates or protofibrils. The Aβ fibrillisation reactions monitored by thioflavin T assays (Figure 3.3) are consistent with the nucleation-dependent elongation model of amyloid assembly (Chapter 1; section 1.9). They exhibit a characteristic sigmoidal curve with an initial lag phase in which the amount of amyloid proteins turned into fibrils is not detectable, an exponential growth phase in which fibril concentration increases rapidly and eventually, a final equilibrium phase when most soluble proteins are converted into fibrils (Lee *et al.*, 2007).

Our aim was to use physiological conditions regarding pH, ionic strength and temperature. Salt accelerates and promotes the transformation of Aβ to β-sheet as it weakens electrostatic forces and as the hydrophobic interaction becomes the dominant driving force (Lin *et al.*, 2008), it enhances aggregation. Higher temperatures also accelerate Aβ aggregation (Wolff *et al.*, 2015). Figure 3.3 shows the time course $A\beta_{1-42}$ fibrillisation under our optimised conditions. In both polystyrene and PEG-coated plates the general features of the fibrillisation reaction are preserved but the reaction is noticeably faster in the PEG-treated plates. Most inhibition studies to date have compared these data using t_{50} values because of their greater reproducibility. From the Aβ growth curves, the half time (t_{50}) or the time for mid-growth phase when the fluorescence reaches

its 50% value was determined. The t_{50} for Aβ fibrillisation curve was 4.2 ± 0.6 and 1.33 ± 0.15 hrs in the polystyrene and PEG plates, respectively.

The morphology of produced $A\beta_{1-42}$ fibrils was analysed using transmission electron microscopy. Electron micrographs of $A\beta_{1-42}$ fibrilisation reactions in the presence of PEG and PS plate surfaces after 24 hours are shown in Figure 3.3c & d respectively. The formation of mature fibrils confirmed in all of the samples. The fibrils are long, straight and unbranched. Little structural variations were between the two different preparations were observed.

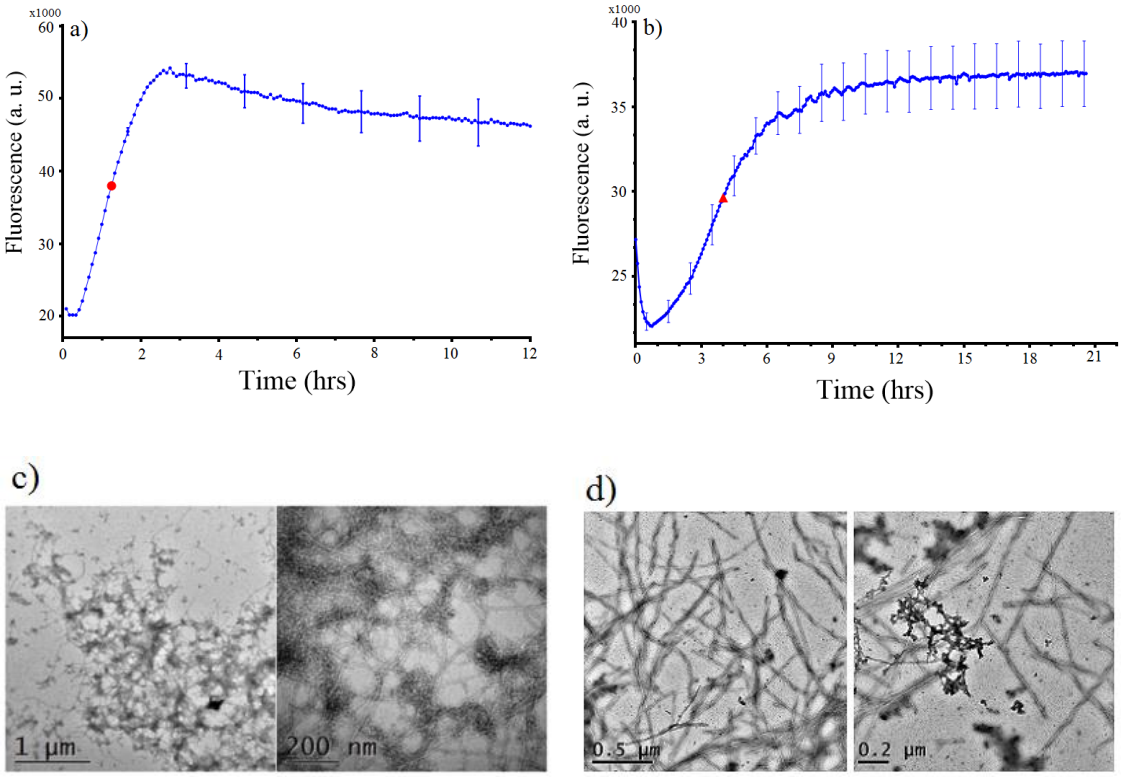

Figure 3. 3. Thioflavin T curves and EM images of $A\beta_{1-42}$ fibrillisation in PS and PEG plates. $A\beta_{1-42}$ fibrilisation curves with error bars displaying the standard error of the mean (SEM) to give an indication of the spread of the data. t_{50} is indicated as a large red spot. a) $A\beta_{1-42}$ in PEG and b) $A\beta_{1-42}$ in polystyrene plates. Electron micrographs of Aβ (11µM) after 24 hrs of incubation. c) $A\beta_{1-42}$ (11µM) in the PEG plate, d) $A\beta_{1-42}$ in the presence of polystyrene plate. The scale bars are indicated.

3.3.2. Addition of WT-TTR to the $A\beta_{1-42}$ fibrillisation reaction

Thioflavin T time-course

The kinetics of $A\beta_{1-42}$ fibrillisation were monitored in the presence of different molar concentrations of WT-TTR in the standard conditions described earlier, with a fixed $A\beta_{1-42}$ concentration of 11 μM, and shown in Figure 3.4. In the PEG plates, different concentrations of TTR were tested ranging from 22 μM (twice the stoichiometric concentration of $A\beta_{1-42}$) to 1 μM (11 times less than the concentration of $A\beta_{1-42}$). Low levels of WT-TTR (1 μM) do not appear to have any effect on Aβ aggregation with the curves showing a similar t_{50}. Equimolar (11μM) and lower concentrations (4μM) of WT-TTR produced an increased t_{50} in a concentration-dependent manner, although the effect is very small. Surprisingly, higher concentrations of WT-TTR (22 μM) do not appear to have a greater effect than equimolar (11 μM) with respect to the t_{50} of Aβ aggregation (see Table 3.1.).

In the polystyrene plates, a fixed $A\beta_{1-42}$ concentration of 11 μM, with different concentrations of TTRs were tested ranging from 11 μM (stoichiometric concentration of $A\beta_{1-42}$) to 1 μM (11 times less than the concentration of $A\beta_{1-42}$). Near equimolar concentrations (9μM) of WT-TTR were able to completely suppress thioflavin T fluorescence, suggesting a complete inhibition of fibril formation. Smaller ratios of WT-TTR (2, 4 and 7.5 μM) lengthened the Aβ fibrillisation time in a concentration dependant manner, producing changes in t_{50} far more significant than for the PEG treated plates. Low concentrations of WT-TTR (1 μM) do not appear to have a significant effect on Aβ aggregation with the curves showing similar t_{50} to the control reaction.

WT TTR conc (μM)	Normalized t_{50} (hrs)				Amplitude (as a fraction of control fluorescence)	
	PEG		Polystyrene		PEG	Polystyrene
	Mean± sem	p> 0.05* p<0.01*	Mean± sem	p> 0.05* p<0.01*		
0	1.33(1)± 0.15	n. a.	3.6 (1) ± 0.6	n. a.	n. a.	n. a.
1	0.95 ± 0.19	0.2 n. s.	1.1 ± 0.13	0.15 n. s.	1.1± 0.06	1.22 ± 0.23
2	n. d.	n. d.	1.7 ± 0.5	0.007**	n. d.	1.53 ± 0.29
4	1.1 ± 0.15	0.08 n. s.	2.1 ± 0.5	0.006**	1.2 ± 0.1	1.58 ± 0.4
7	n. d.	n. d.	2.95 ± 0.8	0.045**	n. d.	1.9 ± 0.45
11	1.32 ± 0.33	0.80 n. s.	n. d.	n. d.	1.07 ± 0.12	n. d.
22	1.3 ± 0.42	n. s.	n. d.	n. d.	1.29 ± 0.42	n. d.

n. a. = not applicable, n. s. = non-significant, n. d. = no data

Table 3.1. Normalised t_{50} and amplitude values for $A\beta_{1-42}$ fibrillisation in the presence of WT TTR in PEG and PS microplates. 11 μM of $A\beta_{1-42}$ and in the presence of different concentrations of WT-TTR with standard errors of mean (sem). The significant differences were calculated using t test and those with p< 0.05 (n. s.), p> 0.05 (*) and p> 0.01 (**) are indicated.

At the end of the reaction (after reaching plateau), in the PEG plates, the amplitude of thioflavin T signal was slightly higher in the presence of the different concentrations of TTR. However, in the polystyrene plates, the amplitude was slightly higher in the presence of (1μM) of TTR than in its absence and significantly higher in the presence of (2, 4 and 7.5 μM) of TTR (Figure 3.4D). Only in the polystyrene plates could the reaction be supressed completely and no fibrils observed even after months of incubation suggesting the reaction is unable to proceed under these conditions. The increase in thioflavin T fluorescence at lower TTR could not be attributed to the independent formation of TTR amyloid because, when incubated alone in these conditions, WT TTR does not form fibrils and there is no increase in thioflavin T fluorescence.

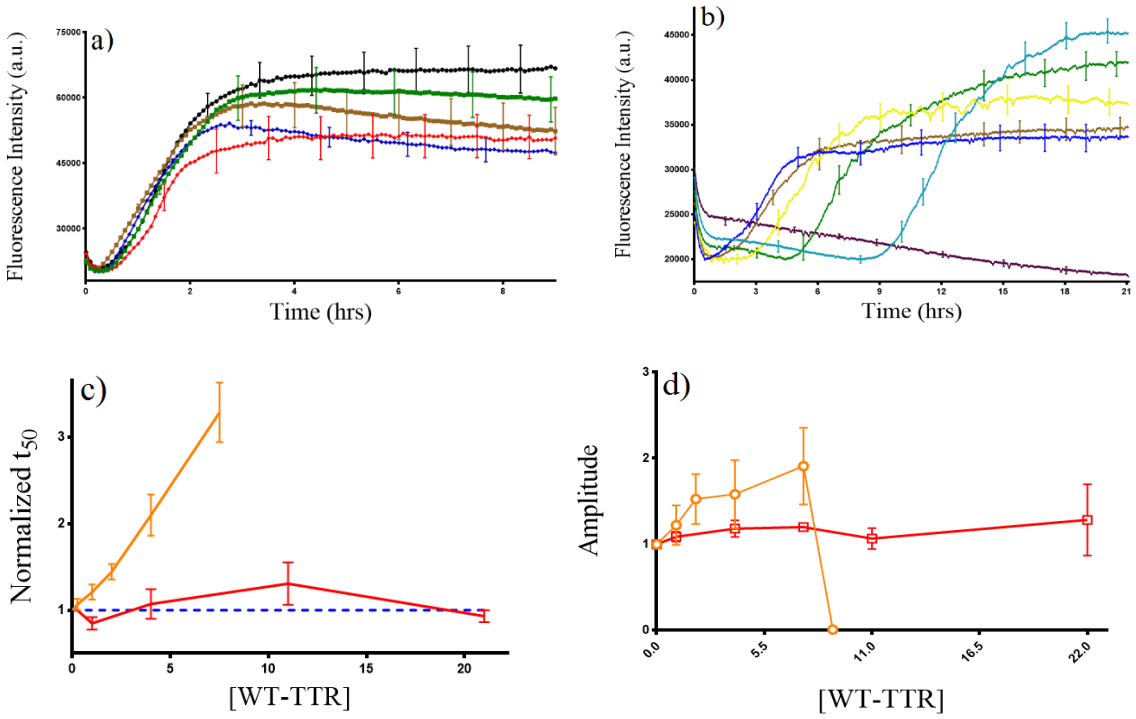

Figure 3. 4. **Thioflavin T curves of $A\beta_{1-42}$ in the presence of WT TTR in both PS and PEG plates**. Each colour coded line represents a different concentration of TTR with 11 µM of Aβ (1µM TTR, brown; 2 µM TTR, yellow; 4 µM, green; 7.5 µM, ocean; 9 µM, purple, 11 µM; black, and 22 µM; red), with SEM bars representing 3 different experiments. a) $A\beta_{1-42}$ with WT-TTR in PEG microplate b) $A\beta_{1-42}$ with WT-TTR in polystyren microplate. c) normalized t_{50} and d) amplitude values calculated for the $A\beta_{1-42}$ with different concentrations of WT-TTR, in PEG (red) and polystyrene (orange) plates, with error bars showing the sem.

Electron Microscopy

While the thioflavin T fluorescence changes suggest that WT TTR affected Aβ fibril formation differently in the presence of PEG and polystyrene microplates, direct observation of the morphology of the structures was still necessary to confirm thioflavin T results. TEM was employed to investigate the morphology of the structures produced at the end of the incubation of Aβ in the presence of equimolar concentration (11µM) of WT-TTR in both PEG and polystyrene microplates. Figure 3.5 shows representative examples of electron micrographs of these different preparations after 24 hours. In PEG microplates, along with mature fibrils, only small amounts of amorphous aggregates also

formed, however in the polystyrene microplates large amounts of amorphous aggregates were found with very small amounts of fibrils observed in some images.

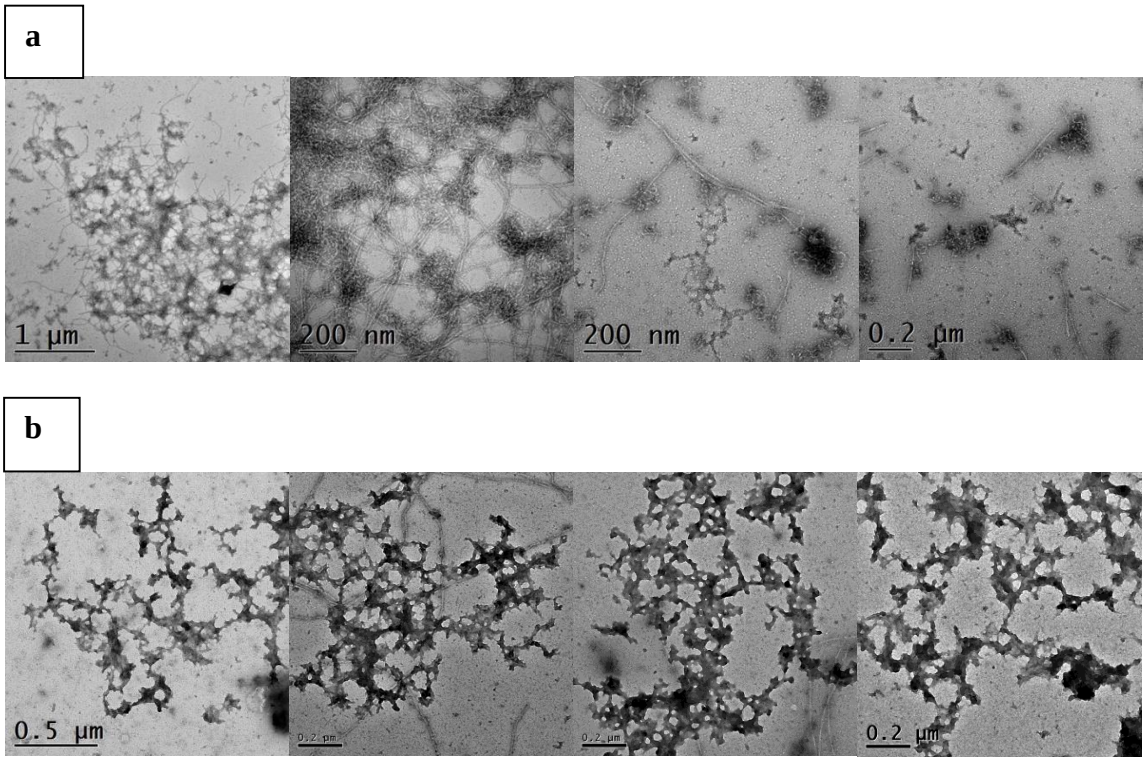

Figure 3.5. Electron micrographs of $A\beta_{1-42}$ in the presence of equimolar concentrations of WT-TTR after 24 hrs. a) in PEG and b) in polystyrene microplates. The scale bars are indicated.

3.3. Discussion

Several studies have suggested an interaction between TTR and Aβ peptides. Transthyretin is one of the amyloidogenic proteins found co-deposited in the plaques. Animal model and cell line studies suggest a protective role for TTR in the pathophysiology of AD. *In vitro* analyses of direct interactions also suggest that sub-stoichiometric concentrations of TTR inhibit Aβ fibrillisation.

In order to study TTR interaction with Aβ fibrillisation, a typical condition was developed for Aβ fibrillisation in both polystyrene and PEG microplates. Under the conditions used in this study Aβ peptides make typical straight, unbranched, thioflavin T positive amyloid fibrils and the aggregation kinetics follow a typical sigmoidal shape with a lag time,

growth phase and then plateau. This pattern fits with a nucleation dependant mechanism of aggregation which is a characteristic of Aβ aggregation. In PEG plates, $A\beta_{1-42}$ exhibits a t_{50} of 1.33 ± 0.15hrs. These results are different from Aβ aggregation rates obtained in polystyrene plates where the aggregation rate is slower, the t_{50} value is about 4.2 ± 0.6 hrs. However, it is consistent with the t_{50} for Aβ aggregation by (Meisl *et al.*, 2016). They found a t_{50} of 0.7 hr for $A\beta_{1-42}$ incubated in 96 well black polystyrene coated with PEG, in 20 mM sodium phosphate, 200 mM EDTA, 2mM NaN_3, pH 7.4. The differences in the aggregation rate in both plates are most likely down to the difference in the Aβ interaction with the different surfaces. As previously mentioned, the deposition of an Aβ film and its nucleation on hydrophobic surfaces is well-supported in the literature. My lab colleague Alex Taylor found evidence for the formation of a tightly bound monolayer of Aβ on polystyrene which enhances Aβ nucleation. However, the lose binding of Aβ on PEG is likely to accelerate Aβ nucleation and aggregation more than the polystyrene plate, presumably because the nuclei can easily come off the surface to the solution and start aggregation. The acceleration of nucleation through loose binding of Aβ to surfaces have been suggested as the local concentration increases upon binding and loose binding allows mobility of the peptide and the ability to aggregate (Shen *et al.*, 2012).

In an attempt to study the binding and inhibition of Aβ by TTR in the presence of different surfaces, thioflavin T experiments were performed using PEG and polystyrene microplates. Results obtained in this study show that the intensity of WT-TTR to inhibit Aβ fibrillisation is significantly lower in the presence of PEG compared to polystyrene surfaces. In the presence of polystyrene plates low concentrations of TTR significantly lengthened the t_{50} of the Aβ fibrillisation and slightly lower than equimolar concentrations were sufficient to completely inhibit Aβ fibrillisation. However, in the presence of PEG surface even twice the equimolar concentration of WT-TTR does not inhibit $A\beta_{1-42}$

fibrillisation. Electron microscopy showed no difference between the morphology of fibrils formed in the presence of an equimolar amount of TTR after 24 hrs in the PEG plates, suggesting no inhibition in Aβ fibrillisation by TTR. However, EM showed that near equimolar concentration of TTR prevented the formation of fibrils by Aβ in the polystyrene plates, and large amounts of amorphous aggregates were observed instead. The results obtained in the presence of PEG disagreed with previous studies suggesting $A\beta_{1-42}$ fibrillisation can be inhibited by sub-stoichiometric amounts of TTR. Li *et al.* (2013a) found the complete inhibition of $A\beta_{1-40}$ by 3μM WT TTR. Our results imply strongly that TTR can only inhibit $A\beta_{1-42}$ fibillisation at these concentrations when it is immobilized on a surface. Indeed, while $A\beta_{1-42}$ forms a tightly bound monolayer on the polystyrene surface, its binding to the PEG-treated plate is very weak suggesting it can only nucleate Aβ aggregation without forming a monolayer.

This interpretation is supported by solution measurements of TTR binding to $A\beta_{1-40}$ monomers: the K_D for TTR tetramer binding to $A\beta_{1-40}$ is 24μM (Li *et al.*, 2013a). However, the K_D for TTR binding to $A\beta_{1-42}$ is much stronger (28 nM) once the Aβ is immobilized as shown by ELISA based studies (Costa *et al.*, 2008).

Aβ forms a monolayer on the surface of the plate which enhances Aβ nucleation to happen faster than it would otherwise occur in solution. The binding occurs on the monolayer surface which enhances nucleation and formation of larger aggregates and then fibrils. Our results imply that disturbance of this layer by TTR prevents nucleation from occurring. On the other hand, nuclei and solution monomer can directly form fibrils as well but this may be extremely slow. It has been found that elimination of both air-liquid interfaces or reactive solid-liquid interfaces can extend nucleation of $A\beta_{1-40}$ for extended periods of time (Garai *et al.*, 2008, Morinaga *et al.*, 2010) and presumably the critical

concentration for primary nucleation may be higher than 11μM in the absence of a polystyrene and/or air water interface.

As the rate of aggregation of Aβ in our conditions was independent of monomer concentration, the increase in lag time and t_{50} in the presence of polystyrene plates cannot be interpreted as the result of TTR binding to Aβ monomer.

It is plausible therefore that TTR binds weakly to the monomer or aggregated structure in the solution and binds much tighter to a rare species of Aβ aggregated structure on the monolayer, causing a delay in the lag time because it delays nucleus formation. However, the fibril formation reaction is more favourable and can drive the species bound to TTR (because the binding is weak) and the same amount of fibrils will form because all the Aβ can convert to fibrils and the final amplitude will be the same or greater than the control as the amount of $A\beta_{1-42}$ which would otherwise bind to the surface is disturbed and able to fibrillise. When the concentration of TTR is higher but not high enough to inhibit Aβ completely, the amplitude becomes lower because a larger amount of TTR will be available at each time point to stay bound to the rare species and not all Aβ will be available to form fibrils. When the concentration of TTR is higher, the on-pathway fibril reaction will no longer be available and the amorphous aggregation will be more favourable.

Chapter Four: Transthyretin and Aβ interaction

4.1. Introduction

The hallmark of Alzheimer's disease is the accumulation of Aβ peptide aggregates into extracellular amyloid plaques in the brain. This leads to major neurodegeneration and the consequent pathology. Whereas in the past, it was believed that Alzheimer's plaques contained only Aβ peptides, recent findings suggest the involvement of multiple amyloid-forming proteins in the plaques and in the pathophysiology of Alzheimer's disease. *In vitro*, the aggregation behaviour of the Aβ peptide has been characterised extensively but the effect of co-deposited proteins on Aβ aggregation is not well established. Different amyloid forming proteins including transthyretin, neuroserpin and cystatin C have been found within amyloid plaques along with Aβ. Although these proteins have similar effects *in vitro* by reducing Aβ toxicity, it seems to be that the different proteins use different mechanisms to do this, as illustrated in Figure 4.1. Perhaps it is unsurprising that nature has evolved alternative natural mechanisms for the modulation of amyloid formation at different stages.

Protein binding to Aβ monomers prevents the formation of nucleating species thus inhibiting fibril formation at the very early stages. Given that the nucleus formation is a rate limiting step, small decreases in protein concentration can significantly reduce the rate of fibril formation under some conditions (Jarrett and Lansbury, 1993). Nucleus stabilisation or restriction of monomer addition may also inhibit fibril formation. Binding to the surface of fibrils and preventing Aβ monomers from using it as a template in secondary nucleation reactions can also limit formation of new fibrils (Cohen *et al.*, 2015). Other factors might defibrillise mature fibrils into smaller aggregates which are susceptible to proteolysis (and therefore can be cleared by the body) or remodel on-

pathway oligomeric species to non-toxic aggregates through transient bi-molecular collisions (Eichner *et al.*, 2011), thus abolishing the potential for amyloid formation. Some other modulator acts as a catalyst by causing the formation of non-toxic species without itself being incorporated into the final product. A better understanding of these natural mechanisms, and how to mimic them, would lead to the development of a therapeutic strategy against AD.

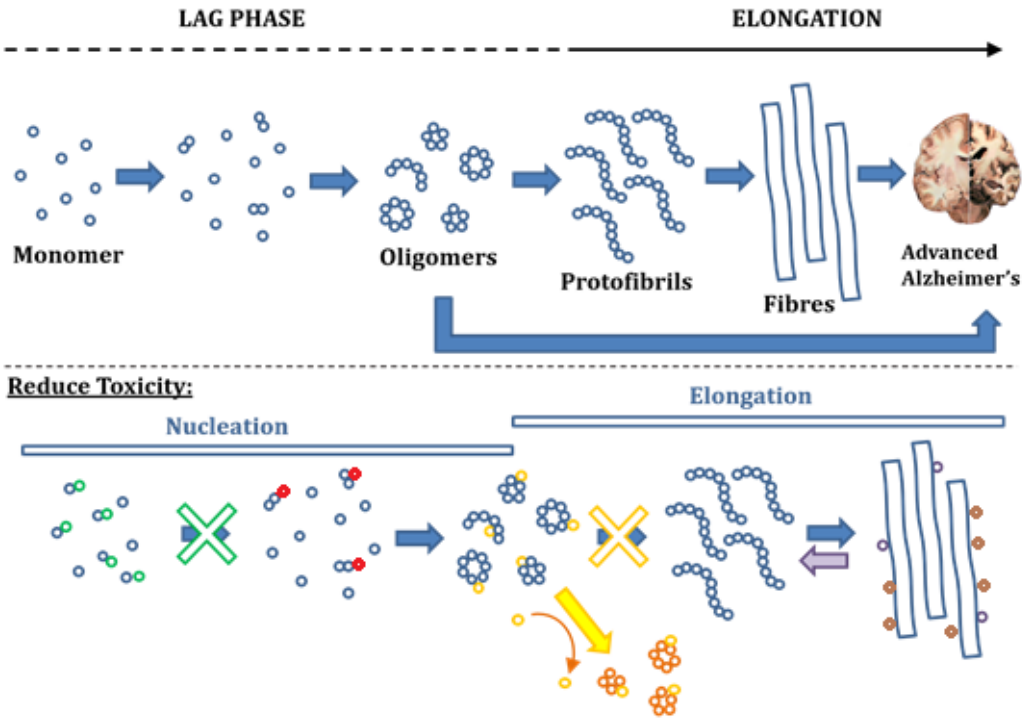

Figure 4.1. The Aggregation of Aβ$_{1-42}$ and Different Methods of Modulation. Schematic illustrating the assembly pathway of Aβ$_{1-42}$ into amyloid fibrils, from the formation of a nucleus through the production of oligomeric species before the assembly of protofibrils and finally mature fibrils, demonstrating the presence of both fibrils and oligomers in advanced AD. Mechanisms for reducing Aβ$_{1-42}$ toxicity at different points in the aggregation process are highlighted, including the formation of a 1:1 complex (green), binding to nuclei (red), binding to oligomers (yellow), dissociation of amyloid (purple) and covering the fibril surface to prevent the use of its surface as an aggregation template (brown) (Adapted from Williams, 2015 with modifications).

Transthyretin and Aβ

Transthyretin is one of several proteins which have been found inside Alzheimer's plaques along with Aβ, is a major constituent of the CSF and can sequester Aβ (Schwarzman *et al.*, 1994). Several studies using either animal models or cell culture supported the TTR's interaction and protective ability against Aβ cytotoxicity. *In vitro* studies then showed a direct inhibitory effect of wild type and mutant TTRs on Aβ aggregation. Although there is clear evidence for the interaction between WT TTR and Aβ, *in vitro* studies have given contradictory results regarding which species of Aβ and TTR are interacting when different methodologies are used. In general, methodologies depending on immobilising one of the proteins like surface plasmon resonance (SPR) and ELISA show that TTR tetramers bind all forms of Aβ (Costa *et al.*, 2008) with preferential binding of TTR tetramers to Aβ aggregates compared to Aβ monomers (Du and Murphy, 2010) and fibrils (Yang *et al.*, 2013a). However, liquid phase NMR experiments showed that TTR tetramers but not monomers bind to Aβ monomers and both TTR tetramers and monomers bind to Aβ aggregates (Li *et al.*, 2013a).

The efficiency of the inhibition remains questionable in the absence of a detailed characterisation of the inhibition of fibril formation in the liquid phase. This chapter is a study of the inhibitory effect of WT and mutant TTRs on Aβ monomers, oligomers and fibrils. To achieve these goals, a number of TTR mutants with different kinetic and thermodynamic stabilities were chosen and their inhibitory effect against different species of Aβ were investigated and compared to the human cystatin C mechanism of inhibition of Aβ fibrillisation (chapter 5).

TTR mutants used in the study

More than 100 natural TTR mutants have been described. Most of these mutants are less stable as tetramers and more amyloidogenic than the wild-type (McCutchen *et al.,* 1995). Four mutants have been used in this study, 3 natural and 1 model (Figure 4.2). All the mutants used exhibited a less stable tetramer and monomer to different degrees, except V122I which has more stable monomers. TTR mutants with unstable tetramers have been shown to be the best inhibitors of Aβ fibrillisation. However, it is not clear whether it is unstable tetramers that are effective or unstable monomers. In order to find whether only unstable tetramers are necessary for inhibition or unstable monomer as well is an important factor. The available data on the stability of WT TTR and its mutants is often difficult to compare due to the difficulty in resolving different unfolding and refolding transitions in this multimeric protein and the different cooperativity of folding observed in different mutants. A summary of the characteristics of the mutants chosen as a result of their different multimeric stabilities is described below (Table 4.1).

1. S85A, is a model mutant TTR which assembles into less stable tetramers (Yang *et al.,* 2013). S85 is one of the retinol binding residues on the EF loop. CD spectra and tryptophan fluorescence data show that S85A retains a native or near-native secondary and tertiary structure. In contrast, ANS fluorescence indicates a loss of the thyroxine-binding channel in this mutant. S85A assembles into a tetramer but these tetramers are less stable than their WT counterparts (Du *et al.,* 2012). Size-exclusion chromatography shows a significant population of monomers at 10^{-5}M.

2. The V122I TTR variant causes a form of late onset familial amyloid cardiomyopathy. The V122I mutant protein is again less stable as a tetramer compared with WT TTR (ΔG_{diss} = +7 ± 1 kcal mole^{-1}) whereas monomers are at least as stable as for the WT TTR.

V122I tetramer destabilisation and monomer stability counteract each other to some extent, leading to the observed similar overall thermodynamic stability of V122I and WT TTR. At physiological concentrations the amount of unfolded V122I monomer (0.15 nM) is 3-fold higher than for WT TTR (0.05 nM). The rate of V122I dissociation is 2-fold faster than WT ($t_{½}$= 19 h vs. 41 h for WT TTR) (Hurshman Babbes *et al.*, 2008).

3. V30M is the most common cause of familial amyloid polyneuropathy (FAP) in heterozygotes (Sanchez-Ruiz, 2010). The V30M stability is lower than WT and this perhaps accounts for its greater capacity to inhibit fibrillogenesis (Li *et al.*, 2013a). The formation of a V30M tetramer happens at a much slower rate than for WT-TTR $t_{1/2}$ is 68 h, compared with 41 h for WT TTR (Hurshman Babbes *et al.*, 2008), which could enhance monomer accumulation (Jesus *et al.*, 2012), resulting in a higher inhibitory effect against Aβ aggregation. V30M monomer is destabilized by ∼2.5 kcal/mol relative to WT TTR monomer, with a ΔG_{unfold}^{H2O} of 3.0 ± 0.2 kcal/mol and compared with a ΔG_{unfold}^{H2O} for WT TTR monomer of 5.5 ± 0.8 kcal/mol under the same conditions (Hurshman Babbes *et al.*, 2008).

4. A25T is a mutant which causes central nervous system (CNS) amyloidosis. A25T is one of the most unstable known tetramers of TTR. The A25T TTR protein exhibits a k_{diss} of 5.4 x 10^{-3} s^{-1}, which equates to a half-life ($t_{1/2}$) of only 2.1 minutes, 1200-fold faster than that of WT TTR. The A25T tetramer is the least stable of all other TTR variant published to date. The A25T mutation significantly destabilises both the TTR quaternary and tertiary structure compared with WT and the other FAP variants (Sekijima *et al.*, 2003). A25T monomer ΔG_{unfold}^{H2O} = 1.8 ± 0.2 kcal mol^{-1} (M urea)$^{-1,}$ and $-m_{unfold}$ = 1.1 kcal mol^{-1} (M urea)$^{-1}$ (Hurshman Babbes *et al.*, 2008). The free energy of monomer

unfolding of A25T is 2.80 kcal/mol (C_m = 2M urea), which indicates that the A25T tertiary structure is less stable than that of WT TTR (C_m = 3.4 M urea) (Sekijima *et al.*, 2003).

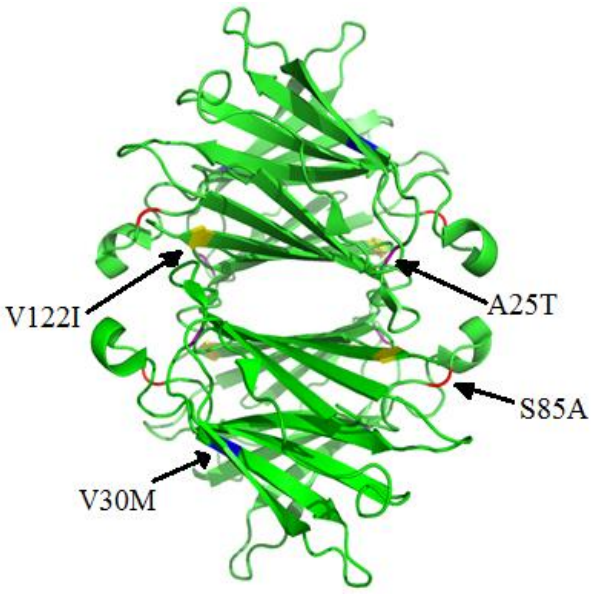

Figure 4.2. The crystal structure of tetrameric TTR with the mutated residues coloured and labelled. The structure adapted from (Klabunde *et al.*, 2000). The structure made by using Pymol (DeLano, UK).

Parameters	WT	V122I	V30M	A25T	S85A
ΔG_{Diss} (kcal mole^{-1})	-32.8 ± 2.2 [(a)]	-25.6±1.0 [(a)]	1.5 M Urea vs 3M for WT at 1.44 µM [TTR]	Very aggregation prone	n. a.
k_{diss} (s^{-1}) t½ (min)	$4.67*10^{-6}$ ± 2460 (41hrs)	10^{-5} ± 1140 (19hrs) [(a)]	$2.8 * 10^{-6}$ ± 4080 (68hrs)	$5.4 * 10^{-3}$ 2.1 (4) [(c)]	n. a.
k_{ass} (s^{-1} M^{-3}), k_1 U→D and k_2 D→T (both $M^{-1}s^{-1}$)	$2.2*10^{6}$ [(a)] $8.1*10^{3}$ [(a)]	n. a.	$1.8*10^{3}$ [(b)] $1.9*10^{2}$ [(b)]	n. a.	n. a.
K_{Diss} (M^3)	10^{-24} [(a)]	10^{-18} [(a)]	Very slow to dissociate	n. a.	10^{-16}
m_{Diss} (kcal mole^{-1} M^{-1})	-2.7± 0.1 [(a)]	-1.5± 0.1 [(a)]	n. a.	n. a.	Very unstable monomers, probably unfolded, open door for Aβ binding site
C_{mDiss} (M)	3.3 M at 1.44 µM [(a)]	n. a.	1.5 M at 1.44 µM	n. a.	
ΔG_{unf} (kcal mole^{-1})	-4± 0.5 [(a)] M-TTR is -5.5±0.8	-5.1± 0.2 [(a)] stable monomers	-1.5 (M-TTR equiv is -3±0.2)	-1.8± 0.2[a] (at low [TTR], 0.7-7µM) Or -2.8 [(c)]	
$K_{U/F}$	$1.3*10^{-3}$	$2.0*10^{-4}$	$8.2*10^{-2}$	$5.0*10^{-2}$	n. a.

m_{unf} (kcal mole^{-1} M^{-1})	-1.4±0.4 [(a)]	-1.6±0.5 [(a)]	n. a.	n. a.	n. a.
C_{munf} (M urea)	3.4 [(a)]	n. a.	n. a.	2	n. a.
ΔGoverall (kcal mole-1)	-48.8	-56.1	n. a.	n. a.	n. a.
Koverall	10^{-27}	10^{-23}	n. a.	n. a.	n. a.

n. a. = not available

Table 4.1. A summary of the characteristics of the WT and mutant TTRs chosen as a result of their different multimeric stabilities. [(a)] (Hurshman Babbes *et al.*, 2008), [(b)] (Jesus *et al.*, 2012), [(c)] (Sekijima *et al.*, 2003).

4.2. Materials and Methods

Aβ monomers for thioflavin T experiments were prepared and fibrillised as described in chapter 2.

4.2.1. Addition of TTRs to Aβ

TTR stocks were kept in PBS (50 mM Na_2HPO_4/NaH_2PO_4, 150mM NaCl, 2mM NaN_3, pH 7.4) at -20 °C. TTR stocks were thawed at room temperature, then filtered through 100KD filters to remove any aggregated structures. TTR solutions were then diluted by adding PBS to the correct final concentration then added directly to the lyophilised Aβ, to prevent the peptide from forming low molecular weight species before the addition of TTR. 100 µl of the mixture was then added to 96 half-well plates and incubated at 37C° with shaking for 10 seconds before taking readings at 5 minutes intervals.

4.2.2. Addition of TTR at different time points

Aβ fibrillisation was started as described previously. After 5 minutes or 1 hr of incubation, 5 µl aliquots of 220 µM of TTRs were added to 95 µl of 11 µM Aβ at each of the time-points to produce a 100 µl sample of 11 µM TTRs and 11 µM Aβ. Controls where PBS buffer was added to the Aβ reactions were also run. The aggregation reaction was then left to proceed by incubation of the plate in the plate reader.

4.2.3. Purification of fibrillar $A\beta_{1-42}$ fibril

After one day of incubation, the produced $A\beta_{1-42}$ aggregates were pelleted by centrifugation at 13, 000 rpm for 20 minutes. The pelleted fractions were re-suspended in 2% SDS to dissolve any non-fibrous aggregates (amorphous and oligomers). The SDS re-suspended fibrils were pelleted again, and then washed twice by re-suspension in PBS, to remove any residual SDS. The fibrils were then re-suspended in a small amount of phosphate buffer and used directly. The concentration of the Aβ fibril fraction was determined by measuring the concentration of soluble Aβ in the supernatant after the 1st and 2nd centrifugation steps and subtracting it from the total monomer concentration of Aβ used at the start of fibrillisation (This method is adapted from Davis, 2013, with modifications).

4.2.4. TTRs binding to $A\beta_{1-42}$ fibrils

Different molar concentrations of TTRs were incubated with different amounts of purified Aβ fibrils for 20 minutes at 37°C. Then the mixture was centrifuged at 13, 000 rpm for 20 minutes to pellet down the fibrils and bound TTR. The concentration of TTR in supernatant was measured at 280 nm. The percentage of disappeared TTR was determined by subtraction of the TTR concentration in the supernatant from the initial TTR concentration.

4.2.5. Defibrillisation of Aβ fibrils by TTRs

Different molar concentrations of TTRs were mixed with different amounts of purified Aβ fibrils. 10μM of ThT was added to the mixture then 100 μl of the mixture was added to microplate wells and incubated at 37ºC for 24 hrs. The ThT fluorescence was recorded as described in chapter 2.

4.2.6. TTR addition to Aβ seeds

Aβ fibrils were purified as described previously then fibril sonicated for 30 minutes to create short fibrils (seeds). The concentration of seeds was determined from the initial Aβ monomer concentration used for making the fibrils. The seeds were mixed with different concentrations of TTR in PBS. Then Aβ monomers added to the mixture. The mixture was added to the plate reader and the thioflavin T fluorescence followed as described previously.

4.2.7. Analytical Size Exclusion Chromatography (SEC)

The $A\beta_{1-42}$ aggregation was monitored in both the absence and presence of TTR by using size-exclusion chromatography in PBS on an analytical gel filtration column Superdex 200 (GE Healthcare, UK). The protein exclusion limit Superdex column is 1,300 kDa, with a separation range between 10 and 600 kDa. 180 µl samples were analysed and the column was run at 0.5ml/minute for 1hr. Samples from thioflavin T experiments performed using the plate reader were collected and analysed after 24 hrs from starting the reaction. The OD was measured at either 280 nm or 230 nm.

4.3. Results

4.3.1. Aβ Fibrillisation

$A\beta_{1-40}$ and $A\beta_{1-42}$ fibril formation was monitored using thioflavin T fluorescence (Figure 4.3). The Aβ fibrillisation reactions monitored by thioflavin T assays are consistent with the nucleation-dependent elongation model of amyloid assembly (Chapter 1; section 1.9) but do not show the concentration dependence implied by this model. Instead the polystyrene surface of the microplates drives the reaction in a manner which is dependent on the available surface area and thus unchanging for all the reactions observed (chapter 3 and Taylor *et al.*, manuscript in preparation).

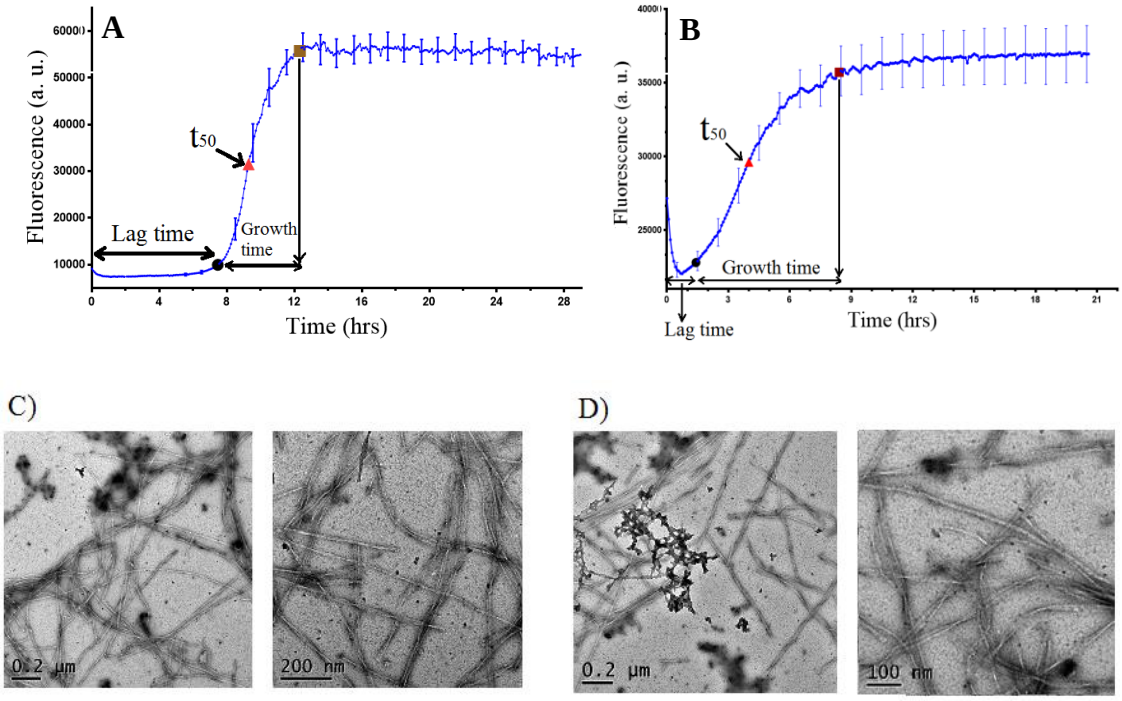

Figure 4. 3. Thioflavin T curves and EM micrographs of Aβ$_{1-40}$ and Aβ$_{1-42}$ fibrillisations. A) Aβ$_{1-40}$, B) Aβ$_{1-42}$. Error bars displaying the standard error of the mean (SEM). t_{lag}, t_{50} and t_{growth} times are indicated. C) EM micrographs of Aβ$_{1-40}$ after 24hrs of fibrillisation, D) EM micrographs of fibrillised Aβ$_{1-42}$ after 24hrs of incubation, scale bars are indicated.

Most published studies have extracted only the half times (t_{50}) for the Aβ fibrillisation reactions. Despite the greater reproducibility of t_{50}, t_{50} is a mix of the lag time (t_{lag}) and growth time (t_{growth}) and these two phases are completely different in their nature. In the current study we calculated lag time, t_{50} and growth times separately, in order to be able to show the effect of TTRs on the primary and secondary nucleation mechanisms and t_{50} to be comparable to the literature. From the Aβ growth curves, the t_{lag}, t_{50} and t_{growth} were determined. The t_{lag} for aggregation is the time when the initial nuclei of aggregation are forming, which is calculated here as the time point when the fluorescence reaches 5% of its final amplitude. t_{50} corresponds to the time for mid growth phase and is the time when the fluorescence reaches its 50% value, this value calculated depending on the lowest and highest fluorescence points during the path of Aβ aggregation. The t_{growth} is the time from

the start of fibrillisation (or end of t_{lag}) to the end of fibrillisation (or reaching equilibrium or plateau), calculated by subtracting t_{lag} from the time when the fluorescence reaches 95% of its maximum value. t_{growth} represents the time needed by Aβ monomers to reach equilibrium with fibrils. The t_{lag} for $A\beta_{1-40}$ fibrillisation were much longer than for $A\beta_{1-42}$, and were 10 ± 2.8 hrs and 1.54 ± 0.3 hrs, respectively under our standard conditions at 11μM peptide. The $A\beta_{1-40}$ t_{50} value was 13.0 + 3.0 hrs while for $A\beta_{1-42}$ was about 4.2 ± 0.6 hrs. The t_{growth} for $A\beta_{1-40}$ was 4.5 ± 0.7 hrs compared to 4.7 ± 0.7 hrs for $A\beta_{1-42}$. This suggests that nucleation events are rarer for $A\beta_{1-40}$ compared with $A\beta_{1-42}$ peptides but that once growth is under way, both elongation and secondary nucleation events must be similar. It is worth mentioning that at the begining of $A\beta_{1-42}$ fibrilisation the fluorescence is decreasing for about 30 minutes which might be due to the formation of non-fibrous but thioflavin T positive species which dissolve and then start aggregation to take fibrillisation pathway.

The morphology of the produced $A\beta_{1-40}$ and $A\beta_{1-42}$ fibrils was investigated by transmission electron microscopy. Electron micrographs showed that mature fibrils had formed in both preparations after 24 hours (Figure 4.3C&D). The fibrils are long, straight and unbranched. There appeared to be very little structural variation between different preparations shown throughout this chapter.

4.3.2. Addition of WT TTR to $A\beta_{1-42}$ Fibrillisation

Thioflavin T Time-course

The kinetics of $A\beta_{1-42}$ fibrillisation were monitored in the presence of different molar ratios of WT TTR in the standard conditions described earlier, with a fixed $A\beta_{1-42}$ concentration of 11 μM, as shown in Figure 4.4. Different concentrations of TTR were tested ranging from 11 μM (stoichiometric concentrations of $A\beta_{1-42}$) to 1 μM (11 times less than the concentration of $A\beta_{1-42}$). Near equimolar concentrations (9μM) of WT TTR

were needed to completely supress thioflavin T fluorescence, suggesting complete inhibition of fibril formation. Smaller ratios of WT TTR lengthened the Aβ fibrillisation time in a concentration dependant manner. Low concentrations of WT TTR (1 µM) do not appear to have a significant effect on Aβ aggregation with the curves showing a similar t_{lag} (1.56 ± 0.12 hrs p= 0.105 ns), t_{50} (3.34 ± 0.30 hrs p=0.15ns) and t_{growth} values (5.84 ± 1.48 hrs p<0.05=0.024*). Intermediate concentrations of WT TTR (2, 4 and 7.5 µM) appeared to have a significant effect on Aβ aggregation with the curves showing a significant increase in t_{lag}, t_{50} and t_{growth} in a concentration dependant manner (Figure 4.4 and table 4.2). Compared with the t_{lag}, the t_{growth} did not increase to the same extent, although it did increase with concentration. The t_{growth} increased by a factor of 1.2-2.2 times the control in the presence of 1 to 7.5 µM TTR.

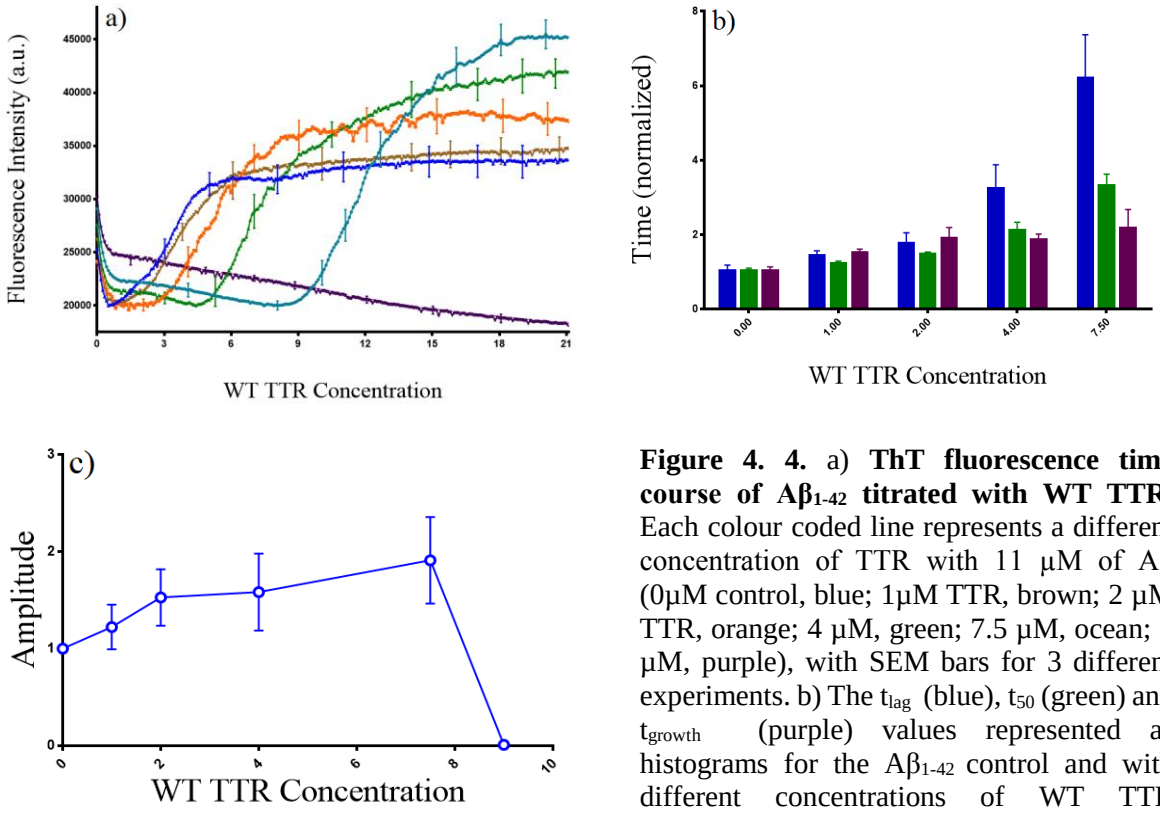

Figure 4. 4. a) **ThT fluorescence time course of $A\beta_{1-42}$ titrated with WT TTR**. Each colour coded line represents a different concentration of TTR with 11 µM of Aβ (0µM control, blue; 1µM TTR, brown; 2 µM TTR, orange; 4 µM, green; 7.5 µM, ocean; 9 µM, purple), with SEM bars for 3 different experiments. b) The t_{lag} (blue), t_{50} (green) and t_{growth} (purple) values represented as histograms for the $A\beta_{1-42}$ control and with different concentrations of WT TTR normalised, with error bars showing the sem. c) The amplitude of the growth curves in the presence of different concentrations of WT TTR normalised to one (Aβ control) with sem bars.

WT TTR conc. (μM)	Normalized t_{lag} (hrs)		Normalized t_{50} (hrs)		Normalized t_{growth} (hrs)	
	Mean± SEM	p> 0.05	Mean± SEM	p> 0.05* p<0.01*	Mean± SEM	p> 0.05
1	1.56 ± 0.12	0.105 ns	3.34 ± 0.30	0.15ns	1.2 ± 0.2	0.024*
2	3.0 ± 0.9	0.0739 ns	5.3 ± 1.1	0.007**	1.8 ± 0.37	0.039*
4	3.2 ± 0.6	0.0252*	5.9 ± 1.0	0.006**	2.1 ± 0.5	0.02*
7.5	6.8 ± 1.35	0.0215*	9.9 ± 1.7	0.045**	2.2 ± 0.4	0.113ns

Table 4.2. The mean of Normalized t_{lag}, t_{50} and t_{growth} values of Aβ fibrillisation (11μM) in the presence of different concentrations of WT-TTR with the calculated standard errors and p-values.

Unexpectedly, at the end of reaction (after reaching plateau), the amplitude of thioflavin T signal was slightly higher in the presence of the different concentrations of TTR. The intensity was slightly higher in the presence of (1μM) of TTR than in its absence and significantly higher in the presence of (2, 4 and 7.5 μM) of TTR (Figure 4.4 C). The increase in thioflavin T fluorescence could not be attributed to the independent formation of TTR amyloid because, when incubated alone in these conditions, WT TTR does not form fibrils and there is no increase in thioflavin T fluorescence. Past a threshold TTR, $A\beta_{1-42}$ no longer fibrillises and the amplitude therefore drops to 0.

4.3.3. Electron Microscopy

Although the reductions in thioflavin T fluorescence suggest that WT TTR inhibits Aβ fibril formation, these changes could also be due to other factors such as changes in morphology and production of thioflavin T negative species. TEM was employed to analyse the morphology of the produced structures at the end of the incubation of Aβ in the presence of a near equimolar concentration (9μM) of WT TTR. Figure 4.5 shows representative examples of electron micrographs of these different preparations after 24

hours. Along with mature fibrils, small amounts of amorphous aggregates also form in the Aβ control samples. The fibrils are long, straight and unbranched.

Although changes in thioflavin T fluorescence suggest that TTR is completely inhibiting $A\beta_{1-42}$ fibril production at equimolar concentration of WT TTR, a small number of single fibrils are present along with large amounts of amorphous aggregates. Re-investigation of this reaction mixtures after long periods of time (months) did not show the formation of large quantities of mature fibrils. Instead a large amount of amorphous aggregate is present along with small amounts of fibrils. In the presence of WT TTR, the most likely explanation is that an off-pathway species is formed and further associates to form large unstructured aggregates. The lack of fibrils even after extended periods of incubation suggests these species are no longer thermodynamically favoured.

a)

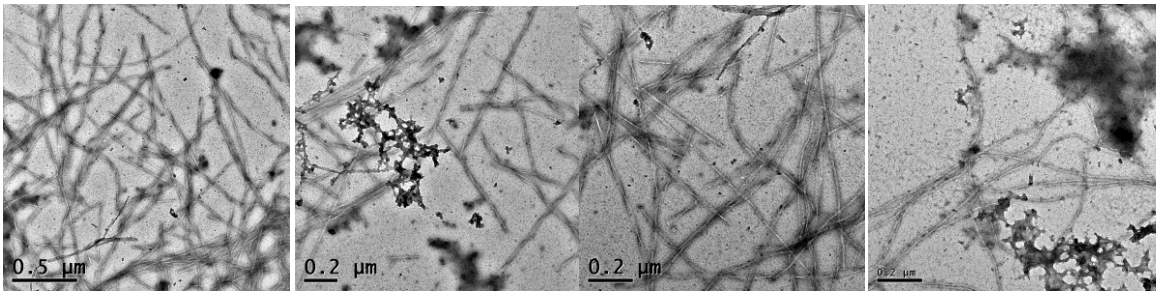

b)

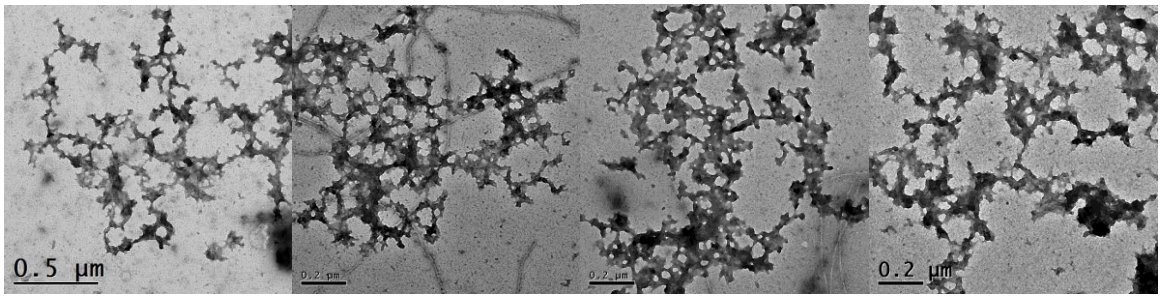

Figure 4.5. Electron micrographs of $A\beta_{1-42}$ in the presence and absence of near equimolar concentrations of WT TTR after 24 hrs. a) Aβ control (11µM), b) Aβ in the presence of 9 µM of WT TTR. The scale bars are indicated.

4.3.4. Analytical Size Exclusion Chromatography (SEC) for $A\beta_{1-42}$ and WT TTR

Figure 4.6 shows SEC elution traces of samples obtained from the fibrillisation reactions of $A\beta_{1-42}$ in the presence of different concentration of wild type TTR after 24hrs of incubation. There are several peaks observable in addition to the tetrameric TTR peak at 28 min and the small monomeric Aβ peak just about detectable at 38.6 min, which is just within the separation range for the column: although Aβ is only a 4KDa peptide, the unfolded nature of the monomer means that it behaves more like a 15 KDa globular protein and is resolvable here. In all reactions, a large peak is observed at the void volume of the column (13min) and represents species in excess of 600kDa but that are not filtered out by the in-line filter, which suggests it was smaller than 13 MDa. This peak represents the aggregated structure larger than 600 KDa, wich could be pure Aβ fibrils or amorphous aggregates or any of them bound to TTR. A further peak at 36.7 mins is representative of large oligomeric species which adhere to the column and are retarded (Williams, 2014). DMSO and buffer peaks appeared at 40.3 and 44 minutes. Aβ monomer, DMSO and buffer peaks were characterised by loading monomeric Aβ and DMSO separately on the column.

The height of the 13 min peak is 50% higher in the $A\beta_{1-42}$ control reaction compared to reactions in the presence of 4 and 7μM concentrations of TTR, and about twice the height of the aggregated structure peak in the presence of 1μM WT TTR. This is consistent with the thioflavin T data which indicates that the proportion of fibril produced by Aβ was relatively higher in the presence of the higher concentrations of TTR, and further confirmed that TTR only delays the lag time of the Aβ aggregation but unless the fibrillisation is started a large amount of fibrils produced at the end. Even in the presence of near equimolar (9 μM) concentration of TTR, the height of the aggregated structure peak was still nearly half of the control.

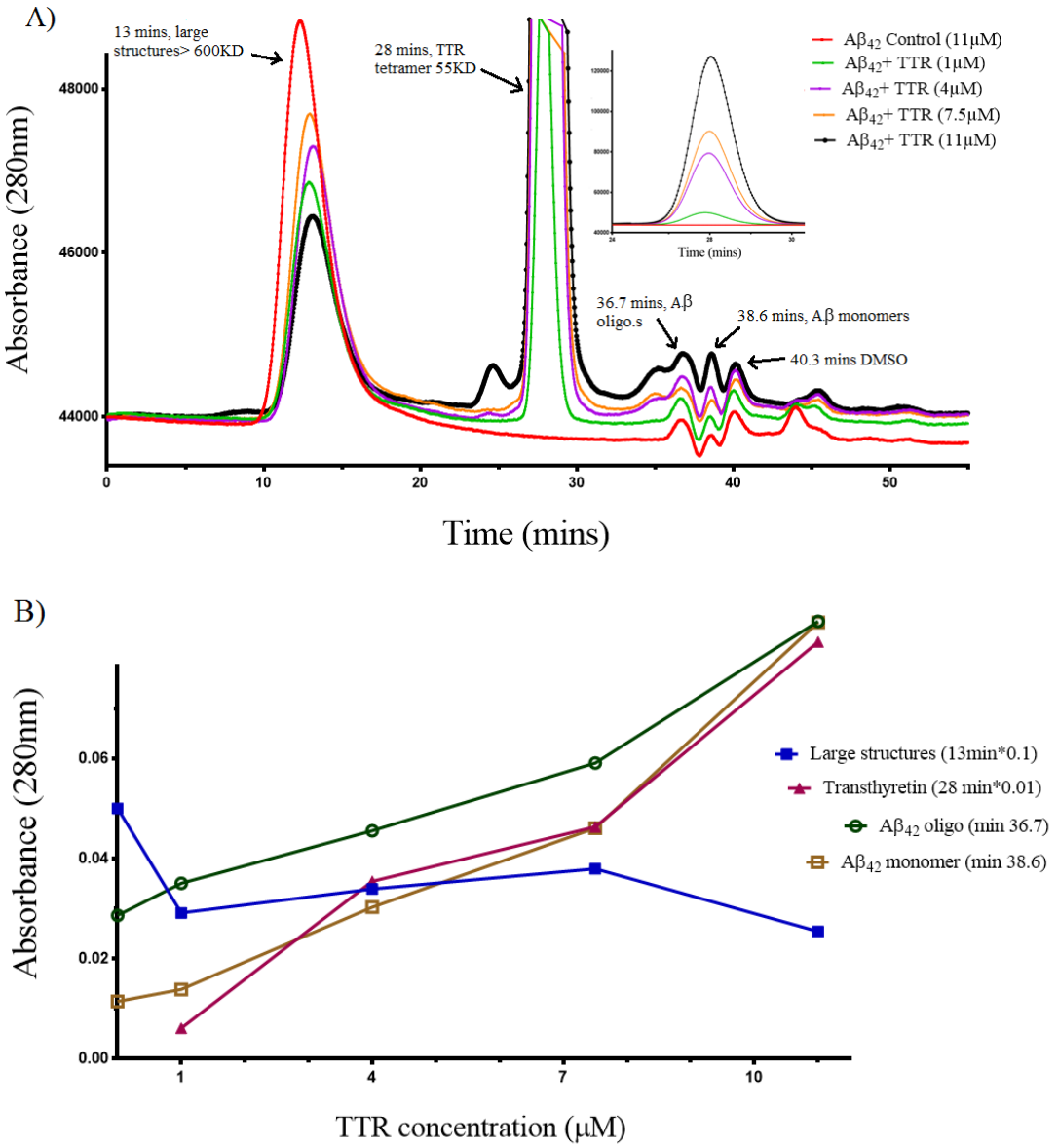

Figure 4.6. SEC of $A\beta_{1-42}$ fibrillisation reactions in the presence of different concentrations of WT TTR. (A) SEC elution profiles of $A\beta_{1-42}$ fibrillisation in the presence of different TTR concentrations after 24 hours. The peak at 13 minutes indicates aggregated structures, and the peak at 28 minutes indicates TTR tetramer. Colours represent different TTR concentrations (0μM control, red; 1μM TTR, green; 4μM, magenta; 7.5μM, orange; 11μM, black), the insert is TTR tetramer peaks. B) Variation of peak heights (absorbance) from incubations with different amounts of WT TTR. Peaks represented are aggregates at 13min (blue), TTR tetramers at 28min (purple), $A\beta_{1-42}$ monomers at 38.6 (brown) and $A\beta_{1-42}$ oligomers at 36.7min (dark green).

This supports the EM observation that even in the absence of a thioflavin T signal increase, there are still some aggregates formed, although the nature of these aggregates may be amorphous rather than fibrous.

This conclusion is supported to some extent by the presence of a concomitant increase in the height of peaks from smaller molecular weight species, which elute at 36 min and 38 min respectively and are likely representative of large oligomeric species which adhere to the column and are retarded (Williams, 2014). It is clear however that there is a large amount of optical density present in the 13 min peak that is not compensated by an increase in the 36 and 38 min peaks, so we examined the profiles for evidence of a TTR-Aβ complex. Tetrameric TTR elutes at 28 min and the observed peak heights are within error of the expected peak heights for the relative amounts of TTR in the absence of Aβ. This suggests that, while most of the TTR remains soluble, most of the Aβ species remain aggregated in one form or the other, but at a smaller molecular weight on average.

4.3.5. Addition of mutant TTRs to $A\beta_{1-42}$ fibrillisation reactions

V122I

The V122I mutant exhibits a less stable tetramer compared with WT TTR while the monomers are at least as stable as WT TTR. This mutant exhibits a 2 fold faster rate of tetramer dissociation compared to WT and so was used to investigate the efficacy of folded monomer in inhibition. The impact of V122I on the $A\beta_{1-42}$ fibrillisation was studied using thioflavin T fluorescence assays, where 11μM samples of $A\beta_{1-42}$ were fibrillised in PBS in the presence of different concentrations of V122I (1, 2, 4, 7.5, 10 and 11μM) (Figure 4.7 A). t_{lag}, t_{50} and t_{growth} values were calculated for all reactions (Figure 4.7 B). The results show that equimolar amounts of V122I are needed to completely inhibit Aβ fibril formation. Smaller ratios of V122I TTR increased the t_{lag} and the t_{50} of Aβ fibrillisation in a concentration dependant manner.

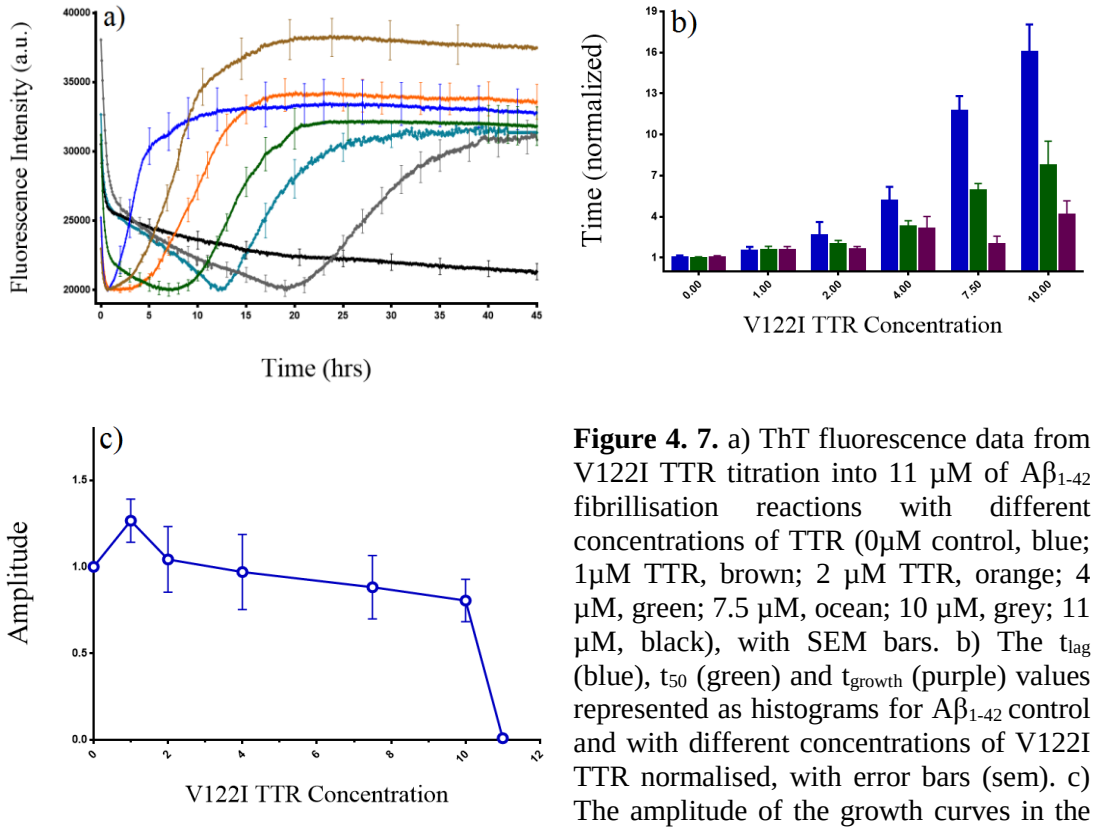

Figure 4. 7. a) ThT fluorescence data from V122I TTR titration into 11 µM of $A\beta_{1-42}$ fibrillisation reactions with different concentrations of TTR (0µM control, blue; 1µM TTR, brown; 2 µM TTR, orange; 4 µM, green; 7.5 µM, ocean; 10 µM, grey; 11 µM, black), with SEM bars. b) The t_{lag} (blue), t_{50} (green) and t_{growth} (purple) values represented as histograms for $A\beta_{1-42}$ control and with different concentrations of V122I TTR normalised, with error bars (sem). c) The amplitude of the growth curves in the presence of different concentrations of V122I TTR, normalised to the Aβ control, with error bars (sem).

As shown in table 4.3, the normalised t_{lag} increased in the presence of 1, 2, 4, 7.5 and 10 µM V122I as well as the normalised t_{50}, indicating a similar efficacy for inhibition as WT TTR. However, unlike with the WT, $A\beta_{1-42}$ fibrils still grow in the presence of 10 µM V122I (Figure 4.7). This result suggests that V122I is slightly less effective compared to WT TTR.

The amplitude of Aβ fibrillisation in the presence of V122I (Figure 4.7C) was slightly different for the Aβ control compared with the different concentrations of V122I. The amplitude increased in the presence of 1 µM (1.27 ± 0.13), and 2 µM (1.14 ± 0.12) of V122I. However, in the presence of higher concentrations 4 µM (1.0 ± 0.15), 7.5 µM (0.9 ± 0.2), 10 µM (0.8 ± 0.12) of V122I the amplitude generally decreased with the increase in V122I concentration, indicating that the bulk of fibril produced was different from

control Aβ. As with the WT, the amplitude shows a dramatic drop past a critical concentration of TTR, in this case at 10μM V122I, which is slightly higher than for WT.

V122I TTR conc. (μM)	Normalized t_{lag}		Normalized t_{50}		Normalized t_{growth}	
	Mean± SEM	p>0.05* p<0.01**	Mean± SEM	p> 0.05* p<0.01**	Mean± SEM	p> 0.05
1	1.5 ± 0.3	0.225ns	1.6+_0.3	0.19ns	1.58± 0.24	0.125ns
2	2.7 ± 0.9	0.18ns	2.0+_0.25	0.04*	1.6 ± 0.2	0.084ns
4	5.2 ± 1.0	0.041*	3.3+_0.4	0.94ns	3.1 ± 0.9	0.14ns
7.5	11.7 ± 1.1	0.002**	6.0+_0.52	0.0096**	2 ± 0.57	0.22ns
10	16 ± 2.0	0.005**	7.5+_1.8	0.042*	4.15 ± 1.0	0.085ns

Table 4.3. The mean of t_{lag}, t_{50} and t_{growth} normalized values of Aβ fibrillisation (11μM) in the presence of different concentrations of V122I-TTR with the calculated standard errors and p-values.

V30M

V30M is less stable than wild type transthyretin, perhaps accounting for its greater capacity to inhibit fibrillogenesis (Li *et al.*, 2013a). The formation of V30M tetramers also happens at a much slower rate than for WT-TTR, which will enhance monomer accumulation (Jesus et al, 2012), resulting in a higher inhibitory effect against Aβ aggregation. However, the lack of stability of the monomer (table 4.1.) may imply that the predominant species populated apart from the tetramer is an unfolded monomer.

The fibrillisation of 11 μM $Aβ_{1-42}$ was monitored in the presence of different concentrations of V30M (0.5, 1, 2, and 2.5μM) (Figure 4.8). The results show that substoichiometric concentrations (less than 1:4, 2.5 μM) of V30M are enough to completely inhibit Aβ fibril formation, which is 3-4 times less than the concentration of WT or V122I TTR needed to achieve the same effect. Smaller amounts of V30M TTR increased the t_{lag} and t_{50} of Aβ fibrillisation in a concentration dependent manner. While

the t_{lag} in the presence of 0.5 µM V30M was not significantly increased (table 4.4), in the presence of 1, 1.5 and 2 µM V30 µM, the lag times were significantly different from the control. This result shows that V30M is significantly more effective than both WT and V122I TTR.

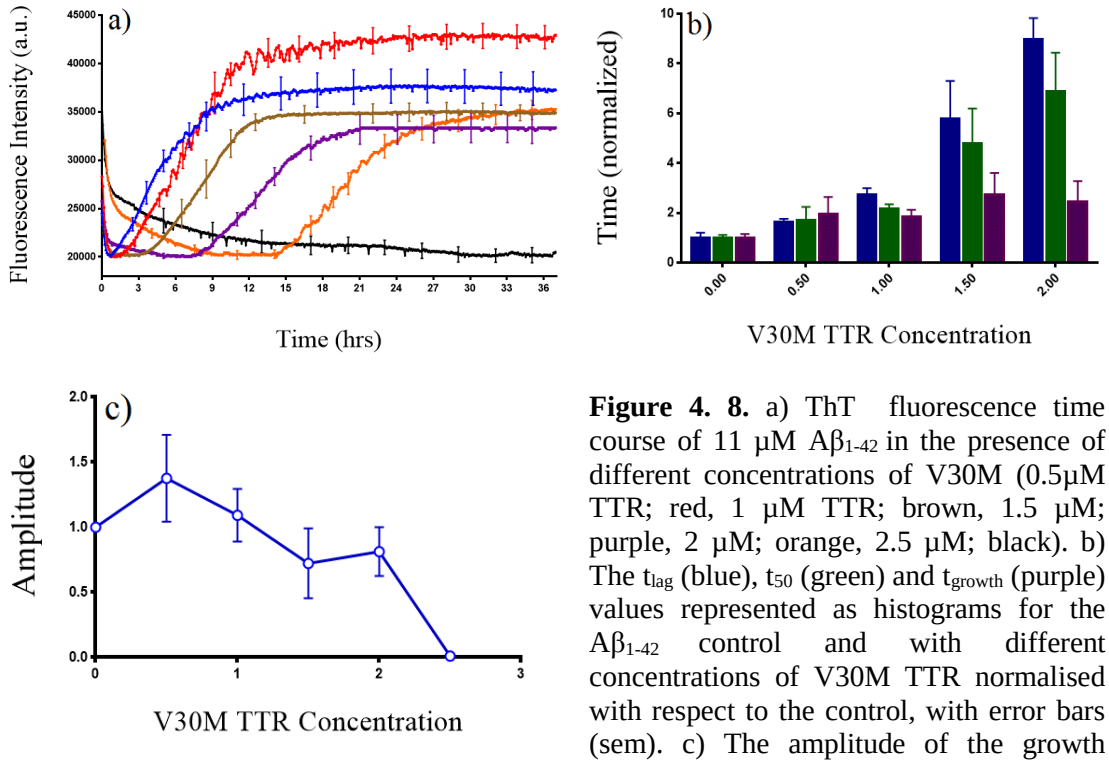

Figure 4. 8. a) ThT fluorescence time course of 11 µM $A\beta_{1-42}$ in the presence of different concentrations of V30M (0.5µM TTR; red, 1 µM TTR; brown, 1.5 µM; purple, 2 µM; orange, 2.5 µM; black). b) The t_{lag} (blue), t_{50} (green) and t_{growth} (purple) values represented as histograms for the $A\beta_{1-42}$ control and with different concentrations of V30M TTR normalised with respect to the control, with error bars (sem). c) The amplitude of the growth curves in the presence of different concentrations of V30M TTR normalised to the Aβ control, with error bars (sem).

The effect of V30M was greater on the t_{lag} compared with its effect on the t_{50} and t_{growth} (Figure 4.8.b) and (table 4.4). The increase in growth time was between 1.8 and 2.7 times the control in the presence of 0.5, 1, 1.5 and 2 µM V30M. However, these rates were not significantly different from the control. The results so far concur to say that the effect of TTR on the fibrillisation of $A\beta_{1-42}$ is principally on the nucleation phase and is enhanced greatly when TTR is unfolded rather than simply dissociated to monomers.

V30M TTR conc (μM)	Normalized t_{lag} (hrs)		Normalized t_{50} (hrs)		Normalized t_{growth} (hrs)	
	Mean± SEM	p> 0.05	Mean± SEM	p> 0.05* p<0.01*	Mean± SEM	p> 0.05
0.5	1.63± 0.13	0.024*	1.75 ± 0.5	0.26ns	2.0 0.7	0.23ns
1	2.7 ± 0.26	0.0037**	2.16 ±0.2	0.08*	1.9 0.3	0.06ns
1.5	5.8 ± 1.1	0.02*	4.8 ±1.4	0.11ns	2.7 ±0.9	0.19ns
2	9.0 ± 0.9	0.0083**	6.9 ±1.6	0.044*	2.5 ± 0.83	0.2ns

Table 4.4. The mean of normalized t_{lag}, t_{50} and t_{growth} values of Aβ fibrillisation (11μM) in the presence of different concentrations of V30M-TTR with the calculated standard errors and p-values.

The amplitude of $A\beta_{1-42}$ fibrillisation in the presence of V30M was also marginally different from the $A\beta_{1-42}$ control (Figure 4.8 C). While the yield was higher in the presence of 0.5 μM V30M, at higher concentrations of the inhibitor, it generally decreased until a cut-off value of 2μM beyond which no fibrillisation occurs.

A25T

A25T is one of the most unstable known tetramers of TTR (Table 4.1) and causes CNS myloidosis. A25T has a half-life ($t_{1/2}$) of only 2.1 minutes, with a k_{diss} of 5.4 x 10^{-3} s^{-1}, some 1200-fold faster than that of WT TTR (Hammarström et al, 2002). The A25T mutation significantly destabilises both the TTR quaternary and tertiary structure compared with WT and the other FAP variants (Sekijima et al., 2003).

11 μM $A\beta_{1-42}$ was fibrillised in the presence of different concentrations of A25T (0.5, 1, 1.5, 2, and 2.5μM) (Figure 4.9). Similarly to V30M, the results show that substoichiometric concentrations (2.5 μM) of A25T TTR were enough to completely inhibit Aβ fibril formation, 3-4 times less than the concentration of WT or V122I TTR needed to achieve the same effect. Smaller ratios of A25T TTR increased the t_{lag} and t_{50}

of Aβ fibrillisation in a concentration dependant manner. The t_{lag} was increased by a factor of 2 to 9 times in the presence of 0.5, 1, 1.5 and 2 µM A25T (Figure 4.9 b) and (table 4.5). t_{50} were increased accordingly to up to 7 times the control. This result shows that A25T TTR is far more effective than WT and V122I TTR.

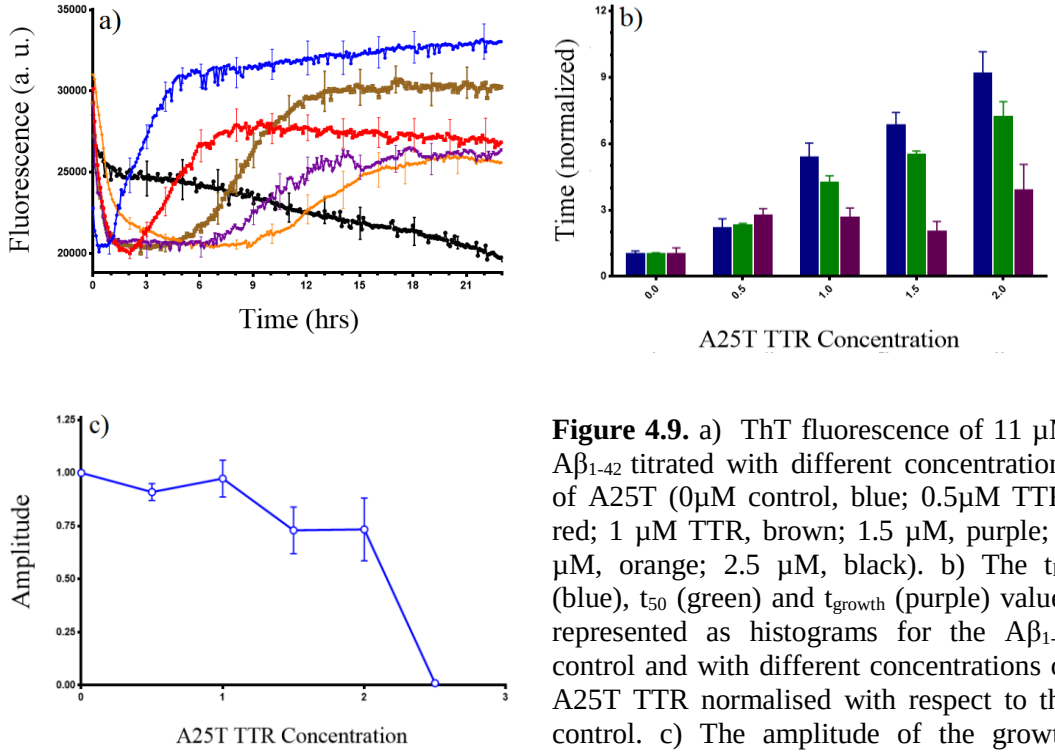

Figure 4.9. a) ThT fluorescence of 11 µM $A\beta_{1-42}$ titrated with different concentrations of A25T (0µM control, blue; 0.5µM TTR, red; 1 µM TTR, brown; 1.5 µM, purple; 2 µM, orange; 2.5 µM, black). b) The t_{lag} (blue), t_{50} (green) and t_{growth} (purple) values represented as histograms for the $A\beta_{1-42}$ control and with different concentrations of A25T TTR normalised with respect to the control. c) The amplitude of the growth curves in the presence of different concentrations of A25T TTR normalised to the Aβ control. All error bars are sem.

Slightly different to WT and all other mutants, the amplitude of Aβ fibrillisation in the presence of A25T TTR was lower than that of the Aβ control for all concentrations (table 4.5), and it generally decreased with the increase in A25T TTR concentration (Figure 4.9 C).

A25T TTR conc. (µM)	Normalized t_{lag} (hrs)		Normalized t_{50} (hrs)		Normalized t_{growth} (hrs)	
	Mean± SEM	p> 0.05 p<0.01**	Mean± SEM	p> 0.05* p<0.01**	Mean± SEM	p> 0.05*

0.5	2.2 ±0.42	0.16	2.3 ±0.1	0.0035**	2.8 ± 0.3	0.04*
1	5.4 ±0.7	0.015*	4.3 ±0.3	0.0042**	2.7 ±0.43	0.048*
1.5	6.8 ±0.58	0.005**	5.5 ± 0.17	0.0001***	2.0 ± 0.45	0.16ns
2	9.17 ±1.9	0.14ns	7.2 ± 0.7	0.06*	3.9 ± 1.17	0.2ns

Table 4.5. The mean of normalized t_{lag}, t_{50} and t_{growth} values of Aβ fibrillisation (11μM) in the presence of different concentrations of A25T-TTR with the calculated standard errors of mean and p-values.

S85A TTR

S85A is a model mutant TTR with the mutation in the EF loop. This mutant assembles into less stable tetramers. The EF loop has been suggested as a binding site to Aβ and as an Aβ sensor (Yang *et al.*, 2013a).

11 μM $Aβ_{1-42}$ was fibrillised in the presence of different concentrations of S85A (0.5, 1, 1.5, 2, and 2.5μM) (Figure 4.10). Similarly to V30M and A25T, the results show that substoichiometric concentrations (2.5 μM) of S85A TTR were enough to completely inhibit Aβ fibril formation, which is 3-4 times less than the concentration of WT and V122I TTR needed to achieve the same effect. However, smaller ratios of S85A TTR increased the t_{lag} and the t_{50} of Aβ fibrillisation in a concentration dependent manner, even more effectively compared to A25T and V30M. The t_{lag} increased by a factor of 4, 6, 8 and 11 times in the presence of 0.5, 1, 1.5 and 2 μM S85A respectively (table 4.6). The t_{50} increases accordingly between 1.5 and 3.5 times the control as S35A TTR concentrations rise to 2 μM. This result shows that S85A TTR is the best inhibitor in terms of increasing the t_{lag}. Even more strikingly than for the other TTRs, the t_{growth} stays unchanged compared to the control and in the presence of different amounts of S85A. These data show that S85A affects only the t_{lag}, with only a very small effect on the t_{growth}.

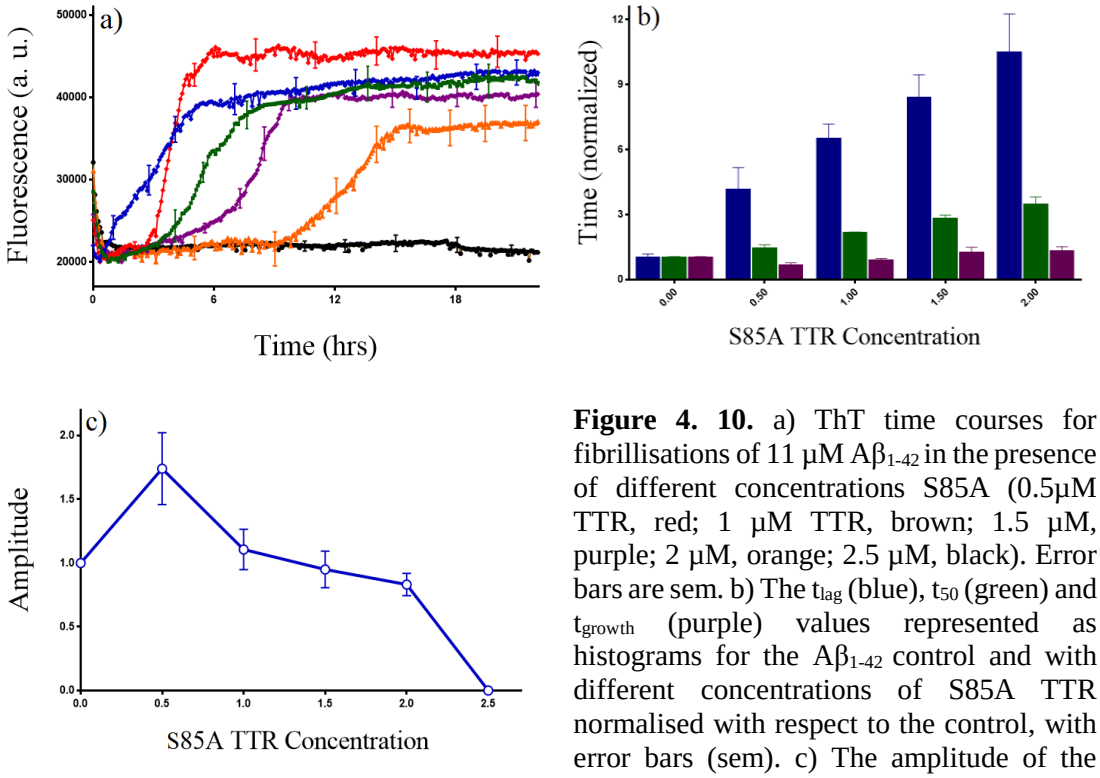

Figure 4. 10. a) ThT time courses for fibrillisations of 11 µM $A\beta_{1-42}$ in the presence of different concentrations S85A (0.5µM TTR, red; 1 µM TTR, brown; 1.5 µM, purple; 2 µM, orange; 2.5 µM, black). Error bars are sem. b) The t_{lag} (blue), t_{50} (green) and t_{growth} (purple) values represented as histograms for the $A\beta_{1-42}$ control and with different concentrations of S85A TTR normalised with respect to the control, with error bars (sem). c) The amplitude of the growth curves in the presence of different concentrations of S85A TTR normalised to the Aβ control, with error bars (sem).

The amplitude of Aβ fibrillisation in the presence of S85A TTR was higher than the control in the presence of 0.5 µM of S85A, however it then decreased with increasing S85A concentration (Fig. 4.10C and table 4.6).

S85A TTR conc. (µM)	Normalized t_{lag} (hrs)		Normalized t_{50} (hrs)		Normalized t_{growth} (hrs)	
	Mean± SEM	p> 0.05* p<0.01**	Mean± SEM	p> 0.05* p<0.01**	Mean± SEM	p> 0.05
0.5	4.15 ±1.0	0.08	1.5 ±0.16	0.09	0.65 ±0.12	0.09ns
1	6.5 ±0.67	0.0076**	2.14 ± 0.07	0.0006***	0.9 ±0.09	0.44ns
1.5	8.4 ± 1.1	0.016*	2.8 0.18	0.0035**	1.25 ±0.25	0.44ns
2	10.5 ± 1.8	0.031*	3.5 ±0.35	0.015*	1.3 ±0.21	0.27ns

Table 4.6. The mean of normalized t_{lag}, t_{50} and t_{growth} values of Aβ fibrillisation (11µM) in the presence of different concentrations of S85A-TTR with the calculated standard errors and p-values.

4.3.6. Comparing WT and mutant TTRs

t_{lag}, t_{50} and t_{growth} of $A\beta_{1-42}$ in the presence of different concentrations of WT and mutant TTR were calculated and plotted together to show the difference between the inhibition intensity of different mutants compared with WT (Figure 4.11).

The t_{lag} of $A\beta_{1-42}$ aggregation increases in a concentration dependent manner as a result of the addition of WT and all mutants. Near stoichiometric concentrations of WT and V122I were needed to completely inhibit Aβ aggregation, however 3-4 times less (only 2.5μM) of V30M, A25T and S85A were needed to do so. S85A was the most effective mutant for extending the lag time, followed by A25T> V30M> WT> V122I. This result indicates that, with the exception of V122I, all other mutants were more effective compared to WT TTR.

Regarding growth time, the results show that in general the TTRs are not as effective on growth time as they are on lag time. The order of effectiveness remains the same, however S85A has no any obvious effect on growth time and is less effective compared with WT and all other mutants. The observed t_{50}s of aggregation reflect a contribution from both lag and growth times, with the pattern of inhibition intensity generally the same except for S85A, which is less effective than A25T and V30M.

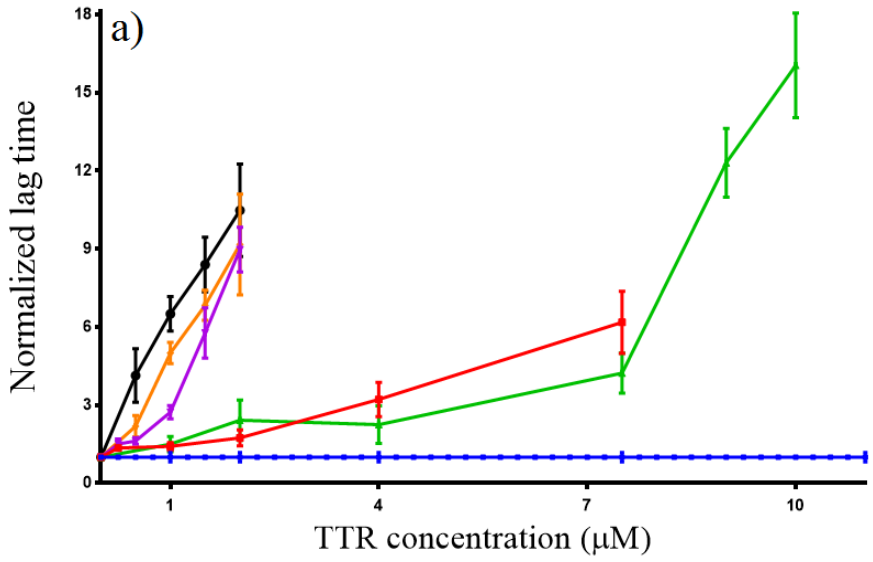

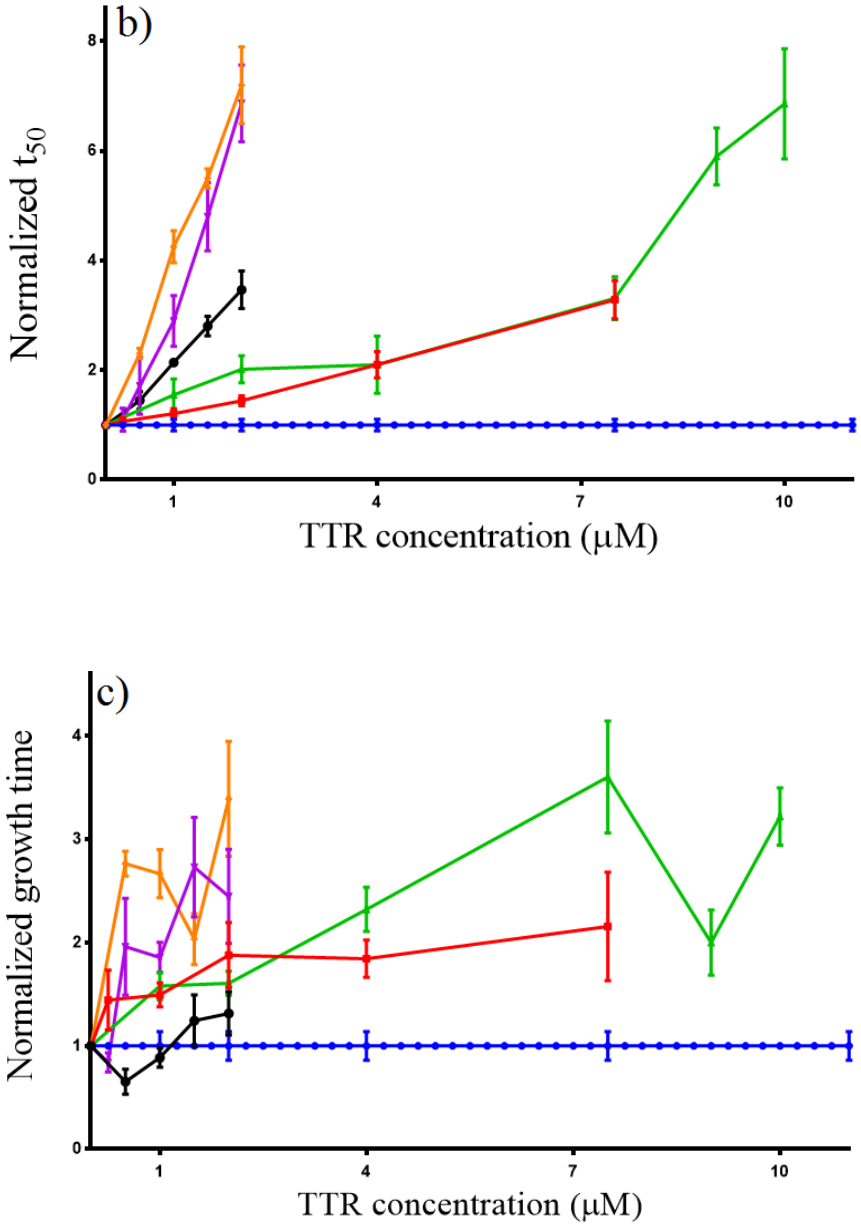

Figure 4.11. Lag, t50 and growth times for Aβ$_{1-42}$ fibrillisation in the presence of TTRs with respect to control Aβ$_{1-42}$ (in blue, 11 μM), for Aβ$_{1-42}$ in the presence of different concentrations of TTR (Red-WT, Green-V122I, Purple-V30M, Orange-A25T, Black-S85A) with error bars representing sem. Values are normalised with respect to the Aβ$_{1-42}$ control mean. a) Normalized lag time (t_{lag}), b) Normalised half time (t_{50}). c) Normalised growth time (t_{growth}).

4.3.7. Addition of TTRs to $A\beta_{1-40}$ Fibrillisation

Thioflavin T Time-course

The kinetics of $A\beta_{1-40}$ fibrillisation were monitored in the presence of different molar ratios of WT TTR in the standard conditions described earlier, with an $A\beta_{1-40}$ concentration of 11 µM (Figure 4.12). Different concentrations of WT TTR were tested ranging from 4 µM (33% of the concentration of $A\beta_{1-40}$) to 0.1 µM (~100 times less than the concentration of $A\beta_{1-40}$). A molar ratio of 1:5 WT TTR to $A\beta_{1-40}$ caused a complete reduction in thioflavin T fluorescence, suggesting that the fibril formation is completely inhibited in the presence of WT TTR. Smaller ratios of WT TTR to Aβ (~1:20 and ~1:10) have an effect on $A\beta_{1-40}$ aggregation with the curves showing significant increases in t_{lag}, and a delay in t_{50}.

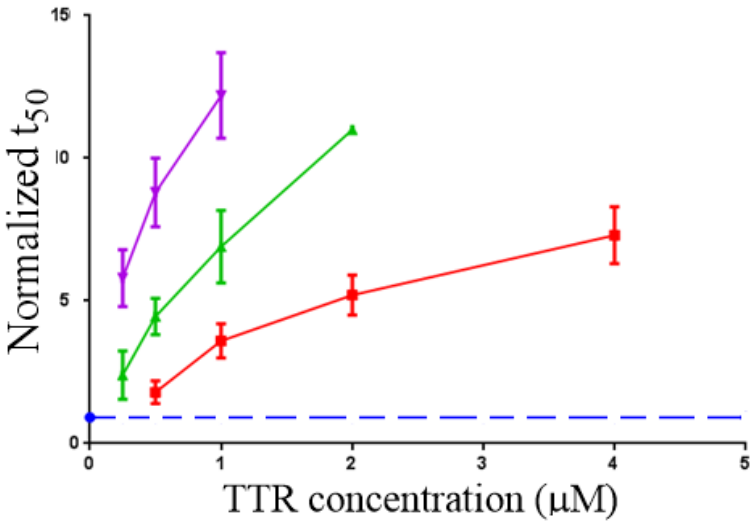

Figure 4.12. TTRs inhibit $A\beta_{1-40}$ fibril formation. WT (green), V122I (red) and V30M (purple) TTRs increased the aggregation t_{50} (i.e. decreased fibril formation) of 11 µM solution of monomeric $A\beta_{1-40}$ monitored by ThT fluorescence, in a concentration dependent manner within concentration ranges (0.2– 4 µM). The blue dashed line shows the t_{50} of $A\beta_{1-40}$ aggregation under the same conditions in the absence of TTR.

In order to investigate different inhibitory behaviours of different TTR mutants on $A\beta_{1-40}$ aggregation and obtain data comparable with $A\beta_{1-42}$, two of the mutants with different inhibitory effects on $A\beta_{1-42}$ fibrillisation were used. The V122I and V30M mutants were chosen. V122I was the least effective and V30M was the most effective (equally to A25T). The order of inhibition of WT and mutants are similar to that of TTRs on $A\beta_{1-42}$, except that the difference in the inhibitory effect of V122I with WT is more obvious. The inhibitory effect of V122I is significantly less than wild type TTR. In the case of $A\beta_{1-40}$, the inhibitory order is V30M>WT>V122I compared to V30M> WT≥ V122I in $A\beta_{1-42}$. Compared to WT TTR, a higher concentration of V122I (5 µM) was needed to completely inhibit $A\beta_{1-40}$ fibrillisation. Lower concentrations of V122I (1, 2, 4 µM) significantly lengthened the t_{50} of Aβ fibrillisation in a concentration dependant manner, however, the intensity of inhibition was smaller compared to WT and the difference between the effect of V122I and WT was significant. V30M was significantly more effective than WT. Only 1.5µM is needed to completely inhibit 11 µM of $A\beta_{1-40}$. Lower concentrations (0.25, 0.5 and 1 µM) extended the t_{50} for much longer time compared to WT TTR (Figure 4.12).

4.3.8. Addition of TTRs at different time points

In order to reveal whether TTRs bind to already aggregated species of Aβ, TTRs were added to $A\beta_{1-40}$ aggregation reactions at different time points and the reaction followed by ThT fluorescence (Figure 4.13). These time points were chosen to be at the beginning of the elongation phase or lag time (5 minutes) and later after (1 hr), where $A\beta_{1-40}$ aggregates are formed.

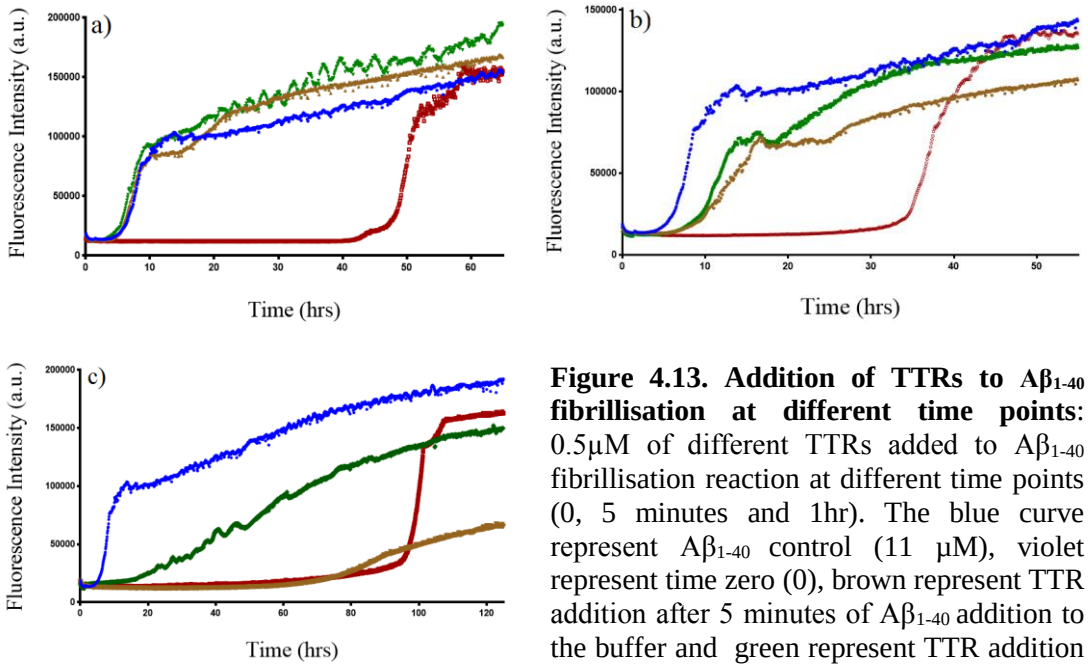

Figure 4.13. Addition of TTRs to $A\beta_{1-40}$ fibrillisation at different time points: 0.5µM of different TTRs added to $A\beta_{1-40}$ fibrillisation reaction at different time points (0, 5 minutes and 1hr). The blue curve represent $A\beta_{1-40}$ control (11 µM), violet represent time zero (0), brown represent TTR addition after 5 minutes of $A\beta_{1-40}$ addition to the buffer and green represent TTR addition after 1 hr of $A\beta_{1-40}$ addition to the buffer a) WT TTR, b) V122I TTR, c) V30M TTR.

The addition of TTRs after both 5 minutes and 1 hour caused differences in their inhibitory effects compared to their addition to fresh monomeric Aβ. The inhibitory capacity of WT TTR was nullified when added after 5 minutes and 1hr. The ability of the V122I variant to delay $A\beta_{1-40}$ aggregation markedly decreased when added after 5 minutes or 1hr. However, its addition after 5 minutes and 1hr were very similar. The inhibitory effect of V30M mutant reduced when added after 1 hr, however, its addition after 5 minutes did not reduce its inhibitory effect and was similar to its addition to fresh Aβ. These results indicate that WT affects Aβ aggregation mainly through monomers or very early events. The effect of the V122I mutant on aggregated structures is very small, while V30M can still affect smaller $A\beta_{1-40}$ species but not larger ones.

4.3.9. TTRs and Aβ fibrils

4.3.9.1. TTR binding to $A\beta_{1-42}$ fibrils

The surface of Aβ fibrils can catalyse production of new aggregates through working as a secondary nucleation template for the formation of new fibrils. Prevention of this

secondary nucleation process is of particular importance in the prevention of toxic oligomer production (Cohen *et al*., 2015). In order to investigate the ability of WT and mutant TTRs to bind to pre-made Aβ fibrils, the co-pelleting of TTRs with $A\beta_{1-42}$ fibrils was measured. TTRs were incubated with equimolar amounts of $A\beta_{1-42}$ fibrils (monomer equivalents) for 20 minutes. After incubation the mixtures were centrifuged at 13, 000 rpm for 20 minutes to pellet the fibrils and any bound TTR. The amount of TTR remaining in the supernatant was measured and the pelleted fraction of TTR calculated by subtracting the remaining amount from the original TTR concentration. The same concentrations of TTR were incubated separately without $A\beta_{1-42}$, centrifuged and TTR concentrations were checked in the supernatant to be used as controls. A25T showed the largest fraction of protein co-pelleting with $A\beta_{1-42}$ fibrils, followed by V30M> WT> S85A> V122I (Table 4.7. and Figure 4.14).

TTRs	Decrease in TTR concentration in TTR controls %	Decrease in TTR concentration in TTR+ $A\beta_{1-42}$ mixtures %	The fraction of TTR co-pelleted with $A\beta_{1-42}$ %
WT	0%	8%	8 ± 1.2 %
V122I	5%	7%	2 ± 0.6 %
V30M	7%	16%	9 ± 1.4 %
A25T	38%	56%	18 ± 3.1 %
S85A	2%	8%	6 ± 0.9 %

Table 4.7. The mean percentage of the bound (co-pelleted) TTRs in the presence of equimolar concentrations of purified $A\beta_{1-42}$ fibrils.

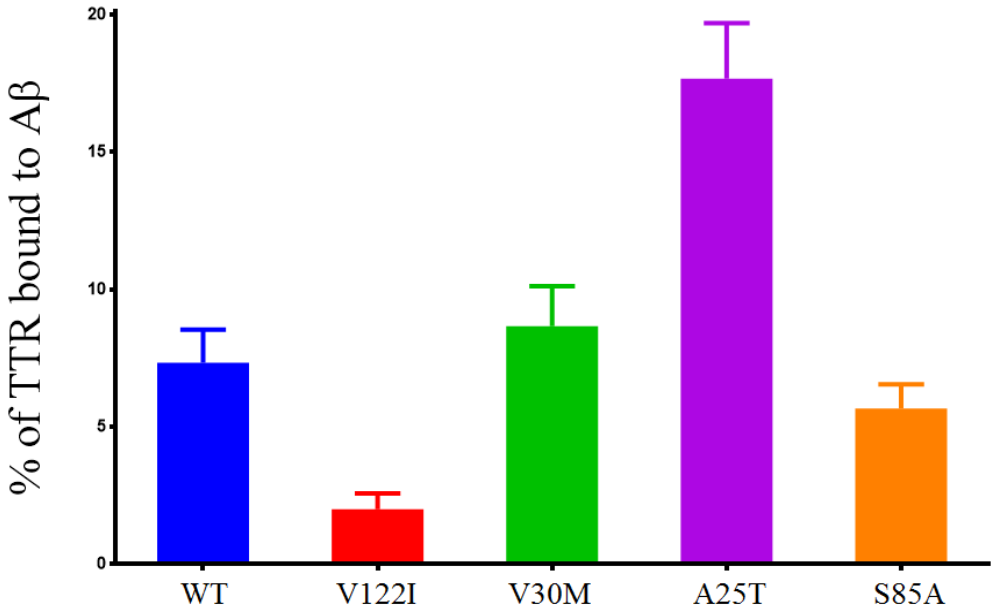

Figure 4. 14. Histogram representation of the percentage of TTRs co-pelleted with $A\beta_{1-42}$ fibril.

4.3.9.2. $A\beta_{1-42}$ defibrillisation by TTRs

Disaggregation of amyloid fibrils is an important step towards its clearance. TTRs can alter the Aβ fibrillisation kinetics and we found evidence on its ability to bind to pre-made fibrils. The ability of WT and mutant TTRs to defibrillise pre-made Aβ fibrils was investigated applying thioflavin T technique. Equimolar amounts of TTRs were incubated with purified $A\beta_{1-42}$ fibrils and the thioflavin T signal monitored to detect any changes. Generally, the addition of TTRs to Aβ fibril shows no difference in thioflavin T fluorescence compared to the control. An initial decrease in the Thio T fluorescence intensity is noticed in the $A\beta_{1-42}$ control and similarly in the presence of TTRs, this could be due to either temperature adjustment or dissociation of the fibrils because of dilution as the reaction started by adding highly concentrated stock of fibrils to the reaction buffer. As no significant differences are detectable with TTR compared with in its absence, these

results suggest that TTRs do not dissolve pre-formed mature Aβ fibrils, but rather have an effect on their formation.

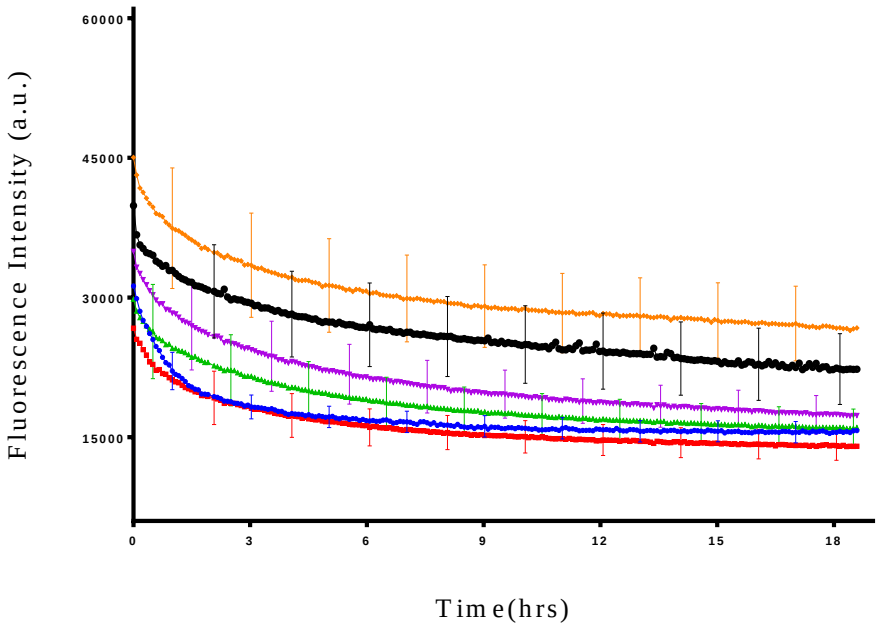

Figure 4.15. **Thio T curves of $A\beta_{1-40}$ defibrillisation by TTRs.** Thio T curves of (11 μM-monomer equivalent) of purified $A\beta_{1-42}$ fibrils in the absence, control (blue) and the presence of equimolar amount of WT TTR (red), V122I (green), V30M (purple), A25T (black), S85A (orange). The error bars represent (sem).

4.3.9.3. TTRs inhibition of $A\beta_{1-42}$ seeding

It has been shown that formation of amyloid fibrils by $A\beta_{1-42}$ happen by a nucleated growth mechanism (Evans *et al.*, 1995). In the absence of an aggregate, a nucleus has to be formed in situ in a process that needs a relatively high concentration of the peptide and significant dead time. When an aggregation seed is present due to addition of exogenous aggregates, the nucleation time of the reaction is reduced and the fibril extension step is more quickly started (Evans *et al.*, 1995). The addition of WT and mutant TTRs to such seeded reactions does not extend the lag time, except for A25T which extends the lag time similarly in the presence and absence of seeds. This result indicates that only the

A25T variant inhibits the ability of added fibrils to act as seeds for fibril formation, suggesting that A25T can prevent addition of monomers through binding to the extension sites of an amyloid fibril and, probably these sites are similar to the binding sites on an in situ generated nucleus in an unseeded reaction (Wood *et al.*, 1996).

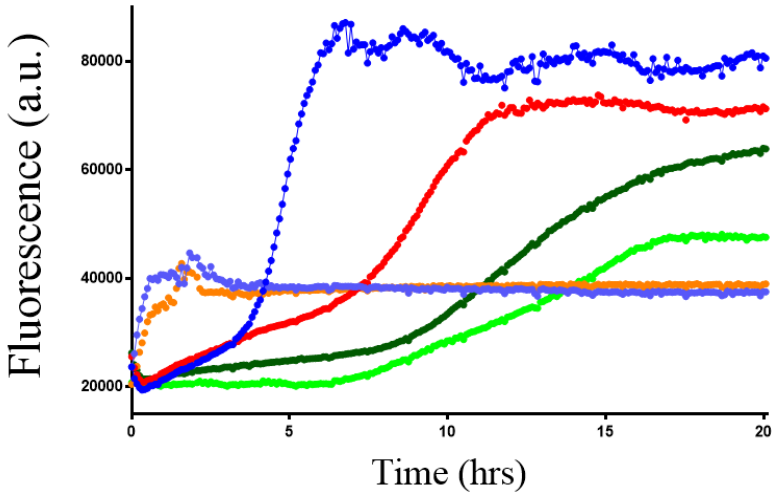

Figure 4. 16. Thiofavin T curves showing the inhibitory effect of WT and A25T TTRs on seeded reaction of Aβ fibrillisation. $A\beta_{1\text{-}42}$ monomer (4μM) without (blue) and with 0.4μM $A\beta_{1\text{-}42}$ seeds (light blue); 0.4μM WT TTR added to Aβ monomers without (red) and with (orange) seeds; 0.4μM A25T TTR added to Aβ monomers without (dark green) and with (light green) seeds.

4.4. Discussion

Several studies have suggested a protective role for TTR in the pathophysiology of AD and a direct interaction between TTR and Aβ peptides. *In vitro* data suggest that sub-stoichiometric concentrations of TTR inhibit Aβ fibrillisation. However, the species of Aβ which TTR binds to prevent its aggregation is still not clear. ELISA based methods suggested that TTR binds to all forms of Aβ including fibril, oligomers and monomer, preferentially to oligomer. However HSQC NMR showed that TTR and specifically the residues around and including the thyroxine binding pocket of the TTR tetramer bind to

$A\beta_{1-40}$ monomers. Most of the studies mentioned above have been performed on $A\beta_{1-40}$. $A\beta_{1-40}$ is 4 times more abundant in the brain, however $A\beta_{1-42}$ is more aggregation prone and pathogenic. This study is an attempt to reveal the species of Aβ which TTR binds to. In this study, conditions were optimized to make both $A\beta_{1-40}$ and $A\beta_{1-42}$ fibrillise, in order to compare the effect of TTRs on the peptides under similar conditions. Under the conditions used in this study both Aβ peptides makes typical straight, unbranched, thioflavin T positive amyloid fibrils and the aggregation kinetics follow a typical sigmoidal shape with a lag time, growth phase and then plateau. This pattern fits with a nucleation dependant mechanism of aggregation which is a characteristic of Aβ aggregation. Our results showed that $A\beta_{1-42}$ is the more aggregation prone and exhibits a lag time of 1.5 hrs, t_{50} of 4.2 hrs and reaches a plateau after 6.2 hrs. $A\beta_{1-40}$ takes 5 times longer to start fibrillisation, with a lag time of 10hrs, a t_{50} of 13hrs and then reaches a plateau after 14.5 hrs. Results obtained by this study show that near equimolar concentrations of WT TTR are needed to completely inhibit $A\beta_{1-42}$ fibrillisation, while a 3-4 times lower concentration was sufficient to completely inhibit $A\beta_{1-40}$ fibrillisation. These results are in agreement with those from Kelly and co-workers (Li et al., 2013) regarding the complete inhibition of $A\beta_{1-40}$ by 3μM WT TTR. However, in the current study, lower concentrations of TTR extended the t_{50} of $A\beta_{1-40}$ for longer compared with the t_{50} times found by Kelly and co-workers. This is most probably due to the later addition of TTR to Aβ by their group, where the peptide is dissolved in buffer before addition of TTR instead of our method which is to dissolve the peptide into a solution already containing TTR. This is validated by our observation that addition of TTR to $A\beta_{1-40}$ after addition of buffer significantly lowers the strength of TTR inhibition, as measured by the fibrillisation lag time (section 4.3.8).

4.4.1. The stoichiometry of transthyretin inhibition implies that it binds to more than just monomeric Aβ.

While TTR binding to immobilised Aβ is strong (28nM), TTR binding to Aβ monomers in solution is relatively weak. The K_D of TTR tetramer binding to $A\beta_{1-40}$ in solution is 24μM (Li *et al.*, 2013a), meaning that only 1/3 of TTR and Aβ monomers are bound at any particular time in an 11μM mixture of equimolar amounts of both TTR and Aβ. Despite this, equimolar concentrations of WT TTR were enough to inhibit $A\beta_{1-42}$ fibrillisation completely. In addition, under our experimental conditions, the lag time is not concentration dependent, so binding of TTR to Aβ monomers can't explain the delays in the lag time of Aβ fibrillisation. At the same time, TTR only significantly increased the t_{lag} and t_{50} rather than t_{growth} which suggests TTR mainly affects the monomeric Aβ or early oligomeric / nucleating species. There are a number of models which can explain these observations. Inhibition may occur in this way due to the fact that both TTR tetramers and monomers can bind to Aβ aggregates as well as monomers. TTR tetramers may inhibit Aβ aggregation through binding to small aggregates (shown by ELISA based methods) and enhancing the formation of off-pathway species rather than fibrils. The observation of large amounts of amorphous aggregates in EM images in the presence of TTR further supports this interpretation. Monomers of TTR may also contribute significantly to this process: at physiological concentrations of TTR, tetramer is in equilibrium with small but significant amounts of monomer (table 4.1.). TTR monomers are more effective than tetramers in inhibiting Aβ fibrillisation and bind preferentially to Aβ aggregates. It has also been suggested that addition of Aβ enhances the destabilisation of the TTR tetramer which then leads to an increase in the observed monomer population. Monomers subsequently bind to newly formed Aβ oligomers to inhibit further fibrillisation. This could explain, why less stable mutants are more effective under our conditions (4 times more effective). Because this mechanism does not depend on

interactions with the monomeric species of Aβ, it permits to inhibition of Aβ fibrillisation at lower than stoichiometric ratios of TTR to $A\beta_{1-42}$ monomers. The implication here is that these secondary mechanisms may be responsible for the segregation of at least 2/3 of the Aβ molecules down alternative pathways.

A further interpretation of this effect would be surface effects given that we found that Aβ binds to the surface of the polystyrene microplates and forms a monolayer. This monolayer can nucleate Aβ aggregation, however, the TTR binding to Aβ on this monolayer is stronger than to Aβ in solution. The TTR stays bound to aggregated Aβ and prevents it from nucleating the fibrillisation reaction.

4.4.2. Mutant TTRs exhibit different inhibitory mechanisms on Aβ fibrillisation.

$A\beta_{1-42}$

The 4 variant TTRs compared in this study exhibited two different types of behaviour. While the inhibitory effect of the V122I mutant is not significantly different from wild type, other mutants were significantly more effective. Nearly four times less V30M, A25T and S85A were required to completely inhibit $A\beta_{1-42}$ fibrillisation, compared with WT and V122I. The S85A mutant was significantly more effective in extending the lag time of Aβ aggregation compared to A25T and V30M. The rank of inhibitory effect of TTR mutants was S85A> A25T>= V30M> V122I>=WT. These results indicate that the inhibitory capacity of mutants is conversely related to their stability, with the less stable mutants acting as the better inhibitors. Even if V122I tetramer is less stable as tetramer compared to wild-type, this mutant is equally effective or even slightly less. This could be because V122I has a more stable monomer compared to other mutants and possibly its binding site to Aβ is not as exposed as other mutants which have unstable monomers as well as tetramers. It has been suggested that addition of Aβ can lead to the dissociation of

TTR tetramers, indicating that both the dissociation of tetramer the unfolded nature of the monomer are important to inhibit Aβ fibril formation.

Costa and colleagues (2009), found that the affinity of V30M for immobilised Aβ is only 60% of WT TTR binding. However, NMR data have shown that V30M binding to soluble $A\beta_{1-40}$ is stronger than WT TTR in solution (Li et al., 2013) and these effects are likely to dominate our experiments. The stronger inhibitory efficacy of the less stable TTR mutants (V30M, A25T and S85A) may be due to the increased exposure and therefore accessibility of their hydrophobic residues to Aβ. Another possibility could be that more than one Aβ molecule can fit within the TTR hydrophobic pocket if these mutants exhibit a more open tetrameric structure (Figure 4.2). For example, with regards to the S85A mutant, it has been suggested that mutation of S85 to alanine leads to better access of other hydrophobic residues to Aβ and consequently a better inhibition of Aβ fibrillisation is achieved (Du and Murphy, 2010). The idea that Aβ destabilises the TTR tetramer and that the increased monomer population can then bind to Aβ oligomers and inhibit fibrillisation may provide a further explanation for the 4-fold greater than WT inhibitory effect of mutants observed here. The observed high efficacy of M-TTRs even at highly substochiometric ratios by (Li *et al.*, 2013) supports this theory.

$A\beta_{1-40}$

The $A\beta_{1-40}$ is less aggregation prone and exhibits a much longer lag time compared with $A\beta_{1-42}$. Results obtained by this study show that only 3 μM WT TTR were needed to completely inhibit $A\beta_{1-40}$ fibrillisation. This results is consistent with published data (Li *et al.*, 2013a). However, in the current study, lower concentrations of TTR extended the $A\beta_{1-40}$ t_{50} time for longer compared to the t_{50} times found by (Li *et al.*, 2013). This could be due to the addition of buffer to Aβ before adding TTR by (Li *et al.*, 2013), considering

that Aβ can form small aggregates rapidly in physiological buffers. This is validated by the addition of TTR to Aβ after addition of buffer which significantly lowered the intensity of TTR inhibition. We found the V122I variant to be less effective at inhibiting $A\beta_{1-40}$ fibrillisation compared with WT and 5 μM was needed to completely inhibit fibrillisation instead of 3μM. This finding is different to the result reported by Li and colleagues (2013), where they found that the V122I mutant was more effective than WT TTR. This could also be due to the late addition of WT TTR to Aβ (their addition of buffer to Aβ before adding TTR) by (Li *et al.*, 2013). This makes the WT inhibition appear far less efficient as it allows the formation of oligomers that the WT TTR cannot reverse. Interestingly, we found that V122I was more effective at lengthening the lag time of Aβ aggregation when added after 5 minutes or 1hr of addition of buffer to Aβ. This could be due to the fact that V122I can also bind to small Aβ aggregates and delay fibrillisation. V30M mutant is even more effective, and compared with both WT and V122I only needs 1.5 μM to completely inhibit $A\beta_{1-40}$ fibrillisation for at least 200 hrs.

4.4.3. Transthyretin did not reduce the fibril yield once a threshold concentration is reached

The amplitude of the ThT fluorescence signal from Aβ and TTR reactions is most likely to represent the amount of fibril produced during the reaction. The intensity is largely the same until it reaches a threshold concentration, then no fibrils are observed. This means that below a certain concentration of TTR, amyloid β fibrillisation is only delayed and the final yield of fibril remains essentially the same. Once a threshold concentration is reached, the reaction is prevented from occurring and the amplitude is 0. The fluorescence amplitude of Aβ and WT TTR mixtures was slightly higher and increased with WT TTR concentration. However, for all mutants, the amplitude was higher than the control in the

presence of lower TTR concentrations and then decreased with further increases in TTR concentration, indicating a possible decrease in the formation of Aβ fibrils. The most obvious idea would be that transthyretin may be co-aggregating and contributing directly to the increase in fluorescence observed. However, the size-exclusion analysis presented in section 4.3.4 suggests this is not true and supports a model where most of the TTR remains in solution. Another explanation is that the increase in fluorescence does not represent an increased yield, rather it could be due to TTR enhancing the formation of morphologically different ThT positive Aβ fibrils with a higher intrinsic fluorescence. However, in the case of higher concentrations of TTR, the same thing is not happening making this hypothesis less likely.

4.4.4. The nature of the growth phase of Aβ fibrillisation – a clue to interpreting the mechanism of inhibition of transthyretins?

From our t_{lag}, t_{50} and t_{growth} calculations, it would appear that the effect of TTRs on t_{growth} is smaller compared with their effect on t_{lag} and is not concentration dependent (i. e. 7.5 μM of WT TTR extends the t_{lag} 7-fold, however the same amount of TTR extends t_{growth} by only 2-fold compared with the control reaction). The nature of the growth phase is controversial and in our conditions has only a very shallow concentration dependence on Aβ concentration, if at all, suggesting that the molecular processes that dominate in this phase are not affected by the concentration of monomer. If TTR exerts most of its effect through monomer binding, then its effect will be to decrease monomer concentration, which is therefore unlikely to have a significant effect on t_{growth}. Given the above discussions, this seems unlikely.

A simpler explanation would be that, despite the importance of other effects, the main impact of TTRs is still to affect Aβ aggregation through delaying the formation of primary nuclei rather than by affecting secondary nucleation. The S85A variant is an extreme case

of this where the effect on t_{growth} is negligible, in spite of the fact that it had the greatest impact of all TTRs on lag time. The Aβ fibril binding assays presented here further support this: S85A was also the odd one out in showing no significant binding to Aβ fibrils. This would indicate that S85A inhibits Aβ fibrillisation entirely through binding to monomers or very early species not present in the growth phase, and not oligomers or fibrils. Experiments performed on TTRs binding to Aβ fibrils and the effects on seeding showed that only in the case of A25T mutant can a relatively large percentage bind to Aβ fibrils and neutralise the seeding effect. These results again shows that most TTRs cannot affect secondary nucleation reactions. As A25T is very unstable and aggregation prone, addition of fibrils can further destabilise and make it aggregate and precipitate during pelleting, however it was effective in controlling the seeding. This could be due to increase in monomer population as monomers suggested to bind Aβ aggregates better. Conversely, mutants which had the greatest impact on growth rate were A25T and V30M, which are most likely to be binding to alternative species of Aβ.

4.4.5. Transthyretin interacts with more than monomers, but does it interact with fibrils?

The current hypothesis of Aβ fibrillisation supports the idea that secondary nucleation plays a key role in fibrillisation. $Aβ_{1-42}$ fibrils are not directly toxic themselves. However, they can help continuous generation of toxic oligomers as they can provide a catalytic surface for this. Consequently the produced oligomeric species can grow and form additional fibrils, which further promoting the production of more toxic species in a catalytic cycle. Accordingly, the fibrils, play a big role in the toxic oligomer by lowering the kinetic barriers. Because of the prominent role of the catalytic cycle in the generation of new toxic oligomers, identification of inhibitors to prevent the catalytic activity of the fibril surfaces would be of a valuable importance.

To explore the potential of this strategy, TTRs were incubated with purified Aβ fibrils and monitored using ThT fluorescence. The data obtained show that TTRs do not exhibit any obvious defibrilisation effect on $A\beta_{1-42}$ fibrils. However, co-pelleting assays showed that a large fraction of the A25T TTR variant protein co-pelleted with Aβ fibrils. This could be due to either binding to Aβ fibrils or destabilisation of A25T by Aβ and consequently amorphous aggregate formation, followed by precipitation of the A25T. Aβ seeding inhibition assays show that only A25T can inhibit seeding of $A\beta_{1-42}$. This result would support the idea that it binds to Aβ fibrils and prevents the fibril surface from acting as a secondary nucleation template for the formation of new fibrils. A25T can inhibit both primary and secondary nucleation processes for generating oligomers. Additionally, because the targets are the catalytic sites on the fibrils, and does not depend on interactions with the monomers, it is possible that even substoichiometric ratios of TTR would be efficient to inhibit the catalytic process.

5 Chapter Five: Human Cystatin C and Aβ interaction

5.1. Introduction

The importance of human Cystatin C (hCC) in Alzheimer's disease is presented in the introduction to this thesis. Here, we consider available data on the direct interaction of hCC with Aβ *in vitro*. The first investigations into the direct interaction between hCC and Aβ revealed a high affinity binding between the two proteins at physiological pH and temperature. ELISA assays revealed a specific, concentration dependant and high affinity binding of hCC to both $A\beta_{1-40}$ and $A\beta_{1-42}$ (Figure 5.1 A) (Sastre *et al.*, 2004b). This study also showed a nanomolar K_D for both proteins. The same study found that hCC inhibited *in vitro* fibril formation by both $A\beta_{1-40}$ and $A\beta_{1-42}$, and promoted the formation of amorphous aggregates rather than mature fibrils (Figure 5.1D). TEM detected that substoichimetric concentrations of hCC can prevent fibril formation by $A\beta_{1-40}$, as no fibrils were observed when 3.75 µM hCC was incubated with 22 µM of $A\beta_{1-40}$. However near stoichiometric amounts of hCC were needed to completely inhibit amyloid fibril formation by $A\beta_{1-42}$ (15 µM hCC for 22 µM $A\beta_{1-42}$) in a 10 µl volume. The binding site of hCC to the extracellular N-terminal region of Aβ was mapped employing co-immunoprecipitation experiments with deletion mutants of APP and *in vitro* binding assays with GST-Aβ.

Selenica *et al.* (2007a), probed the effect of hCC addition to $A\beta_{1-42}$ ADDL and protofibril preparations using western blotting and gel filtration (Figure 5.1 B&C). The authors suggested that the formation of both small and large $A\beta_{1-42}$ oligomers decreased in the presence of hCC, as a decrease in the amount of Aβ trimers, tetramers and high molecular weight oligomers (98-38 kDa) was detected by SDS-PAGE when $A\beta_{1-42}$ was incubated with an equimolar amount of hCC (Figure 5.1B).

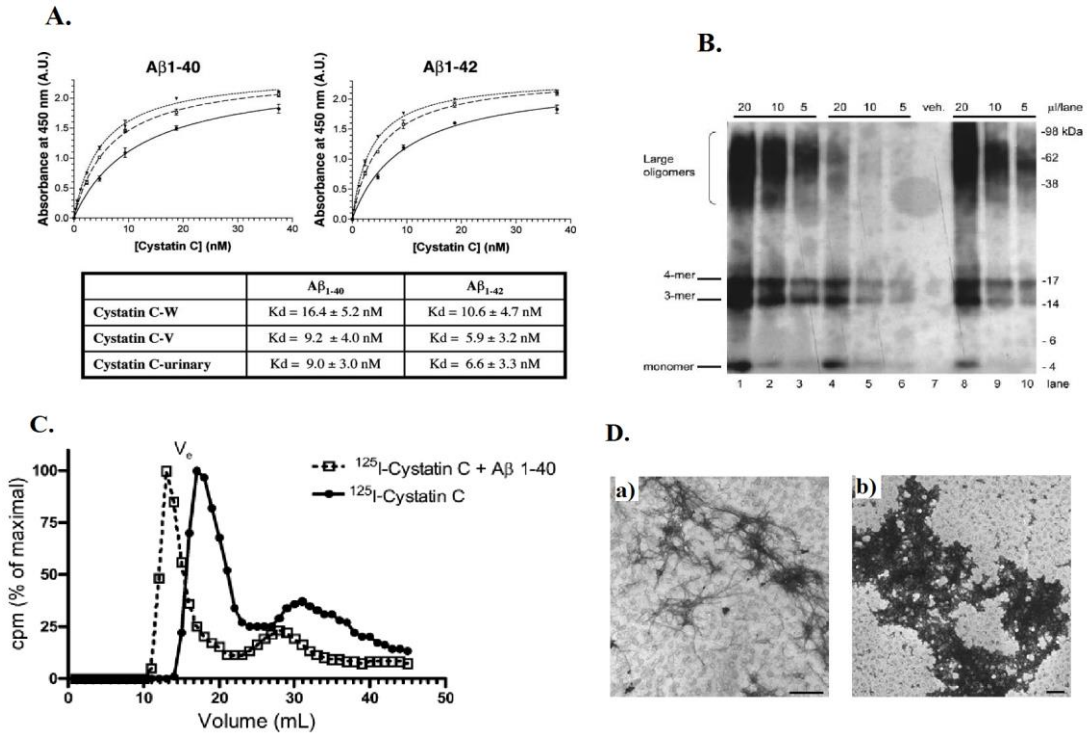

	$A\beta_{1-40}$	$A\beta_{1-42}$
Cystatin C-W	Kd = 16.4 ± 5.2 nM	Kd = 10.6 ± 4.7 nM
Cystatin C-V	Kd = 9.2 ± 4.0 nM	Kd = 5.9 ± 3.2 nM
Cystatin C-urinary	Kd = 9.0 ± 3.0 nM	Kd = 6.6 ± 3.3 nM

Figure 5.1. The Interaction between hCC and Aβ in the Literature

The binding of hCC to Aβ was studied by ELISA (**A**) Different concentrations of wild-type (solid line, solid circles), L68Q variant (dashed line, open squares) and urinary hCC (dotted line, solid triangles) were incubated for 3 h at 37°C with $A\beta_{1-40}$ or $A\beta_{1-42}$ coated wells. Anti-hCC antibody was used to detect bound hCC, and the means and standard deviations were calculated from three independent experiments (image taken from Sastre *et al.* (2004a). (**B**) Western blot of $A\beta_{1-42}$ oligomers with and without hCC (taken from Selenica *et al.* (2007a). SDS-PAGE of the oligomeric preparations was analysed using the anti-Aβ monoclonal antibody 6E10. Lanes 1-6 show different volumes of the supernatants of mixtures in the absence (lanes 1-3) and presence (lanes 4-6) of equimolar hCC after 24 h incubation. Lanes 8-10 represent different volumes of the supernatants of mixtures with preformed Aβ-oligomers to which 100 µM has been added and incubated for a further 24 h. Lane 7 (veh.) is a control of the incubation solution with no proteins present. (**C**) The elution profile of gel filtration of 0.6 nM ^{125}-I-labelled hCC (solid circles) and a solution of 0.6 nM ^{125}I-labelled hCC in the presence of a slight molar excess of $A\beta_{1-40}$ (open squares) (taken from Selenica *et al.* (2007a). The shift in the peak of radioactivity to a volume thought to correspond to a molecular mass of ~17 kDa is explained as the formation of an equimolar complex between ^{125}I-labelled hCC (13 kDa) and $A\beta_{1-40}$ (4 kDa). **D**) Electron micrographs of assemblies formed by (a) Aβ42 (1 µg) or (b) Aβ42 (1 µg) incubated with hCC (2 µg). Scale bars represent 100 nm (taken from Sastre *et al.*

(2004a).

They also found that the amount of precipitate increased in the presence of hCC: TEM revealed that this precipitate was mainly composed of amorphous aggregates with few oligomers and fibrils present. SEC-HPLC was employed to show a reduction in $A\beta_{1-42}$ protofibril formation when $A\beta_{1-42}$ was incubated with both equimolar and 2 x concentrations of hCC. A sephadex G-50 gel filtration column (Amersham) was used to detect Radio-labelled ^{125}I-hCC-$A\beta_{1-40}$ complex after for 35 minutes of incubation of the two proteins. The radioactive peak of hCC (13 kDa) shifted as seen in Figure 5.1C and this was believed to resemble a complex with a molecular weight of 17 kDa, i.e. a 1:1 complex formation between hCC and $A\beta_{1-40}$ (4 kDa). These data are difficult to explain, given the insufficient resolution of Sephadex G-50 and the abnormal behaviour of oligomeric species during gel filtration. The nature of any complex formed in solution is still debatable.

As mentioned above, it has been suggested that there is a single binding site between the two proteins, with a nanomolar range dissociation constant. The hCC binding halts further Aβ aggregation to form amyloid fibrils, and alternatively diverts the assembly pathway to the formation of amorphous aggregates. Despite the fact that hCC interaction with Aβ has been investigated through several different methods, however, the structural details of this association is no well-established yet. In our lab, previously the interaction between hCC and amyloid beta peptide (Aβ) has been studied by Williams (2015). Amyloid β fibrillisation time courses were performed with and without hCC and showed that hCC will inhibit the amyloid fibrils formation by $A\beta_{1-42}$ in a concentration-dependent way, requiring a 2:1 molar ratio of hCC to Aβ to completely inhibit this reaction where complete reduction in the intensity of thioflavin T fluorescence was noticed. At equimolar concentrations, a significant decrease in thioflavin T fluorescence, but not a

complete loss, indicates that a small amount of amyloid fibrils is still present (Figure 5.2).

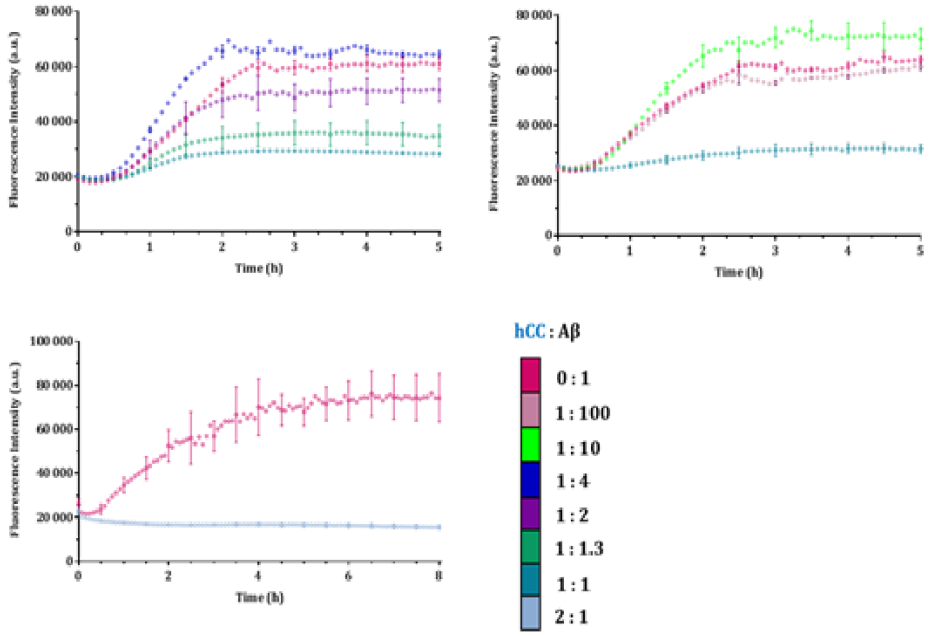

Figure 5.2. Aβ and hCC Dose Dependence

Thioflavin T fluorescence time-courses of $A\beta_{1-42}$ fibrillisation at 11 μM with the addition of different molar ratios of hCC. Each curve is the average of 5 replicates, with error bars indicating the standard error of the mean (SEM). Three separate experimental series done at different times and with different protein stocks are shown for comparison (Adapted from Williams, 2015).

^{1}H ^{15}N-HSQC NMR experiments were also performed for ^{15}N labelled hCC and Aβ to find the binding surface of hCC to Aβ. Despite the fact that hCC inhibited Aβ fibril formation, no chemical shift in amide cross-peaks was observed in ^{1}H ^{15}N-HSQC NMR spectra of hCC incubated with $A\beta_{1-40}$ (Keeley, 2007, Elshawaihde, 2012), and $A\beta_{1-42}$ both in its monomeric and oligomeric forms (Williams, 2015). These data suggest that folded hCC monomers do not interact with $A\beta_{1-42}$ monomers, yet they still effectively inhibit Aβ fibril formation. This was surprising, as it has been shown that hCC tightly binds to monomeric $A\beta_{1-40}$ as determined by ELISA (Sastre *et al.*, 2004a). It is believed that these variations could be accounted for by the fact the ELISA experiment is performed on a

surface, while the NMR experiment is in solution. This is a strong indication that hCC binds non-monomeric species of $A\beta_{1-42}$, most probably some form of the oligomer (Williams, 2015).

In order to identify the species in the Aβ aggregation reaction to which the hCC was binding, hCC was added to Aβ fibrillisation at different time points. These points were the start of the initiating the Aβ fibrillisation, at the mid-elongation phase, and at the plateau. Addition of hCC at the start of the initiating the Aβ fibrillisation, at the mid-elongation phase have also caused inhibition of the aggregation and a reduction in thioflavin T fluorescence intensity, however, hCC addition at these points was not as effective as when it was added at the start of the aggregation reaction. This however indicates that hCC still has an effect on Aβ aggregation at these time-points, suggesting that the hCC binding species are still present. The addition of hCC at the plateau shows no difference in thioflavin T fluorescence compared to the control. This suggests that hCC needs to be present early on in the reaction to have an effect, and hCC does not dissolve pre-formed mature Aβ fibrils, but rather has an effect on their formation. This suggests the interacting Aβ species are likely to be a protofibrillar species present early on in the reaction.

Formation of domain-swapped dimers is one of the characteristics of the cystatin superfamily. As demonstrated by Ekiel & Abrahamson (1996), dimerisation of hCC can be induced by de-stabilising the protein using temperature, pH or chemical denaturants. Dimerisation causes hCC to lose its protease inhibition activity as the active site is included in the process. As oligomeric forms of an intracellular homolog of hCC, cystatin B had been shown to interact with amyloid β (Skerget *et al.*, 2010b), the ability of hCC dimers to inhibit Aβ fibrillisation was also examined. Unlike monomer, the addition of equimolar concentrations of hCC dimer has no effect on the fibril yield, but instead caused

an increase in lag phase, compared to $A\beta_{1-42}$ incubated in the absence of hCC. This suggests a different mechanism of inhibition by the dimer, where it is able to interfere with the reaction progress but not affect its outcome. The notable difference between the inhibitory effect of monomer and dimer gives a strong indication that the region involved in protease binding is responsible (Williams, 2015). The surface of the monomer and the dimer are basically similar in all regions of the molecule except for the loops involved in protease binding (Ekiel *et al.*, 1997a). The hydrophobic nature of this region of the hCC, which is essential for protease binding, makes it a typical surface for interactions with the Aβ peptide.

Given the above findings, the next step in this study was to understand the chemical nature of the binding site and the binding Aβ species. However, re-examination of the concentration dependence of the hCC inhibition and hCC: Aβ complex formation by NMR was necessary. Residue-specific mutagenesis is a powerful technique in the study of protein–protein interactions, allowing identification of key residues in protein–protein interactions. The unusually hydrophobic nature of the protease binding site suggested that hydrophobic residues may be key candidates for the binding of Aβ species. This chapter describes the biochemical identification of the binding interface of hCC with Aβ through mutation of hydrophobic residues to alanine. The interaction between wild-type and variant hCC and different species of Aβ is assessed applying thioflavin T fluorescence assays and electron microscopy techniques. 1D and ^{1}H ^{15}N-HSQC NMR were used to monitor fibrillisation time-courses of $A\beta_{1-42}$ with hCC and detect complex formation/monomer disappearance. A key part of this work is also to validate/rectify previous measurements which I show to be affected by the presence of an *E. coli* contaminant, with a significant anti-amyloid activity (chapter 6).

Establishing the molecular mechanism of how this process works would then allow a

comparison of this with other Aβ-modulating systems to discover if there is a general mechanism for *in vivo* protection which could be exploited for the identification of a therapeutic peptide.

Materials and Methods

5.2.1 Monomeric Aβ preparation and fibrillisation

Monomeric Aβ preparation, fibrillisation and inhibitor addition assays were performed as described in (Chapter 2), except that two different shaking conditions used. First; continuous shaking at 300 r.p.m. Second: minimal shaking at 100 r.p.m for only 10 seconds before each reading.

5.2.2 Purification of fibrillar $A\beta_{1-42}$ fibril

Fibrillar Aβ was prepared, hCC binding to Aβ fibrils, defibrillisation and seeding inhibition assays were performed as described in section (4.2.).

5.2.3. Preparation of hCC Dimer

100 µM hCC in 10 mM sodium phosphate pH 6.0, 100 mM NaCl was incubated for 30 minutes at 68 °C, then loading onto a semi-preparative Superdex 200 (GE Healthcare) gel filtration column equilibrated in 50 mM sodium phosphate pH 7.4, 150 mM NaCl. 0.5 ml fractions were collected and the dimeric peak were collected and quantified by measuring the absorbance at 280 nm, before immediate use in thioflavin T assays.

5.2.4. Nuclear Magnetic Resonance Spectroscopy

Protein preparations.

^{15}N-labelled hCC was expressed and purified as described in section 2.4.3. Before the NMR experiments, the purity and monomeric state of the protein was established through analysis by mass spectrometry and SEC-HPLC.

Lyophilised HFIP-treated $A\beta_{1-42}$ was purchased from rPeptide. 1 mg $A\beta_{1-42}$ was dissolved in 1 ml HFIP and sonicated for 10 minutes in a DECON Ultrasonics sonicator bath (Sussex, UK). The solution was split into 0.1 mg aliquots and HFIP was evaporated under a stream of N_2. Samples were lyophilised to remove any residual HFIP and stored at -20 °C. Monomeric $A\beta_{1-42}$ for subsequent NMR experiments was prepared by dissolving 0.2 mg of HFIP-treated $A\beta_{1-42}$ in 176 µl of 10 mM NaOH, with sonication for 30 minutes. 50 µl of deuterium oxide (D_2O) and 340µl of phosphate buffer saline were added to 100 µl of NaOH dissolved $A\beta_{1-42}$ stock. The final concentration of $A\beta_{1-42}$ was brought to 50 µM in 50 mM phosphate buffer (Na_2HPO_4/NaH_2PO_4), 150mM NaCl, 2mM Sodium azide. The pH was adjusted to 7.4 by adding 10 µl of 100 µM HCl and adjusting the final volume to 500 µl. The concentration of Aβ was quantified by measuring the absorbance at 280 nm, and where necessary adjusted to 50 µM by the addition of Phosphate buffer pH 7.4, 10% D_2O. A 1D ^1H spectrum was recorded at 330 K.

NMR Spectroscopy.

All NMR spectra described in this chapter were recorded on a Bruker DRX spectrometer operating at 600 mHz with a cryogenically cooled probe, and controlled using XWinNMR (Bruker). Spectra were processed and analysed using Felix 2004 (Accelrys) with in-house macros. All heteronuclear single quantum coherence (^1H ^{15}N-HSQC) experiments were acquired using 1024 increments in the proton dimension and 512 increments in the nitrogen dimension. The spectral widths of the proton and nitrogen dimensions were 7507.5 Hz and 2128.6 Hz respectively.

^{1}H-^{15}N HSQC Spectrum of HCC.

A backbone assignment for hCC at the required experimental conditions of 50 mM phosphate buffer (Na2HPO4/NaH2PO4), pH 7.4, 150mM NaCl, 330 K, has been determined through salt titration. This assignment was based on a published assignment for 200 μM hCC in 15 mM Tris-TFA pH 7.5, 278 K (Keeley, 2007). In turn, this assignment was based on a published assignment for 200 μM hCC in 50 μM sodium phosphate pH 6.0, which was recorded at 303 K (Ekiel *et al.*, 1997b).

Salt Titration for ^{15}N-labelled HCC.

The backbone assignment of hCC under the desired experimental conditions, 50 mM phosphate buffer (Na_2HPO_4/NaH_2PO_4), pH 7.4, 150mM NaCl, 330 K was determined by tracking changes in the ^{1}H-^{15}N HSQC spectra as conditions were gradually changed from the previously assigned conditions 15 mM Tris-TFA pH 7.5, 278 K (Keeley, 2007). This assignment was based on a published assignment for 200 μM hCC in 50 μM sodium phosphate pH 6.0, which was recorded at 303 K (Ekiel *et al.*, 1997b). The new assignment was determined in three steps by gradually increasing NaCl concentration, as described below. A 500 μl sample of 50 mM phosphate buffer (Na_2HPO_4/NaH_2PO_4), pH 7.4, was prepared for NMR by the addition of 10% D_2O. The initial spectrum was recorded once the sample was equilibrated to 303°K. The assignment of 15 mM Tris-TFA pH 7.5, 278 K transferred well onto this spectrum. Following this, the sample was removed from the NMR tube so that the NaCl concentration could be increased to 20 mM and 150 mM by the addition small aliquots of 5M NaCl stock. At each new NaCl concentration, a 1D ^{1}H-spectrum of the sample was recorded prior to recording the ^{1}H-^{15}N HSQC spectra.

Time-course of unlabelled $A\beta_{1-42}$

1D time course - 50 µM of $A\beta_{1-42}$ in 50 mM phosphate buffer (Na_2HPO_4/NaH_2PO_4), pH 7.4, 150mM NaCl, 2mM Sodium azide, was prepared as previously described, and 50 µl of deuterium oxide (D_2O) was added to bring the final the final volume to 500 µl. The concentration of $A\beta_{1-42}$ was quantified by measuring the absorbance at 280 nm, and where necessary adjusted to 50 µM by the addition of Phosphate buffer pH 7.4, 10% D_2O. A 1D ^1H spectra were recorded at 15 minute intervals at 303K. The disappearance of $A\beta_{1-42}$ monomer was followed by the reduction in the overall spectral intensity as a function of time by comparing to the 1st time point.

Time-course of unlabelled $A\beta_{1-42}$ with ^{15}N-hCC

1D and ^1H-^{15}N HSQC Time Courses - ^{15}N-labelled hCC in phosphate buffer saline were added to monomeric $A\beta_{1-42}$ to achieve 50 µM of both Aβ and hCC in 50 mM phosphate buffer (Na_2HPO_4/NaH_2PO_4), pH 7.4, 150mM NaCl, 2mM Sodium azide and 50 µl of deuterium oxide (D_2O) was added to bring the final volume to 500 µl. The 1D and 2D HSQC spectra of the sample were obtained every 85 minutes for 24 hours at 303 K.

Results

5.3.1 Design of Mutations

The fact that dimerisation of hCC causes the loss of its inhibitory action implies that the dimerisation interface is the same interface as for binding (Williams, 2015). Given the hydrophobic nature of this site and the affinity of Aβ for hydrophobic surfaces, six hydrophobic residues with large solvent accessible surfaces were selected from different parts of hCC and mutated to alanine (Figure 5.3). Three large hydrophobic patches were identified at the surface of the molecule including the protease binding site, which contains the hCC N-terminal, previously implicated in Aβ binding (Sastre *et al.*, 2004b).

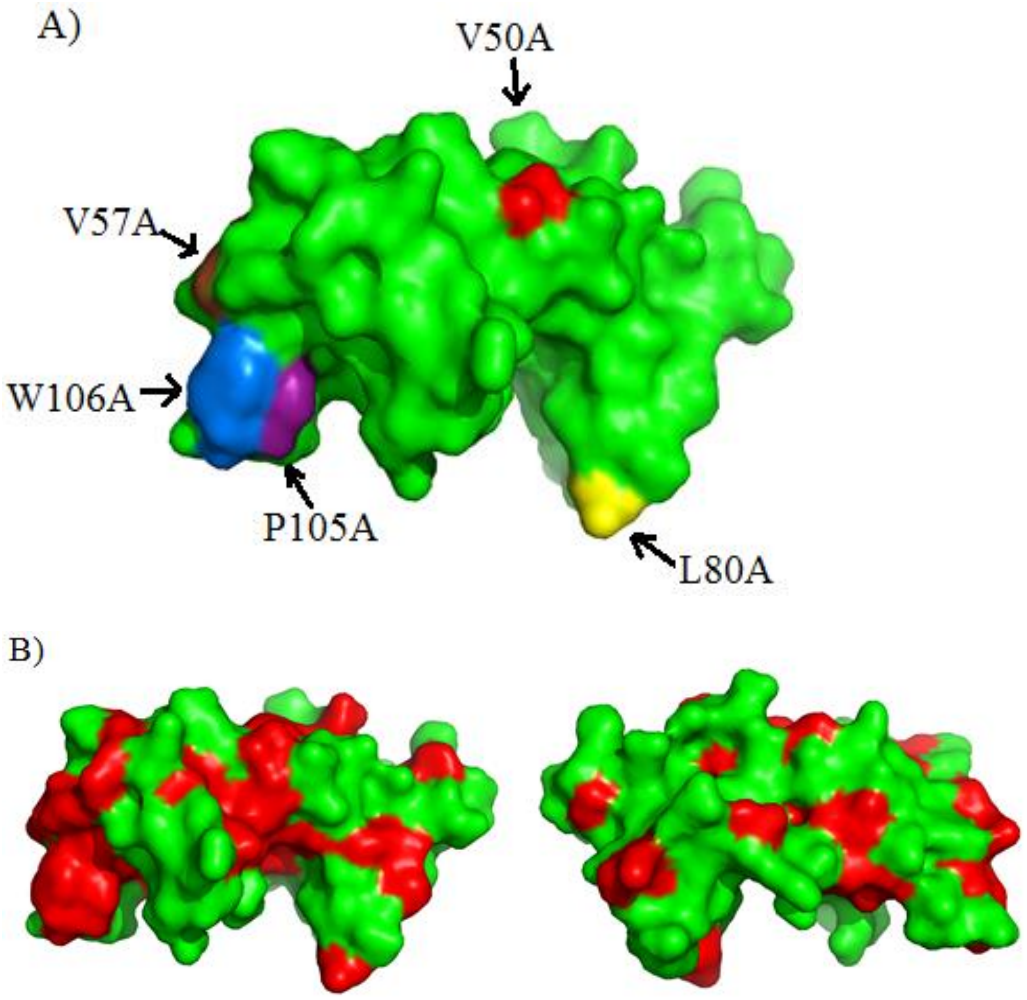

Figure 5.3. Crystal surface structure of hCC showing, A) mutated residues, and B) all hydrophobic residues in red. On the left, view as in A), right, rotated through 180°. Images made using Pymol (Delano, UK).

NMR titrations of hCC with $A\beta_{1\text{-}40}$ and $A\beta_{1\text{-}42}$ had shown that flexibility in this region is gained during the titration: peaks (G4, K5, R8, L9, V10, G11, and G12) from residues at the N-terminal sharpen and increase in intensity (Keeley, 2007). In the N-terminal region, Proline number 6 (P6) was thus mutated, although it is not shown in figure 5.3. as the flexible N-terminal does not appear in the crystal structure. As well as the N-terminal, residue V57 at the first, then P105 and W106 from the second loop of hCC protease inhibition active site were selected. A second hydrophobic patch through the

middle part of the protein was identified and V50 made up a large part of its surface so was chosen. In the third patch, residue L80 from the large loop between strands 3 and 4 was also mutated to Alanine (Figure 5.3.). The total solvent accessible surface area of hCC is 6819 $Å^2$, and the solvent accessible hydrophobic surface area is 2036 $Å^2$. The percentage of solvent accessible surface area of each residue to the total accessible hydrophobic surface area of the protein was calculated and presented in table 5.1.

Mutated residue	Total surface area ($Å^2$)	Solvent accessible surface area ($Å^2$)	% of solvent accessible surface area ($Å^2$)
P6	143*	143	7
V50	96.6	96.6	3.62
V57	95.8	95.8	3.4
L80	117.8	117.8	7.86
P105	84	84	3.93
W106	166.8	163	8

* P6 residue is not included in the crystal structure, so its surface area calculated form Miller *et al.* (1987).

Table 5.1. Total surface area and solvent accessible surface area of each mutated residues calculated from hCC PDB file in PYMOL (Blake *et al.*, 1978). The percentage of accessible surfaces for each residue is calculated with respect to the total solvent accessible hydrophobic surface of hCC.

5.3.2. $A\beta_{1-42}$ Fibrillisation

Previously in our lab, the effect of wild-type hCC on $A\beta_{1-42}$ aggregation kinetics was studied with continuous shaking of the reaction mixture at 300 r.p.m. In this study the same continuous shaking method was used to reproduce comparable data to those obtained from the previous study as shaking is known to affect the reaction both in terms of acceleration of nucleation (Morinaga *et al.*, 2010, Lee *et al.*, 2012), growth rate (Cohen *et al.*, 2013) and changes in fibril structure (Buttstedt *et al.*, 2013). However, in order to

produce comparable data to the data obtained in the study of the TTR effect on Aβ, the minimal shaking condition was also used as presented in section 3. Fibrillisation curves under both conditions are shown in figure 5.4 for comparison.

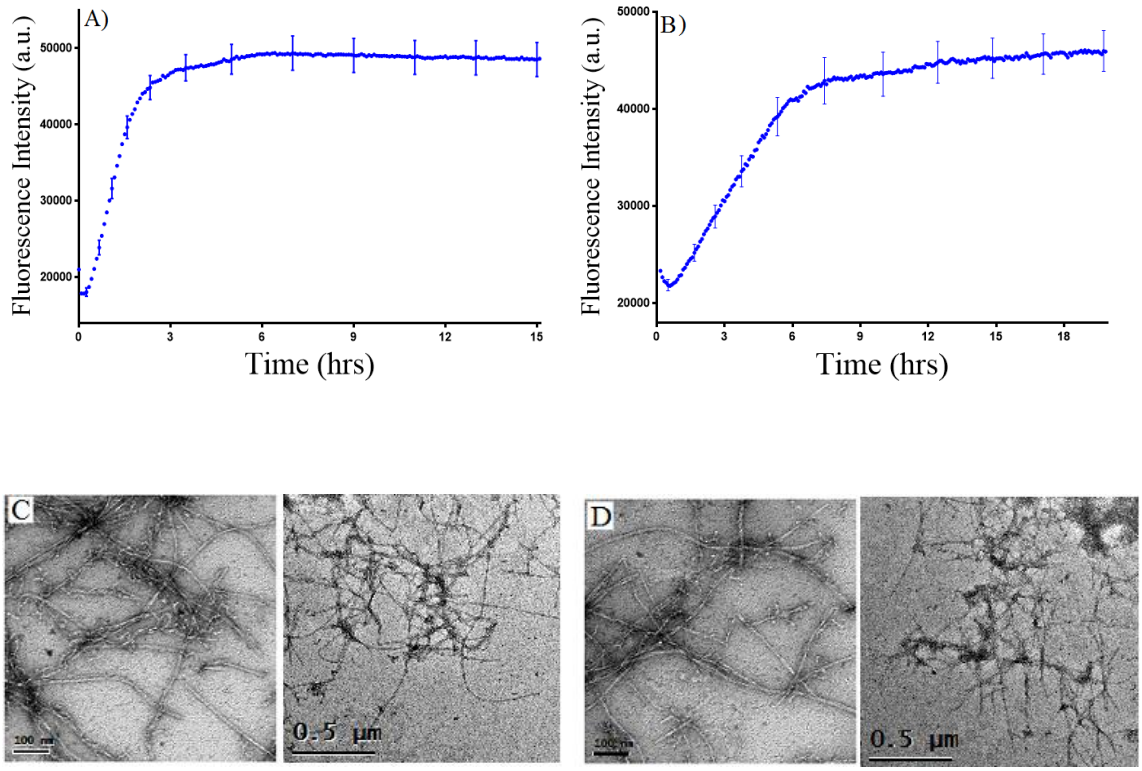

Figure 5.4. Thio T curves and TEM of Aβ$_{1-42}$ fibrillisation in minimal and continuous shaking conditions. Thioflavin T fluorescence curves showing Aβ$_{1-42}$ fibrillisation reactions. Aβ$_{1-42}$ was incubated at 11 µM in 50 mM sodium phosphate pH 7.4, 150 mM NaCl in an Omega plate-reader at 37 °C either with **A)** continuous shaking at 300 r.p.m. or **B)** minimal shaking at 100 r.p.m. for only 10 seconds before each reading. The increase in fluorescence intensity at 482 nm was monitored over several hours. The mean of 3 different experiments with 5 replicates from each experiment was plotted. **C** and **D:** Aβ fibrils produced during thioflavin T experiments at different shaking conditions in 50 mM sodium phosphate pH 7.4, 150 mM NaCl show a similar structural morphology after 24 hours. Scale bars are indicated.

From the Aβ growth curves obtained in continuous and minimal shaking conditions, the lag time (t_{lag}), half time (t_{50}) and growth times (t_{growth}) were determined (as discussed in section 4.3) and presented in table 5.2. The t_{lag} and t_{50} times are much shorter in the case

of continuous shaking, probably due to the fact that shaking can cause fragmentation of the fibrils. Fibril fragmentation can thus accelerate the rate of secondary nucleation. As amyloid aggregation is an autocatalytic process, monomer addition to the ends of preformed fibrils is more favourable and faster than the formation of new fibrils from the monomers and, consequently, the aggregation rate depends on the number of fibril ends.

Conditions \Values	t_{lag} (hours)	t_{50} (hours)	t_{growth} (hours)
Continuous shaking	0.6 ± 0.14	1.3 ± 0.23	2.2 ± 0.4
Minimal shaking	1.54 ± 0.3	4.2 ± 0.2	4.7 ± 0.7

Table 5.2. The mean and sem of t_{lag}, t_{50}, t_{growth} values of Aβ fibrillisation curves in both continuous and minimal shaking conditions.

The morphology of produced $A\beta_{1-42}$ fibrils were analysed by transmission electron microscopy of the fibrils produced. Electron micrographs of the $A\beta_{1-42}$ fibrils in these different conditions after 24 hours are presented in figure 5.4 C&D. TEM confirmed that mature fibrils had formed in all of the samples. The fibrils are long, straight and unbranched. There appeared to be very little structural variation between $A\beta_{1-42}$ fibrils produced in these two different preparations.

5.3.3. Addition of hCC to $A\beta_{1-42}$ Fibrillisation

5.3.3.1. Thioflavin T Time-course

The kinetics of $A\beta_{1-42}$ fibrillisation were monitored in the presence of different molar ratios of hCC, with 11 μM $A\beta_{1-42}$, as shown in Figure 5.5. Each curve is the average of 3-5 different experiments, each experiment with 5 replicates.

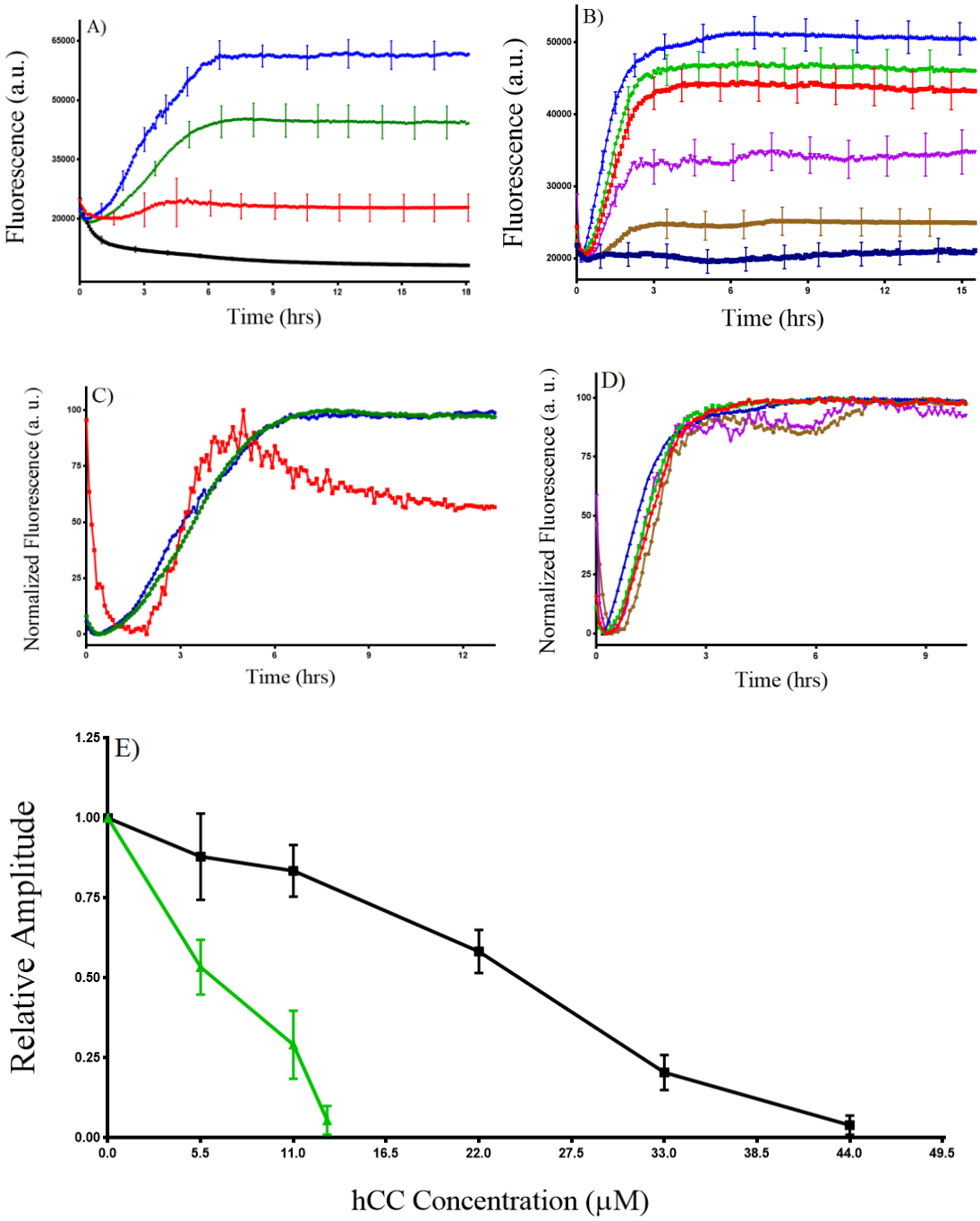

Figure 5.5. Concentration dependence inhibition of $A\beta_{1-42}$ in minimal and continuous shaking conditions. Thioflavin T fluorescence time-courses of $A\beta_{1-42}$ fibrillisation at 11 μM with the addition of different molar ratios of hCC; blue (0 μM), green (5.5 μM), red (11 μM), black (13 μM), purple (22 μM), brown (33 μM) and dark blue (44 μM). Each curve is the average of 5 replicates, with error bars indicating the standard error of the mean (SEM). A) In minimal shaking and B) Continuous shaking conditions. C) and D) normalized data from A) and B), respectively. E) The relative amplitude of thioflavin T curves of Aβ fibrillisation (11μM) in the presence of different concentrations of hCC in minimal shaking (green) and continuous shaking (black) conditions. The error bars represent SEM.

In minimal shaking conditions slightly higher than equimolar concentrations of hCC caused complete inhibition of thioflavin T fluorescence, suggesting complete inhibition of fibril production. hCC concentrations of 11 μM and 5.5 μM caused a reduction in thioflavin T fluorescence of 90% and 40% respectively. However, in continuous shaking conditions, 4 times the equimolar concentration was needed to completely inhibit Aβ aggregation (Figures 5.5.B&E). Equimolar concentration of hCC only slightly reduced the amplitude of Aβ aggregation curves. This suggests that hCC only binds to a subset of $A\beta_{1-42}$ species and that these are less highly populated under shaking conditions.

Unlike TTR, hCC did not show any effect on the shape of the curves of Aβ aggregation time courses with the curves showing similar t_{lag}, t_{50} and t_{growth}. It was not any increase in thioflavin T fluorescence upon incubation of hCC alone, indicating that hCC did not form fibrils in these conditions. Normalisation of the curves shows that superficially there is very little difference in either the lag phase or the elongation rate of the reactions under all conditions (Figures 5.5.C&D).

5.3.3.2. Electron Microscopy

In spite of the fact that reductions in thioflavin T fluorescence suggested that hCC was inhibiting $A\beta_{1-42}$ fibril production, this reduction in fluorescence intensity could be down to other factors such as the formation of different Thioflavin T species or changes in morphology. TEM was employed to investigate the structural morphology of the structures formed at the end of the incubation of $A\beta_{1-42}$ in the presence of inhibitory concentrations of hCC. Figure 5.6 shows electron micrographs of $A\beta_{1-42}$ after at least 24 hours of incubation in the presence of inhibitory concentrations of hCC in two different conditions. In the absence of hCC, $A\beta_{1-42}$ produces long straight unbranched fibrils (Figure 5.4.) while in its presence, a large amount of amorphous aggregate was observed in both conditions (Figure 5.6).

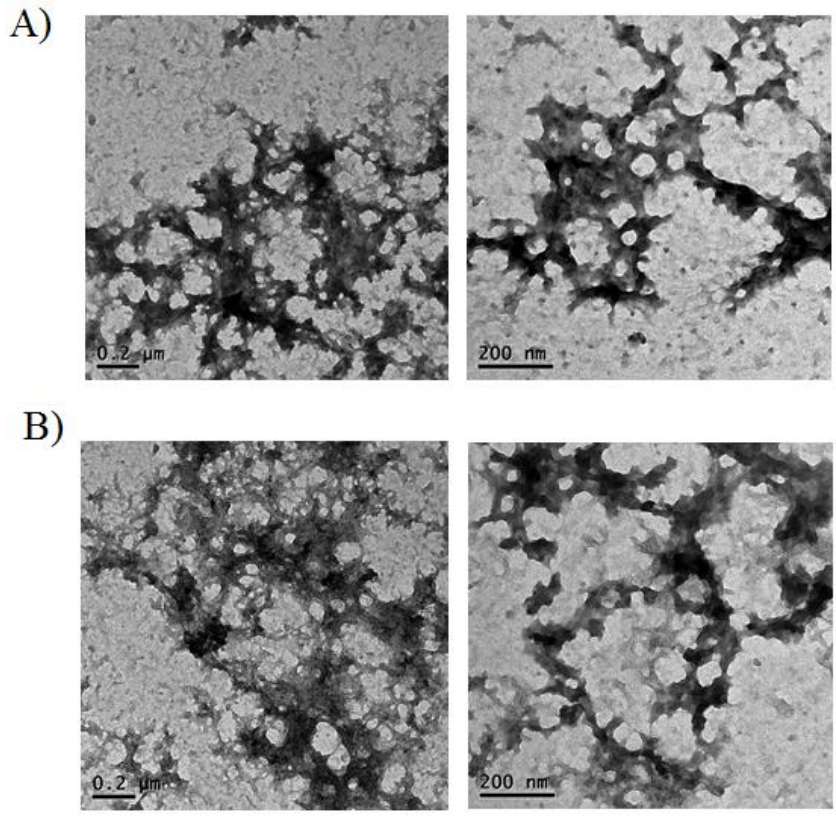

Figure 5.6. TEM of incubated $A\beta_{1-42}$ in the Presence of hCC

Electron micrographs of $A\beta_{1-42}$ (11 µM) in the presence of inhibitory concentrations of hCC after at least 24 hours. A) $A\beta_{1-42}$ in the presence of 13 µM of hCC in minimal shaking conditions and B) $A\beta_{1-42}$ in the presence of 44 µM of hCC in continuous shaking conditions. The scale bars re indicated.

5.3.4. hCC binding to $A\beta_{1-42}$ fibres

Equimolar amounts of purified $A\beta_{1-42}$ fibrils and WT hCC were incubated at 30°C for 2 hrs. The mixture was centrifuged for 20 minutes at 13,000 rpm to co-pellet $A\beta_{1-42}$ fibrils and bound hCC. The concentration of the co-pelleted fraction of hCC was determined by subtracting the hCC concentration left in the supernatant from the original hCC concentration at the start. hCC alone was also incubated, spun down and pelleted as a control.

18% of WT hCC co-pelleted with the $A\beta_{1-42}$ fibrils suggesting that 18% of hCC was bound to $A\beta_{1-42}$ fibrils, which is nearly a ratio of 1:5 of hCC to $A\beta_{1-42}$. This result is

consistent with 18% disappearance of hCC when incubated with the equimolar amounts of $A\beta_{1-42}$ after 24 hrs and monitored by 1D ^{1}H NMR (section 5.3.8.4).

5.3.5. $A\beta_{1-42}$ defibrillisation by hCC

Equimolar amounts of hCC were incubated with purified $A\beta_{1-42}$ fibrils and the thioflavin T signal monitored. Only a very small reduction in thioflavin T fluorescence is observed in both the Aβ control and in the presence of hCC (Figure 5.7.), which might be due to temperature adjustment or dilution of the fibrils. This suggests that WT hCC does not dissolve pre-formed mature $A\beta_{1-42}$ fibrils in the time course of this experiment, but rather has an effect on their formation.

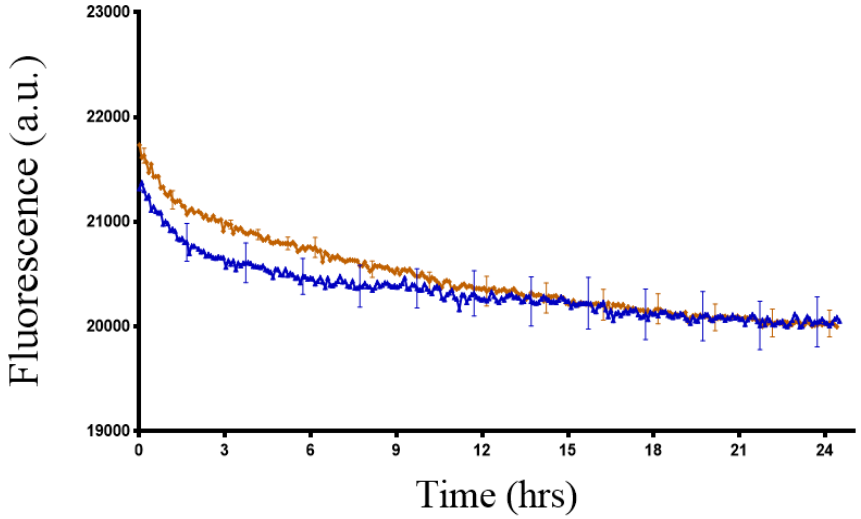

Figure 5.7. $A\beta_{1-42}$ defibrillisation by WT hCC. Thioflavin T curves for the $A\beta_{1-42}$ defibrillisation assay, where blue represents 11μM purified Aβ fibrils in standard phosphate buffer and brown is the same amount of purified fibrils in the presence of an equimolar amount of monomeric WT hCC. The initial decrease is most likely a temperature adjustment.

5.3.6. Inhibition of seeding

$A\beta_{1-42}$ seeds were generated by sonication of purified fibrils for 30 minutes. Addition of 10% of these seeds significantly shortened or removed the lag time of monomeric $A\beta_{1-42}$ aggregation. Compared with WT TTR, which had no impact on seeding, addition of

equimolar amounts of hCC completely inhibited the seeding effect. It has been shown that formation of amyloid fibrils by $A\beta_{1-42}$ happen by a nucleated growth mechanism (Evans *et al.,* 1995). In the absence of an aggregate, a nucleus has to be formed in situ in a process that needs a relatively high concentration of the peptide and significant dead time. When an aggregation seed is present due to addition of exogenous aggregates, the nucleation time of the reaction is reduced and the fibril extension step is more quickly started (Evans *et al.,* 1995). Low concentration (equimolar to Aβ seeds) did not delay the lag time of Aβ fibrillisation. However, higher concentration of WT hCC extended the lag time to what it was in the absence of seeds. This result indicates that WT hCC inhibits the ability of added fibrils to act as seeds for fibril formation only when it is present in excess to seeds. This suggests that despite WT hCC's ability to bind and presumably cover the surface of fibrils, it is not very effective in preventing addition of Aβ monomers to the extension sites of an amyloid fibril.

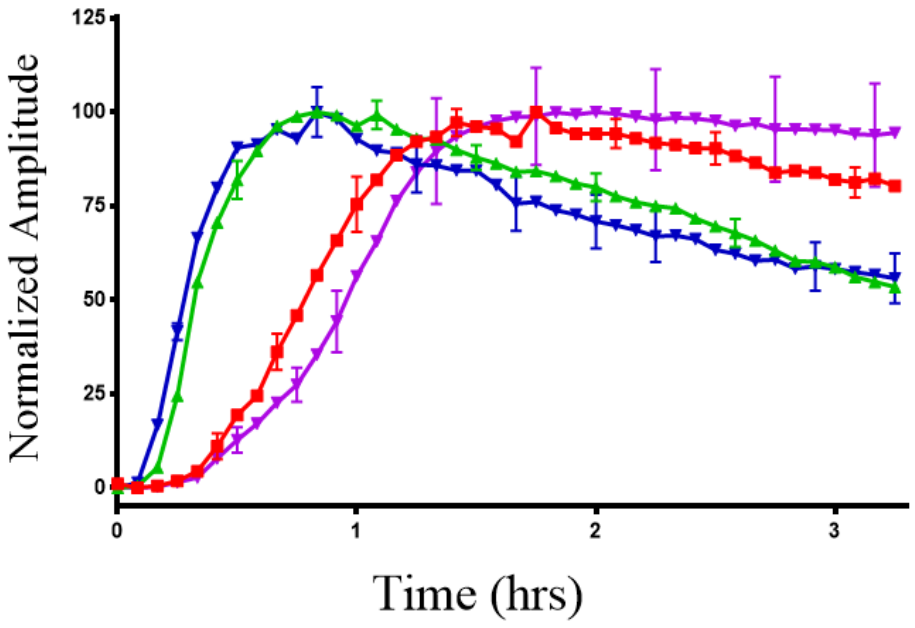

Figure 5.8. Thioflavin T curves of inhibition of Aβ seeding by WT hCC. Red is 6μM of $A\beta_{1-42}$ monomers in phosphate buffer, green is 6μM of $A\beta_{1-42}$ monomers seeded with 1 μM of $A\beta_{1-42}$ seeds, blue is 6μM of $A\beta_{1-42}$ monomers seeded with 1 μM of $A\beta_{1-42}$ seeds in the presence of 1 μM of hCC, purple is 6μM of $A\beta_{1-42}$ monomers seeded with 1 μM of $A\beta_{1-42}$ seeds in the presence of 6 μM of hCC.

5.3.7. Addition of Dimer

Dimers of hCC were produced and characterised and their ability to inhibit Aβ fibrillisation was investigated using thioflavin T fluorescence. An investigation into the effect of cystatin B on amyloid fibril formation by Aβ suggested that tetramers of this wild-type cystatin completely inhibit Aβ fibrillisation, as showed by thioflavin T and TEM, whereas the monomer, dimer and higher oligomeric species do not have this inhibitory effect (Skerget *et al.*, 2010a). Similarly, it has been found that non-native species of transthyretin and neuroserpin are more effective inhibitors, possibly as this favours exposure of the active binding site (Du and Murphy, 2010, Chiou *et al.*, 2009).

Dimers were produced by heating 50 μM hCC in 50 mM sodium phosphate pH 7.4, 150 mM NaCl at 68°C for 30 minutes before purification using a Superdex 200 (GE Healthcare, UK) size exclusion column in 50 mM sodium phosphate pH 7.4, 150 mM NaCl. Figure 5.9. shows the change in thioflavin T fluorescence when the hCC dimer preparation was incubated with 11 μM $A\beta_{1-42}$ at two different dimer concentrations, 11 μM and 22 μM. Unlike the monomers, the addition of dimer has no effect on the final yield of fibrils produced. This confirms the previous work by Abigail Williams in our group (Williams, 2015).

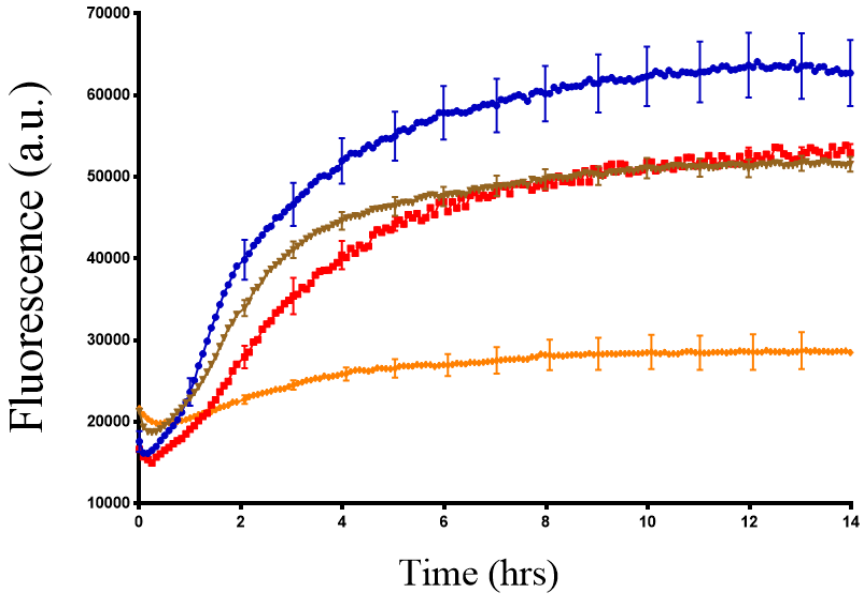

Figure 5.9. Addition of hCC Dimer to $A\beta_{1-42}$ fibrillisation reaction. Molar ratios of 1:2 (brown) and 1:1 (red) $A\beta_{1-42}$ to hCC dimer and 1:1 molar ratio of Aβ with hCC monomers (orange) were incubated and monitored by thioflavin T fluorescence. Each curve is the average of 4 or 5 replicate reactions with the standard error of the mean indicated by the error bars.

5.3.8. NMR Spectroscopy

The nature of the interaction between hCC and $A\beta_{1-40}$ (Keeley, 2007, Elshawaihde, 2012) and $A\beta_{1-42}$ (Williams, 2015) has been investigated by previous lab members through ^{1}H ^{15}N HSQC titration experiments. These studies showed that there are no major chemical shift changes when $A\beta_{1-40}$ or $A\beta_{1-42}$ is titrated into a sample of hCC up to 1:1.2 equivalences, despite the observed inhibition of Aβ fibril formation by hCC. These experiments were performed in different buffer conditions to the Thio T experiments presented here. ^{1}H-^{15}N HSQC NMR experiments were performed in 15mM Tris buffer, pH 7.4, 278K for hCC and Aβ monomer binding in order to prevent oligomerisation of the peptide during the experiment (Williams, 2015). In order to investigate the interaction between hCC and Aβ in the same buffer as used for our thioflavin T experiments, the ^{1}H-^{15}N HSQC spectrum of hCC was first assigned under these buffer conditions based on previous assignments and then the $A\beta_{1-42}$ titrated into hCC.

5.3.8.1. Assignement of the ^{1}H ^{15}N HSQC of hCC in 50 mM phosphate buffer, pH 7.4, 150mM NaCl.

Previously, the ^{1}H ^{15}N hCC HSQC spectrum was assigned in 15 mM Tris-TFA, pH 7.5, with no added salt (Keeley, 2007). This spectrum was used to assign hCC spectra in (50 mM phosphate buffer, pH 7.4, 150mM NaCl) by salt titration and tracking the shifts in the amide peaks.

An ^{1}H ^{15}N HSQC experiment measures the chemical shift of the nitrogen and amide proton. This is attained by modulating each proton signal with the signal of the attached nitrogen. Employing software to deconvolute the two frequencies can generate a two-dimensional plot of the spectrum with a peak for every amide at the intersection of the proton and nitrogen chemical shifts. As each amino acid contains a backbone amide, each peak in the ^{1}H ^{15}N HSQC spectrum will correspond to a specific residue within the protein structure. The chemical shift in amide is directly correlated to its local chemical environment. As a result factors that alter the chemical environment of the amide can be revealed by changes in the ^{1}H ^{15}N HSQC spectral property. Accordingly, peaks may show a shift in position or a change in intensity. Alternatively, they can broaden or fade away completely. It is important to know which amide, and therefore residue, corresponds to which peak in the spectrum to allow changes in the chemical environment to be mapped onto the protein structure. This is achieved through a process known as resonance assignment. The chemical shift is expressed in parts per million (ppm), which accounts for the field strength at which it is measured.

Salt titration

Changes in the ^{1}H ^{15}N HSQC spectrum were successfully tracked as the salt concentration was increased from 0 to 150 mM. The salt concentration was increased from 0 to 20 and then 150mM Figure 5.10. shows the change in chemical shift of each amide in the ^{1}H ^{15}N HSQC spectrum. The majority of peaks can be tracked from their position at no salt to their position at 150 mM NaCl as they showed only very small shifts during the course of the titration. Intensity changes were also only minor for the majority of residues, the gentle decrease that is observed can be attributed to the minor dilution factor caused by addition of salt to the sample. The distribution of amide peaks corresponds well with the established assignment in the conditions used by (Keeley, 2007) and (Williams, 2015). As even small changes in the chemical environment are reflected in the ^{1}H ^{15}N HSQC spectrum, this validates the reproducibility of the sample preparation. There is no evidence for the characteristic shifts in the peaks that are attributed with dimerisation in either the 1D or 2D spectra, confirming that the protein is in the required monomeric state. Out of 120 residues, 87 were successfully; the ones that were excluded were either not present (prolines), significantly overlapped or very weak.

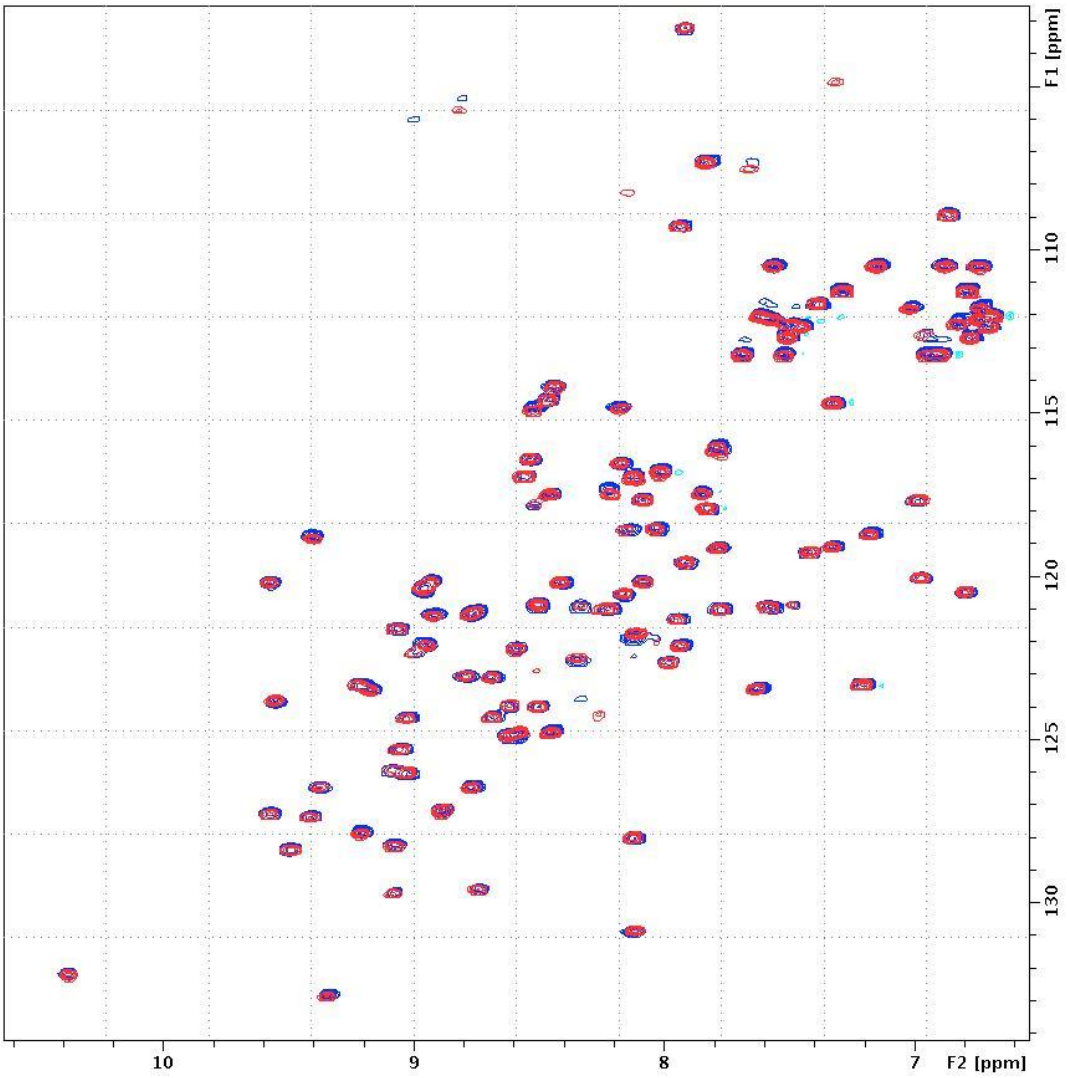

Figure 5.10. ^{1}H-^{15}N HSQC spectrum of hCC salt titration. The associated chemical shift changes observed in the ^{1}H-^{15}N HSQC spectra of hCC as the NaCl concentration increased from 0 (blue) to 150 mM (red positions). The spectra were recorded at 303K using 50 µM hCC in 50 mM phosphate buffer, pH 7.4, 2 mM sodium azide. F1 represents the ^{1}H dimension, F2 represents the ^{15}N dimension.

5.3.8.2. ^{1}H ^{15}N HSQC Spectrum of hCC

The ^{1}H 1D spectrum of 50 µM hCC in 50 mM phosphate buffer, pH 7.4 at 303 K shows a wide dispersion of amide proton resonances (6-10 ppm) and up-field aliphatic proton peaks (below 0 ppm) indicating that hCC is folded. This is reflected in the ^{1}H ^{15}N HSQC spectrum where the amide chemical shifts are also well dispersed (Figure 5.11).

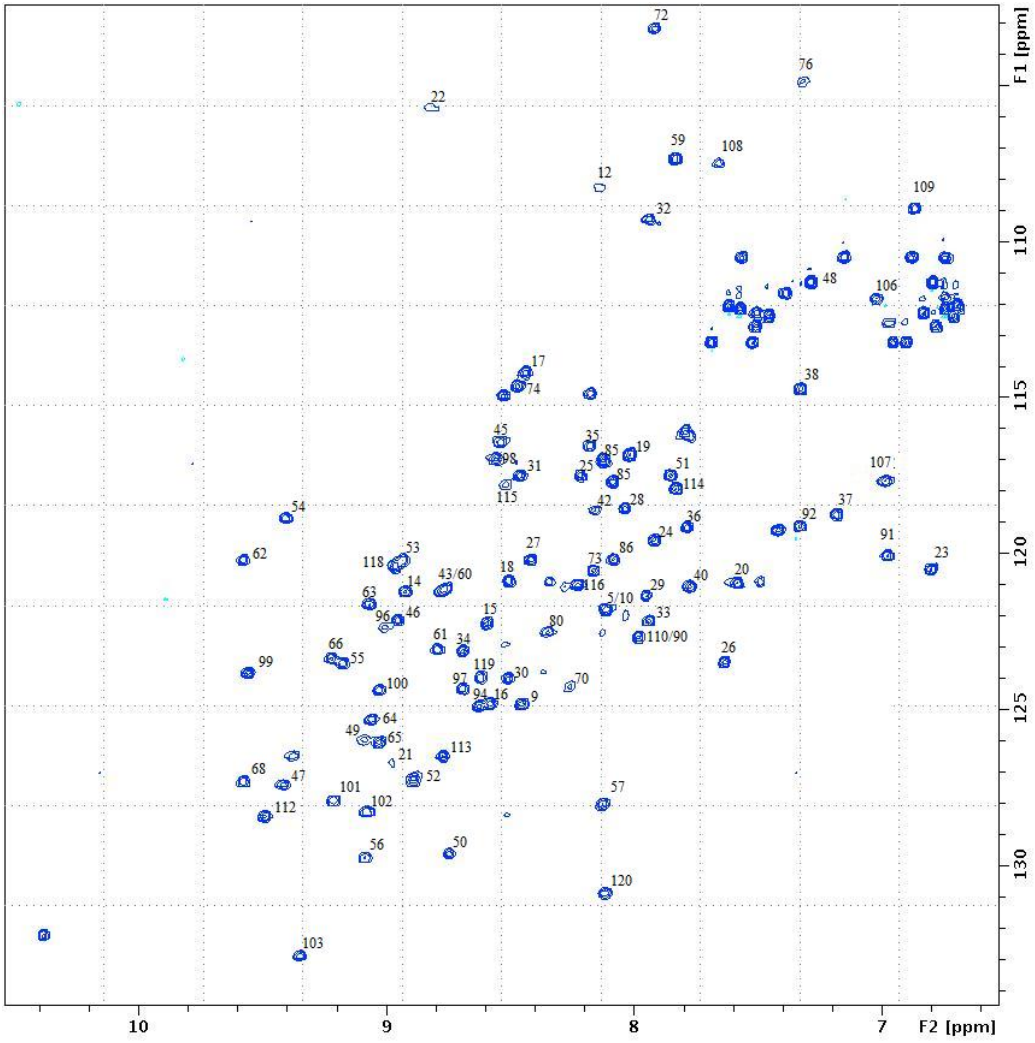

Figure 5.11. ^{1}H ^{15}N HSQC Spectrum of hCC at 303 K. An ^{1}H ^{15}N HSQC spectrum of 50 μM hCC incubated in 50 mM Phosphate buffer, pH 7.4, 150 mM NaCl at 303 K, showing the amide assignment. F1 represents the ^{1}H dimension and F2 represents the ^{15}N dimension.

5.3.8.3. Titration with monomeric Aβ$_{1-42}$

Aβ$_{1-42}$ was added to a monomeric hCC sample. As has been previously observed (Elshawaihde (2012); Williams, 2015) there are only very minor chemical shift changes. The lack of chemical shift changes at equimolar concentrations (1:1 of Aβ$_{1-42}$: hCC) indicates that there is no change in the local chemical environments of any of the residues. This suggests that there is no binding between hCC and Aβ monomers. The solution conditions of the two proteins were the same (no change in pH and salt caused artefacts).

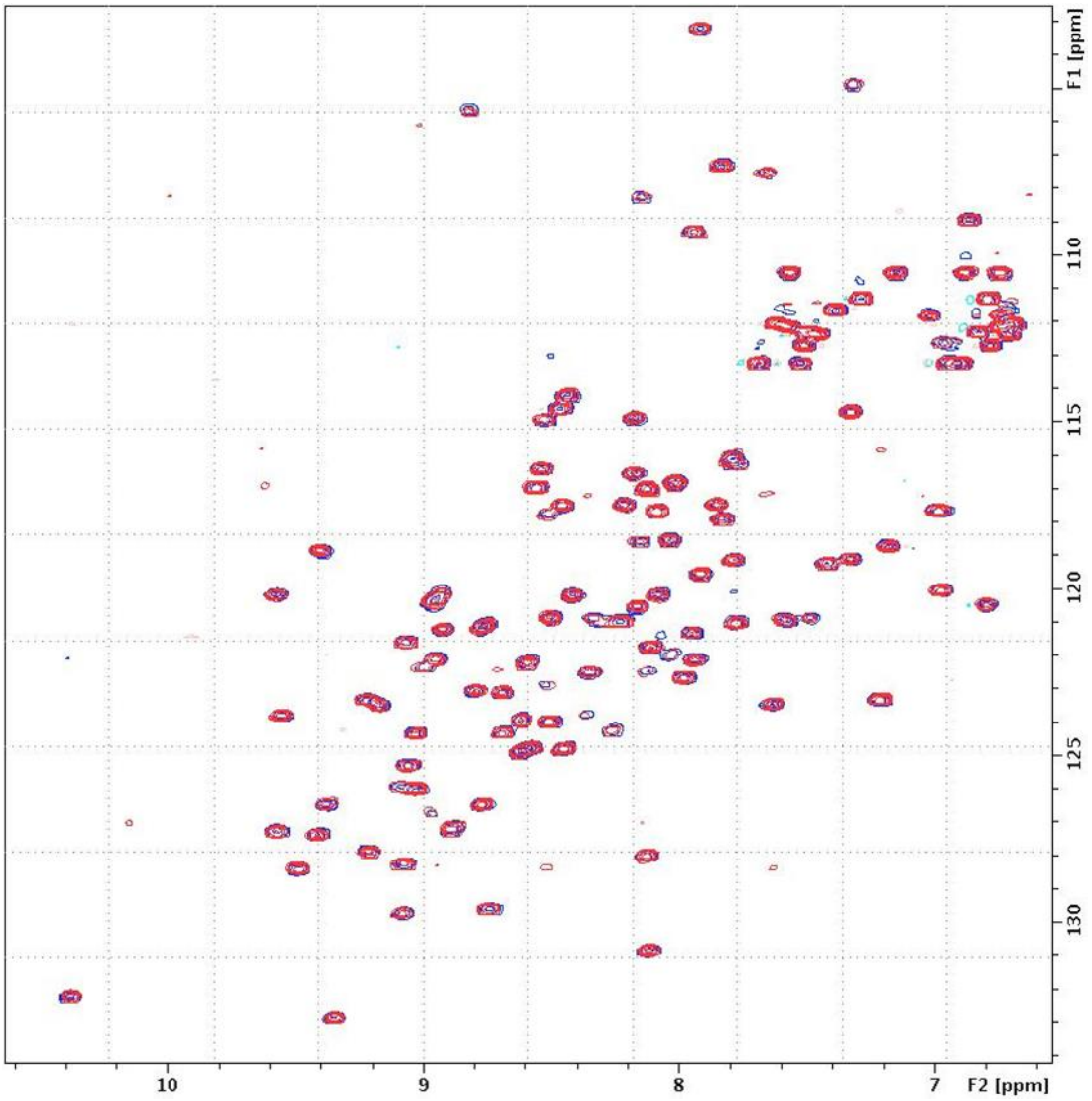

Figure 5.12. Titration of hCC with Aβ$_{1-42}$. A reference ^{1}H ^{15}N HSQC spectrum of ^{15}N labelled 50 µM hCC in 50 mM phosphate buffer, pH 7.4, 150 mM NaCl at 303 K (blue) was overlaid with the spectrum of hCC where an equivalent amount of Aβ$_{1-42}$ has been added (shown in red). F2 represents the ^{1}H dimension and F1 represents the ^{15}N dimension.

5.3.8.4. 1D ^{1}H NMR Time course of the fibrillisation reaction

Measuring the reduction in the ^{1}H 1D NMR spectral intensity of Aβ$_{1-42}$ peptide and hCC over time can give information on the rate of their monomer disappearance, as the intensity of the spectral signal corresponds to the monomer population. Because NMR is unable to detect large molecules, Aβ$_{1-42}$ monomer signal intensity reduces as it forms large aggregates and hCC monomer signal intensity reduces as it binds to large Aβ$_{1-42}$

aggregated structures. 1D ^{1}H spectra of both $A\beta_{1-42}$ and hCC were recorded separately and in the mixture over the time course of the reaction for 24 hrs. The $A\beta_{1-42}$ and hCC spectra were subtracted from the mixture spectrum and the reduction in signal of the spectra was measured (Figure 5.13). In the presence of equimolar amounts (50 μM) of hCC the intensity of the $A\beta_{1-42}$ spectrum was reduced by only 52% compared with the control $A\beta_{1-42}$ which was reduced by 89%. This indicates that in the presence of hCC, 30% more of the $A\beta_{1-42}$ samples is maintained monomeric or as small structures and prevented from going to form large enough aggregates to be invisible by NMR. This result indicates that the hCC prevents $A\beta_{1-42}$ aggregation despite the fact that the ^{1}H ^{15}N HSQC fails to show binding to monomers of $A\beta_{1-42}$. Investigating the hCC 1D ^{1}H spectrum showed that during the same time period, 18% of the hCC disappeared in the mixture with the Aβ compared to 1% in the absence of Aβ, this could be due to hCC molecules binding to the $A\beta_{1-42}$ aggregated structures while they are forming and becoming no longer visible to NMR. The rate of the hCC disappearance was simultaneous with $A\beta_{1-42}$ disappearance further confirming that hCC was binding to the $A\beta_{1-42}$ aggregated structures (figure 5.13B). This result was consistent with the centrifugation results reported here (section 5.3.4.) and the chromatography results obtained by (Williams, 2015) where a percentage (10%) of the monomeric hCC was observed to disappear during incubation with $A\beta_{1-42}$, presumably to go and form a large molecular weight complex with $A\beta_{1-42}$. Both these later experiments were performed at considerably lower concentrations of protein suggesting this binding is significant at micromolar concentrations.

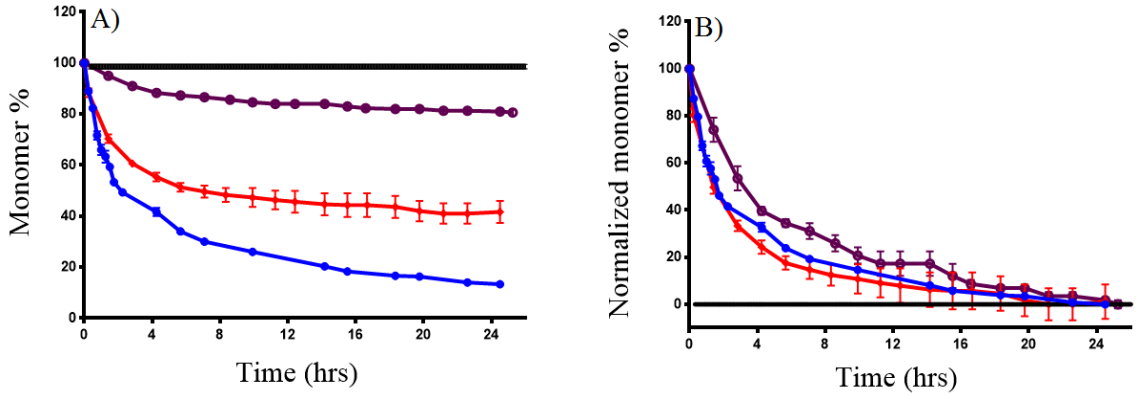

Figure 5.13. The time course of monomer disappearance of both Aβ and hCC obtained by 1D NMR. A) The percentage of Aβ monomer disappearance in Aβ control (blue), Aβ monomer disappearance in the presence of equimolar amount of hCC (red), and hCC disappearance in the Aβ and hCC mixture (purple), hCC disappearance in hCC control (black). The error bars represent (sem). B) The same data normalized to show simultaneous disappearance of Aβ and hCC.

The nature of the species produced in these titrations was verified using TEM and is shown in figure 5.14 where amorphous aggregates are seen in the presence of hCC compared with fibrils in the control. This suggest despite that hCC cause larger fraction of Aβ to stay as monomer or small aggregates, it is also bind to Aβ aggregates and disfavours the fibrillisation pathway of Aβ by leading to the formation of amorphous aggregates.

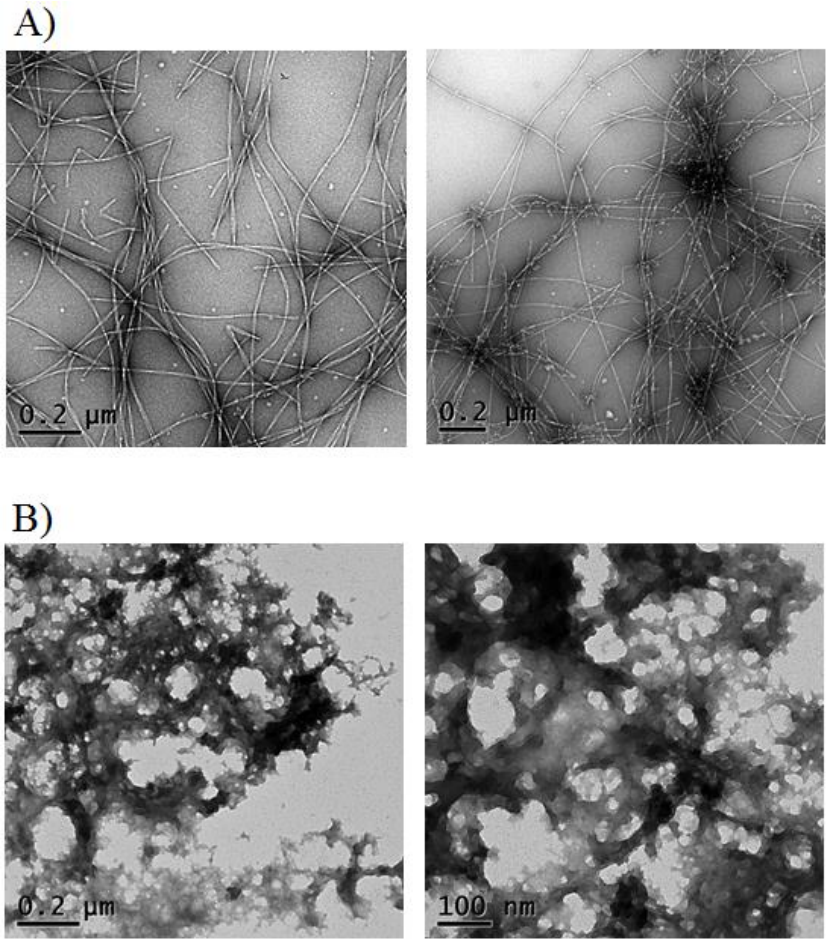

Figure 5.14. TEM of 1D ^{1}H NMR Time-course samples after 24 hrs. Electron micrographs of the 1D ^{1}H NMR time-course experiment where 50 µM $A\beta_{1-42}$ is incubated in the absence (A) and presence (B) of 50 µM hCC in Phosphate pH 7.4, 150 mM NaCl, 2 mM Sodium Azide, at 30°C after 24 hours. The scale bars are indicated.

5.3.9. Addition of different hCC mutants

$A\beta_{1-42}$ fibril formation was monitored in the presence of hCC mutants employing thioflavin T fluorescence in minimal shaking conditions. Slightly higher than equimolar concentrations of wild type hCC caused a complete reduction in thioflavin T fluorescence, suggesting complete inhibition of $A\beta_{1-42}$ fibril formation. All other mutants were less effective compared with wild type hCC. Four times the equimolar

concentration of W106A and three times the equimolar concentration of P6A were needed to completely inhibit $A\beta_{1-42}$ fibrillisation. Around twice the equimolar concentrations of V57A and V50A were needed to inhibit $A\beta_{1-42}$ fibrillisation. Despite their large exposed hydrophobic surfaces, L80A and P105A mutant were very similar to WT hCC. Half molar ratios of hCCs were also used against $A\beta_{1-42}$ to confirm the reproducibility of the results obtained with equimolar concentrations of hCC, and these data confirm that the inhibitory pattern is same.

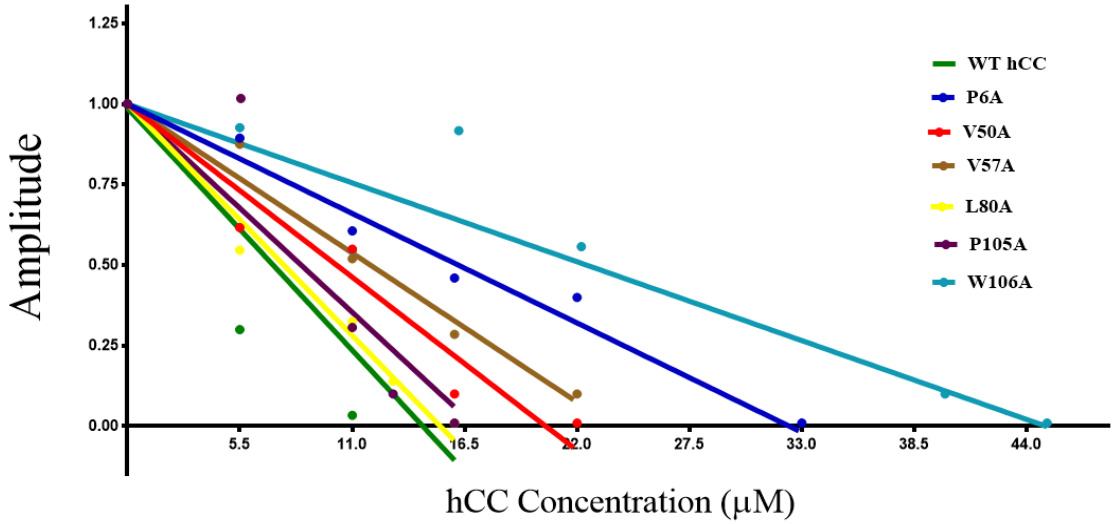

Figure 5.15. $A\beta_{1-42}$ aggregation in the presence of hCC mutants. Linear regression of the amplitudes of thioflavin T curves of Aβ aggregation in the presence of different concentration of WT hCC and mutants, as indicated.

The inhibitory order of mutants compared to WT was WT > L80A> P105A> V50A> V57A> P6A> W106A. These results indicate that hydrophobic residues like P6 which is located in the unstructured N-terminal region and W106 from the protease inhibition part of the protein are mostly involved in Aβ inhibition. Other nearby residues from the

active site region, V57 and V50, were significantly less effective than WT, indicating a lesser involvement in the inhibition. Interestingly, although V50 is well away from the protease binding site, mutation of this residue does affect inhibition suggesting this second hydrophobic patch may be involved, either directly or indirectly, by destabilising the protease binding site. P105, despite its large solvent accessible hydrophobic surface and proximity to W106 is not significantly different from the WT. The last mutated residue, L80, is least involved in $A\beta_{1-42}$ binding suggesting this third hydrophobic region is not involved.

5.4 Discussion

5.4.1. hCC inhibition is strongly affected by shaking the fibrilliation reactions

The kinetics of $A\beta_{1-42}$ fibrillisation was monitored in two different shaking conditions; minimal and continuous shaking. The Aβ fibrillisation was faster in the continuous shaking conditions. The explanation for this could be that shaking accelerates $A\beta_{1-42}$ nucleation (Morinaga *et al.*, 2010, Lee *et al.*, 2012) and fragmentation of the fibrils (Cohen *et al.*, 2013). Accelerating primary nucleation shortens the time $A\beta_{1-42}$ needs to start fibrillisation and fibril fragmentation can accelerate the rate of secondary nucleation. Amyloid aggregation is an autocatalytic process which means that the monomer addition to the ends of preformed fibril is more favourable and faster than the formation of new fibrils from the monomers and, consequently, the aggregation rate depends on the number of fibril ends.

Amyloid β fibrillisation time courses with hCC were carried out and presented in this thesis. We showed that in minimal shaking conditions hCC will inhibit the amyloid fibril formation by $A\beta_{1-42}$ in a concentration-dependent manner, requiring a 1.3:1 molar ratio of

hCC to $A\beta_{1-42}$ to inhibit this reaction completely, where no increase in thioflavin T fluorescence intensity is detected. Equimolar concentrations significantly reduced thioflavin T fluorescence, but not completely, indicating that a considerable amount of amyloid fibre is still present. In continuous shaking conditions a much higher amount of hCC is needed to completely inhibit $A\beta_{1-42}$ fibrillisation; 4 times more than equimolar concentration was needed. Equimolar concentrations only reduced the amplitude of thioflavin T signal by a small percentage. These differences could be due to the fact that shaking either causes acceleration of nucleation and consequently more hCC will be needed to prevent growing nuclei or causes fragmentation and consequently more fibril ends forming - more hCC is then needed to inhibit enhanced secondary nucleation arising from the fragmentation. Another explanation is that shaking might cause formation of a different morphology of $A\beta_{1-42}$ fibrils which hCC can't bind to and therefore stop from fibrillising. Generally, in all conditions, hCC has no measurable effect on the fibrillisation kinetics of the Aβ peptides that escape inhibition as the t_{lag}, t_{50} and t_{growth} measurements showed no significant differences in the presence and the absence of lower than inhibitory amounts of hCC, however the effect of hCC is purely on the yield of amyloid fibrils. As in our conditions, the $A\beta_{1-42}$ aggregation was not concentration dependant, even a small amount of hCC which escapes inhibition will still aggregate at the same rate as a larger amount in the absence of hCC.

It has previously been suggested that ratios of 1:1 hCC to $A\beta_{1-42}$ are needed to completely inhibit the amyloid fibrils formation by $A\beta_{1-42}$ (Sastre *et al.*, 2004a). However, substoichiometric concentrations of hCC (0.3 μM) have been shown to protect both N2a neuroblastoma cells and rat primary hippocampal neurons from Aβ-induced cell death when incubated with 30 μM of $A\beta_{1-42}$. Our results from minimal shaking conditions were consistent with the above study as near equimolar amount of hCC inhibited fibrillisation

completely. It has been previously found in our lab that ratios of 2:1 hCC to $A\beta_{1-42}$ are required to completely inhibit the formation of amyloid fibres by $A\beta_{1-42}$ in continuous shaking conditions (Williams, 2015). The results obtained in the current study were different from the previous results obtained by (Williams A, 2015), as 4 times more than an equimolar amount of hCC was required to completely inhibit Aβ fibrillisation under similar continuous shaking conditions. This might be due to the impurities in the hCC batch used by (Williams A, 2015) as shown by SDS PAGE and HPLC experiments. This is explained in detail in chapter 6.

5.4.2 Aβ forms amorphous aggregates in the presence of hCC

Observation of the sample by TEM indicated that instead of amyloid fibrils, large amounts of amorphous aggregates had been produced through the incubation of $A\beta_{1-42}$ with near equimolar amounts of WT-hCC in minimal shaking conditions and 4 times equimolar concentration in the continuous shaking conditions. It is possible that hCC is stabilising off-pathway states and preventing their further aggregation to produce mature fibrils. This result was consistent with the results obtained by Sastre et al. (2004), when they found that $A\beta_{1-42}$ formed amorphous aggregates in the presence of twice equimolar amounts of hCC. Studies have showed a remarkable reduction in cytotoxicity when hCC is incubated with Aβ (Kaeser *et al.*, 2007a, Mi *et al.*, 2007b, Tizon *et al.*, 2010a), demonstrating that the species forming do not exhibit the toxic activity that is observed with Aβ alone.

One of the challenges in this study was variability in the inhibitory efficacy of WT hCC and variants through different experiments even when the same batch of the inhibitor was used. This variability could be due to the fact that hCCs inhibit Aβ fibrilisation not through binding to monomeric Aβ hence through binding to aggregated structures, like

oligomers and protofibrils of Aβ. As Aβ oligomers are very heterogeneous, different results could be obtained in different experiments, when the pathway of Aβ aggregation is different from one experiment to another. Another explanation of this variability is that handling of the Aβ during the experiment is likely to introduce air to the Aβ: hCC mixture during pipetting, this will enhance Aβ aggregation and reduce hCC efficacy to inhibit aggregation, as the air-water interface is known to interfere with Aβ nucleation (Garai *et al.*, 2008, Morinaga *et al.*, 2010). As the hCC yield was very low, the probability for the presence of contaminants was higher, this could be another reason for the variabilities found in hCCs effects. An *E. coli* protein contaminant co-purifiy with hCC and was later found to have inhibitory effects on Aβ fibrillisation, the details of this can be found in chapter 6.

5.4.3. Aβ and hCC do not bind as monomers but hCC does inhibit Aβ assembly

Previously in our lab, the effect of Aβ addition on the NMR ^{1}H ^{15}N-HSQC spectrum of hCC was investigated to look for clues to possible binding sites. The time course of the interaction was followed in a Tris buffer pH 7 with no added salt, to keep Aβ monomeric for a longer time to detect binding to monomer. Despite the inhibition of Aβ fibril formation, no shifted amide cross-peaks were observed in ^{1}H ^{15}N-HSQC spectra of hCC incubated with Aβ at 30°C (Williams, 2015). In order to exclude the possibility of buffer interference (effects) on hCC binding to Aβ, the same ^{1}H ^{15}N-HSQC NMR experiments were repeated in an identical buffer condition to that used for thioflavin T experiments. No significant chemical shifts in any of the amide cross-peaks were observed in ^{1}H ^{15}N-HSQC spectra of hCC incubated with $A\beta_{1-42}$. Titration results were similar to previous results obtained in our lab confirming no complex formation between monomeric hCC and Aβ. However, this result was inconsistent with published data which suggested the formation of a high-affinity complex between the two proteins as investigated by ELISA

(Sastre *et al.*, 2004a). It is believed that the inconsitency in these results could be due to the fact that the ELISA experiment is carried out on a surface, whereas the NMR experiment is in solution. A similar variation has been showed in experiments with transthyretin, indicating solid-phase binding assays may not be entirely consistent with binding characteristics or inhibition of fibril formation observed in the liquid-phase (Li *et al.*, 2013b). We have also found variations in the inhibitory effect of transthyretin on Aβ fibrillisation in the presence of different surfaces (chapter 3).

1D ^{1}H NMR spectra of both $A\beta_{1-42}$ and hCC were investigated to monitor the reduction in the amount of monomer over the time period of 24 hrs. In the $A\beta_{1-42}$ control 89% of monomers disappeared compared to 52% in the presence of equimolar amounts of hCC. The hCC spectral signal intensity reduced by 18% in the mixture with the $A\beta_{1-42}$ compared to 1% in the absence of $A\beta_{1-42}$. This indicates that hCC reduces the formation of large structures by $A\beta_{1-42}$ and causes a larger fraction of Aβ to stay as monomer or small aggregates. Despite that, the ^{1}H ^{15}N-HSQC fails to show hCC binding to $A\beta_{1-42}$ monomers, the simultaneous disappearance of hCC with $A\beta_{1-42}$ suggests that hCC bind to $A\beta_{1-42}$ aggregated structures in the ratio of 1:3 hCC to $A\beta_{1-42}$, as 18% of hCC disappear compared to 52% of $A\beta_{1-42}$ at the same time. These results are consistent with the chromatography results obtained by (Williams, 2015) as a percentage (10%) of the monomeric hCC was observed to disappear during incubation with $A\beta_{1-42}$. This suggested that hCC forms a large molecular weight complex with $A\beta_{1-42}$.

5.4.4. Does hCC bind to $A\beta_{1-42}$ fibrils?

In order to identify the nature of the $A\beta_{1-42}$ species that interacts with hCC, the inhibitor was added to $A\beta_{1-42}$ fibrils. The hCC incubated with purified $A\beta_{1-42}$ fibrils and the fraction of hCC co-pelleted with fibrils by centrifugation was measured. Nearly 20% of the hCC co-pelleted with the equimolar amount of fibrils (calculated as monomer equivalent). This

result shows that hCC bind and cover the surface of the fibrils in 1 to 5 molar ratio of hCC to $A\beta_{1-42}$. Despite hCC binding to the $A\beta_{1-42}$ fibrils, co-incubation of hCC with $A\beta_{1-42}$ fibrils and monitoring the fibril disaggregation applying thioflavin T did not show disaggregation of $A\beta_{1-42}$ fibrils, at least in the time course of the thioflavin T experiment. Addition of a large amount of hCC was needed to inhibit seeding of the $A\beta_{1-42}$ fibrillisation reaction. Presumably, hCC can only cover the surface of the fibrils as showed by co-pelleting assays, however, it is not active in inhibition of elongation of the seeds from the ends. Overall, results so far suggest that WT hCC can bind and cover the surface of fibrils and prevent $A\beta_{1-42}$ monomers from starting aggregation using the fibril surface as a template. Similar behaviour by another amyloidogenic protein has been suggested. Brichos is an amyloidogenic protein domain which is also found highly concentrated in Aβ amyloid plaques in the brain. It have been showed that Brichos can bind to $A\beta_{1-42}$ fibrils without defibrillising, however, it can prevent the use of the fibre surface as a secondary nucleation template for the formation of new fibrils (Cohen *et al.*, 2015). These findings suggest a different role for hCC and Brichos in preventing amyloid plaque formation in the brain by preventing secondary nucleation.

5.4.5. The hCC interface

The different forms of hCC were also investigated in terms of their inhibitory activity. The addition of an equimolar concentration of hCC dimer to the $A\beta_{1-42}$ aggregation reaction has no effect on the thioflavin T fluorescence changes, showing no decrease in fibril yield, compared to $A\beta_{1-42}$ incubated in the presence of hCC monomer. This reinforced the view that the dimer interface is crucial to the inhibitory activity of hCC.

In order to find the binding surface of the hCC to $A\beta_{1-42}$ protofibrils or fibrils, several hydrophobic residues chosen from 3 identified hydrophobic patches were mutated to alanine. Mutated hCCs were tested for $A\beta_{1-42}$ fibrillisation inhibition. In region 1,

corresponding to the dimer interface the P6 residue from the unstructured N-terminal region of hCC and another residue, W106 from the active site of protease inhibitor significantly reduced the hCC inhibitory effect. V57A in region 1, from the active site and V50A from the second part also reduced hCC's inhibitory effect but to a smaller degree. L80 exhibits a large accessible hydrophobic surface area, however it did not significantly reduce the hCC's ability to inhibit Aβ fibrillisation suggesting that this loop's site of hCC is not involved in the binding. The P105 residue was also unaffected by hCC's inhibitory action despite its large solvent accessible hydrophobic surface and its proximity to the most affected W106 region, this could be due to the direction of the P105 hydrophobic surface which is away from the binding site. These results together suggest that the N-terminal unstructured part and residues with large accessible hydrophobic surface areas located in or close to the active site and the hydrophobic surface facing outward are effectively involving in the hCC binding to $A\beta_{1-42}$ aggregated structures.

A potential model for this system could be that hCC is binding to an aggregated structure of Aβ as the results obtained in this study and previous work in our lab strongly suggest that hCC binds a species of $A\beta_{1-42}$ other than monomer. Presumably, this binding happens through its N-terminal unstructured part and residues with large accessible hydrophobic surface areas located in the active site as the results from mutant hCCs suggest. Our results suggest that the stoichiometry of the binding is about 1 hCC molecule to 3 to 5 $A\beta_{1-42}$ monomers in the aggregated structure. The hCC binding to $A\beta_{1-42}$ aggregated structures diverting the assembly pathway and causing the formation of amorphous non-toxic aggregates and this is consistent with previous studies, in which hCC is shown to cause the production of amorphous aggregates and non-toxic to the cells (Sastre *et al.*, 2004a).

Chapter Six: Variability in the observed activity of recombinant cystatin C on Aβ fibrillisation- Isolation of GLTI, an active inhibitor from *E. Coli* periplasm

As mentioned in chapter 5, WT hCC showed inconsistent results to the previous study regarding the concentration of WT hCC needed for inhibition and the reproducibility of the data. Variable results were obtained using either the same batch of hCC or hCC from different purification preps. The aim of this chapter is to investigate the reasons behind this inconsistency in detail and characterise an active contaminating inhibitor protein from the *Escherichia coli* periplasm.

6.1. Materials and Methods

For purification of hCC, preparation of Aβ monomers, thoflavin T assays and EM see chapter 2.

6.1.1. hCC Re-purification

Previously in our lab, the hCC was purified by periplasmic extraction through applying osmotic shock by 20% sucrose, then loading on a cation exchange chromatography column, and finally, gel filtration. The same purification method was used in this study, however, the observed hCC inhibitory action on Aβ fibrillisation was variable among hCC samples from different purification preps. In order to work out the reasons behind these inconsistencies in the hCC inhibitory action on Aβ fibrillisation, the purified hCC was re-purified by different methodologies. The techniques used for re-purification were anion exchange chromatography, hydrophobic interaction chromatography (HIC), and size exclusion high-pressure liquid chromatography (SEC-HPLC).

6.1.1.1. Anion exchange chromatography

The purified hCC was further purified using anion exchange chromatography. The hCC buffer exchanged to 10mM phosphate buffer pH 9.0 and loaded at a rate of 2 ml/min into the 100 ml Q-Sepharose column equilibrated with the same buffer. The column was washed with 10 mM sodium phosphate pH 9.0 until A_{280} of the eluent stabilized. The hCC was eluted using 10 mM sodium phosphate buffer, pH 9.0, 0.2 M NaCl, and 5 ml fractions collected. Any remaining bound protein was eluted with sodium phosphate buffer pH 9.0, 1 M NaCl. Fractions were analysed by SDS-PAGE and those containing hCC were pooled and stored at -20°C.

6.1.1.2. Hydrophobic interaction chromatography (HIC)

As re-purification with anion exchange chromatography was not successful in separating the contaminants from hCC, re-purification using a hydrophobic interactions column was performed using RESOURCE ETH (GE Healthcare, UK), prepacked with SOURCE™ 15ETH, which are rigid, monodisperse 15 µm beads made of polystyrene/divinyl benzene.

6.1.1.3. Size-exclusion high-pressure liquid chromatography (SEC-HPLC)

The purified hCC was further purified by size exclusion high-pressure liquid chromatography (SEC-HPLC). An analytical Superdex 200 (10/300) column (GE Healthcare, UK) was equilibrated with 50mM phosphate buffer pH 7.0, 100mM NaCl. 180 µl samples of concentrated hCC were loaded on the column with a Perkin Elmer Series 200 HPLC system (Perkin Elmer, UK) equipped with a UV-visible absorbance detector. The OD of eluent monitored at 280nm. The column was run at 0.5ml/min and the 0.5ml fractions of the eluted peaks were collected in eppendorf tubes.

The Superdex column has a protein exclusion limit of 1,300 kDa, with a separation range between 10 and 600 kDa, and a matrix of cross-linked agarose and dextran.

6.1.2. Nuclear Magnetic Resonance Spectroscopy

^{15}N-labelled GLTI was expressed and purified as well as ^{15}N hCC. Before the NMR experiments, the purity of the protein was established through analysis by SDS-PAGE and SEC-HPLC.

6.1.2.1. ^{1}H ^{15}N HSQC NMR for unlabelled Aβ$_{1-42}$ and ^{15}N GLTI

^{1}H ^{15}N HSQC experiments were performed for ^{15}N GLTI in the absence of Aβ and after adding Aβ monomers to GLTI. A final concentration of 50 µM of each protein was achieved in 50 mM phosphate buffer (Na2HPO4/NaH2PO4), pH 7.4, 150mM NaCl, 2mM Sodium azide, and 50 µl (10%) of deuterium oxide (D_2O) added to bring the final volume to 500 µl. The experiments were performed at 330 K.

6.1.2.2. 1 D ^{1}H NMR time-course of unlabelled Aβ$_{1-42}$ with ^{15}N-GLTI

^{15}N-labelled GLTI in phosphate buffer saline was added to monomeric Aβ$_{1-42}$ to achieve 50 µM of both Aβ and GLTI in 50 mM phosphate buffer (Na_2HPO_4/NaH_2PO_4), pH 7.4, 150mM NaCl, 2mM Sodium azide and 50 µl of deuterium oxide (D_2O) added to bring the final volume to 500 µl. A 1D ^{1}H spectrum of the sample was obtained every 2hrs for 24 hours at 303 K.

6.2. Results

6.2.1. Purification-elution profiles

The hCC sample used throughout this study was purified from three different purification preps at different times. The elution profiles and SDS-PAGE from each prep is presented,

(Figures 6.1, 6.2, 6.3). The yield from the first and second prep was low, it was 1-2 mgs per litre of growth. The third prep yielded a much higher amount of hCC, three mgs per litre of growth. The higher yield caused the production of purer hCC, as the amount of contaminant became relatively lower. The first step of hCC purification was anion exchange chromatography. Some other contaminants were co-eluted with hCC form the SP-sepharose column and only a single peak was observed (see figure 6.1.). However, more than one protein appeared in SDS-PAGE in all fractions. The fractions from the peak were identified by SDS-PAGE and fractions (11-1) which contained hCC and less contaminant were pooled together and concentrated using a further step of purification.

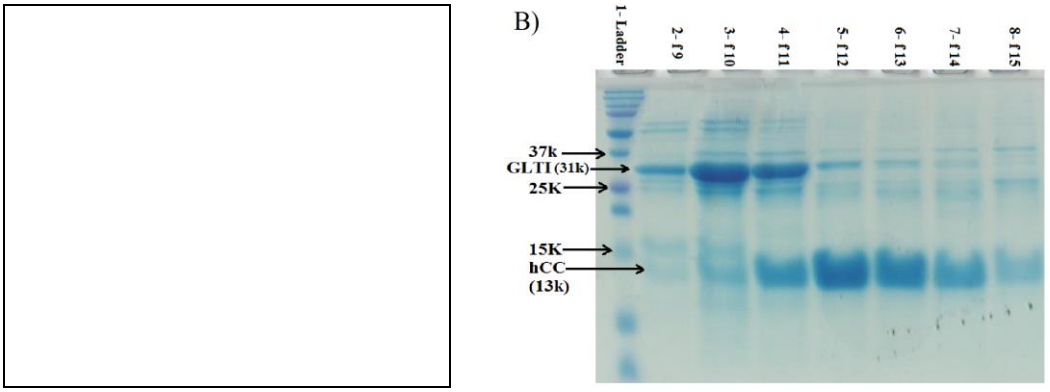

Figure 6.1. Elution profile and SDS-PAGE from loading periplasmic extract onto SP-sepharose. A) showing co-elution of hCC and GLTI as a single peak from fraction number 9 to 15. B) SDS-PAGE of the fractions 9-15 from the SP-sepharose.

The most abundant contaminant was a protein with an apparent MW of 37KD which was later identified as a periplasmic *E. coli* protein; Aspartate/ Glutamate binding protein (GLTI) (section 6.2.5).

The next step of purification was the loading of the co-eluted fractions from the SP-sepharose column onto the gel filtration column. As hCC is smaller than all of the contaminants that co-elute from SP-sepharose, it elutes later from the gel filtration column.

hCC eluted at fraction 31-38 while the periplasmic *E. coli* protein (GLTI) was mostly eluted from fraction 25-28. Fractions 32-38 were pooled together and kept at 8°C.

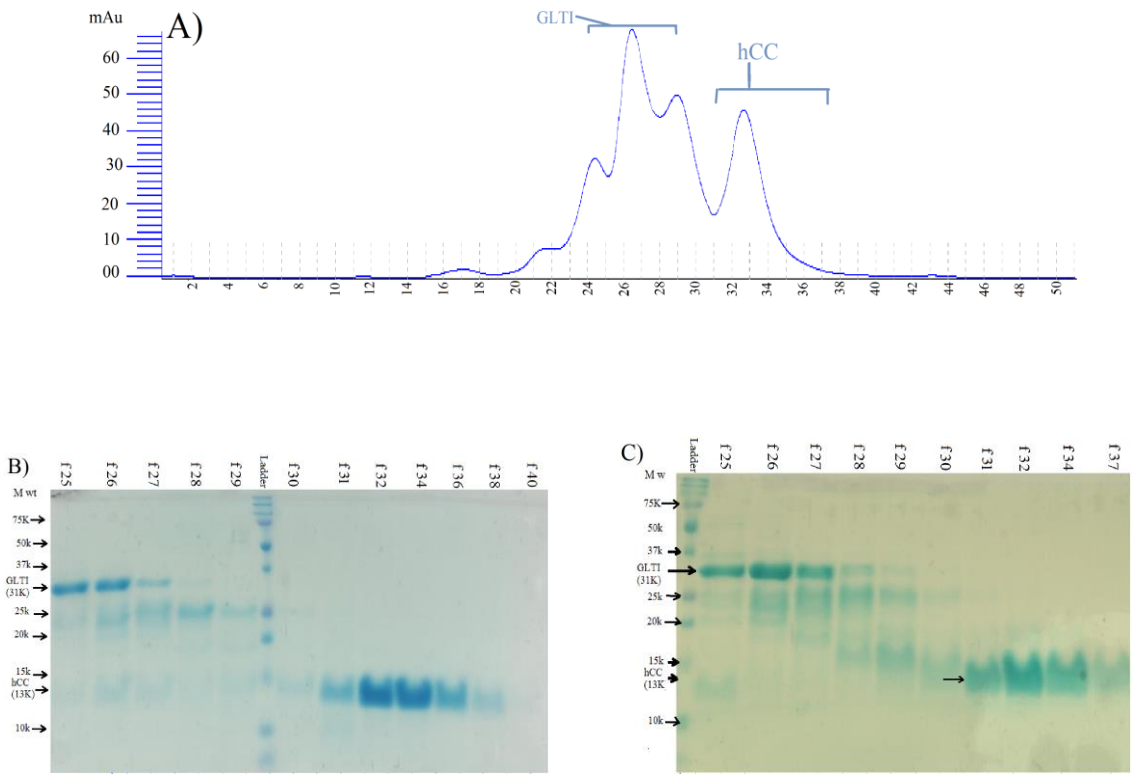

Figure 6.2. The elution profile and SDS PAGEs of 1st and 2nd hCC purification prep. A) The elution profile of hCC gel filtration and B) SDS-PAGE of the eluted fractions from first (B) and second (C) purification prep of hCC after gel filtration (final step of purification), showing hCC and GLTI proteins.

The hCC yield from the third purification prep was much higher compared to the first and second one. The yield from 5L of broth was 13 mg from third prep compared to only 5-7 from the first and second one. The high protein yield from the second prep led to obtaining more pure sample as the amount of contaminant was relatively lower, figure 6.3. Fractions pooled were 40-46 and the SDS-PAGE suggested only very small amounts of co-purified proteins.

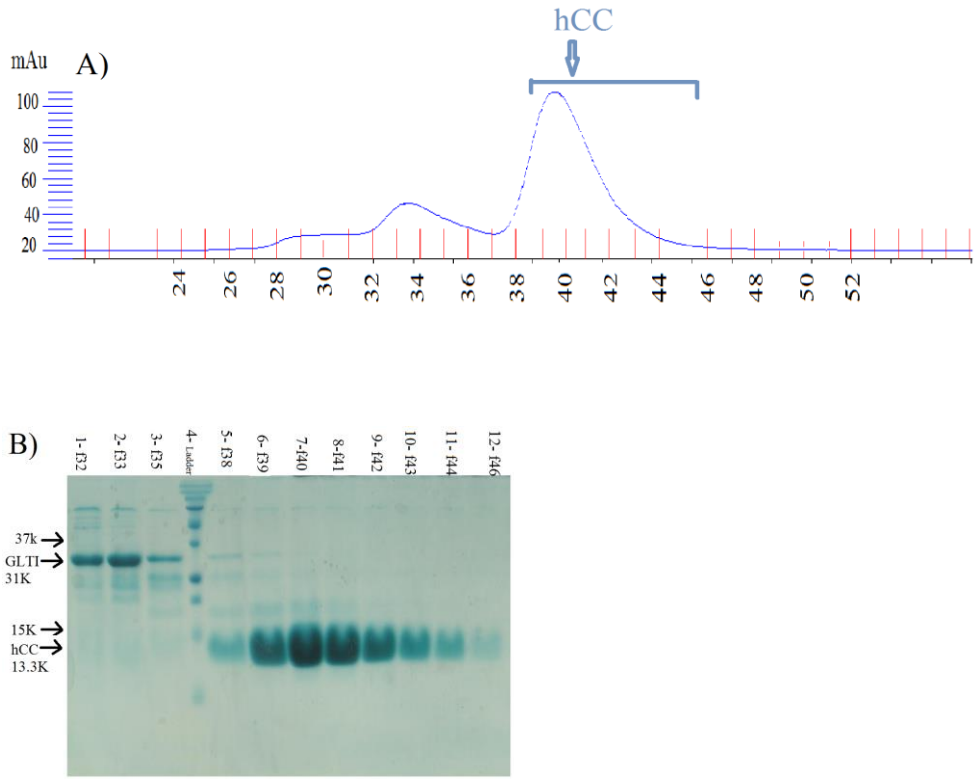

Figure 6.3. The elution profile and SDS PAGE of 3rd hCC purification prep. A) The elution profile from the gel filtration of hCC and B) SDS-PAGE of the eluted fraction from the third purification prep of WT hCC after gel filtration (final step of purification), showing hCC and GLTI proteins.

6.2.2. Re-purifying hCC and GLTI

6.2.2.1. Anion exchange chromatography

Because the iso-electric points of both hCC (8.7) and GLTI (8.5) are very similar, this technique was unsuccessful in separating both proteins. Both proteins were eluted together as two overlapped peaks which are shown in figure 6.4.

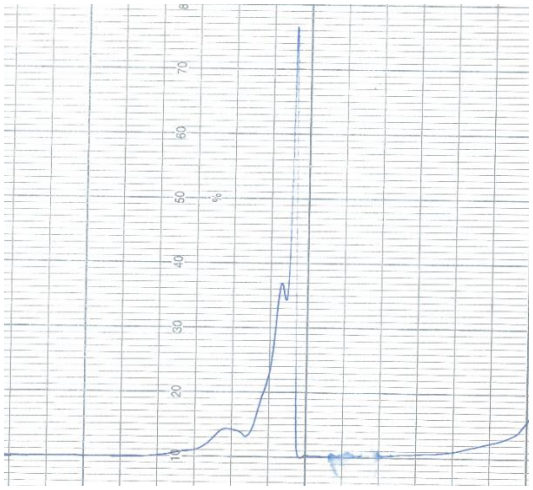

Figure 6.4. Elution profile of hCC re-purification with anion exchange chromatography using Q-sepharose applying pH 9. Both hCC and the contaminant were eluted as two overlapping peaks.

6.2.2.2. Hydrophobic interaction chromatography (HIC)

Both hCC and GLTI are abundant in hydrophobic residues. Although a chemically distinct methodology, HIC did not efficiently separate the two proteins. In thioflavin T experiments, the effect of hCC before then after purification on the Resource ETH column showed no difference in inhibitory efficiency on $A\beta_{1\text{-}42}$ fibrillisation (Figure 6.5).

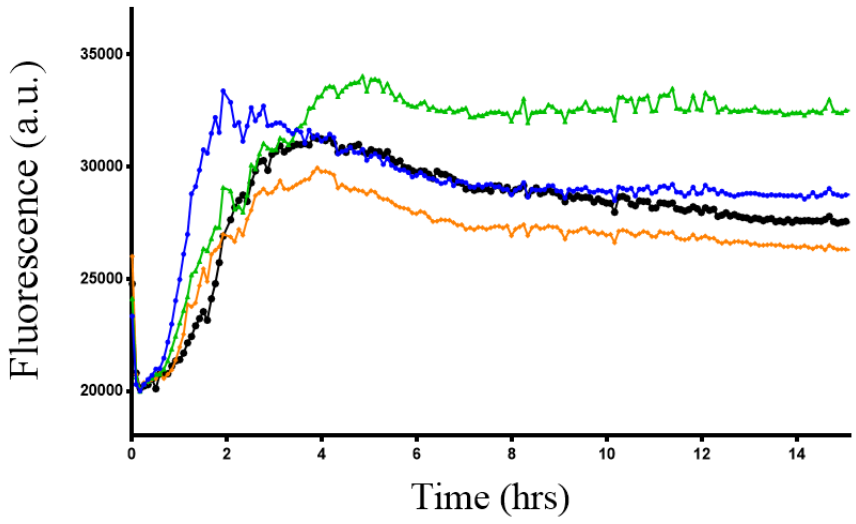

Figure 6.5. Thioflavin T curves for $A\beta_{1\text{-}42}$ fibrillisation in the presence of re-purified hCC by Resource ETH. Blue: $A\beta_{1\text{-}42}$ control, green: Aβ in the presence of equimolar amount of non-purified hCC, orange and black: $A\beta_{1\text{-}42}$ in the presence of equimolar amount of hCC from the first and second parts of overlapped peaks, respectively.

6.2.2.3. Size exclusion high-pressure liquid chromatography (SEC-HPLC)

hCC was further purified by size exclusion high-pressure liquid chromatography (SEC-HPLC). An analytical Superdex 200 column was a good choice to re-purify concentrated hCC without losing a significant amount of the protein and the two proteins were clearly separated and recovered. The *E. coli* periplasmic contaminant (GLTI) was eluted at 15.5 ml and hCC eluted at 17.5 ml (Figure 6.7 A). The middle part of both peaks were collected as pure proteins.

6.2.3. Addition of hCC to $A\beta_{1-42}$ Fibrillisation

Thioflavin T Time-course

The kinetics of $A\beta_{1-42}$ fibrillisation was monitored in the presence of different molar ratios of hCC to $A\beta_{1-42}$, as shown in Figure 6.6. Each bar represents the amplitude of the thioflavin T curve of $A\beta_{1-42}$ fibrilisation in the presence of equimolar and half equimolar amount of hCC in experiments, each experiment with 5 replicates. hCC samples used from all the different preps showed inconsistent results compared with previous results and even between different preps. Impure hCC samples exhibit the greater inhibitory action, purer hCC from the third prep was shown to be less effective on $A\beta_{1-42}$ fibrillisation: up to 3 times the equimolar concentration of the less pure (first and second preps) hCC (Figure 6.6 A&B) and 4 times the equimolar concentration of the purer (third prep) sample were needed to complete inhibition of $A\beta_{1-42}$ fibrillisation as monitored by thioflavin T fluorescence (figure 6.6C). This contrasts with a 2-fold excess in the previous results obtained by (Williams, 2015). The results obtained in minimal shaking conditions (red bars in figure 6.6) were more consistent among different experiments using the same hCC sample and between different preps, indicating that continuous shaking (blue bars) is also one of the reasons behind these inconsistencies despite the presence of various amounts of contaminant in different hCC preps.

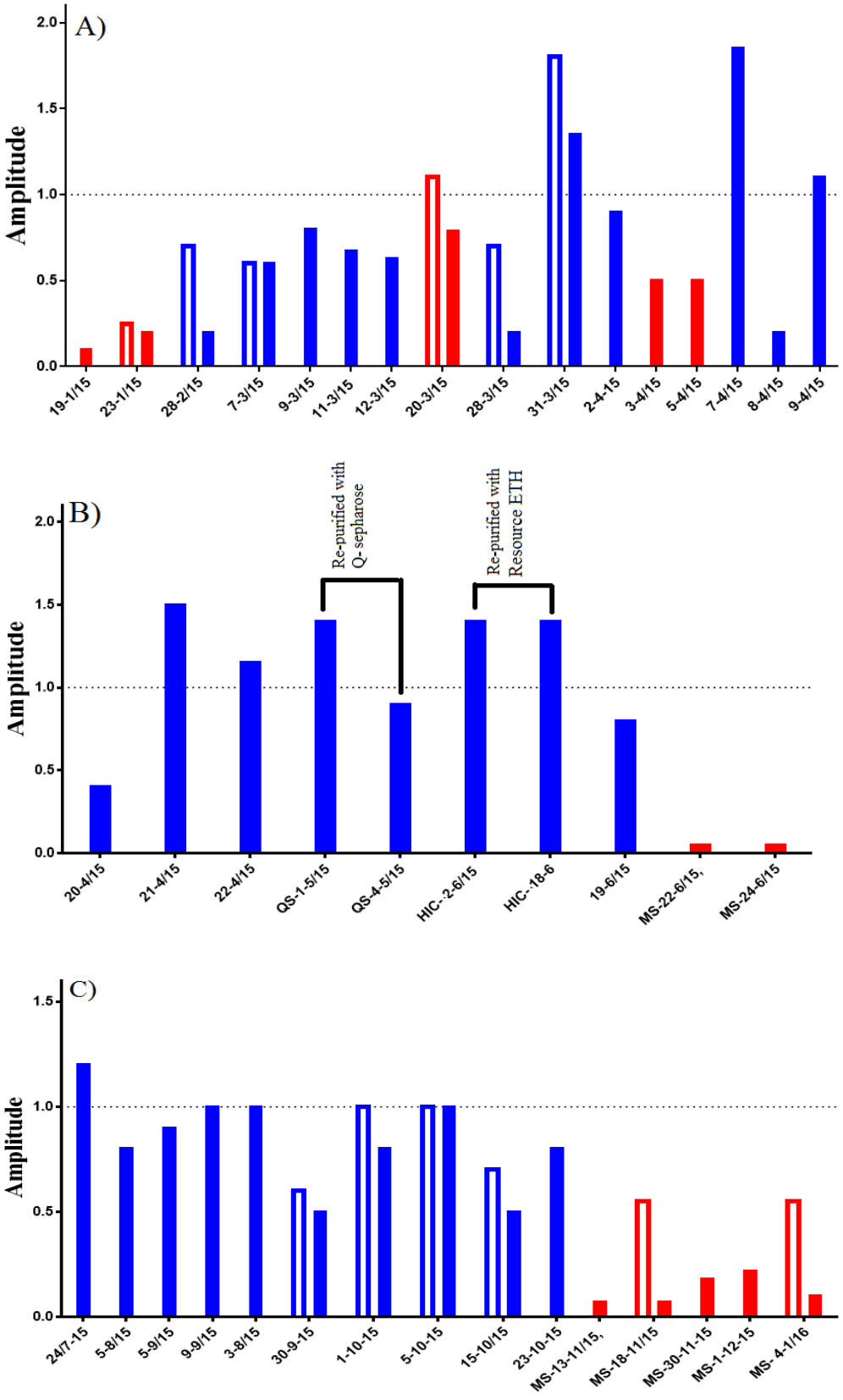

Figure 6.6. Amplitude of Aβ fibrillisation curves in the presence of WT hCC. The x axis represent different experiments and y axis is the relative amplitude of Aβ fibrillisation curves in the presence of equimolar (solid bars) or half equimolar (empty bars) concentrations of hCC. The blue

bar charts represent continuous shaking and red ones represent minimal shaking conditions. The hCC sample used during the study was from 3 different purification preps, first prep (A), second prep (B) and third prep (C). Showing the inconsistency between different experiments. In graph (B) the bar charts labelled with re-purified with Q-sepharose to represent purified hCC with cation exchange chromatography and bar charts labelled with re-purified with Resource ETH represent purified hCC with hydrophobic interaction chromatography. The dates of the experiments are shown to allow evaluation of the effect of sample age on the results obtained.

6.2.4. Purification of GLTI

GLTI co-purified with hCC through periplasmic extraction, cation exchange and size exclusion chromatography (FPLC). As reported in section 6.2.2.3, GLTI separated from hCC through another round of size exclusion using analytical HPLC superdex 200 colum, figure 6.7 A. The GLTI was eluted at 15.5 ml (31 minutes). SDS-PAGE of the collected 0.5 ml fractions is shown in Figure 6.7 C. The purest fractions were collected and analysed by HPLC-SEC (Figure 6.7 B) and used for thioflavin T and NMR experiments.

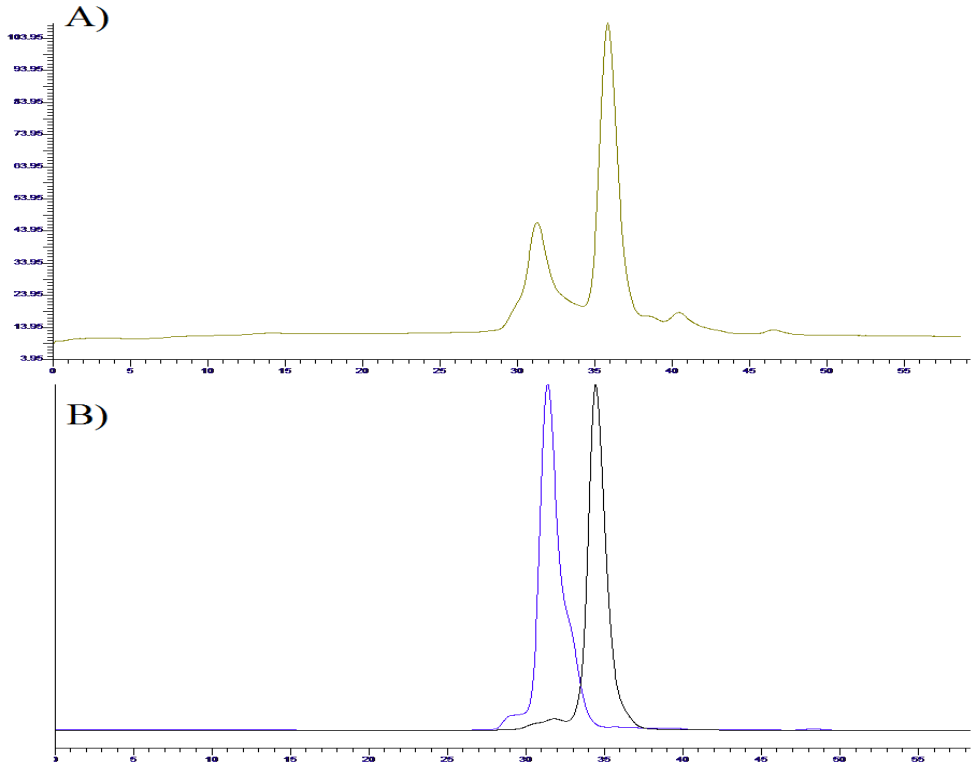

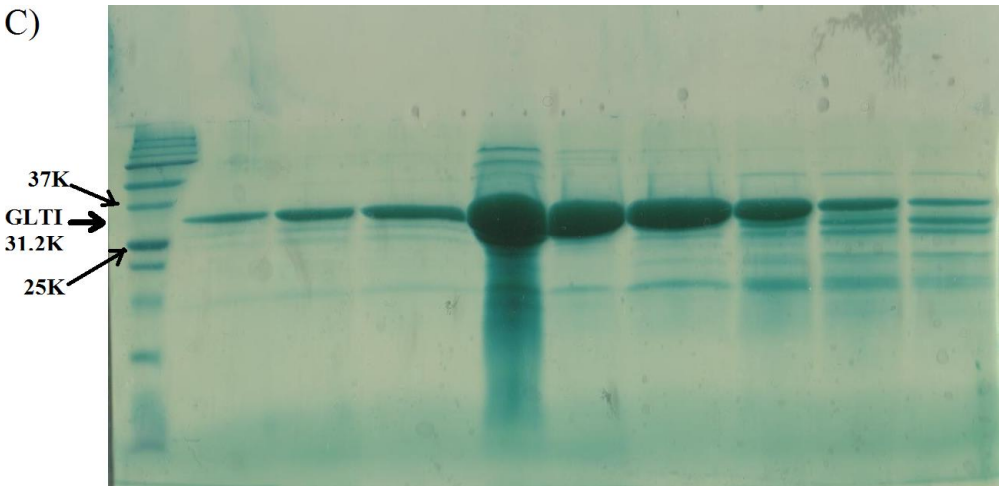

Figure 6.7. SEC-HPLC Elution profile and SDS-PAGE of hCC and GLTI. A) Elution profile of the mixture of hCC and GLTI from size exclusion (HPLC), showing the peaks from GLTI and hCC, GLTI eluted at 15.1ml (31 mins) and hCC at 18ml (36 mins). B) Elution profile of the HPLC purified GLTI and hCC, showing the peaks from GLTI (blue) and hCC (black). C) SDS-PAGE of the eluted fractions form GLTI purification by HPLC.

6.2.5. Characterisation of GLTI

Mass spectrometry

Purified GLTI and ^{15}N GLTI were investigated by mass spectrometry. The size of GLTI was 31,170.5 Dalton. This mass was different from the theoretical mass of GLTI without the first 22 amino acid signal peptide (31229D when it's 280 residues). ^{15}N GLTI was 31525 Dalton, but the protein contains 377 nitrogen atoms, which theoretically should be 31607D. These differences might be due to a mutation in the protein like mutation of a K or Q to A or D to G as a small part of the sequence did not match the theoretical sequence: specifically residues number 240-246 (KDDPQFK) (see next section). Minor peaks of other contaminants were also observed.

A)

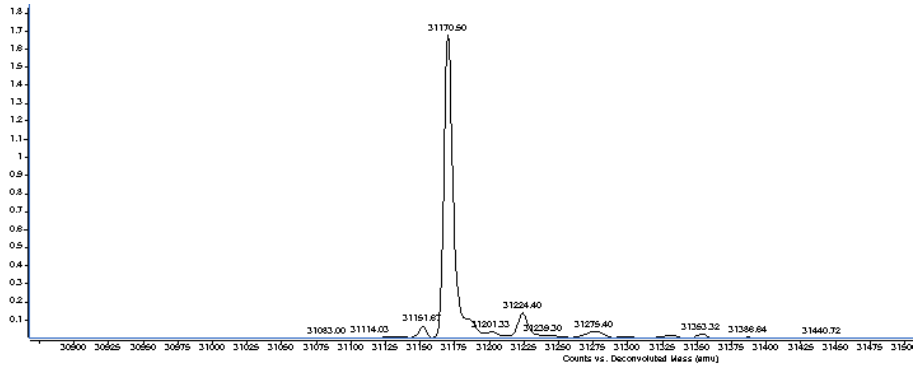

B)

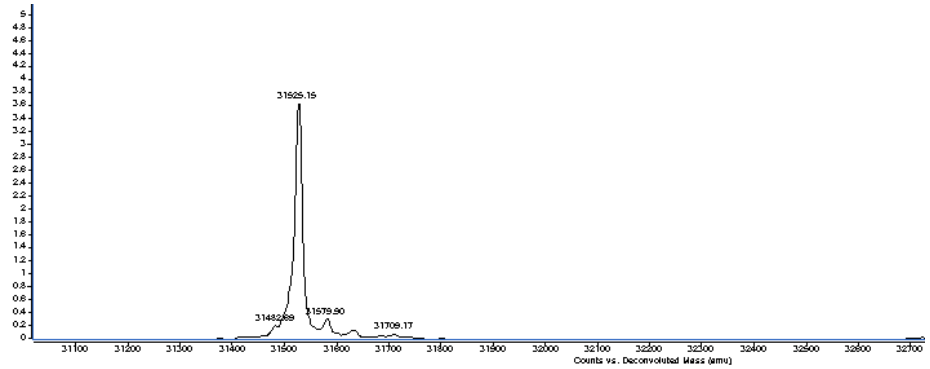

Figure 6.8. Mass spectrometry results of purified A) GLTI which is 31170 D, and B) ^{15}N GLTI which is 31525 D.

Sequencing

Purified GLTI was characterised by mass spectrometry. The protein identified by Peptide mass fingerprinting; in which the proteins digested by proteolytic enzymes, then the masses of the produced peptides are compared to a database of predicted masses that created from the digestion of known proteins. If a significant number of produced peptides masses matched the protein sequence in the reference list, this indicates that the protein was present in the original sample. 118 out of 121 peptides which generated from the enzymatic digestion of the protein sample were unique to GLTI (Figure 6.9). 84% of the GLTI sequence was identified and if we exclude the first 22 signal peptide amino acids, the percentage of coverage would be as high as 95%. The percentage coverage

refers to the percentage of found peptides matched to database peptides. The higher the coverage the greater the probability of the presence of particular protein.

A)

Accession	Description	Score	Coverage	Protein	Unique Peptides	Peptides	PSMs	AAs	MW [kDa]
P37902	Glutamate/aspartate periplasmic-binding protein OS	29799.63	84.11	1	118	121	730	302	33.4
P0A911	Outer membrane protein A OS=Escherichia coli O15	2111.19	40.46	1	24	24	70	346	37.2
P76341	5-hydroxyisourate hydrolase OS=Escherichia coli (st	1775.63	64.23	2	25	25	65	137	15.5
P0AFG1	Transcription termination/antitermination protein Nu	1773.70	72.38	2	31	31	67	181	20.5
Q8X9X2	Uncharacterized protein YncE OS=Escherichia coli O	1294.75	58.92	2	18	18	35	353	38.6
A7ZV18	Elongation factor P OS=Escherichia coli O139:H28 (s	1180.77	52.66	1	20	20	53	188	20.6

B)

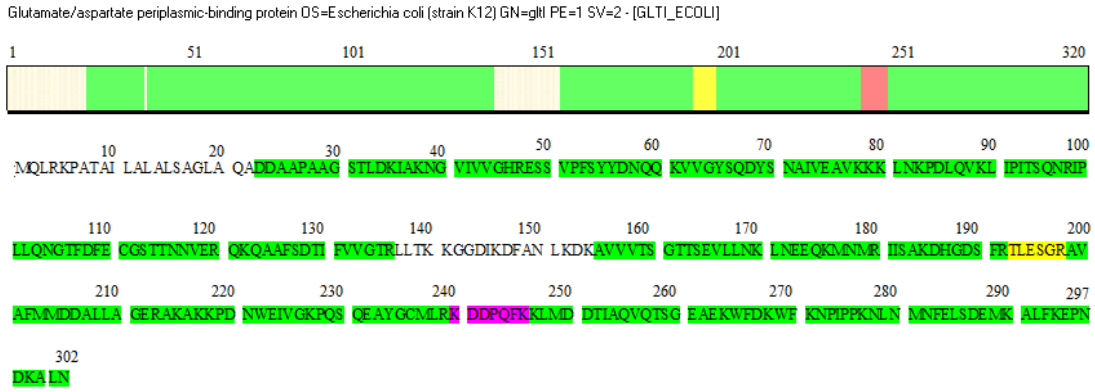

Figure 6.9. Mass Spec Results of GLTI Characterisation. A) List of the proteins identified in the sample. B) The sequence of GLTI (including first 22 signal peptide) with identified regions highlighted in green.

6.2.6. Background information on GLTI

The periplasmic contaminant was identified as the aspartate/glutamate binding protein (GLTI). GLTI is an *E. Coli* periplasmic protein which binds both glutamate (K_D = 0.8 pM) and aspartate (K_D = 1.2 pM) (Willis and Furlong, 1975a) with only one binding site is indicated per molecule of protein.

GLTI belongs to the DEBP family of binding proteins. DEBP is one of the constituents of ATP-binding cassette (ABC) transport systems. These systems transport solutes across membranes through coupling to ATP hydrolysis. These systems include a periplasmic

binding protein (PBP), an integral membrane protein, and two cytoplasmic nucleotide-binding domains that hydrolyze ATP. The periplasmic protein, like GLTI, is responsible for ligand capture and then passes it to a transmembrane protein for transport into the cell. At the time of binding to their ligands, the DEBPs exhibits a remarkable conformational change that enhances the formation of a complex with a corresponding membrane-bound component of the transport system (Sun *et al.*, 1998).

Periplasmic glutamate/aspartate binding protein was first purified and identified from *Escherichia coli* K12 (Willis and Furlong, 1975b). A DEBP from *Shigella flexneri* (sfDEBP) has more recently been reported which is almost identical to the *E. coli* DEBP (GLTI) in amino acid sequence. The only difference is that a nonessential residue (Val5) in GLTI, is replaced with an Alanine in sfDEBP (Hu *et al.*, 2008). The *E. coli* DEBP (GLTI) structure is not solved yet. However, its similarity to *Shigella flexneri* DEBP (sfDEBP) can provide information on its possible structure and role.

DEBP structures consist of two asymmetric domains, and the two domains are similarly folded. Two antiparallel strands link the two domains together. The ligand binding site located at the intersection of two domains. The centre of each domain consist of a five-stranded beta sheet surrounded by12 α-helices (Figure 6.10 A).

The DEBP protein binding to ligands is achieved by hydrogen bonding and salt bridges between the side chains and the main chain of the DEBP protein and the ligand molecules. Hydrogen bonds form between the side chains of the Arg24, Ser72, Arg75, Ser90, His164, Thr92 and Thr140 and the ligand. The side chains of Arg75, Arg90 and Asp 182 and the main chain carbonyl oxygen of Ser90 form salt bridges with the glutamate (Hu *et al.*, 2008).

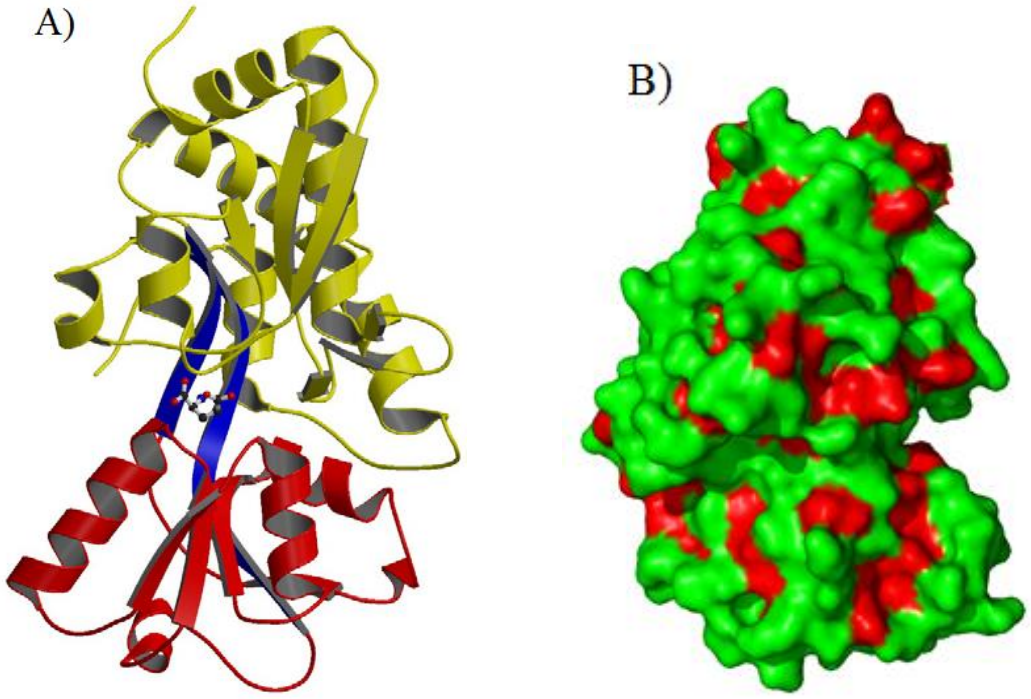

Figure 6.10. **The crystal structure of *Shigella flexneri* DEBP (sfDEBP).** A) cartoon structure; Domains I and II are colored yellow and red, respectively. The two β-strands that connect domains I and II are colored blue. The bound glutamate molecule is shown as ball-and-stick model Adapted from (Hu *et al.*, 2008). B) the surface structure of sfDEBP with the hydrophobic residues coloured in red (drawn using pdb code 2VHA using Pymol).

6.2.7. Interaction between $A\beta_{1-42}$ and GLTI

6.2.7.1. Thioflavin T of $A\beta_{1-42}$ and GLTI

The kinetics of $A\beta_{1-42}$ fibrillisation were measured in the presence of different molar ratios of GLTI in the standard conditions described earlier, with an $A\beta_{1-42}$ concentration of 11 µM, as shown in Figure 6.11. Each curve is the average of 5 replicates with error bars displaying the standard error of the mean (SEM) to give an indication of the spread of the data. Different concentrations of GLTI were tested ranging from 5 µM (half the concentration of $A\beta_{1-42}$) to 1.25 µM (8 times less than the concentration of $A\beta_{1-42}$). Half equimolar concentrations of GLTI caused a complete reduction in thioflavin T fluorescence. In the presence of 3.75 µM GLTI the intensity of the thioflavin T curve is

about 17% of the $A\beta_{1-42}$ control curve, suggesting that the amount of fibril being produced was significantly less than in the absence of GLTI. GLTI concentrations of 2.5 µM and 1.25 µM caused reductions in thioflavin T fluorescence of 40% and 30% respectively.

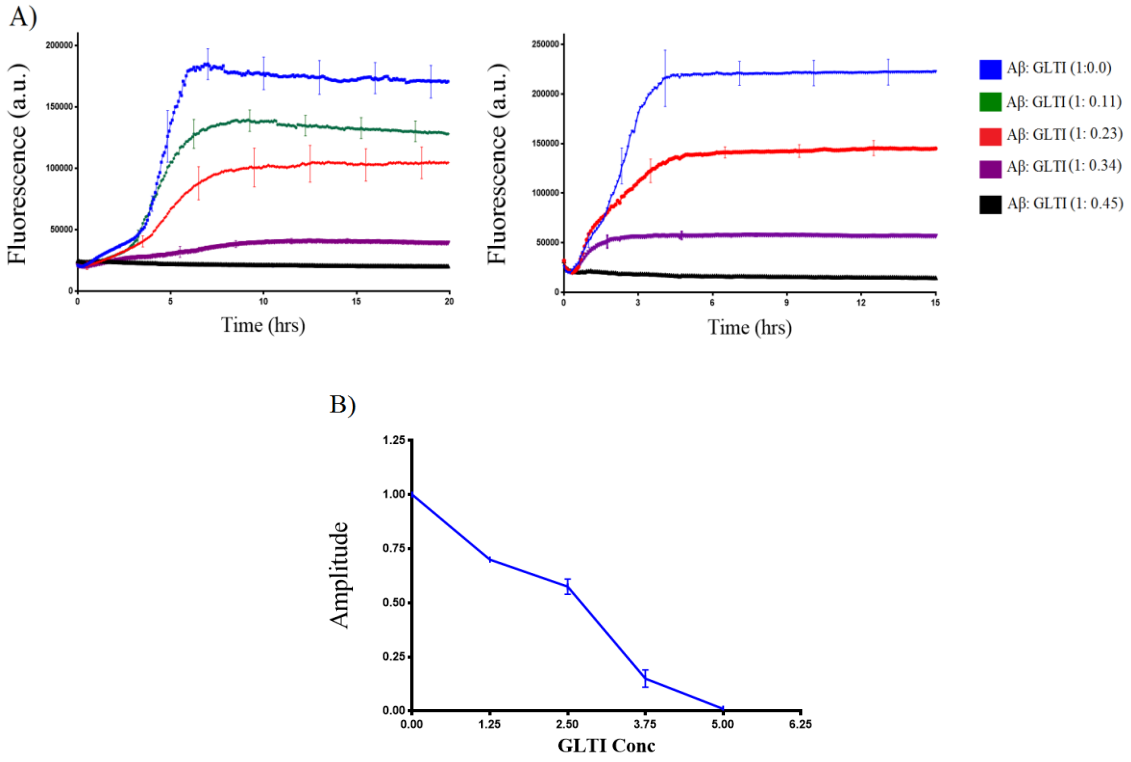

Figure 6.12. Dose Dependence of the inhibitory activity of GLTI on $A\beta_{1-42}$ fibrillisation. A) Thioflavin T fluorescence time-courses of $A\beta_{1-42}$ fibrillisation at 11 µM with the addition of different molar ratios of GLTI. Each curve is the average of 5 replicates, with error bars indicating the standard error of the mean (SEM). Eight separate experiments have been done at different times and with different protein stocks, the data summarized in two graphs. B) The amplitude of Thioflavin T curve in the presence of different concentrations of GLTI, normalised to the $A\beta_{1-42}$ control.

6.2.7.2. Electron Microscopy

Although changes in thioflavin T fluorescence suggested that GLTI inhibits $A\beta_{1-42}$ fibril production, this reduction in intensity could be attributed to other factors such as changes in morphology or the production of alternative species which also bind thioflavin T. TEM

was used to study the structural morphology of the structures produced at the end of the incubation of $A\beta_{1-42}$ in the presence of half equimolar concentration of GLTI. Figure 6.12 shows electron micrographs of equimolar concentrations of $A\beta_{1-42}$ and GLTI in the same conditions after at least 24 hours of incubation. In the absence of GLTI, $A\beta_{1-42}$ produces fibrils. In its presence, a large amount of amorphous aggregate observed with some curly structures is seen.

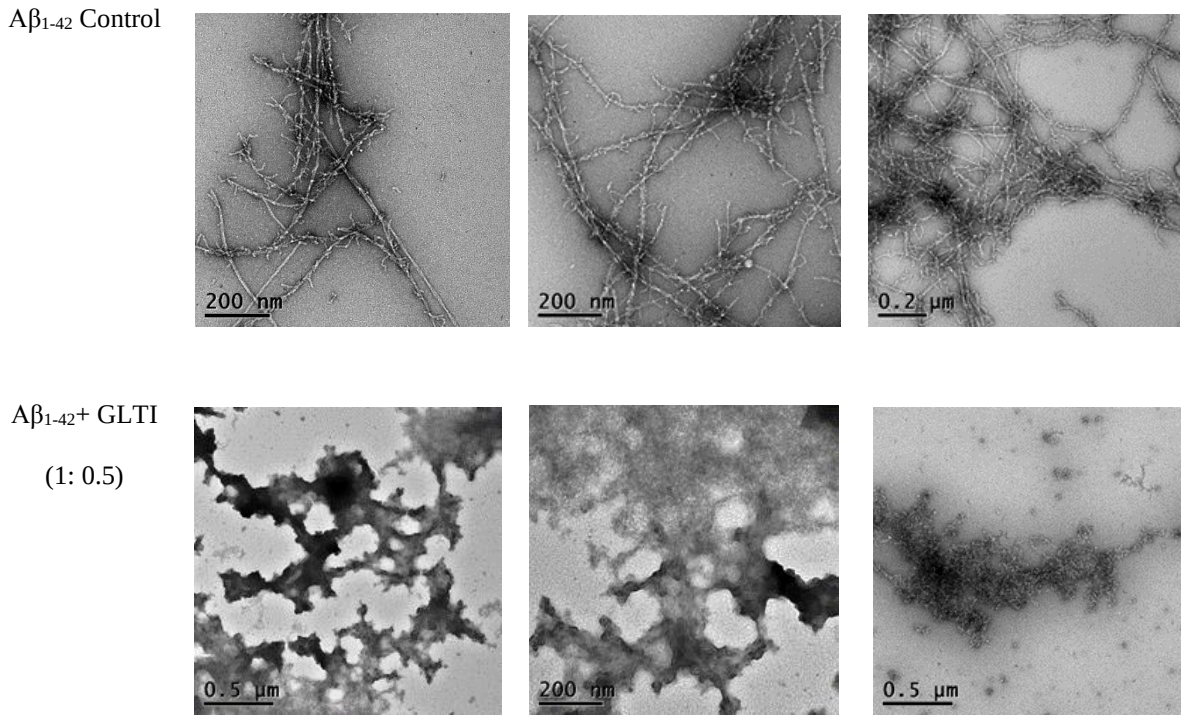

Figure 6.13. TEM micrographs of $A\beta_{1-42}$ and GLTI after 24 hrs of A) Aβ control after 24hrs of aggregation. B) Aβ aggregation reaction in the presence of half equimolar amount of GLTI.

6.2.7.3. NMR Spectroscopy

6.2.7.3.1. ^{1}H ^{15}N HSQC Spectrum of GLTI

The ^{1}H spectrum of 50 µM GLTI in 50 mM phosphate buffer, pH 7.4 at 303 K shows a wide dispersion of amide proton resonances (6-10 ppm) indicating that GLTI is folded. This is reflected in the ^{1}H ^{15}N HSQC spectrum where the amide chemical shifts are also

well dispersed (Figure 6.13.). Out of 280 residues, 220 were observed, 12 are prolines, the rest of the peaks (48) were either not present, very weak or significantly overlapped. The peaks were dispersed between 6-11 ppm indicating proper folding of the protein. $A\beta_{1-42}$ was then titrated to the GLTI to achieve equimolar concentration. The ^{1}H ^{15}N HSQC for ^{15}N GLTI has not been assigned yet, so the observed residues are not identified.

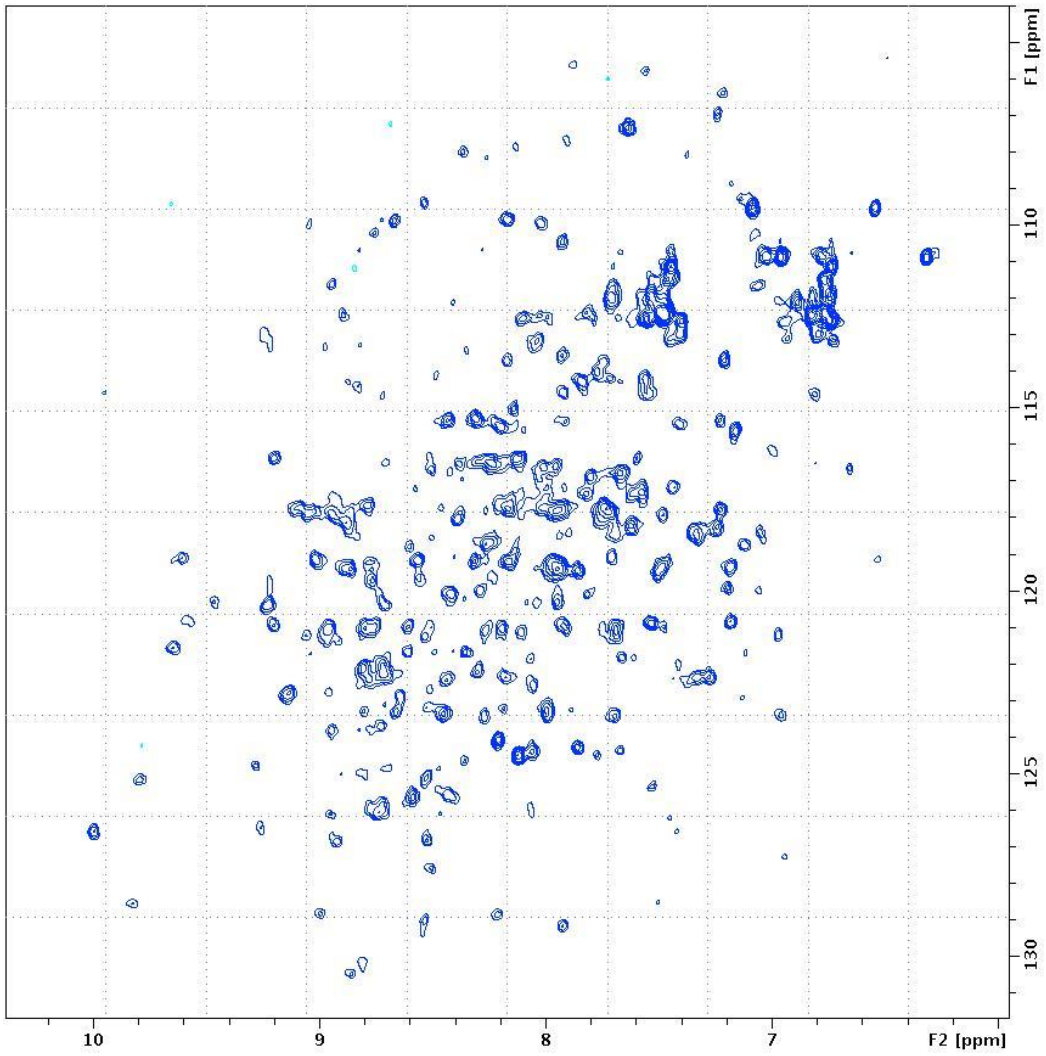

Figure 6.14. **^{1}H ^{15}N HSQC Spectrum of ^{15}N GLTI at 303 K.** An ^{1}H ^{15}N HSQC spectrum of 50 µM GLTI incubated in 50 mM Phosphate buffer, ph 7.4, 150 mM NaCl at 303 K showing the amide peaks. F1 represents the ^{1}H dimension and F2 represents the ^{15}N dimension.

6.2.7.3.2. Titration with monomeric Aβ$_{1-42}$

Figure 6.14 shows an overlay of a reference ^{1}H ^{15}N HSQC spectra overlaid with the spectrum that were obtained after addition of monomeric ^{15}N-labelled GLTI with unlabelled monomeric Aβ$_{1-42}$. Because the ^{1}H ^{15}N HSQC is not assigned yet and the intensity of the peaks was not uniform, it was difficult to find the amide chemical shifts. However, there were some shifts in the position of some of the residues and some other residues were completely disappeared.

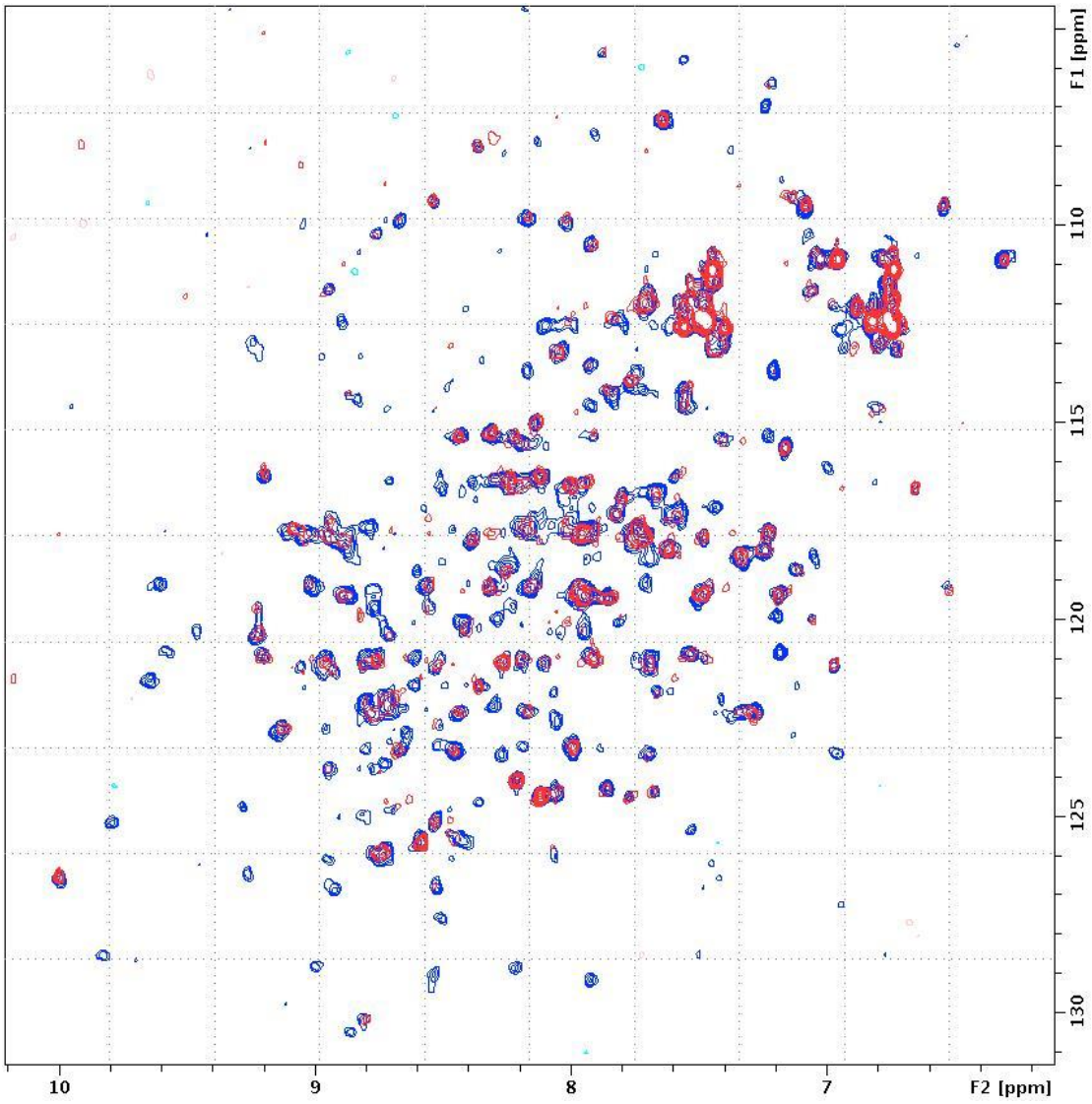

Figure 6.15. Titration of ^{1}H ^{15}N GLTI with Aβ$_{1-42}$. A reference spectrum of ^{15}N labelled 50 µM GLTI in 50 mM phosphate buffer, pH 7.4, NaCl 150 mM at 303 K (blue) was overlaid with the ^{1}H ^{15}N HSQC spectrum of Aβ$_{1-42}$ have been added (shown in red). F2 represents the ^{1}H dimension and F1 represents the ^{15}N dimension.

6.2.7.3.3. 1D ^{1}H NMR Time-course of GLTI with $A\beta_{1-42}$

1D ^{1}H NMR can monitor the disappearance of $A\beta_{1-42}$ monomers during the time course of Aβ aggregation as the intensity of the spectra reduces with the reduction of the amount of the monomer. 1D NMR spectra, a total of 12, were obtained over 24 hours, with each experiment lasting 2 hours and 8 minutes. The aim was to compare the reduction in $A\beta_{1-42}$ spectrum intensity in the absence and presence of GLTI. The substraction of the $A\beta_{1-42}$ spectra from the GLTI and $A\beta_{1-42}$ mixture was not possible because of the change in the position of the peaks. It is clear therefore that large conformational changes in GLTI, $A\beta_{1-42}$ or both are occurring. The $A\beta_{1-42}$ control (Figure 6.15) showed 87% reduction in the intensity of its spectrum over 24 hrs at 37°C, indicating that a significant fraction of $A\beta_{1-42}$ monomers participate in the formation of large aggregated structures.

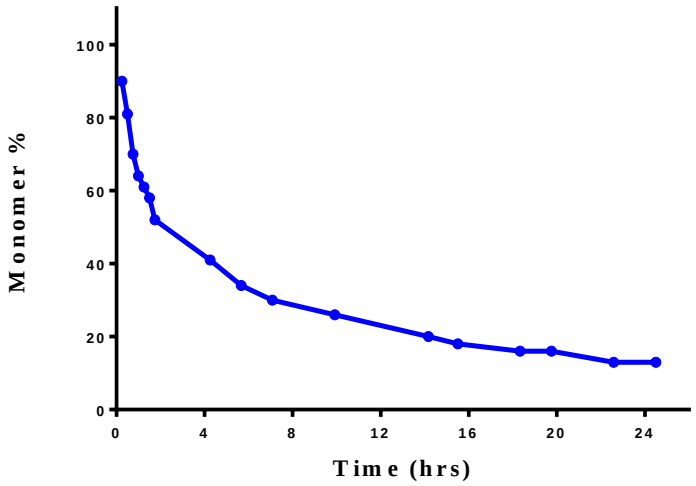

Figure 6.15. The intensity of $A\beta_{1-42}$ 1D 1H NMR spectrum over the time course of 24 hrs. 50 μM of $A\beta_{1-42}$ in phosphate buffer, pH 7.4 and temperature 37°C. The reduction happens as the monomers form large structures.

6.3. Discussion and Future work

Confirmation of existing data and further characterisation of the inhibition of Aβ fibrillisation by WT hCC meant working with purer hCC samples. In the current study, attempts to replicate the same results as the previous study were confronted with some issues. Inconsistent results were obtained regarding the amount of hCC required to inhibit $A\beta_{1-42}$ fibrillisation completely. Unlike the previous study, the current study demonstrates that twice equimolar concentration is not enough to completely inhibit the formation of amyloid fibrils by $A\beta_{1-42}$ in the same continuous shaking conditions. Also, the thioflavin T data obtained from different experiments using either the same batch of hCC or hCC from different purification preps were variable, as the amplitude of thioflavin T curves was variable through using different experiments.

Trying to work out the reasons behind these inconsistencies and keeping the possibility of contaminants in mind, some different purification strategies like repurifying through hydrophobic interaction chromatography and re-purifying by anion exchange chromatography at pH 9. These techniques were unsuccessful in resolving the inconsistency issues as they failed to separate the contaminant and the hCC, probably because of similar iso-electric point and similar abundance in hydrophobic residues in both proteins. Size-exclusion chromatography using an analytical superdex 200 column was successful in separating an *E. coli* priplasmic protein which showed an inhibitory effect on $A\beta_{1-42}$ fibrillisation at a much lower stoichiometric concentration compared to hCC.

These differences could be due to the fact that the amount of contaminant present was different between the various purification preps, as the contaminant had some ability to inhibit $A\beta_{1-42}$ fibrillisation. Shaking might also be another reason for the inconsistency, as shaking leads to an increase in a species of $A\beta_{1-42}$ aggregates that hCC is less able to

bind (chapter 5). Non-shaking conditions produced more consistent results and hCC was more efficient.

Thioflavin T experiments performed with $A\beta_{1-42}$ in the presence of GLTI showed that GLTI can inhibit $A\beta_{1-42}$ fibrillisation at a much lower molar concentration compared to hCC. The stoichiometry of 1:0.45 of $A\beta_{1-42}$: GLTI was sufficient to completely inhibit $A\beta_{1-42}$ fibrillisation. The structure of GLTI has not been solved yet, however, the structure of the homologous *Shigella* DEBP protein has many hydrophobic patches (Figure 6.10B). These hydrophobic patches could be behind GLTI's ability to bind to $A\beta_{1-42}$ and inhibit its fibrillisation as $A\beta_{1-42}$ binds to hydrophobic surfaces. Another explanation of this inhibition activity could be down to the ability of GLTI to bind to both glutamate and aspartate very tightly. The $A\beta_{1-42}$ structure includes 3 aspartic acids and 3 glutamic acids (D1, E3, D7, E12, E23, and D24), and GLTI may bind to one or more of these residues with sufficient affinity to inhibit the peptide from aggregation, especially if it binds to the ones which take part in the fibril structure (Figure 1.3.)

Observation of the sample by TEM indicated that instead of amyloid fibrils, large amounts of amorphous aggregates had been produced through the incubation of $A\beta_{1-42}$ with GLTI. It is possible that GLTI is stabilising off-pathway states and preventing their further aggregation to produce mature fibrils.

The ^{1}H ^{15}N NMR HSQC spectrum of GLTI has not been assigned previously. The ^{1}H ^{15}N HSQC spectrum of the GLTI was measured. We observed chemical shifts in some residues and a complete disappearance of some other peaks. Because of the lack of GLTI HSQC assignment, it is very difficult to find any clue on which interface and residues of the GLTI bind to $A\beta_{1-42}$. Future work has to be performed to find the species of $A\beta_{1-42}$ the GLTI binds to and to identify residues of both GLTI and $A\beta_{1-42}$ which form the interface.

In an attempt to assess the rate of $A\beta_{1-42}$ monomer disappearance in the presence of GLTI, a 1D ^{1}H NMR time course was performed. In the case of the $A\beta_{1-42}$ control the intensity of the spectra was reduced by 87% in 24 hrs, suggesting that a big fraction of monomers were forming larger aggregates not visible by NMR. Since chemical shift changes were observed, subtraction of the $A\beta_{1-42}$ spectra from the $A\beta_{1-42}$ and GLTI mixture was difficult and the rate of $A\beta_{1-42}$ monomer disappearance in the presence of GLTI was not deduced here. The large conformational changes which occur in this family of proteins on substrate binding suggest that similar events may be occurring on binding $A\beta_{1-42}$.

Further analysis will be required to understand the nature of interaction sites. The first step towards this goal is developing an overexpression system for GLTI to produce a sufficient amount of the protein. An ^{1}H ^{15}N HSQC assignment would then provide the ability to identify the binding sites of GLTI to $A\beta_{1-42}$.

Chapter Seven: Final Conclusions and Future Work

The initial aim of this project was to reveal the nature of interaction between the Aβ peptide and the proteins, transthyretin and human cystatin C (hCC). Both TTR and hCC have been found inside and in the periphery of Aβ plaques in the brains of people with Alzheimer's disease (Deng *et al.*, 2001). Animal models and cell assay experiments suggest a protective role for these two amyloidogenic proteins in the pathophysiology of Alzheimer's (Stein *et al.*, 2004, Tizon *et al.*, 2010b). Direct interactions between these proteins and the Aβ peptide had been studied *in vitro* using techniques based mostly on the immobilisation of one of the proteins (Sastre *et al.*, 2004b, Selenica *et al.*, 2007b, Costa *et al.*, 2008, Du and Murphy, 2010). However, the details of the direct interactions in solution were unknown. The main aim of this project was to study the details of the direct *in vitro* interactions between these proteins and the Aβ peptide.

The deposition of an Aβ film and its nucleation on hydrophobic surfaces is well-supported in the literature (Kowalewski and Holtzman, 1999, Rocha *et al.*, 2005, Shen *et al.*, 2012). In our lab, we found evidence for the formation of a tightly bound monolayer of $A\beta_{1-42}$ on the surface of polystyrene microplates. We also found that both polystyrene (PS) and polyethyl glycate (PEG) surfaces enhance the nucleation of Aβ. However, the loose binding of Aβ on PEG is likely to accelerate Aβ nucleation and aggregation more than the polystyrene plate, presumably because the nuclei can easily come off the surface to the solution and start aggregation.

Inhibition of Aβ firbillisation by TTR occurs at the surface

Previous reports suggested that TTR tetramers bind to Aβ monomers in solution and inhibition mainly happen through binding to Aβ monomers (Costa *et al.*, 2008, Li *et al.*,

2013a). This was inconsistent with the low K_d of binding between TTR and Aβ monomers in solution (24μM) as this suggests that only one third of the Aβ molecules are bound to TTR tetramers in the solution with the equimolar amount of both proteins at 11μM. Despite this, we have found that an equimolar concentration of TTR is enough to inhibit Aβ aggregation. Additionally, as the rate of aggregation of Aβ in our conditions was independent of monomer concentration, the observed increase in lag time in the presence of polystyrene plates cannot be interpreted as the result of TTR binding to Aβ monomer. This study further confirmed the difference in TTR's ability to bind Aβ when the second is in solution or it is immobilised on a surface. Results obtained in this study show that the ability of WT TTR to inhibit Aβ fibrillisation is significantly lower in the presence of PEG compared to polystyrene, indicating that TTR binding to solution Aβ is much weaker. These results suggested stronger binding of TTR to immobilised Aβ on PS. It is plausible therefore that TTR binds weakly to the monomer or aggregated structure in the solution and binds much tighter to a rare species of Aβ aggregated structure on the monolayer, causing a delayed nucleus formation. Given the above discussion, we suggest that TTR prevents the nucleation of Aβ on the surface. Our results imply that disturbance of this layer by TTR prevents nucleation from occurring. It follows that TTR may also prevent the binding of oligomeric Aβ to membranes and other surfaces *in vivo*. As it is well-known that oligomers are the most toxic forms of Aβ and these oligomers exert their toxicity via affecting the cell membranes, validating TTR binding to oligomeric species on surfaces would be of a particular importance for revealing the nature of TTR modulation of Aβ *in vivo*. Performing Aβ inhibition experiments by TTR in the presence of other surfaces with different hydrophobicities, inert surfaces like glass and lipid bilayer coated surfaces would be invaluable to find clues to understanding the TTR inhibitory effect on Aβ fibrillisation *in vivo*.

WT TTR inhibits Aβ fibrillisation using a different mechanism to its amyloidgenic mutants

In order to study TTR interaction with Aβ in detail, four different TTR mutants were chosen with different kinetic and thermodynamic stabilities in terms of their tetramer stability and the folded state of their monomers. It had been previously shown that the residues around and including the thyroxine binding pocket of the TTR tetramer bind to Aβ monomers and Aβ inhibition by TTR was suggested to occur through binding to solution Aβ monomers. However, our results suggest that WT TTR works through tetramer binding to a very early nucleating species, supported by the observation that late addition of WT TTR to Aβ fibrillisation reactions abolishes its ability to inhibit Aβ fibrillisation, and this interaction occurs mainly at the surface. The WT TTR and its mutants inhibit Aβ fibrillisation via different pathways. Mutants interact with larger Aβ aggregates via exposing hydrophobic patches on their monomers. TTR mutants used in this study showed two different types of behaviour. TTR mutants study showed that their ability to inhibit Aβ aggregation is inversely related to their stability as a tetramer and folding state of monomer. Less stable mutants as a tetramer with unfolded monomers were the strongest inhibitors. V122I tetramer V122I has a more stable monomer compared to other mutants yet even though its tetramer is strongly destabilised, it is similarly effective or even slightly less than WT TTR. This could be because its binding site to Aβ is not as exposed as that of other mutants which have unstable monomers as well as dissociating tetramers.

$A\beta_{1\text{-}42}$ fibrils are not directly toxic themselves. However, they can help the continuous generation of toxic oligomers as they can provide a catalytic surface for this. To explore the potential of TTRs to bind Aβ fibrils, TTRs were incubated with purified Aβ fibrils

and co-pelleted to show binding between TTRs and Aβ fibrils. The percentage of TTRs showed to bind Aβ fibrils was consistent with the instability of their tetramers and unfolded state of their monomers. Addition of TTRs to seeded Aβ fibrillisation reactions showed that the TTR mutant with the most unstable tetramer with significantly populated unfolded monomers (A25T mutant) was the only inhibitor of seeding, presumably via binding to the fibrils ends through its exposed hydrophobic patches of monomer. These results indicates that mutant TTRs bind to aggregated structures, seeds and fibrils in the same way by using exposed hydrophobic patches of their monomers.

It has been suggested that TTR monomers are more effective than tetramers in inhibiting Aβ fibrillisation presumably through stronger binding to Aβ aggregates. It has been found that F78M/L110M (M-TTR) TTR mutant is unable to assemble to tetramers and it stays as monomers (Du and Murphy, 2010). Designing M-TTR mutants to produce TTR monomers with different folding states and investigation of its ability to inhibit Aβ fibrillisation could validate the relationship between the unfolding of TTR monomer and ability to inhibit Aβ aggregation.

Monitoring the time course and size distribution of aggregates forming during Aβ fibrillisation in the presence and absence of TTRs and the effect of different TTRs on the formation of ADDLs would give an idea of the nature of the Aβ oligomers that TTRs bind.

Cystatin C inhibits Aβ fibrillisation through binding of a specific type of oligomer

The second part of this project was to study the interaction between human cystatin C (hCC) and Aβ. It had been suggested that monomer-monomer binding occurs between hCC and Aβ and this results in the prevention of Aβ fibrillisation (Sastre *et al.*, 2004b, Selenica *et al.*, 2007b). However, previously in our lab the interaction between WT cystatin C and $A\beta_{1-42}$ was investigated and led to the proposal that monomeric hCC

inhibits the formation of amyloid fibrils by Aβ through binding to an oligomeric form of the peptide. hCC does not bind to monomeric Aβ but instead appears to be binding to an oligomeric species causing the formation of non-toxic assemblies. Similarly, PrP^C selectively binds to oligomers (Lauren *et al.*, 2009), however in this system the producing species are more toxic than those formed in the absence of PrP^C. In the current study, again NMR experiments failed to find the interaction between monomeric Aβ and hCC. However, the concentration dependence of Aβ inhibition by hCC was confirmed by thioflavin T assays. Although the formation of the complex between Aβ and hCC was not observable using ^{15}N ^{1}H HSQC, it is possible that alternative NMR methods, for example relaxation experiments, could be performed to monitor this interaction.

A major challenge in this part of the study was the insufficient production of hCC and co-purifying of an *E. coli* protein mutants. This problem was solved by adding another round of size exclusion to separate out the contaminants. The concentration dependence confirmed, however in slightly different conditions, as it was found that in continuous shaking conditions hCC is less efficient in inhibiting Aβ fibrillisation. Slightly higher than equimolar concentration of hCC were enough to completely inhibit Aβ fibrillisation in minimal shaking conditions compared to about 4 times of the equimolar concentration in the continuous shaking conditions. This differences could be down to the acceleration of nuclei generation by Aβ or production of the different oligomeric forms that hCC is unable to bind (and thus avoid their growth to form fibrils). Another factor could be due to the fragmentation of the produced Aβ fibrils during shaking which causes generation of more ends and a faster rate of aggregation.

Investigation of the morphology and size distribution of the Aβ oligomers forming in these two different shaking conditions is important to find the nature of oligomers that hCC can bind and its implication *in vivo*.

The inhibition interface of Cystatin C

Mutagenesis of hydrophobic residues over different regions of the hCC structure was used as a crude biochemical method to find the binding interface to Aβ oligomers through their impact on the inhibition of Aβ fibrillisation measured through thioflavin T fluorescence assays. The addition of hCC dimers to the $A\beta_{1-42}$ aggregation reaction has no effect on the fibril yield. This reinforced the view that the dimer interface is crucial to the inhibitory activity of hCC. The major limitation of this strategy were reproducibility of the inhibitory effect of WT and mutants, which could be due to binding of hCC to heterogenous oligomers, however an order of inhibitory effect of mutants were possible. The likely binding interface of Aβ binding on the hCC is the unstructured N-terminal region represented by P6 residue and protease inhibitor active site represented strongly by W106 residue and less intensely by V57. Close to dimer interface (V50A) also reduced hCC's inhibitory effect but to a smaller degree. Despite its large hydrophobic surfaces L80 from the biggest loop's site of hCC and P105A which is close to W106 is not involved in the binding. These results together suggest that the N-terminal unstructured part and residues with large accessible hydrophobic surface areas located in or close to the active site and the hydrophobic surface facing outward are effectively involved in hCC binding to $A\beta_{1-42}$ aggregated structures. Presumably hCC bind to Aβ aggregated structures via this binding site and inhibit its further aggregation to form fibrils.

A study using short peptides of hCC could also be employed to find which region of hCC is involved in binding Aβ, as has been successful in the transthyretin system (Du and Murphy, 2010). Additionally, it may be interesting to investigate the effect of mixtures of modulating proteins on Aβ fibril formation.

As TTR's effect was significantly different in the presence of different surface and all the hCC: Aβ experiments were performed in the presence of polystyrene microplates.

Preliminary work in our lab shows that unlike TTR, hCC does inhibit Aβ fibrillisation in the presence of PEG microplates. This result indicates that hCC can bind and inhibit Aβ oligomers both in the solution and on the surface which indicates the potential importance of hCC in the inhibition of Aβ aggregation *in vivo* in different compartments. This, in addition to its ability to prevent fibrillisation at later stages of assembly, makes cystatin C a particularly interesting regulator of amyloid formation.

Identification of a novel inhibitor of Aβ fribrillisation from *E. coli*

While trying to work out the reasons behind the variability in the intensity of hCC to inhibit Aβ fibrillisation. An *E. coli* contaminant was found to co-purify with hCC. This contaminant separated from hCC by adding another round of size exclusion. The purified contaminant was found to have an inhibitory effect against Aβ. Half equimolar amounts of the contaminant were enough to completely inhibit Aβ fibrillisation and EM observation confirmed the formation of amorphous aggregates instead of fibrils by Aβ. The contaminant identified and sequenced by mass spectrometry was the periplasmic glutamate/ aspartate binding (GLTI) *E. coli* protein. This protein is part of an amino acid transport system which transfer the aspartate and glutamate ligands from the periplasm to an inner membrane protein (Sun *et al.*, 1998). The ability of this protein to inhibit Aβ fibrillisation could be due to binding to Aβ through its hydrophobic patches as its *Shigella* homologus structure is abundant in hydrophobic patches. Alternatively, binding to aspartate or glutamate residues in the Aβ sequence may avoid interactions with other monomers. Specific binding between an *E. coli* protein and Aβ peptide might not be very likely. However, the *E. coli* periplasm has a system to control the production of the right amounts of curli fibrils. *E. coli* curli is a natural amyloidogenic protein which the bacterium uses for attachment to surfaces. The GLTI protein might have a dual role

related to the curli controlling system and it might be designed to prevent fibrillisation of amyloidogenic proteins as well as its function as a transporter of amino acids. This may be similar to the observation that TTR, cystatin C and other brain proteins regulate amyloid β fibrillisation as well as carrying out their natural roles in the human body.

Future work will require designing a GLTI construct to produce it in sufficient amounts to study. The GLTI ^{15}N ^{1}H HSQC is not assigned yet. Production of triple labelled GLTI will allow the assignment of its HSQC then titrating Aβ will identify the binding site of Aβ on GLTI. Based on this binding region to the Aβ, short peptides can be designed and used as a potential small molecule therapeutic. Looking for human homologs and investigation of its activity against Aβ aggregation and toxicity is also one of the future works which can be performed.

7. References

ABRAHAMSON, M., ISLAM, M. Q., SZPIRER, J., SZPIRER, C. & LEVAN, G. 1989. The Human Cystatin C Gene (Cst3), Mutated in Hereditary Cystatin C Amyloid Angiopathy, Is Located on Chromosome 20. *Hum Genet,* 82**,** 223-6.

ABRAHAMSON, M., MASON, R. W., HANSSON, H., BUTTLE, D. J., GRUBB, A. & OHLSSON, K. 1991. Human Cystatin-C - Role of the N-Terminal Segment in the Inhibition of Human Cysteine Proteinases and in Its Inactivation by Leukocyte Elastase. *Biochemical Journal,* 273**,** 621-626.

ABRAHAMSON, M. & GRUBB, A. 1994. Increased Body-Temperature Accelerates Aggregation of the Leu-68 -] Gln Mutant Cystatin-C, the Amyloid-Forming Protein in Hereditary Cystatin-C Amyloid Angiopathy. *Proceedings of the National Academy of Sciences of the United States of America,* 91**,** 1416-1420.

ABRAHAMSON, M. 1996. Molecular Basis for Amyloidosis Related to Hereditary Brain Hemorrhage. *Scand J Clin Lab Invest Suppl,* 226**,** 47-56.

ALBERS, D. S. & BEAL, M. F. 2000. Mitochondrial Dysfunction and Oxidative Stress in Aging and Neurodegenerative Disease. *J Neural Transm Suppl,* 59**,** 133-54.

ANCOLIO, K., DUMANCHIN, C., BARELLI, H., WARTER, J. M., BRICE, A., CAMPION, D., FREBOURG, T. & CHECLER, F. 1999. Unusual Phenotypic Alteration of Beta Amyloid Precursor Protein (Beta App) Maturation by a New Val-715 -> Met Beta App-770 Mutation Responsible for Probable Early-Onset Alzheimer's Disease. *Proceedings of the National Academy of Sciences of the United States of America,* 96**,** 4119-4124.

ANCSIN, J. B. 2003. Amyloidogenesis: Historical and Modern Observations Point to Heparan Sulfate Proteoglycans as a Major Culprit. *Amyloid,* 10**,** 67-79.

ANNAERT, W. & DE STROOPER, B. 2002. A Cell Biological Perspective on Alzheimer's Disease. *Annual Review of Cell and Developmental Biology,* 18**,** 25-51.

ARIGA, T., MIYATAKE, T. & YU, R. K. 2010. Role of Proteoglycans and Glycosaminoglycans in the Pathogenesis of Alzheimer's Disease and Related Disorders: Amyloidogenesis and Therapeutic Strategies--a Review. *J Neurosci Res,* 88**,** 2303-15.

ARISPE, N., POLLARD, H. B. & ROJAS, E. 1993. Giant Multilevel Cation Channels Formed by Alzheimer Disease Amyloid Beta-Protein [a Beta P-(1-40)] in Bilayer Membranes. *Proc Natl Acad Sci U S A,* 90**,** 10573-7.

ARONICA, E., VAN VLIET, E. A., HENDRIKSEN, E., TROOST, D., LOPES DA SILVA, F. H. & GORTER, J. A. 2001. Cystatin C, a Cysteine Protease Inhibitor, Is Persistently up-Regulated in Neurons and Glia in a Rat Model for Mesial Temporal Lobe Epilepsy. *Eur J Neurosci,* 14**,** 1485-91.

ARORA, A., HA, C. & PARK, C. B. 2004. Inhibition of Insulin Amyloid Formation by Small Stress Molecules. *Febs Letters,* 564**,** 121-125.

BAI, Y., MILNE, J. S., MAYNE, L. & ENGLANDER, S. W. 1993. Primary Structure Effects on Peptide Group Hydrogen Exchange. *Proteins,* 17**,** 75-86.

BALDUCCI, C., BEEG, M., STRAVALACI, M., BASTONE, A., SCLIP, A., BIASINI, E., TAPELLA, L., COLOMBO, L., MANZONI, C., BORSELLO, T., CHIESA, R., GOBBI, M., SALMONA, M. & FORLONI, G. 2010. Synthetic Amyloid-Beta Oligomers Impair Long-Term Memory Independently of Cellular Prion Protein. *Proc Natl Acad Sci U S A,* 107**,** 2295-300.

BALGUERIE, A., DOS REIS, S., RITTER, C., CHAIGNEPAIN, S., COULARY-SALIN, B., FORGE, V., BATHANY, K., LASCU, I., SCHMITTER, J. M., RIEK, R. & SAUPE, S. J. 2003. Domain Organization and Structure-Function Relationship of the Het-S Prion Protein of Podospora Anserina. *EMBO J,* 22**,** 2071-81.

BARTOLINI, M., NALDI, M., FIORI, J., VALLE, F., BISCARINI, F., NICOLAU, D. V. & ANDRISANO, V. 2011. Kinetic Characterization of Amyloid-Beta 1-42 Aggregation with a Multimethodological Approach. *Anal Biochem,* 414**,** 215-25.

BASSETT, C. N. & MONTINE, T. J. 2003. Lipoproteins and Lipid Peroxidation in Alzheimer's Disease. *J Nutr Health Aging,* 7**,** 24-9.

BAUER, M., GOETZ, T., GLENN, T. & WHYBROW, P. C. 2008. The Thyroid-Brain Interaction in Thyroid Disorders and Mood Disorders. *J Neuroendocrinol,* 20**,** 1101-14.

BAXA, U., TAYLOR, K. L., WALL, J. S., SIMON, M. N., CHENG, N., WICKNER, R. B. & STEVEN, A. C. 2003. Architecture of Ure2p Prion Filaments: The N-Terminal Domains Form a Central Core Fiber. *J Biol Chem,* 278**,** 43717-27.

BENILOVA, I., KARRAN, E. & DE STROOPER, B. 2012. The Toxic a Beta Oligomer and Alzheimer's Disease: An Emperor in Need of Clothes. *Nature Neuroscience,* 15**,** 349-357.

BENSON, M. D., JAMES, S., SCOTT, K., LIEPNIEKS, J. J. & KLUVE-BECKERMAN, B. 2008. Leukocyte Chemotactic Factor 2: A Novel Renal Amyloid Protein. *Kidney Int,* 74**,** 218-22.

BERGAMASCHINI, L., ROSSI, E., VERGANI, C. & DE SIMONI, M. G. 2009. Alzheimer's Disease: Another Target for Heparin Therapy. *ScientificWorldJournal,* 9**,** 891-908.

BERNACKI, J. P. & MURPHY, R. M. 2009. Model Discrimination and Mechanistic Interpretation of Kinetic Data in Protein Aggregation Studies. *Biophys J,* 96**,** 2871-87.

BERTRAM, L., MCQUEEN, M. B., MULLIN, K., BLACKER, D. & TANZI, R. E. 2007. Systematic Meta-Analyses of Alzheimer Disease Genetic Association Studies: The Alzgene Database. *Nat Genet,* 39**,** 17-23.

BERTRAM, L. & TANZI, R. E. 2008. Thirty Years of Alzheimer's Disease Genetics: The Implications of Systematic Meta-Analyses. *Nat Rev Neurosci,* 9**,** 768-78.

BHATTACHARYYA, R. & KOVACS, D. M. 2010. Acat Inhibition and Amyloid Beta Reduction. *Biochim Biophys Acta,* 1801**,** 960-5.

BIASINI, E., TURNBAUGH, J. A., UNTERBERGER, U. & HARRIS, D. A. 2012. Prion Protein at the Crossroads of Physiology and Disease. *Trends Neurosci,* 35**,** 92-103.

BIERE, A. L., OSTASZEWSKI, B., STIMSON, E. R., HYMAN, B. T., MAGGIO, J. E. & SELKOE, D. J. 1996. Amyloid Beta-Peptide Is Transported on Lipoproteins and Albumin in Human Plasma. *Journal of Biological Chemistry,* 271**,** 32916-32922.

BITAN, G., KIRKITADZE, M. D., LOMAKIN, A., VOLLERS, S. S., BENEDEK, G. B. & TEPLOW, D. B. 2003. Amyloid Beta -Protein (Abeta) Assembly: Abeta 40 and Abeta 42 Oligomerize through Distinct Pathways. *Proc Natl Acad Sci U S A,* 100**,** 330-5.

BLAKE, C. & SERPELL, L. 1996. Synchrotron X-Ray Studies Suggest That the Core of the Transthyretin Amyloid Fibril Is a Continuous Beta-Sheet Helix. *Structure,* 4**,** 989-98.

BLAKE, C. C., GEISOW, M. J., OATLEY, S. J., RERAT, B. & RERAT, C. 1978. Structure of Prealbumin: Secondary, Tertiary and Quaternary Interactions Determined by Fourier Refinement at 1.8 A. *J Mol Biol,* 121**,** 339-56.

BLAKE, C. C. F., SWAN, I. D. A., RERAT, C., BERTHOU, J., LAURENT, A. & RERAT, B. 1971. X-Ray Study of Subunit Structure of Prealbumin. *Journal of Molecular Biology,* 61**,** 217-&.

BOADA, M., ORTIZ, P., ANAYA, F., HERNANDEZ, I., MUNOZ, J., NUNEZ, L., OLAZARAN, J., ROCA, I., CUBERAS, G., TARRAGA, L., BUENDIA, M., PLA, R. P., FERRER, I. & PAEZ, A. 2009. Amyloid-Targeted Therapeutics in Alzheimer's Disease: Use of Human Albumin in Plasma Exchange as a Novel Approach for a Beta Mobilization. *Drug News & Perspectives,* 22**,** 325-339.

BOBEK, L. A. & LEVINE, M. J. 1992. Cystatins--Inhibitors of Cysteine Proteinases. *Crit Rev Oral Biol Med,* 3**,** 307-32.

BOHRMANN, B., TJERNBERG, L., KUNER, P., POLI, S., LEVET-TRAFIT, B., NASLUND, J., RICHARDS, G., HUBER, W., DOBELI, H. & NORDSTEDT, C. 1999. Endogenous Proteins Controlling Amyloid Beta-Peptide Polymerization. Possible Implications for Beta-Amyloid Formation in the Central Nervous System and in Peripheral Tissues. *J Biol Chem,* 274**,** 15990-5.

BOOTH, D. R., SUNDE, M., BELLOTTI, V., ROBINSON, C. V., HUTCHINSON, W. L., FRASER, P. E., HAWKINS, P. N., DOBSON, C. M., RADFORD, S. E., BLAKE, C. C. & PEPYS, M. B. 1997. Instability, Unfolding and Aggregation of Human Lysozyme Variants Underlying Amyloid Fibrillogenesis. *Nature,* 385**,** 787-93.

BRYLEVA, E. Y., ROGERS, M. A., CHANG, C. C., BUEN, F., HARRIS, B. T., ROUSSELET, E., SEIDAH, N. G., ODDO, S., LAFERLA, F. M., SPENCER, T. A., HICKEY, W. F. & CHANG, T. Y. 2010. Acat1 Gene Ablation Increases 24(S)-Hydroxycholesterol Content in the Brain and Ameliorates Amyloid Pathology in Mice with Ad. *Proc Natl Acad Sci U S A,* 107**,** 3081-6.

BU, G. 2009. Apolipoprotein E and Its Receptors in Alzheimer's Disease: Pathways, Pathogenesis and Therapy. *Nat Rev Neurosci,* 10**,** 333-44.

BUCCIANTINI, M., GIANNONI, E., CHITI, F., BARONI, F., FORMIGLI, L., ZURDO, J., TADDEI, N., RAMPONI, G., DOBSON, C. M. & STEFANI, M. 2002. Inherent Toxicity of Aggregates Implies a Common Mechanism for Protein Misfolding Diseases. *Nature,* 416**,** 507-11.

BUELL, A. K., GALVAGNION, C., GASPAR, R., SPARR, E., VENDRUSCOLO, M., KNOWLES, T. P., LINSE, S. & DOBSON, C. M. 2014. Solution Conditions Determine the Relative Importance of Nucleation and Growth Processes in Alpha-Synuclein Aggregation. *Proc Natl Acad Sci U S A,* 111**,** 7671-6.

BURKE, K. A., YATES, E. A. & LEGLEITER, J. 2013. Biophysical Insights into How Surfaces, Including Lipid Membranes, Modulate Protein Aggregation Related to Neurodegeneration. *Front Neurol,* 4**,** 17.

BURNS, A. & ILIFFE, S. 2009. Dementia. *British Medical Journal,* 338.

BUTTERFIELD, S. M. & LASHUEL, H. A. 2010. Amyloidogenic Protein-Membrane Interactions: Mechanistic Insight from Model Systems. *Angew Chem Int Ed Engl,* 49**,** 5628-54.

BUTTSTEDT, A., WOSTRADOWSKI, T., IHLING, C., HAUSE, G., SINZ, A. & SCHWARZ, E. 2013. Different Morphology of Amyloid Fibrils Originating from Agitated and Non-Agitated Conditions. *Amyloid,* 20**,** 86-92.

BUXBAUM, J. N., YE, Z., REIXACH, N., FRISKE, L., LEVY, C., DAS, P., GOLDE, T., MASLIAH, E., ROBERTS, A. R. & BARTFAI, T. 2008. Transthyretin Protects Alzheimer's Mice from the Behavioral and Biochemical Effects of Abeta Toxicity. *Proc Natl Acad Sci U S A,* 105**,** 2681-6.

BUXBAUM, J. N. & REIXACH, N. 2009. Transthyretin: The Servant of Many Masters. *Cell Mol Life Sci,* 66**,** 3095-101.

BUXBAUM, J. N., TAGOE, C., GALLO, G., WALKER, J. R., KURIAN, S. & SALOMON, D. R. 2012. Why Are Some Amyloidoses Systemic? Does Hepatic "Chaperoning at a Distance" Prevent Cardiac Deposition in a Transgenic Model of Human Senile Systemic (Transthyretin) Amyloidosis? *FASEB J,* 26**,** 2283-93.

BUXBAUM, J. N., ROBERTS, A. J., ADAME, A. & MASLIAH, E. 2014. Silencing of Murine Transthyretin and Retinol Binding Protein Genes Has Distinct and Shared Behavioral and Neuropathologic Effects. *Neuroscience,* 275**,** 352-64.

CALAMAI, M., CHITI, F. & DOBSON, C. M. 2005. Amyloid Fibril Formation Can Proceed from Different Conformations of a Partially Unfolded Protein. *Biophys J,* 89**,** 4201-10.

CALELLA, A. M., FARINELLI, M., NUVOLONE, M., MIRANTE, O., MOOS, R., FALSIG, J., MANSUY, I. M. & AGUZZI, A. 2010. Prion Protein and Abeta-Related Synaptic Toxicity Impairment. *EMBO Mol Med,* 2**,** 306-14.

CAMPIONI, S., MANNINI, B., ZAMPAGNI, M., PENSALFINI, A., PARRINI, C., EVANGELISTI, E., RELINI, A., STEFANI, M., DOBSON, C. M., CECCHI, C. & CHITI, F. 2010. A Causative Link between the Structure of Aberrant Protein Oligomers and Their Toxicity. *Nat Chem Biol,* 6**,** 140-7.

CARTER, D. C. & HO, J. X. 1994. Structure of Serum Albumin. *Adv Protein Chem,* 45**,** 153-203.

CARULLA, N., CADDY, G. L., HALL, D. R., ZURDO, J., GAIRI, M., FELIZ, M., GIRALT, E., ROBINSON, C. V. & DOBSON, C. M. 2005. Molecular Recycling within Amyloid Fibrils. *Nature,* 436**,** 554-8.

CASTILLO, G. M., NGO, C., CUMMINGS, J., WIGHT, T. N. & SNOW, A. D. 1997. Perlecan Binds to the Beta-Amyloid Proteins (a Beta) of Alzheimer's Disease, Accelerates a Beta Fibril Formation, and Maintains a Beta Fibril Stability. *J Neurochem,* 69**,** 2452-65.

CASTILLO, G. M., LUKITO, W., WIGHT, T. N. & SNOW, A. D. 1999. The Sulfate Moieties of Glycosaminoglycans Are Critical for the Enhancement of Beta-Amyloid Protein Fibril Formation. *J Neurochem,* 72**,** 1681-7.

CAUGHEY, B. & LANSBURY, P. T. 2003. Protofibrils, Pores, Fibrils, and Neurodegeneration: Separating the Responsible Protein Aggregates from the Innocent Bystanders. *Annual Review of Neuroscience,* 26**,** 267-298.

CHANDRASEKARAN, R. & STUBBS, G. 2006. Fibre Diffraction. *International Tables for Crystallography.* John Wiley & Sons, Ltd.

CHANG, T. Y., CHANG, C. C., BRYLEVA, E., ROGERS, M. A. & MURPHY, S. R. 2010. Neuronal Cholesterol Esterification by Acat1 in Alzheimer's Disease. *IUBMB Life,* 62**,** 261-7.

CHEN, S., YADAV, S. P. & SUREWICZ, W. K. 2010. Interaction between Human Prion Protein and Amyloid-Beta (Abeta) Oligomers: Role of N-Terminal Residues. *J Biol Chem,* 285**,** 26377-83.

CHENG, H., XU, J., MCKEEL, D. W., JR. & HAN, X. 2003. Specificity and Potential Mechanism of Sulfatide Deficiency in Alzheimer's Disease: An Electrospray Ionization Mass Spectrometric Study. *Cell Mol Biol (Noisy-le-grand),* 49**,** 809-18.

CHIOU, A., HAGGLOF, P., ORTE, A., CHEN, A. Y., DUNNE, P. D., BELORGEY, D., KARLSSON-LI, S., LOMAS, D. A. & KLENERMAN, D. 2009. Probing Neuroserpin Polymerization and Interaction with Amyloid-Beta Peptides Using Single Molecule Fluorescence. *Biophys J,* 97**,** 2306-15.

CHITI, F., WEBSTER, P., TADDEI, N., CLARK, A., STEFANI, M., RAMPONI, G. & DOBSON, C. M. 1999. Designing Conditions for in Vitro Formation of Amyloid Protofilaments and Fibrils. *Proc Natl Acad Sci U S A,* 96**,** 3590-4.

CHITI, F., TADDEI, N., STEFANI, M., DOBSON, C. M. & RAMPONI, G. 2001. Reduction of the Amyloidogenicity of a Protein by Specific Binding of Ligands to the Native Conformation. *Protein Sci,* 10**,** 879-86.

CHITI, F., STEFANI, M., TADDEI, N., RAMPONI, G. & DOBSON, C. M. 2003. Rationalization of the Effects of Mutations on Peptide and Protein Aggregation Rates. *Nature,* 424**,** 805-8.

CHITI, F. & DOBSON, C. M. 2006a. Protein Misfolding, Functional Amyloid, and Human Disease. *Annual Review of Biochemistry,* 75**,** 333-366.

CHITI, F. & DOBSON, C. M. 2006b. Protein Misfolding, Functional Amyloid, and Human Disease. *Annu Rev Biochem,* 75**,** 333-66.

CHO, P. Y., JOSHI, G., JOHNSON, J. A. & MURPHY, R. M. 2014. Transthyretin-Derived Peptides as Beta-Amyloid Inhibitors. *ACS Chem Neurosci,* 5**,** 542-51.

CHOI, S. H., LEIGHT, S. N., LEE, V. M., LI, T., WONG, P. C., JOHNSON, J. A., SARAIVA, M. J. & SISODIA, S. S. 2007. Accelerated Abeta Deposition in Appswe/Ps1deltae9 Mice with Hemizygous Deletions of Ttr (Transthyretin). *J Neurosci,* 27**,** 7006-10.

CIRRITO, J. R., MAY, P. C., O'DELL, M. A., TAYLOR, J. W., PARSADANIAN, M., CRAMER, J. W., AUDIA, J. E., NISSEN, J. S., BALES, K. R., PAUL, S. M., DEMATTOS, R. B. & HOLTZMAN, D. M. 2003. In Vivo Assessment of Brain Interstitial Fluid with Microdialysis Reveals Plaque-Associated Changes in Amyloid-Beta Metabolism and Half-Life. *J Neurosci,* 23**,** 8844-53.

CISSE, M., SANCHEZ, P. E., KIM, D. H., HO, K., YU, G. Q. & MUCKE, L. 2011. Ablation of Cellular Prion Protein Does Not Ameliorate Abnormal Neural Network Activity or Cognitive Dysfunction in the J20 Line of Human Amyloid Precursor Protein Transgenic Mice. *J Neurosci,* 31**,** 10427-31.

COHEN, D. H., FEINER, H., JENSSON, O. & FRANGIONE, B. 1983. Amyloid Fibril in Hereditary Cerebral-Hemorrhage with Amyloidosis (Hchwa) Is Related to the Gastroentero-Pancreatic Neuroendocrine Protein, Gamma Trace *Journal of Experimental Medicine,* 158**,** 623-628.

COHEN, S. I., LINSE, S., LUHESHI, L. M., HELLSTRAND, E., WHITE, D. A., RAJAH, L., OTZEN, D. E., VENDRUSCOLO, M., DOBSON, C. M. & KNOWLES, T. P. 2013. Proliferation of Amyloid-

Beta42 Aggregates Occurs through a Secondary Nucleation Mechanism. *Proc Natl Acad Sci U S A,* 110**,** 9758-63.

COHEN, S. I., AROSIO, P., PRESTO, J., KURUDENKANDY, F. R., BIVERSTAL, H., DOLFE, L., DUNNING, C., YANG, X., FROHM, B., VENDRUSCOLO, M., JOHANSSON, J., DOBSON, C. M., FISAHN, A., KNOWLES, T. P. & LINSE, S. 2015. A Molecular Chaperone Breaks the Catalytic Cycle That Generates Toxic Abeta Oligomers. *Nat Struct Mol Biol,* 22**,** 207-13.

COIMBRA, A., WILLIAMS, D. S. & HOSTETLER, E. D. 2006. The Role of Mri and Pet/Spect in Alzheimer's Disease. *Current Topics in Medicinal Chemistry,* 6**,** 629-647.

COLLINGE, J. 2001. Prion Diseases of Humans and Animals: Their Causes and Molecular Basis. *Annual Review of Neuroscience,* 24**,** 519-550.

CORDER, E. H., SAUNDERS, A. M., STRITTMATTER, W. J., SCHMECHEL, D. E., GASKELL, P. C., SMALL, G. W., ROSES, A. D., HAINES, J. L. & PERICAK-VANCE, M. A. 1993. Gene Dose of Apolipoprotein E Type 4 Allele and the Risk of Alzheimer's Disease in Late Onset Families. *Science,* 261**,** 921-3.

CORREIA, B. E., LOUREIRO-FERREIRA, N., RODRIGUES, J. R. & BRITO, R. M. M. 2006. A Structural Model of an Amyloid Protofilament of Transthyretin. *Protein Science,* 15**,** 28-32.

COSTA, R., GONCALVES, A., SARAIVA, M. J. & CARDOSO, I. 2008. Transthyretin Binding to a-Beta Peptide--Impact on a-Beta Fibrillogenesis and Toxicity. *FEBS Lett,* 582**,** 936-42.

CRAWFORD, F. C., FREEMAN, M. J., SCHINKA, J. A., ABDULLAH, L. I., GOLD, M., HARTMAN, R., KRIVIAN, K., MORRIS, M. D., RICHARDS, D., DUARA, R., ANAND, R. & MULLAN, M. J. 2000. A Polymorphism in the Cystatin C Gene Is a Novel Risk Factor for Late-Onset Alzheimer's Disease. *Neurology,* 55**,** 763-8.

CURRY, S., MANDELKOW, H., BRICK, P. & FRANKS, N. 1998. Crystal Structure of Human Serum Albumin Complexed with Fatty Acid Reveals an Asymmetric Distribution of Binding Sites. *Nat Struct Biol,* 5**,** 827-35.

DAVIS, J. B. 1996. Oxidative Mechanisms in Beta-Amyloid Cytotoxicity. *Neurodegeneration,* 5**,** 441-4.

DAVIS, P. J., HOLMES, D., WALTHO, J. P. & STANIFORTH, R. A. 2015. Limited Proteolysis Reveals That Amyloids from the 3d Domain-Swapping Cystatin B Have a Non-Native Beta-Sheet Topology. *J Mol Biol,* 427**,** 2418-34.

DAVIS, R. L., SHRIMPTON, A. E., HOLOHAN, P. D., BRADSHAW, C., FEIGLIN, D., COLLINS, G. H., SONDEREGGER, P., KINTER, J., BECKER, L. M., LACBAWAN, F., KRASNEWICH, D., MUENKE, M., LAWRENCE, D. A., YERBY, M. S., SHAW, C. M., GOOPTU, B., ELLIOTT, P. R., FINCH, J. T., CARRELL, R. W. & LOMAS, D. A. 1999. Familial Dementia Caused by Polymerization of Mutant Neuroserpin. *Nature,* 401**,** 376-9.

DAVIS, R. L., SHRIMPTON, A. E., CARRELL, R. W., LOMAS, D. A., GERHARD, L., BAUMANN, B., LAWRENCE, D. A., YEPES, M., KIM, T. S., GHETTI, B., PICCARDO, P., TAKAO, M., LACBAWAN, F., MUENKE, M., SIFERS, R. N., BRADSHAW, C. B., KENT, P. F., COLLINS, G. H., LAROCCA, D. & HOLOHAN, P. D. 2002. Association between Conformational Mutations in Neuroserpin and Onset and Severity of Dementia. *Lancet,* 359**,** 2242-7.

DE LA MONTE, S. M. & TONG, M. 2014. Brain Metabolic Dysfunction at the Core of Alzheimer's Disease. *Biochem Pharmacol,* 88**,** 548-59.

DE LAURETO, P. P., TADDEI, N., FRARE, E., CAPANNI, C., COSTANTINI, S., ZURDO, J., CHITI, F., DOBSON, C. M. & FONTANA, A. 2003. Protein Aggregation and Amyloid Fibril Formation by an Sh3 Domain Probed by Limited Proteolysis. *Journal of Molecular Biology,* 334**,** 129-141.

DE LAURETO, P. P., FRARE, E., BATTAGLIA, F., MOSSUTO, M. F., UVERSKY, V. N. & FONTANA, A. 2005. Protein Dissection Enhances the Amyloidogenic Properties of Alpha-Lactalbumin. *FEBS J,* 272**,** 2176-88.

DENG, A., IRIZARRY, M. C., NITSCH, R. M., GROWDON, J. H. & REBECK, G. W. 2001. Elevation of Cystatin C in Susceptible Neurons in Alzheimer's Disease. *American Journal of Pathology,* 159**,** 1061-1068.

DI PAOLO, G. & KIM, T. W. 2011. Linking Lipids to Alzheimer's Disease: Cholesterol and Beyond. *Nat Rev Neurosci,* 12**,** 284-96.
DIETSCHY, J. M. & TURLEY, S. D. 2001. Cholesterol Metabolism in the Brain. *Curr Opin Lipidol,* 12**,** 105-12.
DOBSON, C. M. 1999. Protein Misfolding, Evolution and Disease. *Trends Biochem Sci,* 24**,** 329-32.
DOBSON, C. M. 2002. Protein-Misfolding Diseases: Getting out of Shape. *Nature,* 418**,** 729-730.
DOBSON, C. M. 2003. Protein Folding and Misfolding. *Nature,* 426**,** 884-90.
DOBSON, C. M. 2004. Principles of Protein Folding, Misfolding and Aggregation. *Seminars in Cell & Developmental Biology,* 15**,** 3-16.
DODEL, R. C., DU, Y., DEPBOYLU, C., KURZ, A., EASTWOOD, B., FARLOW, M., OERTEL, W. H., MULLER, U. & RIEMENSCHNEIDER, M. 2002. A Polymorphism in the Cystatin C Promoter Region Is Not Associated with an Increased Risk of Ad. *Neurology,* 58**,** 664.
DU, J. & MURPHY, R. M. 2010. Characterization of the Interaction of Beta-Amyloid with Transthyretin Monomers and Tetramers. *Biochemistry,* 49**,** 8276-89.
DU, J., CHO, P. Y., YANG, D. T. & MURPHY, R. M. 2012. Identification of Beta-Amyloid-Binding Sites on Transthyretin. *Protein Eng Des Sel,* 25**,** 337-45.
EKIEL, I. & ABRAHAMSON, M. 1996. Folding-Related Dimerization of Human Cystatin C. *Journal of Biological Chemistry,* 271**,** 1314-1321.
EKIEL, I., ABRAHAMSON, M., FULTON, D. B., LINDAHL, P., STORER, A. C., LEVADOUX, W., LAFRANCE, M., LABELLE, S., POMERLEAU, Y., GROLEAU, D., LESAUTEUR, L. & GEHRING, K. 1997a. Nmr Structural Studies of Human Cystatin C Dimers and Monomers. *J Mol Biol,* 271**,** 266-77.
EKIEL, I., ABRAHAMSON, M., FULTON, D. B., LINDAHL, P., STORER, A. C., LEVADOUX, W., LAFRANCE, M., LABELLE, S., POMERLEAU, Y., GROLEAU, D., LESAUTEUR, L. & GEHRING, K. 1997b. Nmr Structural Studies of Human Cystatin C Dimers and Monomers. *Journal of Molecular Biology,* 271**,** 266-277.
ELGHETANY, M. T., SALEEM, A. & BARR, K. 1989. The Congo Red Stain Revisited. *Ann Clin Lab Sci,* 19**,** 190-5.
ELSHAWAIHDE, A. 2012. Role of Human Cystatin C in Alzheimer's Disease. Doctor of Philosophy, University of Sheffield.
ENGEL, M. F., KHEMTEMOURIAN, L., KLEIJER, C. C., MEELDIJK, H. J., JACOBS, J., VERKLEIJ, A. J., DE KRUIJFF, B., KILLIAN, J. A. & HOPPENER, J. W. 2008. Membrane Damage by Human Islet Amyloid Polypeptide through Fibril Growth at the Membrane. *Proc Natl Acad Sci U S A,* 105**,** 6033-8.
ENGLANDER, S. W., SOSNICK, T. R., ENGLANDER, J. J. & MAYNE, L. 1996. Mechanisms and Uses of Hydrogen Exchange. *Curr Opin Struct Biol,* 6**,** 18-23.
EULITZ, M., WEISS, D. T. & SOLOMON, A. 1990. Immunoglobulin Heavy-Chain-Associated Amyloidosis. *Proc Natl Acad Sci U S A,* 87**,** 6542-6.
FABBRO, S. & SEEDS, N. W. 2009. Plasminogen Activator Activity Is Inhibited While Neuroserpin Is up-Regulated in the Alzheimer Disease Brain. *J Neurochem,* 109**,** 303-15.
FABBRO, S., SCHALLER, K. & SEEDS, N. W. 2011. Amyloid-Beta Levels Are Significantly Reduced and Spatial Memory Defects Are Rescued in a Novel Neuroserpin-Deficient Alzheimer's Disease Transgenic Mouse Model. *J Neurochem,* 118**,** 928-38.
FANDRICH, M., FLETCHER, M. A. & DOBSON, C. M. 2001. Amyloid Fibrils from Muscle Myoglobin. *Nature,* 410**,** 165-6.
FANDRICH, M. 2012a. Oligomeric Intermediates in Amyloid Formation: Structure Determination and Mechanisms of Toxicity. *Journal of Molecular Biology,* 421**,** 427-440.
FANDRICH, M. 2012b. Oligomeric Intermediates in Amyloid Formation: Structure Determination and Mechanisms of Toxicity. *J Mol Biol,* 421**,** 427-40.
FANTINI, J., GARMY, N., MAHFOUD, R. & YAHI, N. 2002. Lipid Rafts: Structure, Function and Role in Hiv, Alzheimer's and Prion Diseases. *Expert Rev Mol Med,* 4**,** 1-22.

FASSBENDER, K., SIMONS, M., BERGMANN, C., STROICK, M., LUTJOHANN, D., KELLER, P., RUNZ, H., KUHL, S., BERTSCH, T., VON BERGMANN, K., HENNERICI, M., BEYREUTHER, K. & HARTMANN, T. 2001. Simvastatin Strongly Reduces Levels of Alzheimer's Disease Beta - Amyloid Peptides Abeta 42 and Abeta 40 in Vitro and in Vivo. *Proc Natl Acad Sci U S A,* 98**,** 5856-61.

FINCKH, U., VON DER KAMMER, H., VELDEN, J., MICHEL, T., ANDRESEN, B., DENG, A., ZHANG, J., MULLER-THOMSEN, T., ZUCHOWSKI, K., MENZER, G., MANN, U., PAPASSOTIROPOULOS, A., HEUN, R., ZURDEL, J., HOLST, F., BENUSSI, L., STOPPE, G., REISS, J., MISEREZ, A. R., STAEHELIN, H. B., REBECK, G. W., HYMAN, B. T., BINETTI, G., HOCK, C., GROWDON, J. H. & NITSCH, R. M. 2000. Genetic Association of a Cystatin C Gene Polymorphism with Late-Onset Alzheimer Disease. *Arch Neurol,* 57**,** 1579-83.

FRARE, E., MOSSUTO, M. F., POLVERINO DE LAURETO, P., DUMOULIN, M., DOBSON, C. M. & FONTANA, A. 2006. Identification of the Core Structure of Lysozyme Amyloid Fibrils by Proteolysis. *J Mol Biol,* 361**,** 551-61.

FREIR, D. B., NICOLL, A. J., KLYUBIN, I., PANICO, S., MC DONALD, J. M., RISSE, E., ASANTE, E. A., FARROW, M. A., SESSIONS, R. B., SAIBIL, H. R., CLARKE, A. R., ROWAN, M. J., WALSH, D. M. & COLLINGE, J. 2011. Interaction between Prion Protein and Toxic Amyloid Beta Assemblies Can Be Therapeutically Targeted at Multiple Sites. *Nat Commun,* 2**,** 336.

FUNG, J., DARABIE, A. A. & MCLAURIN, J. 2005. Contribution of Simple Saccharides to the Stabilization of Amyloid Structure. *Biochemical and Biophysical Research Communications,* 328**,** 1067-1072.

GARAI, K., SAHOO, B., SENGUPTA, P. & MAITI, S. 2008. Quasihomogeneous Nucleation of Amyloid Beta Yields Numerical Bounds for the Critical Radius, the Surface Tension, and the Free Energy Barrier for Nucleus Formation. *J Chem Phys,* 128**,** 045102.

GEDDES, A. J., PARKER, K. D., ATKINS, E. D. & BEIGHTON, E. 1968. "Cross-Beta" Conformation in Proteins. *J Mol Biol,* 32**,** 343-58.

GHISO, J., PONS-ESTEL, B. & FRANGIONE, B. 1986a. Hereditary Cerebral Amyloid Angiopathy: The Amyloid Fibrils Contain a Protein Which Is a Variant of Cystatin C, an Inhibitor of Lysosomal Cysteine Proteases. *Biochem Biophys Res Commun,* 136**,** 548-54.

GHISO, J., PONSESTEL, B. & FRANGIONE, B. 1986b. Hereditary Cerebral Amyloid Angiopathy - the Amyloid Fibrils Contain a Protein Which Is a Variant of Cystatin-C, an Inhibitor of Lysosomal Cysteine Proteases. *Biochemical and Biophysical Research Communications,* 136**,** 548-554.

GIACOMELLI, C. E. & NORDE, W. 2005. Conformational Changes of the Amyloid Beta-Peptide (1-40) Adsorbed on Solid Surfaces. *Macromol Biosci,* 5**,** 401-7.

GINSBERG, L., RAFIQUE, S., XUEREB, J. H., RAPOPORT, S. I. & GERSHFELD, N. L. 1995. Disease and Anatomic Specificity of Ethanolamine Plasmalogen Deficiency in Alzheimer's Disease Brain. *Brain Res,* 698**,** 223-6.

GINSBERG, L., XUEREB, J. H. & GERSHFELD, N. L. 1998. Membrane Instability, Plasmalogen Content, and Alzheimer's Disease. *J Neurochem,* 70**,** 2533-8.

GIUNTA, S., VALLI, M. B., GALEAZZI, R., FATTORETTI, P., CORDER, E. H. & GALEAZZI, L. 2005. Transthyretin Inhibition of Amyloid Beta Aggregation and Toxicity. *Clin Biochem,* 38**,** 1112-9.

GLABE, C. G. 2006. Common Mechanisms of Amyloid Oligomer Pathogenesis in Degenerative Disease. *Neurobiol Aging,* 27**,** 570-5.

GLABE, C. G. 2008. Structural Classification of Toxic Amyloid Oligomers. *J Biol Chem,* 283**,** 29639-43.

GLENNER, G. G., EANES, E. D. & PAGE, D. L. 1972. The Relation of the Properties of Congo Red-Stained Amyloid Fibrils to the -Conformation. *J Histochem Cytochem,* 20**,** 821-6.

GOLDSBURY, C., KISTLER, J., AEBI, U., ARVINTE, T. & COOPER, G. J. S. 1999. Watching Amyloid Fibrils Grow by Time-Lapse Atomic Force Microscopy. *Journal of Molecular Biology,* 285**,** 33-39.

GOLDSBURY, C., GOLDIE, K., PELLAUD, J., SEELIG, J., FREY, P., MULLER, S. A., KISTLER, J., COOPER, G. J. & AEBI, U. 2000. Amyloid Fibril Formation from Full-Length and Fragments of Amylin. *J Struct Biol,* 130**,** 352-62.

GRIFFITH, J. S. 1967. Self-Replication and Scrapie. *Nature,* 215**,** 1043-4.

GRIMM, M. O., GRIMM, H. S., PATZOLD, A. J., ZINSER, E. G., HALONEN, R., DUERING, M., TSCHAPE, J. A., DE STROOPER, B., MULLER, U., SHEN, J. & HARTMANN, T. 2005. Regulation of Cholesterol and Sphingomyelin Metabolism by Amyloid-Beta and Presenilin. *Nat Cell Biol,* 7**,** 1118-23.

GRUBB, A. & LOFBERG, H. 1985. Human Gamma-Trace - Structure, Function and Clinical Use of Concentration Measurements. *Scandinavian Journal of Clinical & Laboratory Investigation,* 45**,** 7-13.

GRUBB, A. 1992. Diagnostic Value of Analysis of Cystatin C and Protein Hc in Biological Fluids. *Clin Nephrol,* 38 Suppl 1**,** S20-7.

GUAN, Z., WANG, Y., CAIRNS, N. J., LANTOS, P. L., DALLNER, G. & SINDELAR, P. J. 1999. Decrease and Structural Modifications of Phosphatidylethanolamine Plasmalogen in the Brain with Alzheimer Disease. *J Neuropathol Exp Neurol,* 58**,** 740-7.

GUIJARRO, J. I., SUNDE, M., JONES, J. A., CAMPBELL, I. D. & DOBSON, C. M. 1998. Amyloid Fibril Formation by an Sh3 Domain. *Proc Natl Acad Sci U S A,* 95**,** 4224-8.

GUSTAFSSON, M., THYBERG, J., NASLUND, J., ELIASSON, E. & JOHANSSON, J. 1999. Amyloid Fibril Formation by Pulmonary Surfactant Protein C. *FEBS Lett,* 464**,** 138-42.

HAAN, J. & ROOS, R. A. C. 1992. Comparison between the Icelandic and Dutch Forms of Hereditary Cerebral Amyloid Angiopathy. *Clinical Neurology and Neurosurgery,* 94**,** S82-S83.

HAAN, J., MAAT-SCHIEMAN, M. L., VAN DUINEN, S. G., JENSSON, O., THORSTEINSSON, L. & ROOS, R. A. 1994. Co-Localization of Beta/A4 and Cystatin C in Cortical Blood Vessels in Dutch, but Not in Icelandic Hereditary Cerebral Hemorrhage with Amyloidosis. *Acta Neurol Scand,* 89**,** 367-71.

HAASS, C. & SELKOE, D. J. 2007. Soluble Protein Oligomers in Neurodegeneration: Lessons from the Alzheimer's Amyloid Beta-Peptide. *Nat Rev Mol Cell Biol,* 8**,** 101-12.

HABICHT, G., HAUPT, C., FRIEDRICH, R. P., HORTSCHANSKY, P., SACHSE, C., MEINHARDT, J., WIELIGMANN, K., GELLERMANN, G. P., BRODHUN, M., GOTZ, J., HALBHUBER, K. J., ROCKEN, C., HORN, U. & FANDRICH, M. 2007. Directed Selection of a Conformational Antibody Domain That Prevents Mature Amyloid Fibril Formation by Stabilizing Abeta Protofibrils. *Proc Natl Acad Sci U S A,* 104**,** 19232-7.

HAMILTON, J. A. & BENSON, M. D. 2001. Transthyretin: A Review from a Structural Perspective. *Cell Mol Life Sci,* 58**,** 1491-521.

HAMMARSTROM, P., JIANG, X., DEECHONGKIT, S. & KELLY, J. W. 2001. Anion Shielding of Electrostatic Repulsions in Transthyretin Modulates Stability and Amyloidosis: Insight into the Chaotrope Unfolding Dichotomy. *Biochemistry,* 40**,** 11453-9.

HAMMARSTROM, P., WISEMAN, R. L., POWERS, E. T. & KELLY, J. W. 2003. Prevention of Transthyretin Amyloid Disease by Changing Protein Misfolding Energetics. *Science,* 299**,** 713-6.

HAN, X. 2005. Lipid Alterations in the Earliest Clinically Recognizable Stage of Alzheimer's Disease: Implication of the Role of Lipids in the Pathogenesis of Alzheimer's Disease. *Curr Alzheimer Res,* 2**,** 65-77.

HANNUN, Y. A. & OBEID, L. M. 2008. Principles of Bioactive Lipid Signalling: Lessons from Sphingolipids. *Nat Rev Mol Cell Biol,* 9**,** 139-50.

HARDY, J. 1997. The Alzheimer Family of Diseases: Many Etiologies, One Pathogenesis? *Proc Natl Acad Sci U S A,* 94**,** 2095-7.

HARDY, J. 1999. The Shorter Amyloid Cascade Hypothesis. *Neurobiol Aging,* 20**,** 85; discussion 87.

HARIK, S. I., KALARIA, R. N., WHITNEY, P. M., ANDERSSON, L., LUNDAHL, P., LEDBETTER, S. R. & PERRY, G. 1990. Glucose Transporters Are Abundant in Cells with "Occluding" Junctions at the Blood-Eye Barriers. *Proc Natl Acad Sci U S A,* 87**,** 4261-4.

HARPER, J. D., LIEBER, C. M. & LANSBURY, P. T., JR. 1997. Atomic Force Microscopic Imaging of Seeded Fibril Formation and Fibril Branching by the Alzheimer's Disease Amyloid-Beta Protein. *Chem Biol,* 4**,** 951-9.

HASTINGS, G. A., COLEMAN, T. A., HAUDENSCHILD, C. C., STEFANSSON, S., SMITH, E. P., BARTHLOW, R., CHERRY, S., SANDKVIST, M. & LAWRENCE, D. A. 1997. Neuroserpin, a Brain-Associated Inhibitor of Tissue Plasminogen Activator Is Localized Primarily in Neurons. Implications for the Regulation of Motor Learning and Neuronal Survival. *J Biol Chem,* 272**,** 33062-7.

HE, X., HUANG, Y., LI, B., GONG, C. X. & SCHUCHMAN, E. H. 2010. Deregulation of Sphingolipid Metabolism in Alzheimer's Disease. *Neurobiol Aging,* 31**,** 398-408.

HEBDA, J. A. & MIRANKER, A. D. 2009. The Interplay of Catalysis and Toxicity by Amyloid Intermediates on Lipid Bilayers: Insights from Type Ii Diabetes. *Annu Rev Biophys,* 38**,** 125-52.

HELISALMI, S., VAKEVA, A., HILTUNEN, M. & SOININEN, H. 2009. Flanking Markers of Cystatin C (Cst3) Gene Do Not Show Association with Alzheimer's Disease. *Dement Geriatr Cogn Disord,* 27**,** 318-21.

HERBERT, J., WILCOX, J. N., PHAM, K. T., FREMEAU, R. T., JR., ZEVIANI, M., DWORK, A., SOPRANO, D. R., MAKOVER, A., GOODMAN, D. S., ZIMMERMAN, E. A. & ET AL. 1986. Transthyretin: A Choroid Plexus-Specific Transport Protein in Human Brain. The 1986 S. Weir Mitchell Award. *Neurology,* 36**,** 900-11.

HOCHWALD, G. M., PEPE, A. J. & THORBECKE, G. J. 1967. Trace Proteins in Biological Fluids. Iv. Physicochemical Properties and Sites of Formation of Gamma-Trace and Beta-Trace Proteins. *Proc Soc Exp Biol Med,* 124**,** 961-6.

HOLTON, J. L., LASHLEY, T., GHISO, J., BRAENDGAARD, H., VIDAL, R., GUERIN, C. J., GIBB, G., HANGER, D. P., ROSTAGNO, A., ANDERTON, B. H., STRAND, C., AYLING, H., PLANT, G., FRANGIONE, B., BOJSEN-MOLLER, M. & REVESZ, T. 2002. Familial Danish Dementia: A Novel Form of Cerebral Amyloidosis Associated with Deposition of Both Amyloid-Dan and Amyloid-Beta. *J Neuropathol Exp Neurol,* 61**,** 254-67.

HORNBERG, A., ENEQVIST, T., OLOFSSON, A., LUNDGREN, E. & SAUER-ERIKSSON, A. E. 2000. A Comparative Analysis of 23 Structures of the Amyloidogenic Protein Transthyretin. *J Mol Biol,* 302**,** 649-69.

HORTSCHANSKY, P., SCHROECKH, V., CHRISTOPEIT, T., ZANDOMENEGHI, G. & FANDRICH, M. 2005. The Aggregation Kinetics of Alzheimer's Beta-Amyloid Peptide Is Controlled by Stochastic Nucleation. *Protein Sci,* 14**,** 1753-9.

HORWICH, A. 2002. Protein Aggregation in Disease: A Role for Folding Intermediates Forming Specific Multimeric Interactions. *Journal of Clinical Investigation,* 110**,** 1221-1232.

HOSHINO, M., KATOU, H., HAGIHARA, Y., HASEGAWA, K., NAIKI, H. & GOTO, Y. 2002. Mapping the Core of the Beta(2)-Microglobulin Amyloid Fibril by H/D Exchange. *Nat Struct Biol,* 9**,** 332-6.

HOYER, S. 1998. Risk Factors for Alzheimer's Disease During Aging. Impacts of Glucose/Energy Metabolism. *J Neural Transm Suppl,* 54**,** 187-94.

HU, Y., FAN, C. P., FU, G., ZHU, D., JIN, Q. & WANG, D. C. 2008. Crystal Structure of a Glutamate/Aspartate Binding Protein Complexed with a Glutamate Molecule: Structural Basis of Ligand Specificity at Atomic Resolution. *J Mol Biol,* 382**,** 99-111.

HUA, Y., ZHAO, H., LU, X., KONG, Y. & JIN, H. 2012. Meta-Analysis of the Cystatin C(Cst3) Gene G73a Polymorphism and Susceptibility to Alzheimer's Disease. *Int J Neurosci,* 122**,** 431-8.

HUBBARD, S. J. 1998. The Structural Aspects of Limited Proteolysis of Native Proteins. *Biochim Biophys Acta,* 1382**,** 191-206.

HURLE, M. R., HELMS, L. R., LI, L., CHAN, W. & WETZEL, R. 1994. A Role for Destabilizing Amino Acid Replacements in Light-Chain Amyloidosis. *Proc Natl Acad Sci U S A,* 91**,** 5446-50.

HURSHMAN BABBES, A. R., POWERS, E. T. & KELLY, J. W. 2008. Quantification of the Thermodynamically Linked Quaternary and Tertiary Structural Stabilities of Transthyretin and Its Disease-Associated Variants: The Relationship between Stability and Amyloidosis. *Biochemistry,* 47**,** 6969-84.

HUTTER-PAIER, B., HUTTUNEN, H. J., PUGLIELLI, L., ECKMAN, C. B., KIM, D. Y., HOFMEISTER, A., MOIR, R. D., DOMNITZ, S. B., FROSCH, M. P., WINDISCH, M. & KOVACS, D. M. 2004. The Acat Inhibitor Cp-113,818 Markedly Reduces Amyloid Pathology in a Mouse Model of Alzheimer's Disease. *Neuron,* 44**,** 227-38.

IPPEL, J. H., OLOFSSON, A., SCHLEUCHER, J., LUNDGREN, E. & WIJMENGA, S. S. 2002. Probing Solvent Accessibility of Amyloid Fibrils by Solution Nmr Spectroscopy. *Proc Natl Acad Sci U S A,* 99**,** 8648-53.

IRVINE, G. B., EL-AGNAF, O. M., SHANKAR, G. M. & WALSH, D. M. 2008. Protein Aggregation in the Brain: The Molecular Basis for Alzheimer's and Parkinson's Diseases. *Molecular Medicine,* 14**,** 451-464.

ITOH, Y., YAMADA, M., HAYAKAWA, M., OTOMO, E. & MIYATAKE, T. 1993. Cerebral Amyloid Angiopathy: A Significant Cause of Cerebellar as Well as Lobar Cerebral Hemorrhage in the Elderly. *J Neurol Sci,* 116**,** 135-41.

IWATA, K., FUJIWARA, T., MATSUKI, Y., AKUTSU, H., TAKAHASHI, S., NAIKI, H. & GOTO, Y. 2006. 3d Structure of Amyloid Protofilaments of Beta(2)-Microglobulin Fragment Probed by Solid-State Nmr. *Proceedings of the National Academy of Sciences of the United States of America,* 103**,** 18119-18124.

JARRETT, J. T., BERGER, E. P. & LANSBURY, P. T., JR. 1993. The C-Terminus of the Beta Protein Is Critical in Amyloidogenesis. *Ann N Y Acad Sci,* 695**,** 144-8.

JARRETT, J. T. & LANSBURY JR., P. T. 1993. Seeding "One-Dimensional Crystallization" of Amyloid: A Pathogenic Mechanism in Alzheimer's Disease and Scrapie? *Cell,* 73**,** 1055-1058.

JARRETT, J. T. & LANSBURY, P. T., JR. 1993. Seeding "One-Dimensional Crystallization" of Amyloid: A Pathogenic Mechanism in Alzheimer's Disease and Scrapie? *Cell,* 73**,** 1055-8.

JESUS, C. S. H., VAZ, D. C., SARAIVA, M. J. M. & BRITO, R. M. M. 2012. The V30m Amyloidogenic Mutation Decreases the Rate of Refolding Kinetics of the Tetrameric Protein Transthyretin. *Spectroscopy: An International Journal,* 27**,** 6.

JIANG, X., BUXBAUM, J. N. & KELLY, J. W. 2001. The V122i Cardiomyopathy Variant of Transthyretin Increases the Velocity of Rate-Limiting Tetramer Dissociation, Resulting in Accelerated Amyloidosis. *Proc Natl Acad Sci U S A,* 98**,** 14943-8.

JIMENEZ, J. L., GUIJARRO, J. L., ORLOVA, E., ZURDO, J., DOBSON, C. M., SUNDE, M. & SAIBIL, H. R. 1999. Cryo-Electron Microscopy Structure of an Sh3 Amyloid Fibril and Model of the Molecular Packing. *Embo Journal,* 18**,** 815-821.

JIMENEZ, J. L., NETTLETON, E. J., BOUCHARD, M., ROBINSON, C. V., DOBSON, C. M. & SAIBIL, H. R. 2002. The Protofilament Structure of Insulin Amyloid Fibrils. *Proc Natl Acad Sci U S A,* 99**,** 9196-201.

KAD, N. M., THOMSON, N. H., SMITH, D. P., SMITH, D. A. & RADFORD, S. E. 2001. Beta(2)-Microglobulin and Its Deamidated Variant, N17d Form Amyloid Fibrils with a Range of Morphologies in Vitro. *J Mol Biol,* 313**,** 559-71.

KAESER, S. A., HERZIG, M. C., COOMARASWAMY, J., KILGER, E., SELENICA, M. L., WINKLER, D. T., STAUFENBIEL, M., LEVY, E., GRUBB, A. & JUCKER, M. 2007a. Cystatin C Modulates Cerebral Beta-Amyloidosis. *Nature Genetics,* 39**,** 1437-1439.

KAESER, S. A., HERZIG, M. C., COOMARASWAMY, J., KILGER, E., SELENICA, M. L., WINKLER, D. T., STAUFENBIEL, M., LEVY, E., GRUBB, A. & JUCKER, M. 2007b. Cystatin C Modulates Cerebral Beta-Amyloidosis. *Nat Genet,* 39**,** 1437-9.

KAUR, G., MOHAN, P., PAWLIK, M., DEROSA, S., FAJICULAY, J., CHE, S., GRUBB, A., GINSBERG, S. D., NIXON, R. A. & LEVY, E. 2010. Cystatin C Rescues Degenerating Neurons in a Cystatin

B-Knockout Mouse Model of Progressive Myoclonus Epilepsy. *Am J Pathol,* 177**,** 2256-67.

KAUR, G. & LEVY, E. 2012. Cystatin C in Alzheimer's Disease. *Front Mol Neurosci,* 5**,** 79.

KAYED, R., HEAD, E., THOMPSON, J. L., MCINTIRE, T. M., MILTON, S. C., COTMAN, C. W. & GLABE, C. G. 2003. Common Structure of Soluble Amyloid Oligomers Implies Common Mechanism of Pathogenesis. *Science,* 300**,** 486-9.

KEELEY, E. 2007. Folding, Dimerisation and the Interaction with Abeta 1-40 of Human Cystatin C*.* Doctor of Philosophy, University of Sheffield.

KELLY, J. W. 1998. The Alternative Conformations of Amyloidogenic Proteins and Their Multi-Step Assembly Pathways. *Curr Opin Struct Biol,* 8**,** 101-6.

KELLY, J. W. 2000. Mechanisms of Amyloidogenesis. *Nat Struct Biol,* 7**,** 824-6.

KESSELS, H. W., NGUYEN, L. N., NABAVI, S. & MALINOW, R. 2010. The Prion Protein as a Receptor for Amyloid-Beta. *Nature,* 466**,** E3-4; discussion E4-5.

KHETERPAL, I., ZHOU, S., COOK, K. D. & WETZEL, R. 2000. Abeta Amyloid Fibrils Possess a Core Structure Highly Resistant to Hydrogen Exchange. *Proc Natl Acad Sci U S A,* 97**,** 13597-601.

KHETERPAL, I., WILLIAMS, A., MURPHY, C., BLEDSOE, B. & WETZEL, R. 2001. Structural Features of the Abeta Amyloid Fibril Elucidated by Limited Proteolysis. *Biochemistry,* 40**,** 11757-67.

KHETERPAL, I., WETZEL, R. & COOK, K. D. 2003. Enhanced Correction Methods for Hydrogen Exchange-Mass Spectrometric Studies of Amyloid Fibrils. *Protein Sci,* 12**,** 635-43.

KHURANA, R., COLEMAN, C., IONESCU-ZANETTI, C., CARTER, S. A., KRISHNA, V., GROVER, R. K., ROY, R. & SINGH, S. 2005. Mechanism of Thioflavin T Binding to Amyloid Fibrils. *J Struct Biol,* 151**,** 229-38.

KIM, J., BASAK, J. M. & HOLTZMAN, D. M. 2009. The Role of Apolipoprotein E in Alzheimer's Disease. *Neuron,* 63**,** 287-303.

KIM, Y. S., CAPE, S. P., CHI, E., RAFFEN, R., WILKINS-STEVENS, P., STEVENS, F. J., MANNING, M. C., RANDOLPH, T. W., SOLOMON, A. & CARPENTER, J. F. 2001. Counteracting Effects of Renal Solutes on Amyloid Fibril Formation by Immunoglobulin Light Chains. *Journal of Biological Chemistry,* 276**,** 1626-1633.

KINGHORN, K. J., CROWTHER, D. C., SHARP, L. K., NERELIUS, C., DAVIS, R. L., CHANG, H. T., GREEN, C., GUBB, D. C., JOHANSSON, J. & LOMAS, D. A. 2006a. Neuroserpin Binds Abeta and Is a Neuroprotective Component of Amyloid Plaques in Alzheimer Disease. *J Biol Chem,* 281**,** 29268-77.

KINGHORN, K. J., CROWTHER, D. C., SHARP, L. K., NERELIUS, C., DAVIS, R. L., CHANG, H. T., GREEN, C., GUBB, D. C., JOHANSSON, J. & LOMAS, D. A. 2006b. Neuroserpin Binds a Beta and Is a Neuroprotective Component of Amyloid Plaques in Alzheimer Disease. *Journal of Biological Chemistry,* 281**,** 29268-29277.

KIVIPELTO, M., HELKALA, E. L., LAAKSO, M. P., HANNINEN, T., HALLIKAINEN, M., ALHAINEN, K., SOININEN, H., TUOMILEHTO, J. & NISSINEN, A. 2001. Midlife Vascular Risk Factors and Alzheimer's Disease in Later Life: Longitudinal, Population Based Study. *BMJ,* 322**,** 1447-51.

KLABUNDE, T., PETRASSI, H. M., OZA, V. B., RAMAN, P., KELLY, J. W. & SACCHETTINI, J. C. 2000. Rational Design of Potent Human Transthyretin Amyloid Disease Inhibitors. *Nat Struct Biol,* 7**,** 312-21.

KNIGHT, J. D. & MIRANKER, A. D. 2004. Phospholipid Catalysis of Diabetic Amyloid Assembly. *J Mol Biol,* 341**,** 1175-87.

KODALI, R. & WETZEL, R. 2007. Polymorphism in the Intermediates and Products of Amyloid Assembly. *Curr Opin Struct Biol,* 17**,** 48-57.

KOO, E. H., LANSBURY, P. T., JR. & KELLY, J. W. 1999. Amyloid Diseases: Abnormal Protein Aggregation in Neurodegeneration. *Proc Natl Acad Sci U S A,* 96**,** 9989-90.

KOWALEWSKI, T. & HOLTZMAN, D. M. 1999. In Situ Atomic Force Microscopy Study of Alzheimer's Beta-Amyloid Peptide on Different Substrates: New Insights into Mechanism of Beta-Sheet Formation. *Proc Natl Acad Sci U S A,* 96**,** 3688-93.

KREMER, J. J. & MURPHY, R. M. 2003. Kinetics of Adsorption of Beta-Amyloid Peptide Abeta(1-40) to Lipid Bilayers. *J Biochem Biophys Methods,* 57**,** 159-69.

KUMADA, T., HASEGAWA, A., IWASAKI, Y., BABA, H. & IKENAKA, K. 2004. Isolation of Cystatin C Via Functional Cloning of Astrocyte Differentiation Factors. *Dev Neurosci,* 26**,** 68-76.

KUMAR-SINGH, S., DE JONGHE, C., CRUTS, M., KLEINERT, R., WANG, R., MERCKEN, M., DE STROOPER, B., VANDERSTICHELE, H., LOFGREN, A., VANDERHOEVEN, I., BACKHOVENS, H., VANMECHELEN, E., KROISEL, P. M. & VAN BROECKHOVEN, C. 2000. Nonfibrillar Diffuse Amyloid Deposition Due to a Gamma(42)-Secretase Site Mutation Points to an Essential Role for N-Truncated a Beta(42) in Alzheimer's Disease. *Human Molecular Genetics,* 9**,** 2589-2598.

KUO, Y. M., KOKJOHN, T. A., KALBACK, W., LUEHRS, D., GALASKO, D. R., CHEVALLIER, N., KOO, E. H., EMMERLING, M. R. & ROHER, A. E. 2000a. Amyloid-Beta Peptides Interact with Plasma Proteins and Erythrocytes: Implications for Their Quantitation in Plasma. *Biochem Biophys Res Commun,* 268**,** 750-6.

KUO, Y. M., KOKJOHN, T. A., KALBACK, W., LUEHRS, D., GALASKO, D. R., CHEVALLIER, N., KOO, E. H., EMMERLING, M. R. & ROHER, A. E. 2000b. Amyloid-Beta Peptides Interact with Plasma Proteins and Erythrocytes: Implications for Their Quantitation in Plasma. *Biochemical and Biophysical Research Communications,* 268**,** 750-756.

KUPERSTEIN, I., BROERSEN, K., BENILOVA, I., ROZENSKI, J., JONCKHEERE, W., DEBULPAEP, M., VANDERSTEEN, A., SEGERS-NOLTEN, I., VAN DER WERF, K., SUBRAMANIAM, V., BRAEKEN, D., CALLEWAERT, G., BARTIC, C., D'HOOGE, R., MARTINS, I. C., ROUSSEAU, F., SCHYMKOWITZ, J. & DE STROOPER, B. 2010. Neurotoxicity of Alzheimer's Disease Abeta Peptides Is Induced by Small Changes in the Abeta42 to Abeta40 Ratio. *EMBO J,* 29**,** 3408-20.

LAMARK, T. & JOHANSEN, T. 2012. Aggrephagy: Selective Disposal of Protein Aggregates by Macroautophagy. *Int J Cell Biol,* 2012**,** 736905.

LAMBERT, M. P., BARLOW, A. K., CHROMY, B. A., EDWARDS, C., FREED, R., LIOSATOS, M., MORGAN, T. E., ROZOVSKY, I., TROMMER, B., VIOLA, K. L., WALS, P., ZHANG, C., FINCH, C. E., KRAFFT, G. A. & KLEIN, W. L. 1998. Diffusible, Nonfibrillar Ligands Derived from Abeta1-42 Are Potent Central Nervous System Neurotoxins. *Proc Natl Acad Sci U S A,* 95**,** 6448-53.

LANG, A. E. & LOZANO, A. M. 1998. Parkinson's Disease - First of Two Parts. *New England Journal of Medicine,* 339**,** 1044-1053.

LANSBURY, P. T. & LASHUEL, H. A. 2006. A Century-Old Debate on Protein Aggregation and Neurodegeneration Enters the Clinic. *Nature,* 443**,** 774-9.

LANSBURY, P. T., JR. 1999. Evolution of Amyloid: What Normal Protein Folding May Tell Us About Fibrillogenesis and Disease. *Proc Natl Acad Sci U S A,* 96**,** 3342-4.

LASHUEL, H. A., LAI, Z. & KELLY, J. W. 1998. Characterization of the Transthyretin Acid Denaturation Pathway: Implications for Amyloid Fibril Formation. *Abstracts of Papers American Chemical Society,* 216**,** 70-BIOL 70.

LASHUEL, H. A., HARTLEY, D., PETRE, B. M., WALZ, T. & LANSBURY, P. T., JR. 2002. Neurodegenerative Disease: Amyloid Pores from Pathogenic Mutations. *Nature,* 418**,** 291.

LAUREN, J., GIMBEL, D. A., NYGAARD, H. B., GILBERT, J. W. & STRITTMATTER, S. M. 2009. Cellular Prion Protein Mediates Impairment of Synaptic Plasticity by Amyloid-Beta Oligomers. *Nature,* 457**,** 1128-32.

LEDESMA, M. D., DA SILVA, J. S., CRASSAERTS, K., DELACOURTE, A., DE STROOPER, B. & DOTTI, C. G. 2000. Brain Plasmin Enhances App Alpha-Cleavage and Abeta Degradation and Is Reduced in Alzheimer's Disease Brains. *EMBO Rep,* 1**,** 530-5.

LEE, C. C., NAYAK, A., SETHURAMAN, A., BELFORT, G. & MCRAE, G. J. 2007. A Three-Stage Kinetic Model of Amyloid Fibrillation. *Biophys J,* 92**,** 3448-58.

LEE, C. F., BIRD, S., SHAW, M., JEAN, L. & VAUX, D. J. 2012. Combined Effects of Agitation, Macromolecular Crowding, and Interfaces on Amyloidogenesis. *J Biol Chem,* 287**,** 38006-19.

LEVINE, H., 3RD 1993. Thioflavine T Interaction with Synthetic Alzheimer's Disease Beta-Amyloid Peptides: Detection of Amyloid Aggregation in Solution. *Protein Sci,* 2**,** 404-10.

LEVY, E., SASTRE, M., KUMAR, A., GALLO, G., PICCARDO, P., GHETTI, B. & TAGLIAVINI, F. 2001. Codeposition of Cystatin C with Amyloid-Beta Protein in the Brain of Alzheimer Disease Patients. *J Neuropathol Exp Neurol,* 60**,** 94-104.

LI, X., MASLIAH, E., REIXACH, N. & BUXBAUM, J. N. 2011. Neuronal Production of Transthyretin in Human and Murine Alzheimer's Disease: Is It Protective? *J Neurosci,* 31**,** 12483-90.

LI, X., ZHANG, X., LADIWALA, A. R., DU, D., YADAV, J. K., TESSIER, P. M., WRIGHT, P. E., KELLY, J. W. & BUXBAUM, J. N. 2013a. Mechanisms of Transthyretin Inhibition of Beta-Amyloid Aggregation in Vitro. *J Neurosci,* 33**,** 19423-33.

LI, X. Y. & BUXBAUM, J. N. 2011. Transthyretin and the Brain Re-Visited: Is Neuronal Synthesis of Transthyretin Protective in Alzheimer's Disease? *Molecular Neurodegeneration,* 6.

LI, X. Y., ZHANG, X., LADIWALA, A. R. A., DU, D. G., YADAV, J. K., TESSIER, P. M., WRIGHT, P. E., KELLY, J. W. & BUXBAUM, J. N. 2013b. Mechanisms of Transthyretin Inhibition of Beta-Amyloid Aggregation in Vitro. *Journal of Neuroscience,* 33**,** 19423-19433.

LIN, H., BHATIA, R. & LAL, R. 2001. Amyloid Beta Protein Forms Ion Channels: Implications for Alzheimer's Disease Pathophysiology. *FASEB J,* 15**,** 2433-44.

LIN, M. S., CHIU, H. M., FAN, F. J., TSAI, H. T., WANG, S. S., CHANG, Y. & CHEN, W. Y. 2007. Kinetics and Enthalpy Measurements of Interaction between Beta-Amyloid and Liposomes by Surface Plasmon Resonance and Isothermal Titration Microcalorimetry. *Colloids Surf B Biointerfaces,* 58**,** 231-6.

LIN, M. S., CHEN, L. Y., TSAI, H. T., WANG, S. S., CHANG, Y., HIGUCHI, A. & CHEN, W. Y. 2008. Investigation of the Mechanism of Beta-Amyloid Fibril Formation by Kinetic and Thermodynamic Analyses. *Langmuir,* 24**,** 5802-8.

LINK, C. D. 1995. Expression of Human Beta-Amyloid Peptide in Transgenic Caenorhabditis Elegans. *Proc Natl Acad Sci U S A,* 92**,** 9368-72.

LIU, L., HOU, J., DU, J., CHUMANOV, R. S., XU, Q., GE, Y., JOHNSON, J. A. & MURPHY, R. M. 2009. Differential Modification of Cys10 Alters Transthyretin's Effect on Beta-Amyloid Aggregation and Toxicity. *Protein Eng Des Sel,* 22**,** 479-88.

LIU, R., BARKHORDARIAN, H., EMADI, S., PARK, C. B. & SIERKS, M. R. 2005. Trehalose Differentially Inhibits Aggregation and Neurotoxicity of Beta-Amyloid 40 and 42. *Neurobiology of Disease,* 20**,** 74-81.

LUKASIUK, K., PIRTTILA, T. J. & PITKANEN, A. 2002. Upregulation of Cystatin C Expression in the Rat Hippocampus During Epileptogenesis in the Amygdala Stimulation Model of Temporal Lobe Epilepsy. *Epilepsia,* 43 Suppl 5**,** 137-45.

MACKIC, J. B., STINS, M., MCCOMB, J. G., CALERO, M., GHISO, J., KIM, K. S., YAN, S. D., STERN, D., SCHMIDT, A. M., FRANGIONE, B. & ZLOKOVIC, B. V. 1998. Human Blood-Brain Barrier Receptors for Alzheimer's Amyloid-Beta 1- 40. Asymmetrical Binding, Endocytosis, and Transcytosis at the Apical Side of Brain Microvascular Endothelial Cell Monolayer. *J Clin Invest,* 102**,** 734-43.

MAKIN, O. S., ATKINS, E., SIKORSKI, P., JOHANSSON, J. & SERPELL, L. C. 2005. Molecular Basis for Amyloid Fibril Formation and Stability. *Proc Natl Acad Sci U S A,* 102**,** 315-20.

MAKIN, O. S. & SERPELL, L. C. 2005. Structures for Amyloid Fibrils. *FEBS J,* 272**,** 5950-61.

MARKESBERY, W. R. & CARNEY, J. M. 1999. Oxidative Alterations in Alzheimer's Disease. *Brain Pathol,* 9**,** 133-46.

MARUYAMA, H., IZUMI, Y., ODA, M., TORII, T., MORINO, H., TOJI, H., SASAKI, K., TERASAWA, H., NAKAMURA, S. & KAWAKAMI, H. 2001. Lack of an Association between Cystatin C Gene Polymorphisms in Japanese Patients with Alzheimer's Disease. *Neurology,* 57**,** 337-9.

MARUYAMA, K., IKEDA, S., ISHIHARA, T., ALLSOP, D. & YANAGISAWA, N. 1990. Immunohistochemical Characterization of Cerebrovascular Amyloid in 46 Autopsied Cases Using Antibodies to Beta Protein and Cystatin C. *Stroke,* 21**,** 397-403.

MARUYAMA, K., KAMETANI, F., IKEDA, S., ISHIHARA, T. & YANAGISAWA, N. 1992. Characterization of Amyloid Fibril Protein from a Case of Cerebral Amyloid Angiopathy Showing Immunohistochemical Reactivity for Both Beta Protein and Cystatin C. *Neurosci Lett,* 144**,** 38-42.

MASSI, F., PENG, J. W., LEE, J. P. & STRAUB, J. E. 2001. Simulation Study of the Structure and Dynamics of the Alzheimer's Amyloid Peptide Congener in Solution. *Biophys J,* 80**,** 31-44.

MCCUTCHEN, S. L., LAI, Z., MIROY, G. J., KELLY, J. W. & COLON, W. 1995. Comparison of Lethal and Nonlethal Transthyretin Variants and Their Relationship to Amyloid Disease. *Biochemistry,* 34**,** 13527-36.

MCDONALD, M., BOX, H., BIAN, W., KENDALL, A., TYCKO, R. & STUBBS, G. 2012. Fiber Diffraction Data Indicate a Hollow Core for the Alzheimer's Abeta 3-Fold Symmetric Fibril. *J Mol Biol,* 423**,** 454-61.

MCLAURIN, J., FRANKLIN, T., KUHNS, W. J. & FRASER, P. E. 1999. A Sulfated Proteoglycan Aggregation Factor Mediates Amyloid-Beta Peptide Fibril Formation and Neurotoxicity. *Amyloid,* 6**,** 233-43.

MEDINA, M. G., LEDESMA, M. D., DOMINGUEZ, J. E., MEDINA, M., ZAFRA, D., ALAMEDA, F., DOTTI, C. G. & NAVARRO, P. 2005. Tissue Plasminogen Activator Mediates Amyloid-Induced Neurotoxicity Via Erk1/2 Activation. *EMBO J,* 24**,** 1706-16.

MEISL, G., YANG, X., FROHM, B., KNOWLES, T. P. & LINSE, S. 2016. Quantitative Analysis of Intrinsic and Extrinsic Factors in the Aggregation Mechanism of Alzheimer-Associated Abeta-Peptide. *Sci Rep,* 6**,** 18728.

MELCHOR, J. P., PAWLAK, R. & STRICKLAND, S. 2003. The Tissue Plasminogen Activator-Plasminogen Proteolytic Cascade Accelerates Amyloid-Beta (Abeta) Degradation and Inhibits Abeta-Induced Neurodegeneration. *J Neurosci,* 23**,** 8867-71.

MI, W., PAWLIK, M., SASTRE, M., JUNG, S. S., RADVINSKY, D. S., KLEIN, A. M., SOMMER, J., SCHMIDT, S. D., NIXON, R. A., MATHEWS, P. M. & LEVY, E. 2007a. Cystatin C Inhibits Amyloid-Beta Deposition in Alzheimer's Disease Mouse Models. *Nat Genet,* 39**,** 1440-2.

MI, W., PAWLIK, M., SASTRE, M., JUNG, S. S., RADVINSKY, D. S., KLEIN, A. M., SOMMER, J., SCHMIDT, S. D., NIXON, R. A., MATHEWS, P. M. & LEVY, E. 2007b. Cystatin C Inhibits Amyloid-Beta Deposition in Alzheimer's Disease Mouse Models. *Nature Genetics,* 39**,** 1440-1442.

MIAKE, H., MIZUSAWA, H., IWATSUBO, T. & HASEGAWA, M. 2002. Biochemical Characterization of the Core Structure of Alpha-Synuclein Filaments. *J Biol Chem,* 277**,** 19213-9.

MILLER, S., JANIN, J., LESK, A. M. & CHOTHIA, C. 1987. Interior and Surface of Monomeric Proteins. *J Mol Biol,* 196**,** 641-56.

MILLER, S. R., SEKIJIMA, Y. & KELLY, J. W. 2004. Native State Stabilization by Nsaids Inhibits Transthyretin Amyloidogenesis from the Most Common Familial Disease Variants. *Lab Invest,* 84**,** 545-52.

MILOJEVIC, J., ESPOSITO, V., DAS, R. & MELACINI, G. 2007. Understanding the Molecular Basis for the Inhibition of the Alzheimer's Abeta-Peptide Oligomerization by Human Serum Albumin Using Saturation Transfer Difference and Off-Resonance Relaxation Nmr Spectroscopy. *J Am Chem Soc,* 129**,** 4282-90.

MILOJEVIC, J., RADITSIS, A. & MELACINI, G. 2009. Human Serum Albumin Inhibits Abeta Fibrillization through a "Monomer-Competitor" Mechanism. *Biophys J,* 97**,** 2585-94.

MILOJEVIC, J. & MELACINI, G. 2011. Stoichiometry and Affinity of the Human Serum Albumin-Alzheimer's Abeta Peptide Interactions. *Biophys J,* 100**,** 183-92.

MILOJEVIC, J., COSTA, M., ORTIZ, A. M., JORQUERA, J. I. & MELACINI, G. 2014. In Vitro Amyloid-Beta Binding and Inhibition of Amyloid-Beta Self-Association by Therapeutic Albumin. *J Alzheimers Dis,* 38**,** 753-65.

MIRANDA, E. & LOMAS, D. A. 2006. Neuroserpin: A Serpin to Think About. *Cell Mol Life Sci,* 63**,** 709-22.

MONACO, H. L. 2000. The Transthyretin-Retinol-Binding Protein Complex. *Biochimica Et Biophysica Acta-Protein Structure and Molecular Enzymology,* 1482**,** 65-72.

MOORADIAN, A. D., CHUNG, H. C. & SHAH, G. N. 1997. Glut-1 Expression in the Cerebra of Patients with Alzheimer's Disease. *Neurobiol Aging,* 18**,** 469-74.

MOORE, B. D., CHAKRABARTY, P., LEVITES, Y., KUKAR, T. L., BAINE, A. M., MORONI, T., LADD, T. B., DAS, P., DICKSON, D. W. & GOLDE, T. E. 2012. Overlapping Profiles of Abeta Peptides in the Alzheimer's Disease and Pathological Aging Brains. *Alzheimers Res Ther,* 4**,** 18.

MORGADO, I. & FANDRICH, M. 2011. Assembly of Alzheimer's a Beta Peptide into Nanostructured Amyloid Fibrils. *Current Opinion in Colloid & Interface Science,* 16**,** 508-514.

MORGAN, G. J., GIANNINI, S., HOUNSLOW, A. M., CRAVEN, C. J., ZEROVNIK, E., TURK, V., WALTHO, J. P. & STANIFORTH, R. A. 2008. Exclusion of the Native Alpha-Helix from the Amyloid Fibrils of a Mixed Alpha/Beta Protein. *J Mol Biol,* 375**,** 487-98.

MORINAGA, A., HASEGAWA, K., NOMURA, R., OOKOSHI, T., OZAWA, D., GOTO, Y., YAMADA, M. & NAIKI, H. 2010. Critical Role of Interfaces and Agitation on the Nucleation of Abeta Amyloid Fibrils at Low Concentrations of Abeta Monomers. *Biochim Biophys Acta,* 1804**,** 986-95.

MYERS, S. L., THOMSON, N. H., RADFORD, S. E. & ASHCROFT, A. E. 2006. Investigating the Structural Properties of Amyloid-Like Fibrils Formed in Vitro from Beta2-Microglobulin Using Limited Proteolysis and Electrospray Ionisation Mass Spectrometry. *Rapid Commun Mass Spectrom,* 20**,** 1628-36.

NAG, S., SARKAR, B., BANDYOPADHYAY, A., SAHOO, B., SREENIVASAN, V. K., KOMBRABAIL, M., MURALIDHARAN, C. & MAITI, S. 2011. Nature of the Amyloid-Beta Monomer and the Monomer-Oligomer Equilibrium. *J Biol Chem,* 286**,** 13827-33.

NAGAI, A., KOBAYASHI, S., SHIMODE, K., IMAOKA, K., UMEGAE, N., FUJIHARA, S. & NAKAMURA, M. 1998. No Mutations in Cystatin C Gene in Cerebral Amyloid Angiopathy with Cystatin C Deposition. *Mol Chem Neuropathol,* 33**,** 63-78.

NAIRISMAGI, J., GROHN, O. H., KETTUNEN, M. I., NISSINEN, J., KAUPPINEN, R. A. & PITKANEN, A. 2004. Progression of Brain Damage after Status Epilepticus and Its Association with Epileptogenesis: A Quantitative Mri Study in a Rat Model of Temporal Lobe Epilepsy. *Epilepsia,* 45**,** 1024-34.

NAITO, A. & KAWAMURA, I. 2007. Solid-State Nmr as a Method to Reveal Structure and Membrane-Interaction of Amyloidogenic Proteins and Peptides. *Biochimica Et Biophysica Acta-Biomembranes,* 1768**,** 1900-1912.

NAKAMURA, Y., TAKEDA, M., SUZUKI, H., HATTORI, H., TADA, K., HARIGUCHI, S., HASHIMOTO, S. & NISHIMURA, T. 1991. Abnormal Distribution of Cathepsins in the Brain of Patients with Alzheimer's Disease. *Neurosci Lett,* 130**,** 195-8.

NETTLETON, E. J., TITO, P., SUNDE, M., BOUCHARD, M., DOBSON, C. M. & ROBINSON, C. V. 2000. Characterization of the Oligomeric States of Insulin in Self-Assembly and Amyloid Fibril Formation by Mass Spectrometry. *Biophys J,* 79**,** 1053-65.

OHNISHI, S. & TAKANO, K. 2004. Amyloid Fibrils from the Viewpoint of Protein Folding. *Cell Mol Life Sci,* 61**,** 511-24.

OLAFSSON, I., GUDMUNDSSON, G., ABRAHAMSON, M., JENSSON, O. & GRUBB, A. 1990. The Amino Terminal Portion of Cerebrospinal-Fluid Cystatin-C in Hereditary Cystatin-C Amyloid Angiopathy Is Not Truncated - Direct Sequence-Analysis from Agarose-Gel

Electropherograms. *Scandinavian Journal of Clinical & Laboratory Investigation,* 50**,** 85-93.

OSTERWALDER, T., CONTARTESE, J., STOECKLI, E. T., KUHN, T. B. & SONDEREGGER, P. 1996. Neuroserpin, an Axonally Secreted Serine Protease Inhibitor. *EMBO J,* 15**,** 2944-53.

PALSDOTTIR, A., SNORRADOTTIR, A. O. & THORSTEINSSON, L. 2006. Hereditary Cystatin C Amyloid Angiopathy: Genetic, Clinical, and Pathological Aspects. *Brain pathology (Zurich, Switzerland),* 16**,** 55-9.

PAPASSOTIROPOULOS, A., LUTJOHANN, D., BAGLI, M., LOCATELLI, S., JESSEN, F., RAO, M. L., MAIER, W., BJORKHEM, I., VON BERGMANN, K. & HEUN, R. 2000. Plasma 24s-Hydroxycholesterol: A Peripheral Indicator of Neuronal Degeneration and Potential State Marker for Alzheimer's Disease. *Neuroreport,* 11**,** 1959-62.

PARENT, J. M., YU, T. W., LEIBOWITZ, R. T., GESCHWIND, D. H., SLOVITER, R. S. & LOWENSTEIN, D. H. 1997. Dentate Granule Cell Neurogenesis Is Increased by Seizures and Contributes to Aberrant Network Reorganization in the Adult Rat Hippocampus. *J Neurosci,* 17**,** 3727-38.

PARFITT, M., CROOK, R., ROQUES, P., ROSSOR, M. & CHARTIER-HARLIN, M. C. 1993. The Cystatin-C Gene Is Not Linked to Early Onset Familial Alzheimer's Disease. *Neurosci Lett,* 154**,** 81-3.

PENG, L., MINBO, H., FANG, C., XI, L. & CHAOCAN, Z. 2008. The Interaction between Cholesterol and Human Serum Albumin. *Protein Pept Lett,* 15**,** 360-4.

PERANI, D. 1999. The Role of Emission Tomography in Dementia. *Ital J Neurol Sci,* 20**,** S254-7.

PERUTZ, M. F. 1999. Glutamine Repeats and Neurodegenerative Diseases: Molecular Aspects. *Trends in Biochemical Sciences,* 24**,** 58-63.

PERVUSHIN, K., RIEK, R., WIDER, G. & WUTHRICH, K. 1997. Attenuated T2 Relaxation by Mutual Cancellation of Dipole-Dipole Coupling and Chemical Shift Anisotropy Indicates an Avenue to Nmr Structures of Very Large Biological Macromolecules in Solution. *Proc Natl Acad Sci U S A,* 94**,** 12366-71.

PETERSON, S. A., KLABUNDE, T., LASHUEL, H. A., PURKEY, H., SACCHETTINI, J. C. & KELLY, J. W. 1998. Inhibiting Transthyretin Conformational Changes That Lead to Amyloid Fibril Formation. *Proc Natl Acad Sci U S A,* 95**,** 12956-60.

PETKOVA, A. T., ISHII, Y., BALBACH, J. J., ANTZUTKIN, O. N., LEAPMAN, R. D., DELAGLIO, F. & TYCKO, R. 2002a. A Structural Model for Alzheimer's Beta-Amyloid Fibrils Based on Experimental Constraints from Solid State Nmr. *Proceedings of the National Academy of Sciences of the United States of America,* 99**,** 16742-16747.

PETKOVA, A. T., ISHII, Y., BALBACH, J. J., ANTZUTKIN, O. N., LEAPMAN, R. D., DELAGLIO, F. & TYCKO, R. 2002b. A Structural Model for Alzheimer's Beta -Amyloid Fibrils Based on Experimental Constraints from Solid State Nmr. *Proc Natl Acad Sci U S A,* 99**,** 16742-7.

PFRIEGER, F. W. 2003. Cholesterol Homeostasis and Function in Neurons of the Central Nervous System. *Cell Mol Life Sci,* 60**,** 1158-71.

PIRTTILA, T. J. & PITKANEN, A. 2006. Cystatin C Expression Is Increased in the Hippocampus Following Photothrombotic Stroke in Rat. *Neurosci Lett,* 395**,** 108-13.

POLVERINO DE LAURETO, P., TADDEI, N., FRARE, E., CAPANNI, C., COSTANTINI, S., ZURDO, J., CHITI, F., DOBSON, C. M. & FONTANA, A. 2003a. Protein Aggregation and Amyloid Fibril Formation by an Sh3 Domain Probed by Limited Proteolysis. *Journal of Molecular Biology,* 334**,** 129-141.

POLVERINO DE LAURETO, P., TADDEI, N., FRARE, E., CAPANNI, C., COSTANTINI, S., ZURDO, J., CHITI, F., DOBSON, C. M. & FONTANA, A. 2003b. Protein Aggregation and Amyloid Fibril Formation by an Sh3 Domain Probed by Limited Proteolysis. *J Mol Biol,* 334**,** 129-41.

POSSE DE CHAVES, E. & SIPIONE, S. 2010. Sphingolipids and Gangliosides of the Nervous System in Membrane Function and Dysfunction. *FEBS Lett,* 584**,** 1748-59.

PRINCE, M. J., WU, F., GUO, Y. F., ROBLEDO, L. M. G., O'DONNELL, M., SULLIVAN, R. & YUSUF, S. 2015. The Burden of Disease in Older People and Implications for Health Policy and Practice. *Lancet,* 385**,** 549-562.

PRUSINER, S. B. 1982. Novel Proteinaceous Infectious Particles Cause Scrapie. *Science,* 216**,** 136-44.

PRUSINER, S. B. 1998. Prions. *Proceedings of the National Academy of Sciences of the United States of America,* 95**,** 13363-13383.

PUGLIELLI, L. & KOVACS, D. M. 2001. Alzheimer Disease: 100 Years Later. *Rev Med Chil,* 129**,** 569-75.

PUGLIELLI, L., TANZI, R. E. & KOVACS, D. M. 2003. Alzheimer's Disease: The Cholesterol Connection. *Nat Neurosci,* 6**,** 345-51.

RAFFA, D. F. & RAUK, A. 2007. Molecular Dynamics Study of the Beta Amyloid Peptide of Alzheimer's Disease and Its Divalent Copper Complexes. *J Phys Chem B,* 111**,** 3789-99.

RAGHU, P. & SIVAKUMAR, B. 2004. Interactions Amongst Plasma Retinol-Binding Protein, Transthyretin and Their Ligands: Implications in Vitamin a Homeostasis and Transthyretin Amyloidosis. *Biochimica Et Biophysica Acta-Proteins and Proteomics,* 1703**,** 1-9.

RASCHKE, T. M. & MARQUSEE, S. 1998. Hydrogen Exchange Studies of Protein Structure. *Curr Opin Biotechnol,* 9**,** 80-6.

REFOLO, L. M., PAPPOLLA, M. A., LAFRANCOIS, J., MALESTER, B., SCHMIDT, S. D., THOMAS-BRYANT, T., TINT, G. S., WANG, R., MERCKEN, M., PETANCESKA, S. S. & DUFF, K. E. 2001. A Cholesterol-Lowering Drug Reduces Beta-Amyloid Pathology in a Transgenic Mouse Model of Alzheimer's Disease. *Neurobiol Dis,* 8**,** 890-9.

REIXACH, N., DEECHONGKIT, S., JIANG, X., KELLY, J. W. & BUXBAUM, J. N. 2004. Tissue Damage in the Amyloidoses: Transthyretin Monomers and Nonnative Oligomers Are the Major Cytotoxic Species in Tissue Culture. *Proc Natl Acad Sci U S A,* 101**,** 2817-22.

REVESZ, T., GHISO, J., LASHLEY, T., PLANT, G., ROSTAGNO, A., FRANGIONE, B. & HOLTON, J. L. 2003. Cerebral Amyloid Angiopathies: A Pathologic, Biochemical, and Genetic View. *J Neuropathol Exp Neurol,* 62**,** 885-98.

RICHARDSON, S. J. 2007a. Cell and Molecular Biology of Transthyretin and Thyroid Hormones. *Int Rev Cytol,* 258**,** 137-93.

RICHARDSON, S. J. 2007b. Cell and Molecular Biology of Transthyretin and Thyroid Hormones. *In:* JEON, K. W. (ed.) *International Review of Cytology - a Survey of Cell Biology, Vol 258.*

RITTER, C., MADDELEIN, M. L., SIEMER, A. B., LUHRS, T., ERNST, M., MEIER, B. H., SAUPE, S. J. & RIEK, R. 2005. Correlation of Structural Elements and Infectivity of the Het-S Prion. *Nature,* 435**,** 844-8.

ROCHA, S., KRASTEV, R., THUNEMANN, A. F., PEREIRA, M. C., MOHWALD, H. & BREZESINSKI, G. 2005. Adsorption of Amyloid Beta-Peptide at Polymer Surfaces: A Neutron Reflectivity Study. *Chemphyschem,* 6**,** 2527-34.

ROCHA, S., LOUREIRO, J. A., BREZESINSKI, G. & PEREIRA MDO, C. 2012. Peptide-Surfactant Interactions: Consequences for the Amyloid-Beta Structure. *Biochem Biophys Res Commun,* 420**,** 136-40.

ROKS, G., CRUTS, M., SLOOTER, A. J., DERMAUT, B., HOFMAN, A., VAN BROECKHOVEN, C. & VAN DUIJN, C. M. 2001. The Cystatin C Polymorphism Is Not Associated with Early Onset Alzheimer's Disease. *Neurology,* 57**,** 366-7.

ROZGA, M., KLONIECKI, M., JABLONOWSKA, A., DADLEZ, M. & BAL, W. 2007. The Binding Constant for Amyloid Abeta40 Peptide Interaction with Human Serum Albumin. *Biochem Biophys Res Commun,* 364**,** 714-8.

SAITOH, E., SABATINI, L. M., EDDY, R. L., SHOWS, T. B., AZEN, E. A., ISEMURA, S. & SANADA, K. 1989. The Human Cystatin C Gene (Cst3) Is a Member of the Cystatin Gene Family Which Is Localized on Chromosome 20. *Biochem Biophys Res Commun,* 162**,** 1324-31.

SAMBROOK, J., FRITSCH, E. F. & MANIATIS, T. 1989. *Molecular Cloning: A Laboratory Manual*, Cold Spring Harbour Laboratory Press.

SANCHEZ-RUIZ, J. M. 2010. Protein Kinetic Stability. *Biophys Chem,* 148**,** 1-15.

SANCHEZ, L., MADURGA, S., PUKALA, T., VILASECA, M., LOPEZ-IGLESIAS, C., ROBINSON, C. V., GIRALT, E. & CARULLA, N. 2011. Abeta40 and Abeta42 Amyloid Fibrils Exhibit Distinct Molecular Recycling Properties. *J Am Chem Soc,* 133**,** 6505-8.

SANDBERG, A., LUHESHI, L. M., SOLLVANDER, S., PEREIRA DE BARROS, T., MACAO, B., KNOWLES, T. P., BIVERSTAL, H., LENDEL, C., EKHOLM-PETTERSON, F., DUBNOVITSKY, A., LANNFELT, L., DOBSON, C. M. & HARD, T. 2010. Stabilization of Neurotoxic Alzheimer Amyloid-Beta Oligomers by Protein Engineering. *Proc Natl Acad Sci U S A,* 107**,** 15595-600.

SANDERS, H. M., LUST, R. & TELLER, J. K. 2009. Amyloid-Beta Peptide a Beta P3-42 Affects Early Aggregation of Full-Length a Beta 1-42. *Peptides,* 30**,** 849-854.

SANDWALL, E., O'CALLAGHAN, P., ZHANG, X., LINDAHL, U., LANNFELT, L. & LI, J. P. 2010. Heparan Sulfate Mediates Amyloid-Beta Internalization and Cytotoxicity. *Glycobiology,* 20**,** 533-41.

SANI, M. A., GEHMAN, J. D. & SEPAROVIC, F. 2011. Lipid Matrix Plays a Role in Abeta Fibril Kinetics and Morphology. *FEBS Lett,* 585**,** 749-54.

SARAIVA, A. M., PEREIRA, M. C. & BREZESINSKI, G. 2010. Is the Viscoelasticity of Alzheimer's Abeta42 Peptide Oligomers a General Property of Protein Oligomers Related to Their Toxicity? *Langmuir,* 26**,** 12060-7.

SARAIVA, M. J., BIRKEN, S., COSTA, P. P. & GOODMAN, D. S. 1984. Family Studies of the Genetic Abnormality in Transthyretin (Prealbumin) in Portuguese Patients with Familial Amyloidotic Polyneuropathy. *Ann N Y Acad Sci,* 435**,** 86-100.

SASTRE, M., CALERO, M., PAWLIK, M., MATHEWS, P. M., KUMAR, A., DANILOV, V., SCHMIDT, S. D., NIXON, R. A., FRANGIONE, B. & LEVY, E. 2004a. Binding of Cystatin C to Alzheimer's Amyloid Beta Inhibits in Vitro Amyloid Fibril Formation. *Neurobiology of Aging,* 25**,** 1033-1043.

SASTRE, M., CALERO, M., PAWLIK, M., MATHEWS, P. M., KUMAR, A., DANILOV, V., SCHMIDT, S. D., NIXON, R. A., FRANGIONE, B. & LEVY, E. 2004b. Binding of Cystatin C to Alzheimer's Amyloid Beta Inhibits in Vitro Amyloid Fibril Formation. *Neurobiol Aging,* 25**,** 1033-43.

SAWAMURA, N., KO, M., YU, W., ZOU, K., HANADA, K., SUZUKI, T., GONG, J. S., YANAGISAWA, K. & MICHIKAWA, M. 2004. Modulation of Amyloid Precursor Protein Cleavage by Cellular Sphingolipids. *J Biol Chem,* 279**,** 11984-91.

SCHEIDT, H. A., MORGADO, I., ROTHEMUND, S., HUSTER, D. & FANDRICH, M. 2011. Solid-State Nmr Spectroscopic Investigation of Abeta Protofibrils: Implication of a Beta-Sheet Remodeling Upon Maturation into Terminal Amyloid Fibrils. *Angew Chem Int Ed Engl,* 50**,** 2837-40.

SCHEUNER, D., ECKMAN, C., JENSEN, M., SONG, X., CITRON, M., SUZUKI, N., BIRD, T. D., HARDY, J., HUTTON, M., KUKULL, W., LARSON, E., LEVYLAHAD, E., VIITANEN, M., PESKIND, E., POORKAJ, P., SCHELLENBERG, G., TANZI, R., WASCO, W., LANNFELT, L., SELKOE, D. & YOUNKIN, S. 1996. Secreted Amyloid Beta-Protein Similar to That in the Senile Plaques of Alzheimer's Disease Is Increased in Vivo by the Presenilin 1 and 2 and App Mutations Linked to Familial Alzheimer's Disease. *Nature Medicine,* 2**,** 864-870.

SCHMIDT, M., ROHOU, A., LASKER, K., YADAV, J. K., SCHIENE-FISCHER, C., FANDRICH, M. & GRIGORIEFF, N. 2015. Peptide Dimer Structure in an Abeta(1-42) Fibril Visualized with Cryo-Em. *Proc Natl Acad Sci U S A,* 112**,** 11858-63.

SCHOLEFIELD, Z., YATES, E. A., WAYNE, G., AMOUR, A., MCDOWELL, W. & TURNBULL, J. E. 2003. Heparan Sulfate Regulates Amyloid Precursor Protein Processing by Bace1, the Alzheimer's Beta-Secretase. *J Cell Biol,* 163**,** 97-107.

SCHOLTZ, J. M. & ROBERTSON, A. D. 1995. Hydrogen Exchange Techniques. *Methods Mol Biol,* 40**,** 291-311.

SCHWARZMAN, A. L., GREGORI, L., VITEK, M. P., LYUBSKI, S., STRITTMATTER, W. J., ENGHILDE, J. J., BHASIN, R., SILVERMAN, J., WEISGRABER, K. H., COYLE, P. K. & ET AL. 1994. Transthyretin Sequesters Amyloid Beta Protein and Prevents Amyloid Formation. *Proc Natl Acad Sci U S A,* 91**,** 8368-72.

SEKIJIMA, Y., TOKUDA, T., KAMETANI, F., TANAKA, K., MARUYAMA, K. & IKEDA, S. 2001. Serum Transthyretin Monomer in Patients with Familial Amyloid Polyneuropathy. *Amyloid,* 8**,** 257-62.

SEKIJIMA, Y., HAMMARSTROM, P., MATSUMURA, M., SHIMIZU, Y., IWATA, M., TOKUDA, T., IKEDA, S. & KELLY, J. W. 2003. Energetic Characteristics of the New Transthyretin Variant A25t May Explain Its Atypical Central Nervous System Pathology. *Lab Invest,* 83**,** 409-17.

SELENICA, M. L., WANG, X., OSTERGAARD-PEDERSEN, L., WESTLIND-DANIELSSON, A. & GRUBB, A. 2007a. Cystatin C Reduces the in Vitro Formation of Soluble a Beta 1-42 Oligomers and Protofibrils. *Scandinavian Journal of Clinical & Laboratory Investigation,* 67**,** 179-190.

SELENICA, M. L., WANG, X., OSTERGAARD-PEDERSEN, L., WESTLIND-DANIELSSON, A. & GRUBB, A. 2007b. Cystatin C Reduces the in Vitro Formation of Soluble Abeta1-42 Oligomers and Protofibrils. *Scand J Clin Lab Invest,* 67**,** 179-90.

SELKOE, D. J. 2001. Clearing the Brain's Amyloid Cobwebs. *Neuron,* 32**,** 177-80.

SELKOE, D. J. & SCHENK, D. 2003a. Alzheimer's Disease: Molecular Understanding Predicts Amyloid-Based Therapeutics. *Annual Review of Pharmacology and Toxicology,* 43**,** 545-584.

SELKOE, D. J. & SCHENK, D. 2003b. Alzheimer's Disease: Molecular Understanding Predicts Amyloid-Based Therapeutics. *Annu Rev Pharmacol Toxicol,* 43**,** 545-84.

SERIO, T. R., CASHIKAR, A. G., KOWAL, A. S., SAWICKI, G. J., MOSLEHI, J. J., SERPELL, L., ARNSDORF, M. F. & LINDQUIST, S. L. 2000. Nucleated Conformational Conversion and the Replication of Conformational Information by a Prion Determinant. *Science,* 289**,** 1317-21.

SERPELL, L. C., SUNDE, M., FRASER, P. E., LUTHER, P. K., MORRIS, E. P., SANGREN, O., LUNDGREN, E. & BLAKE, C. C. 1995. Examination of the Structure of the Transthyretin Amyloid Fibril by Image Reconstruction from Electron Micrographs. *J Mol Biol,* 254**,** 113-8.

SERPELL, L. C. 2000. Alzheimer's Amyloid Fibrils: Structure and Assembly. *Biochimica Et Biophysica Acta-Molecular Basis of Disease,* 1502**,** 16-30.

SERPELL, L. C. & SMITH, J. M. 2000a. Direct Visualisation of the Beta-Sheet Structure of Synthetic Alzheimer's Amyloid. *J Mol Biol,* 299**,** 225-31.

SERPELL, L. C. & SMITH, J. M. 2000b. Direct Visualisation of the Beta-Sheet Structure of Synthetic Alzheimer's Amyloid. *Journal of Molecular Biology,* 299**,** 225-231.

SERPELL, L. C., SUNDE, M., BENSON, M. D., TENNENT, G. A., PEPYS, M. B. & FRASER, P. E. 2000. The Protofilament Substructure of Amyloid Fibrils. *J Mol Biol,* 300**,** 1033-9.

SHAI, Y. 1999. Mechanism of the Binding, Insertion and Destabilization of Phospholipid Bilayer Membranes by Alpha-Helical Antimicrobial and Cell Non-Selective Membrane-Lytic Peptides. *Biochim Biophys Acta,* 1462**,** 55-70.

SHEN, L., ADACHI, T., VANDEN BOUT, D. & ZHU, X. Y. 2012. A Mobile Precursor Determines Amyloid-Beta Peptide Fibril Formation at Interfaces. *J Am Chem Soc,* 134**,** 14172-8.

SHIE, F. S., JIN, L. W., COOK, D. G., LEVERENZ, J. B. & LEBOEUF, R. C. 2002. Diet-Induced Hypercholesterolemia Enhances Brain a Beta Accumulation in Transgenic Mice. *Neuroreport,* 13**,** 455-9.

SHIRAHAMA, T. & COHEN, A. S. 1967. Reconstitution of Amyloid Fibrils from Alkaline Extracts. *J Cell Biol,* 35**,** 459-64.

SINGER, M. A. & LINDQUIST, S. 1998. Multiple Effects of Trehalose on Protein Folding in Vitro and in Vivo. *Molecular Cell,* 1**,** 639-648.

SIPE, J. D. & COHEN, A. S. 2000. Review: History of the Amyloid Fibril. *Journal of Structural Biology,* 130**,** 88-98.

SIPE, J. D., BENSON, M. D., BUXBAUM, J. N., IKEDA, S., MERLINI, G., SARAIVA, M. J. M. & WESTERMARK, P. 2014. Nomenclature 2014: Amyloid Fibril Proteins and Clinical Classification of the Amyloidosis. *Amyloid-Journal of Protein Folding Disorders,* 21**,** 221-224.

SISODIA, S. S., ANNAERT, W., KIM, S. H. & DE STROOPER, B. 2001. Gamma-Secretase: Never More Enigmatic. *Trends Neurosci,* 24**,** S2-6.

SKERGET, K., TALER-VERCIC, A., BAVDEK, A., HODNIK, V., CERU, S., TUSEK-ZNIDARIC, M., KUMM, T., PITSI, D., POMPE-NOVAK, M., PALUMAA, P., SORIANO, S., KOPITAR-JERALA, N., TURK, V., ANDERLUH, G. & ZEROVNIK, E. 2010a. Interaction between Oligomers of Stefin B and Amyloid-Beta in Vitro and in Cells. *Journal of Biological Chemistry,* 285**,** 3201-3210.

SKERGET, K., TALER-VERCIC, A., BAVDEK, A., HODNIK, V., CERU, S., TUSEK-ZNIDARIC, M., KUMM, T., PITSI, D., POMPE-NOVAK, M., PALUMAA, P., SORIANO, S., KOPITAR-JERALA, N., TURK, V., ANDERLUH, G. & ZEROVNIK, E. 2010b. Interaction between Oligomers of Stefin B and Amyloid-Beta in Vitro and in Cells. *J Biol Chem,* 285**,** 3201-10.

SMALL, D. H., MOK, S. S. & BORNSTEIN, J. C. 2001. Alzheimer's Disease and Ap Toxicity: From Top to Bottom. *Nature Reviews Neuroscience,* 2**,** 595-598.

SNOW, A. D., MAR, H., NOCHLIN, D., SEKIGUCHI, R. T., KIMATA, K., KOIKE, Y. & WIGHT, T. N. 1990. Early Accumulation of Heparan Sulfate in Neurons and in the Beta-Amyloid Protein-Containing Lesions of Alzheimer's Disease and Down's Syndrome. *Am J Pathol,* 137**,** 1253-70.

SOUSA, M. M., CARDOSO, I., FERNANDES, R., GUIMARAES, A. & SARAIVA, M. J. 2001. Deposition of Transthyretin in Early Stages of Familial Amyloidotic Polyneuropathy: Evidence for Toxicity of Nonfibrillar Aggregates. *Am J Pathol,* 159**,** 1993-2000.

SPARKS, D. L., SABBAGH, M. N., CONNOR, D. J., LOPEZ, J., LAUNER, L. J., BROWNE, P., WASSER, D., JOHNSON-TRAVER, S., LOCHHEAD, J. & ZIOLWOLSKI, C. 2005. Atorvastatin for the Treatment of Mild to Moderate Alzheimer Disease: Preliminary Results. *Arch Neurol,* 62**,** 753-7.

STANYON, H. F. & VILES, J. H. 2012a. Human Serum Albumin Can Regulate Amyloid-Beta Peptide Fiber Growth in the Brain Interstitium: Implications for Alzheimer Disease. *J Biol Chem,* 287**,** 28163-8.

STANYON, H. F. & VILES, J. H. 2012b. Human Serum Albumin Can Regulate Amyloid-Beta Peptide Fiber Growth in the Brain Interstitium Implications for Alzheimer Disease. *Journal of Biological Chemistry,* 287**,** 28163-28168.

STEIN, T. D. & JOHNSON, J. A. 2002. Lack of Neurodegeneration in Transgenic Mice Overexpressing Mutant Amyloid Precursor Protein Is Associated with Increased Levels of Transthyretin and the Activation of Cell Survival Pathways. *J Neurosci,* 22**,** 7380-8.

STEIN, T. D., ANDERS, N. J., DECARLI, C., CHAN, S. L., MATTSON, M. P. & JOHNSON, J. A. 2004. Neutralization of Transthyretin Reverses the Neuroprotective Effects of Secreted Amyloid Precursor Protein (App) in Appsw Mice Resulting in Tau Phosphorylation and Loss of Hippocampal Neurons: Support for the Amyloid Hypothesis. *J Neurosci,* 24**,** 7707-17.

STEINHOFF, T., MORITZ, E., WOLLMER, M. A., MOHAJERI, M. H., KINS, S. & NITSCH, R. M. 2001. Increased Cystatin C in Astrocytes of Transgenic Mice Expressing the K670n-M671l Mutation of the Amyloid Precursor Protein and Deposition in Brain Amyloid Plaques. *Neurobiology of Disease,* 8**,** 647-654.

STEVENS, R. W., ELMENDORF, D., GOURLAY, M., STROEBEL, E. & GAAFAR, H. A. 1979. Application of Fluoroimmunoassay to Cerebrospinal Fluid Immunoglobulin G and Albumin. *J Clin Microbiol,* 10**,** 346-50.

STOPPINI, M. & BELLOTTI, V. 2015. Systemic Amyloidosis: Lessons from Beta2-Microglobulin. *J Biol Chem,* 290**,** 9951-8.

STOREY, E. & CAPPAI, R. 1999. The Amyloid Precursor Protein of Alzheimer's Disease and the Abeta Peptide. *Neuropathol Appl Neurobiol,* 25**,** 81-97.

STUBBS, G. 1999. Developments in Fiber Diffraction. *Curr Opin Struct Biol,* 9**,** 615-9.

SUN, B., ZHOU, Y., HALABISKY, B., LO, I., CHO, S. H., MUELLER-STEINER, S., DEVIDZE, N., WANG, X., GRUBB, A. & GAN, L. 2008. Cystatin C-Cathepsin B Axis Regulates Amyloid Beta Levels and Associated Neuronal Deficits in an Animal Model of Alzheimer's Disease. *Neuron,* 60**,** 247-57.

SUN, Q. 1989. Growth Stimulation of 3t3 Fibroblasts by Cystatin. *Exp Cell Res,* 180**,** 150-60.

SUN, Y. J., ROSE, J., WANG, B. C. & HSIAO, C. D. 1998. The Structure of Glutamine-Binding Protein Complexed with Glutamine at 1.94 a Resolution: Comparisons with Other Amino Acid Binding Proteins. *J Mol Biol,* 278**,** 219-29.

SUNDE, M., SERPELL, L. C., BARTLAM, M., FRASER, P. E., PEPYS, M. B. & BLAKE, C. C. 1997. Common Core Structure of Amyloid Fibrils by Synchrotron X-Ray Diffraction. *J Mol Biol,* 273**,** 729-39.

TANAKA, M., MACHIDA, Y., NIU, S. Y., IKEDA, T., JANA, N. R., DOI, H., KUROSAWA, M., NEKOOKI, M. & NUKINA, N. 2004. Trehalose Alleviates Polyglutamine-Mediated Pathology in a Mouse Model of Huntington Disease. *Nature Medicine,* 10**,** 148-154.

TANAKA, M., MACHIDA, Y. & NUKINA, N. 2005. A Novel Therapeutic Strategy for Polyglutamine Diseases by Stabilizing Aggregation-Prone Proteins with Small Molecules. *Journal of Molecular Medicine-Jmm,* 83**,** 343-352.

TAVERA, C., LEUNG-TACK, J., PREVOT, D., GENSAC, M. C., MARTINEZ, J., FULCRAND, P. & COLLE, A. 1992. Cystatin C Secretion by Rat Glomerular Mesangial Cells: Autocrine Loop for in Vitro Growth-Promoting Activity. *Biochem Biophys Res Commun,* 182**,** 1082-8.

THOMAS, P. J., QU, B. H. & PEDERSEN, P. L. 1995. Defective Protein Folding as a Basis of Human Disease. *Trends Biochem Sci,* 20**,** 456-9.

TIZON, B., RIBE, E. M., MI, W., TROY, C. M. & LEVY, E. 2010a. Cystatin C Protects Neuronal Cells from Amyloid-Beta-Induced Toxicity. *Journal of Alzheimers Disease,* 19**,** 885-894.

TIZON, B., RIBE, E. M., MI, W., TROY, C. M. & LEVY, E. 2010b. Cystatin C Protects Neuronal Cells from Amyloid-Beta-Induced Toxicity. *J Alzheimers Dis,* 19**,** 885-94.

TIZON, B., SAHOO, S., YU, H., GAUTHIER, S., KUMAR, A. R., MOHAN, P., FIGLIOLA, M., PAWLIK, M., GRUBB, A., UCHIYAMA, Y., BANDYOPADHYAY, U., CUERVO, A. M., NIXON, R. A. & LEVY, E. 2010c. Induction of Autophagy by Cystatin C: A Mechanism That Protects Murine Primary Cortical Neurons and Neuronal Cell Lines. *PLoS One,* 5**,** e9819.

TU, G. F., ALDRED, A. R., SOUTHWELL, B. R. & SCHREIBER, G. 1992. Strong Conservation of the Expression of Cystatin C Gene in Choroid Plexus. *Am J Physiol,* 263**,** R195-200.

TURK, B., TURK, D. & TURK, V. 2000. Lysosomal Cysteine Proteases: More Than Scavengers. *Biochim Biophys Acta,* 1477**,** 98-111.

TURK, V., STOKA, V. & TURK, D. 2008. Cystatins: Biochemical and Structural Properties, and Medical Relevance. *Front Biosci,* 13**,** 5406-20.

VALLE-DELGADO, J. J., ALFONSO-PRIETO, M., DE GROOT, N. S., VENTURA, S., SAMITIER, J., ROVIRA, C. & FERNANDEZ-BUSQUETS, X. 2010. Modulation of Abeta42 Fibrillogenesis by Glycosaminoglycan Structure. *FASEB J,* 24**,** 4250-61.

VANCE, J. E., HAYASHI, H. & KARTEN, B. 2005. Cholesterol Homeostasis in Neurons and Glial Cells. *Semin Cell Dev Biol,* 16**,** 193-212.

VANDER JAGT, D. L. & GARCIA, K. B. 1987. Immunochemical Comparisons of Proteins That Bind Heme and Bilirubin: Human Serum Albumin, Alpha-Fetoprotein and Glutathione S-Transferases from Liver, Placenta and Erythrocyte. *Comp Biochem Physiol B,* 87**,** 527-31.

VINTERS, H. V., NISHIMURA, G. S., SECOR, D. L. & PARDRIDGE, W. M. 1990a. Immunoreactive A4 and Gamma-Trace Peptide Colocalization in Amyloidotic Arteriolar Lesions in Brains of Patients with Alzheimer's Disease. *Am J Pathol,* 137**,** 233-40.

VINTERS, H. V., SECOR, D. L., PARDRIDGE, W. M. & GRAY, F. 1990b. Immunohistochemical Study of Cerebral Amyloid Angiopathy. Iii. Widespread Alzheimer A4 Peptide in Cerebral Microvessel Walls Colocalizes with Gamma Trace in Patients with Leukoencephalopathy. *Ann Neurol,* 28**,** 34-42.

WALL, J. S., SIMON, M. N., LIN, B. Y. & VINOGRADOV, S. N. 2008. Mass Mapping of Large Globin Complexes by Scanning Transmission Electron Microscopy. *In:* POOLE, R. K. (ed.) *Globins and Other Nitric Oxide-Reactive Proteins, Pt A.* San Diego: Elsevier Academic Press Inc.

WALSH, D. M., LOMAKIN, A., BENEDEK, G. B., CONDRON, M. M. & TEPLOW, D. B. 1997. Amyloid Beta-Protein Fibrillogenesis. Detection of a Protofibrillar Intermediate. *J Biol Chem,* 272**,** 22364-72.

WANG, B., XIE, Y. C., YANG, Z., PENG, D., WANG, J., ZHOU, S., LI, S. & MA, X. 2008. Lack of an Association between Alzheimer's Disease and the Cystatin C (Cst3) Gene G73a Polymorphism in Mainland Chinese. *Dement Geriatr Cogn Disord,* 25**,** 461-4.

WARFEL, A. H., ZUCKER-FRANKLIN, D., FRANGIONE, B. & GHISO, J. 1987. Constitutive Secretion of Cystatin C (Gamma-Trace) by Monocytes and Macrophages and Its Downregulation after Stimulation. *J Exp Med,* 166**,** 1912-7.

WASMER, C., LANGE, A., VAN MELCKEBEKE, H., SIEMER, A. B., RIEK, R. & MEIER, B. H. 2008. Amyloid Fibrils of the Het-S(218-289) Prion Form a Beta Solenoid with a Triangular Hydrophobic Core. *Science,* 319**,** 1523-1526.

WEI, L., BERMAN, Y., CASTANO, E. M., CADENE, M., BEAVIS, R. C., DEVI, L. & LEVY, E. 1998. Instability of the Amyloidogenic Cystatin C Variant of Hereditary Cerebral Hemorrhage with Amyloidosis, Icelandic Type. *J Biol Chem,* 273**,** 11806-14.

WEISNER, B. & ROETHIG, H. J. 1983. The Concentration of Prealbumin in Cerebrospinal Fluid (Csf), Indicator of Csf Circulation Disorders. *Eur Neurol,* 22**,** 96-105.

WELLS, K., FAROOQUI, A. A., LISS, L. & HORROCKS, L. A. 1995. Neural Membrane Phospholipids in Alzheimer Disease. *Neurochem Res,* 20**,** 1329-33.

WESTERMARK, P., SLETTEN, K., JOHANSSON, B. & CORNWELL, G. G., 3RD 1990. Fibril in Senile Systemic Amyloidosis Is Derived from Normal Transthyretin. *Proc Natl Acad Sci U S A,* 87**,** 2843-5.

WESTERMARK, P., BENSON, M. D., BUXBAUM, J. N., COHEN, A. S., FRANGIONE, B., IKEDA, S., MASTERS, C. L., MERLINI, G., SARAIVA, M. J., SIPE, J. D. & AMYLOID, N. C. I. S. 2002. Amyloid Fibril Protein Nomenclature - 2002. *Amyloid-Journal of Protein Folding Disorders,* 9**,** 197-200.

WHITE, H. E., HODGKINSON, J. L., JAHN, T. R., COHEN-KRAUSZ, S., GOSAL, W. S., MUELLER, S., ORLOVA, E. V., RADFORD, S. E. & SAIBIL, H. R. 2009. Globular Tetramers of Beta(2)-Microglobulin Assemble into Elaborate Amyloid Fibrils. *Journal of Molecular Biology,* 389**,** 48-57.

WILLIAMS, T. L., JOHNSON, B. R., URBANC, B., JENKINS, A. T., CONNELL, S. D. & SERPELL, L. C. 2011. Abeta42 Oligomers, but Not Fibrils, Simultaneously Bind to and Cause Damage to Ganglioside-Containing Lipid Membranes. *Biochem J,* 439**,** 67-77.

WILLIAMS, T. L. & SERPELL, L. C. 2011. Membrane and Surface Interactions of Alzheimer's Abeta Peptide--Insights into the Mechanism of Cytotoxicity. *FEBS J,* 278**,** 3905-17.

WILLIS, R. C. & FURLONG, C. E. 1975a. Interactions of a Glutamate-Aspartate Binding Protein with the Glutamate Transport System of Escherichia Coli. *J Biol Chem,* 250**,** 2581-6.

WILLIS, R. C. & FURLONG, C. E. 1975b. Purification and Properties of a Periplasmic Glutamate-Aspartate Binding Protein from Escherichia Coli K12 Strain W3092. *J Biol Chem,* 250**,** 2574-80.

WINKLER, E. A., NISHIDA, Y., SAGARE, A. P., REGE, S. V., BELL, R. D., PERLMUTTER, D., SENGILLO, J. D., HILLMAN, S., KONG, P., NELSON, A. R., SULLIVAN, J. S., ZHAO, Z., MEISELMAN, H. J., WENBY, R. B., SOTO, J., ABEL, E. D., MAKSHANOFF, J., ZUNIGA, E., DE VIVO, D. C. & ZLOKOVIC, B. V. 2015. Glut1 Reductions Exacerbate Alzheimer's Disease Vasculo-Neuronal Dysfunction and Degeneration. *Nat Neurosci,* 18**,** 521-30.

WOLFE, L. S., CALABRESE, M. F., NATH, A., BLAHO, D. V., MIRANKER, A. D. & XIONG, Y. 2010. Protein-Induced Photophysical Changes to the Amyloid Indicator Dye Thioflavin T. *Proc Natl Acad Sci U S A,* 107**,** 16863-8.

WOLFF, M., UNUCHEK, D., ZHANG, B., GORDELIY, V., WILLBOLD, D. & NAGEL-STEGER, L. 2015. Amyloid Beta Oligomeric Species Present in the Lag Phase of Amyloid Formation. *PLoS One,* 10**,** e0127865.

WOOD, S. J., CHAN, W. & WETZEL, R. 1996. Seeding of a Beta Fibril Formation Is Inhibited by All Three Isotypes of Apolipoprotein E. *Biochemistry,* 35**,** 12623-8.

XUE, W. F., HELLEWELL, A. L., GOSAL, W. S., HOMANS, S. W., HEWITT, E. W. & RADFORD, S. E. 2009. Fibril Fragmentation Enhances Amyloid Cytotoxicity. *J Biol Chem,* 284**,** 34272-82.

YAMADA, M., SODEYAMA, N., ITOH, Y., SUEMATSU, N., OTOMO, E., MATSUSHITA, M. & MIZUSAWA, H. 1997. Association of Presenilin-1 Polymorphism with Cerebral Amyloid Angiopathy in the Elderly. *Stroke,* 28**,** 2219-2221.

YAMADA, M. 2000. Cerebral Amyloid Angiopathy: An Overview. *Neuropathology,* 20**,** 8-22.

YAMAGUCHI, K., KATOU, H., HOSHINO, M., HASEGAWA, K., NAIKI, H. & GOTO, Y. 2004. Core and Heterogeneity of Beta2-Microglobulin Amyloid Fibrils as Revealed by H/D Exchange. *J Mol Biol,* 338**,** 559-71.

YAMASAKI, M., LI, W., JOHNSON, D. J. & HUNTINGTON, J. A. 2008. Crystal Structure of a Stable Dimer Reveals the Molecular Basis of Serpin Polymerization. *Nature,* 455**,** 1255-8.

YANG, D. S., YIP, C. M., HUANG, T. H. J., CHAKRABARTTY, A. & FRASER, P. E. 1999. Manipulating the Amyloid-Beta Aggregation Pathway with Chemical Chaperones. *Journal of Biological Chemistry,* 274**,** 32970-32974.

YANG, D. T., JOSHI, G., CHO, P. Y., JOHNSON, J. A. & MURPHY, R. M. 2013a. Transthyretin as Both a Sensor and a Scavenger of Beta-Amyloid Oligomers. *Biochemistry,* 52**,** 2849-61.

YANG, X., XIE, H., CHEN, J. & LI, X. 2013b. Anionic Phenolic Compounds Bind Stronger with Transthyretin Than Their Neutral Forms: Nonnegligible Mechanisms in Virtual Screening of Endocrine Disrupting Chemicals. *Chem Res Toxicol,* 26**,** 1340-7.

YEPES, M. & LAWRENCE, D. A. 2004. New Functions for an Old Enzyme: Nonhemostatic Roles for Tissue-Type Plasminogen Activator in the Central Nervous System. *Exp Biol Med (Maywood),* 229**,** 1097-104.

YOUNG, I. D., AILLES, L., NARINDRASORASAK, S., TAN, R. & KISILEVSKY, R. 1992. Localization of the Basement Membrane Heparan Sulfate Proteoglycan in Islet Amyloid Deposits in Type Ii Diabetes Mellitus. *Arch Pathol Lab Med,* 116**,** 951-4.

ZAHN, R., LIU, A., LUHRS, T., RIEK, R., VON SCHROETTER, C., LOPEZ GARCIA, F., BILLETER, M., CALZOLAI, L., WIDER, G. & WUTHRICH, K. 2000. Nmr Solution Structure of the Human Prion Protein. *Proc Natl Acad Sci U S A,* 97**,** 145-50.

ZHANG, Y., RANTA, F., TANG, C., SHUMILINA, E., MAHMUD, H., FOLLER, M., ULLRICH, S., HARING, H. U. & LANG, F. 2009. Sphingomyelinase Dependent Apoptosis Following Treatment of Pancreatic Beta-Cells with Amyloid Peptides Abeta(1-42) or Iapp. *Apoptosis,* 14**,** 878-89.

ZHOU, J. & LIU, B. 2013. Alzheimer's Disease and Prion Protein. *Intractable Rare Dis Res,* 2**,** 35-44.

ZUNSZAIN, P. A., GHUMAN, J., KOMATSU, T., TSUCHIDA, E. & CURRY, S. 2003. Crystal Structural Analysis of Human Serum Albumin Complexed with Hemin and Fatty Acid. *BMC Struct Biol,* 3**,** 6.